CZECH TECHNICAL UNIVERSITY IN PRAGUE

FACULTY OF CIVIL ENGINEERING

Department of Steel and Timber structures

Ing. Tomáš Hána

TIME AND TEMPERATURE DEPENDENT SHEAR STIFFNESS OF POLYMERIC INTERLAYERS AND ITS EFFECT ON LAMINATED GLASS IN BENDING

DOCTORAL THESIS FOR Ph.D. DEGREE

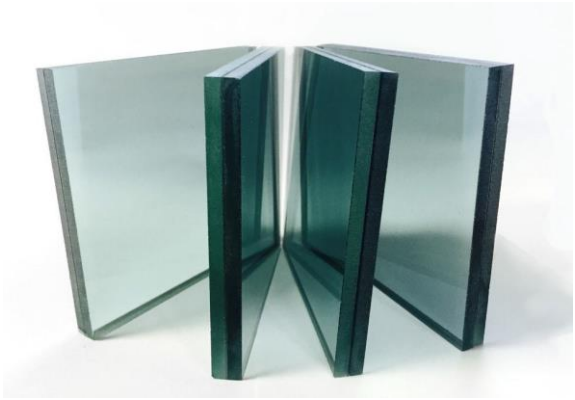

Supervisors

doc. Ing. Martina Eliášová, CSc.

Ing. Miroslav Vokáč, Ph.D.

2022

PROHLÁŠENÍ

DECLARATION

Aspirant: Tomáš Hána

Název disertační práce: Smyková tuhost polymerních folií v závislosti na čase a teplotě a její vliv na odezvu vrstveného skla v ohybu

Title of doctoral thesis: Time and temperature dependent shear stiffness of polymeric interlayers and its effect on laminated glass in bending

Prohlašuji, že jsem předloženou disertační práci vypracoval samostatně pod vedením školitelů paní doc. Ing. Martiny Eliášové, CSc. a pana Ing. Miroslava Vokáče, Ph.D.

Použitou literaturu a další zdroje uvádím v seznamu použité literatury.

Tato disertační práce vznikla v souvislosti s řešením projektů GA 14-17950S, GA 16-14770S a GA 16-17461S.

I declare I wrote the submitted thesis on my own under the supervision of Dr. Martina Eliášová and a Dr. Miroslav Vokáč.

Literature and other sources are stated in the list of references.

This thesis arose in relation to solution of projects GA 14-17950S, GA 16-14770S, and GA 16-17461S.

V Praze dne / *In Prague on*

Podpis / *Signature*

Poděkování

Tato práce, kterou si Vám dovoluji předložit, vznikala v letech 2016 – 2022 na půdě Kloknerova ústavu a Fakulty stavební Českého vysokého učení technického v Praze v rámci mého doktorského studia. Práce je shrnutím rozsáhlého výzkumu, který byl zaměřen na mechanické vlastnosti polymerních folií používaných pro vrstvená skla a na chování těchto skel při zatížení působící kolmo na jejich střednicovou rovinu. Práci jsem pro lepší dostupnost zahraniční veřejnosti napsal v anglickém jazyce.

Chtěl bych zde velmi poděkovat zejména své školitelce doc. Ing. Martině Eliášové, CSc. za její odborné vedení a za připomínky, náměty a podporu, které mi po celou dobu mého doktorského studia vždy ochotně poskytla.

Velké poděkování patří mému školiteli specialistovi Ing. Miroslavu Vokáčovi, Ph.D., jehož cenné rady, zázemí a vřelý přístup pro mne byly důležitou oporou při tvorbě této práce.

Celý výzkum byl od počátku podporován Grantovou agenturou České republiky, konkrétně projekty GA 14-17950S, GA 16-14770S a GA 16-17461S, a také Programem podpory aplikovaného výzkumu a vývoje "TRIO" č. FV 10295. Za tuto podporu děkuji.
Dále bych rád poděkoval Ing. Jakubu Čulkovi z firmy AGC a.s., Ing. Evženu Rainerovi z firmy OGB s.r.o. a Ing. Ondřeji Jarešovi z firmy ROVER s.r.o. za poskytnuté odborné konzultace, které mi pomohly porozumět podstatě obdržených experimentálních výsledků.

V neposlední řadě děkuji kolegům Ing. Kláře V. Machalické, Ph.D. a Ing. Petru Sejkotovi, Ph.D., kteří věnovali svůj čas a pomocnou ruku pro část mého výzkumu.

Nakonec bych chtěl poděkovat svým rodičům Janě a Miroslavovi a dalším členům své nejbližší rodiny, kteří pro mne byli v době mého doktorského studia významnou oporou. Za pomoc s grafickou úpravou práce děkuji Helence Fišarové.

Acknowledgment

This submitted thesis arose in years 2016 – 2022 in Klokner Insitute and Faculty of Civil Engineering CTU during my doctoral studies. The thesis concludes an extensive research aimed at mechanical properties of polymeric interlayers used in laminated glass and on the behaviour of laminated glass in out of plane loading.

I would like to thank my supervisor Dr. Martina Eliášová for professional supervision and for comments, suggestions, and support she kindly provided during my entire doctoral studies.

Special thanks belongs to my co-supervisor Dr. Miroslav Vokáč whose kind approach, background and valuable advice meant important support for my thesis.

Entire experimental campaign was from the beginnings supported by Grant agency of the Czech Republic, particularly by projects GA 14-17950S, GA 16-14770S, and GA 16-17461S and also by Program of applied research and development "TRIO" č. FV 10295. I gratefully acknowledge this support.
Further, I would like to thank Ing. Jakub Čulek from AGC a.s. company, Ing. Evžen Rainer from OGB s.r.o. company, and Ing. Ondřej Jareš from ROVER s.r.o. company for professional consultations which helped me understand the essence of obtained experimental results.

I also thank my colleagues and friends Dr. Klára V. Machalická and Dr. Peter Sejkot who dedicated their time and assisstance for part of my research.

Finally, I want to thank my parents and other members of my family who supported me during my doctoral studies. I also thank dear Helenka Fišarová for a help with graphics.

Abstrakt

Tato doktorská práce je zaměřena na vrstvené sklo, které se v současnosti ve stavebnictví používá i pro nosné prvky. Zvláštní pozornost je věnována chování vrstveného skla zatíženého kolmo na svoji rovinu v závislosti na okolní teplotě a délce trvání statického zatížení. Práce shrnuje současný stav poznání této problematiky a rozebírá mechanické vlastnosti polymerních folií, které se používají do vrstvených skel. Tyto folie mohou za určitých podmínek zajistit smykové spolupůsobení jednotlivých skleněných desek v ohýbaném panelu z vrstveného skla. Vrstvené sklo v ohybu je předmětem intenzivního výzkumu na mnoha evropských pracovištích. Nedostatek znalostí a jednotných evropských norem pro navrhování nosného ohýbaného vrstveného skla vyžaduje nutnost experimentální a výzkumné činnosti v této oblasti stavebního inženýrství. Hlavní část této předložené práce mapuje výsledky autorova výzkumu na ČVUT v Praze, který měl za cíl popsat smykovou tuhost běžných polymerních folií používaných do vrstvených skel v závislosti na teplotě a délce trvání statického zatížení a který měl popsat vliv této tuhosti na odezvu vrstveného skla v ohybu. Vytyčené cíle byly dosaženy provedením reálných experimentů s vrstveným sklem, které byly doplněny četnými analytickými a numerickými výpočty.

Abstract

This doctoral thesis is focused on laminated glass as a new load bearing element in a contemporary architecture. Special attention is paid to the performance of laminated glass in out of plane loading in scope of temperature and load duration. Thesis maps current knowledge in this engineering area. Further, general mechanical properties of polymeric interlayers, which may ensure a certain degree of shear coupling of the individual glass plies in laminated panel in bending, are discussed. Laminated glass in bending is the subject of an intensive research in several European workplaces. The lack of knowledge and uniform European standards aimed at load bearing capacity of laminated glass in out of plane loading requires experimental efforts in this field of civil engineering. The main part of this thesis maps complete research conducted by the author at CTU in Prague to achieve the main goal which consisted in the description of time and temperature stiffness characteristics of selected polymeric interlayers as well as in their effect on the response of laminated glass panels in out of plane static loading. The goal was achieved using real experiments with laminated glass supported by extensive analytical and numerical studies.

Key words: Laminated glass, Polymeric interlayer, Shear stiffness, Time, Temperature, Shear stress, Shear strain, Normal stress, Normal strain, Shear, Torsion, Maxwell-Weichert model, Shear coupling, Bending, Viscoelasticity, Loading rate, Effective thickness, Force, Deflection

List of abbreviations

FG = float glass
HTG = heat toughened glass
HSG = heat strengthened glass
LG = laminated glass
LSG = laminated safety glass
PVB = polyvinyl butyral
EVA = ethylene-vinyl acetate
TPU = thermoplastic polyurethane
SGP = SentryGlas Plus
DIC = digital image correlation
W-B = Wölfel-Bennison
EET = Enhanced Effective Thickness
DS = displacement sensor
SG = strain gauge
1D = one dimensional problem
2D = two dimensional problem
3D = three dimensional problem
PE = polyethylene
PVC = polyvinyl chloride
PC = polycarbonate
FVS = full viscoelastic solution
TTSP = Time Temperature Superposition Principle
LE = linear elastic
LVE = linear viscoelastic
GM = Generalized Maxwell
GMF = Generalized Maxwell fluid
GK-V = Generalized Kelvin-Voigt
M-W = Maxwell-Weichert
SH = shear
TS = torsion
ULS = ultimate limit state
SLS = serviceability limit state
Trosifol BG or only BG = Trosifol BG R20
Trosifol ES or only ES = Trosifol Extra Strong
EVA L = Evalam 80/120
EVA S = Evasafe
SG 5000 = SentryGlas 5000
TPU KF = Krystalflex PE399
DMTA = Dynamic mechanical thermal analysis
FE = finite element
FEM = finite element method
PVD = principle of virtual displacement

FE: SH = numerial results using Maxwell-Weichert model of interlayer from DMTA in shear mode
FE: SH+TS = numerial results using Maxwell-Weichert model of interlayer from combined results of DMTA in shear + torsion mode

List of symbols

t	time
G	shear elastic modulus analogously as shear stiffness
$G(t)$	shear elastic stiffness in time analogously as shear relaxation modulus/function in time
$G(t, T)$	shear elastic stiffness analogously as shear relaxation modulus/function in time and temperature
G_{init}	initial shear stiffness/modulus
G_{inst}	instantaneous shear elastic modulus given by Maxwell-Weichert model
G_{∞}	equilibrium shear stiffness analogously as equilibrium shear relaxation modulus in Maxwell-Weichert model
E	Young elastic modulus analogously as normal (tensile/compressive) elastic stiffness
$E(t)$	Young relaxation modulus/function analogously as normal (tensile/compressive) elastic stiffness in time
$E(t, T)$	Young relaxation modulus/function analogously as normal (tensile/compressive) elastic stiffness in time and temperature

E_{init}	initial tensile stiffness/modulus
E_0	normal stiffness of added elastic component in Generalized Kelvin-Voigt models of polymers
E_{inst}	instantaneous Young elastic modulus given by Maxwell-Weichert model
E_∞	equilibrium normal stiffness analogously as equilibrium normal relaxation modulus in Maxwell-Weichert m.
K	bulk elastic modulus
K(t)	bulk relaxation modulus/function in time
K_{inst}	instantaneous bulk elastic modulus given by Maxwell-Weichert model
K_∞	equilibrium bulk stiffness analogously as equilibrium bulk relaxation modulus in Maxwell-Weichert model
ρ	density
α	thermal expansion coefficient
λ	heat conductivity
σ	normal stress
ε	normal strain
ε_{max}	amplitude of dynamic normal strain at DMTA
τ	shear stress
τ_{init}	initial shear stress related to initial shear modulus
γ	shear strain
γ_{init}	initial shear strain related to initial shear modulus
γ_{fail}	shear strain at failure
γ_{tot}	total shear strain of interlayer at DMTA
τ_{tot}	total shear stress of interlayer at DMTA
γ(t)	dynamic shear strain of interlayer at DMTA
τ(t)	dynamic shear stress of interlayer at DMTA
γ_s	static shear strain of interlayer at DMTA
τ_s	static shear stress of interlayer at DMTA
γ_{max}	amplitude of dynamic shear strain of interlayer at DMTA
δ	phase shift between stress and strain during DMTA
σ_0	applied normal stress at a creep test or instantaneous normal stress at a relaxation test
σ_∞	equilibrium normal stress at a relaxation test
ε_0	instantaneous normal strain at creep test or constant normal strain at a relaxation test
ε_∞	equilibrium normal strain at creep test
J	normal compliance
J(t)	normal compliance in time analogously as compliance function in time
T	temperature
+…°C	temperature in Celsius above zero, these temperatures are usually stated without “+” symbol
-…°C	temperature in Celsius below zero, symbol “-” is never ommited for these temperatures
T_g	glass transition temperature
T_f	flow temperature
T_m	melt temperature
T_{cm}	crystal melting temperature

T_d	degradation temperature
a_T	temperature shift coefficient
T_{ref}	reference temperature
t_{ref}	time related to relaxation modulus at reference temperature
WLF	Williams-Landel-Ferry equation/model
C_1, C_2	dimensionless constants in Williams-Landel-Ferry equation
R	universal gas constant
E_a	activation energy of a polymer
η	viscosity of a damper or coefficient of shear forces in Enhanced Effective Thickness method
θ	retardation or relaxation time
υ	Poisson ratio
$H(\theta)$	relaxation spectrum of a polymer
E^*	normal dynamic complex modulus
E'	normal storage modulus
E''	normal loss modulus
G^*	shear dynamic complex modulus
G'	shear storage modulus
G''	shear loss modulus
i	complex unit
ω	angular velocity
f	frequency
w	midspan vertical displacement (deflection)
w_{max}	maximum midspan vertical displacement (deflection)
F	force
F_{max}	maximum force analogously as maximum load bearing capacity
F_{res}	residual force analogously as residual load bearing capacity
F_s	prestressing tensile force at DMTA
$F(t)$	measured dynamic force at DMTA
M	bending moment or number of Maxwell (Kelvin) models in parallel (series)
m	proportional bending moment
Γ	coefficient of shear forces in Wölfel-Bennison method
L, l	span of glass panel
b	width of laminated panel´s cross section
A	area or surface
β	boundary conditions coefficient in Wölfel-Bennison method
$h_{ef,w}$	effective thickness for vertical deflection
$h_{ef,\sigma}$	effective thickness for stress
h	thickness of glass ply
p	thickness of interlayer
I_s	baricentrical intertia of laminated glass cross section

I	moment of inertia
I_{tot}	moment of inertia of the monolithic cross section
D	flexural rigidity
D_{tot}	flexural rigidity of the monolithic cross section
Ψ	shape coefficient related to boundary conditions in Enhanced Effective Thickness method
u	displacement
u_{max}	amplitude of MTS loading cylinder dynamic displacement at DMTA
$\{\sigma\}$	stress tensor in Voigt notation
$\{\varepsilon\}$	strain tensor in Voigt notation
$\{X\}$	vector of volume forces
$\{p\}$	vector of surface forces
$\{\delta u\}$	vector of virtual displacement
$\{\delta\varepsilon\}$	tensor of virtual strain in Voigt notation
$\{u\}$	vector of displacement
$\{r\}$	displacement vector of discrete nodes
$\{f\}$	load vector of discrete nodes
$\{e\}$	deviatoric part of strain tensor in Voigt notation
ε_V	volumetric part of strain
[K]	stiffness matrix of the structure
[E]	elastic stiffness matrix of a material
[P]	scaling matrix
k	bending stiffness
·	the multiplication symbol used in for clarity of equations (this symbol is omitted where possible)
×	the multiplication symbol used in the text or for numbers in text
$\{E_\infty, E_i, \theta_i\}$ or $\{E_0, E_i, \theta_i\}$	Young Prony series
$\{G_\infty, G_i, \theta_i\}$	shear Prony series
$\{K_\infty, K_i, \theta_i\}$	bulk Prony series
$\{\tau_{init}, \gamma_{init}\}$	shear stress and shear strain related to the initial shear stiffness modulus

Content

1. Introduction

Architecture as well as other human activities develops and requirements for an aesthetic effect of structures are increasing. In the last few years, architects and civil engineers focused on light, transparent, and recyclable structures – structures made of glass. With respect to requirements of modern concept of architecture, glass is currently used more often even for load bearing elements. It means, glass in structure does not serve as a transparent filling material, but it must be resistant to wind load, snow load, and to other variable or permanent loads [1]. Load bearing function of glass elements is enabled due to an intensive development of new technologies used in manufacturing process of glass and, also, of polymeric materials glass elements are usually bonded with. For a design and reliable assessment of glass structures, sufficient knowledge of their performance under loading as well as uniform European standards are missing, therefore use of every new glass load bearing element is regularly followed by series of experiments and studies. Transparency is unique property of glass due to which this material has become popular in a civil engineering. On the other hand, glass is a brittle material and broken glass panel has no residual load bearing capacity. Therefore, load bearing glass panels should be designed with respect to the prevention of an abrupt collapse. This approach brings a different concept of design reliability, robustness, and safety which is ensured by use of laminated glass.

2. Laminated glass – state of art

Load bearing glass elements are, apart from window infill panels, always made of laminated glass. Laminated glass is formed of at least two glass plies bonded with polymeric interlayer. Polymeric interlayer embedded between glass plies enables their shear interaction in out of plane loading and improves the safety of laminated glass. Lamination process does not interfere the transparency of laminated glass, therefore laminated glass can still form transparent structures and fulfil aesthetic requirements. Use of laminated glass in civil structures satisfy new trends in a current architecture, enable to utilize new technologies in a production of building materials and meet safety requirements. Many research workplaces and universities around the world deal with the performance of laminated glass in out of plane loading – this is a fundamental problem whose solution will contribute to more precise and economic design of structures made of laminated glass. Performance of laminated glass in out of plane loading is strongly affected by temperature and duration of load. Due to the lack of knowledge in this engineering area, only approximate methods are used when dealing with design of load bearing laminated glass in daily practice. Therefore, this thesis aims at the performance of laminated glass in static out of plane loading right in scope of temperature and load duration to contribute to a solution of this burning problem.

2.1. Types of glass and material properties of glass

Glass is a brittle material which fails by brittle fracture. This occurs abruptly, without any signs of warning. Therefore, it is not possible to consider the redistribution of local peaks of stress enabled by material plasticization. Typical stress-strain relation of glass is in Fig. 1. Chart shows glass is linearly elastic material. Basic material properties of float glass including characteristic strengths are shown in Tab. 1.

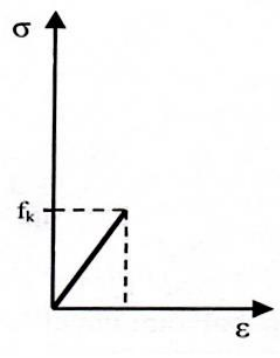

Fig. 1: Schematic stress-strain diagram of glass [1]

Tab. 1: Material properties of float glass [2]

Material property	Value	Unit
Density ρ	2500	kg/m^3
Young modulus of elasticity E	70 000	MPa
Shear modulus of elasticity G	30 000	MPa
Poisson ratio υ	0.23	-
Thermal expansion coefficient α	$7.7 – 8.8 \times 10^{-6}$	1/K
Heat conductivity λ	1.0	W/mK
Characteristic compressive strength	>1000	MPa
Characteristic tensile strength	10 – 100	MPa

Crucial mechanical property of glass is a tensile strength. When glass has perfectly homogenous microstructure and undamaged surface, theoretical value of tensile strength may reach thousands of MPa. Although, experiments showed that real glass tensile strength is 10 – 100 MPa [2]. Lower value of real strength is caused by the presence of macro and microcracks on the glass surface. These may arise in a manufacturing process, improper handling, drilling, installation, or maintenance. Apart from steel or aluminium, glass tensile strength depends also on the load duration and humidity. The development and increase of cracks in the zones of tensile stress accelerates with increased humidity and duration of the load [3]. The example of tensile strength of float glass with respect to the load duration is in Tab. 2.

Glass consists of various chemical substances. Most representative are oxides of silicon (Si), calcium (Ca), boron (B), phosphorus (P), or sodium (Na). Soda-lime glass is mostly used glass in

civil structures. Regarding temperature dependence, glass is an anorganic substance that solidifies without “crystallization”. It is, in fact, a viscoelastic material that is rigid at room temperature but gets to liquid at temperatures above transition zone (approx. 580 °C) [4].

As every structural material, glass has many advantages such as transparency, high compressive strength, corrosion resistance, electrical non-conductivity, and recyclability. Disadvantages are brittle fracture, low tensile strength, impact sensitivity, difficult structural joints and details, and increased requirements on construction and maintenance.

Tab. 2: Example of float glass tensile strength with respect to the load duration [5]

Tensile strength	**Type of the load**	**Example**
32 MPa	short-term load	Wind
11 MPa	long-term load	Self-weight

There are many parameters according to which glass can be sorted. When using glass for structural load members, decisive factors are tensile strength and a type of failure. These factors are determined by the manufacturing process. In scope of this, structural glass can be classified as:

- Float glass
- Strength treated glass (heat toughened, heat strengthened, or chemically toughened)
- Laminated glass

Float glass (FG) is made by float process developed by Pilkington (1952). Basic raw materials are silica (SiO_2), sodium oxide (Na_2O), and calcium oxide (CaO). These substances are heated up in a furnace to 1500 °C to a liquid state. Molten glass is then at the temperature around 1000 °C constantly floated from the furnace to a liquid bed of tin. Glass floats on the tin bath and makes a flat surface. FG is cooled down very slowly which means the residual stress almost disappears. After a cooling process, it is forwarded to the next treatment. Typical thickness of glass ply is 4, 6, 8, 10, 12, 15, or 19 mm [6].

In spite of relatively low characteristic tensile strength – 45 MPa [5], this type of glass is frequently used. At failure, float glass breaks into large shards which are dangerous for structure users. If increased tensile strength of glass surface is desirable, float glass can be in the manufacturing process further thermally modified and it becomes heat toughened or heat strengthened.

Heat toughened glass (HTG) is made of float glass ply by its heating up to 650 °C and subsequent fast cooling. This means the arise of pressure stress on the surface and tensile stress in the core of a glass ply. The course of residual stress over the thickness of a ply is parabolic, see Fig. 2. Compressive stress on the surface, between 90 – 150 MPa [1], means HTG is more resistant to bending. Collapse of HTG ply occurs in the entire volume as the effect of energy decrease. HTG ply breaks, apart from FG, into very small shards which are not so dangerous for structure users.

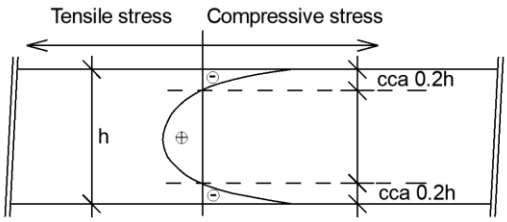

Fig. 2: Stress distribution over the thickness of heat toughened glass ply [1]

Heat strengthened glass (HSG) is manufactured using similar process as HTG, but the level of induced compressive prestress is lower – between 35 MPa and 55 MPa [1]. The level of residual stress over the thickness of ply is also parabolic. At failure, this type of glass breaks in a similar fashion as FG, i.e. large sharp shards. Collapse of HSG occurs in the entire volume as in case of HTG. Visual comparison of glass shards for FG, HTG, and HSG is shown in Fig. 3.

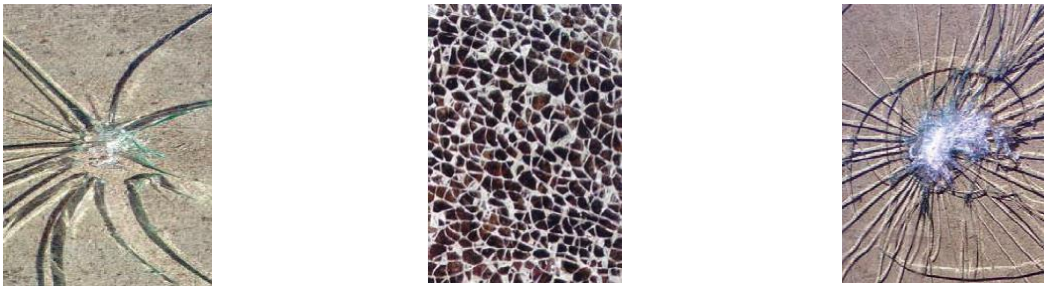

a) Float glass b) Heat toughened glass c) Heat strengthened glass

Fig. 3: Typical failure modes for various types of glass [3]

Laminated glass (LG) is a composition of two or more glass plies bonded together with polymeric interlayer. This is typical for load bearing elements used in civil structures. Glass plies are usually made of float glass (FG), heat strengthened glass (HSG), or heat toughened glass (HTG).

2.2. Composition and performance of laminated glass in bending

Cross section of laminated glass may be of various compositions. Illustrative example of triple laminated cross section is shown in Fig. 4. Usual thickness of glass plies is between 6 mm and 19 mm. Nominal thickness of interlayer is usually in multiples of 0.38 mm depending on the certain product. Main advantage of LG in civil structures is that in case of glass failure, shards of broken glass ply stay adhered to the interlayer, and LG panel is still able to resist a certain load [7] due to remaining undamaged glass plies. Although polymeric interlayers are of much lower stiffness than glass, they can ensure a certain mechanical interaction of the individual glass plies in a panel [8]. Increased economical requirements on LG structures result in experimental effort and research in

the field of mechanical properties of polymeric interlayers, and in their effect on shear interaction of the individual glass plies in out of plane loaded panel.

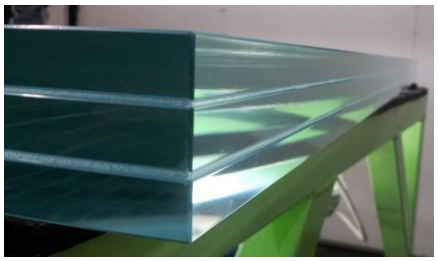

Fig. 4: Composition of triple laminated glass panel in detail, picture by author

If the laminate fulfils certain safety requirements regarding breakage and post-breakage behaviour to guarantee a restraint of glass fragments after the brittle failure, it is referred as laminated safety glass (LSG). LSG is required in case of fall protection glazing, walk-on glazing, or overhead glazing. In the sequel, no distinction will be made between LG and LSG.

Interlayers are usually made of polyvinyl butyral (PVB) or ethylene-vinyl acetate (EVA). Fast development of a chemical industry also introduced new progressive materials such as thermoplastic polyurethanes (TPU) or ionomers. Thickness of glass plies in a panel is usually identical. In case multi laminated walk-on glazing, thickness of upper glass ply may be lower. Examples of double or multi laminated cross sections are shown in Fig. 5.

Fig. 5: Cross section examples of double and multi laminated glass panel

LG panels are mostly loaded in bending which results from their applications in civil structures. Crucial factors on the performance of LG panel in bending are material characteristics of used interlayer, particularly its shear modulus *G*. This physical quantity is time and temperature dependent. The value of interlayer´s shear modulus *G* influences the distribution of normal stress over the cross section of LG panel in bending [9]. Theoretically speaking, for long-term load or high temperatures, shear modulus is low, glass plies "slide" over each other, and their shear coupling is eliminated. For short-term load or low temperatures, shear modulus is high and ensures full shear coupling of glass plies. The panel then acts in bending as a "monolithic". In common practice, shear modulus of the interlayer lies in wide range values and mostly ensures only limited shear coupling of glass plies in bending [9]. The example of normal stress distribution in bended LG panel over its cross section based on the theoretical value of interlayer´s shear modulus *G* is

plotted in Fig. 6. This figure shows that peak of normal stress decreases as the value of *G* increases. Problem is that producers usually do not specify shear moduli of most interlayers and stimulate the need of experimental research.

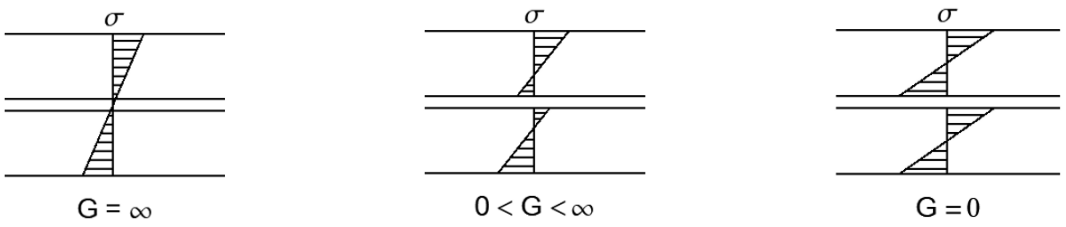

a) Full shear copling b) Limited shear coupling c) No shear coupling

Fig. 6: Distribution of normal stress over the cross section of bended LG panel depending on the theoretical value of interlayer´s shear modulus *G* [9]

Performance of double LG panel in bending, in scope of damage, is schematically shown in Fig. 7. There are generally three phases: 1st phase – both glass plies are intact and carry the load (pre-breakage); 2nd phase – lower glass ply is broken and inactive, upper glass ply is intact and is able to transfer tensile stress (post-breakage); 3rd phase – tensile strength of upper glass ply has been exceeded, its shards are still adhered to the interlayer and transfer only compressive stress by mechanical contact that is in equilibrium with tensile stress in the interlayer (post-breakage, after total failure) [10]. This is the reason why LG panel may carry a certain load even after total failure. Detail of glass shards adhered to the interlayer after failure of LG panel in bending is shown in Fig. 8. The value of residual load bearing capacity of the panel after total failure is dependent on the type of interlayer, namely on its stiffness and tensile strength, and on the type of glass [1], [11]. Comparison of different behaviour of the panels after total failure in relation to the material of interlayer is shown in Fig. 9.

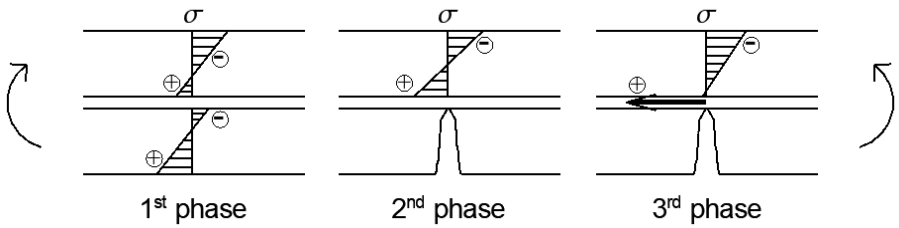

Fig. 7: Three phases of LG performance in bending in scope of damage [10]

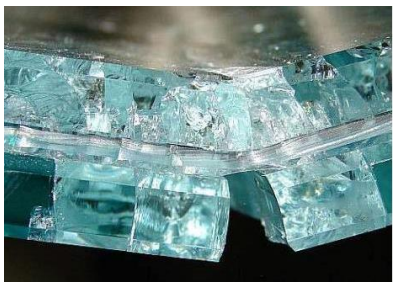

Fig. 8: Shards adhered to the interlayer after failure of LG panel in bending [1]

a) LG panel with polyethylene-co-methacrylid acid ionomer interlayer

b) LG panel with polyvinyl butyral interlayer

Fig. 9: Behaviour of LG panels after total failure laminated with different interlayers [12]

2.3. Structural elements made of laminated glass in practice

Manufacturing process must ensure sufficient cohesion, transparency, and durability of LG panel. Glass surface before lamination must be degreased, the interlayer is then embedded between prepared glass plies which are stacked on a top of each other. This composite is heated up at the temperature around 70 °C and the plies are pressed between rollers to displace air bubbles. The composite is further processed in autoclave or in laminator machine where the bonding process occurs. Whether to use laminator or autoclave depends on the certain type of interlayer as well as on the temperature and the pressure of lamination. Lamination process is schematically shown in Fig. 10.

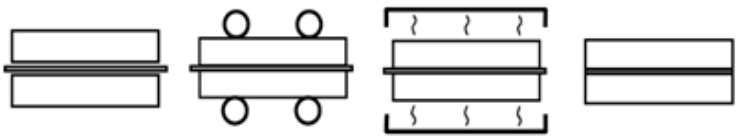

Fig. 10: Schematic manufacturing process of LG panel [1]

Load bearing LG panels are, in civil structures, used as atrium roofing, stairs, balustrades, canopies, floor members, façade panels, etc. Examples of such members are shown in Fig. 11. These members are usually supported by steel structure that transmits the load from the panel. The interaction of LG panel with steel supporting structure is a subject of a contemporary research [13], [14]. There are, in general, two structural options how to connect LG panel with supporting structure: (i) linear support (on the top of steel flange, into U profile, etc.); and (ii) point fixing. Illustrative examples of linear U profile and point drilled "spider" structural connections of LG panels with supporting structure are shown in Fig. 12.

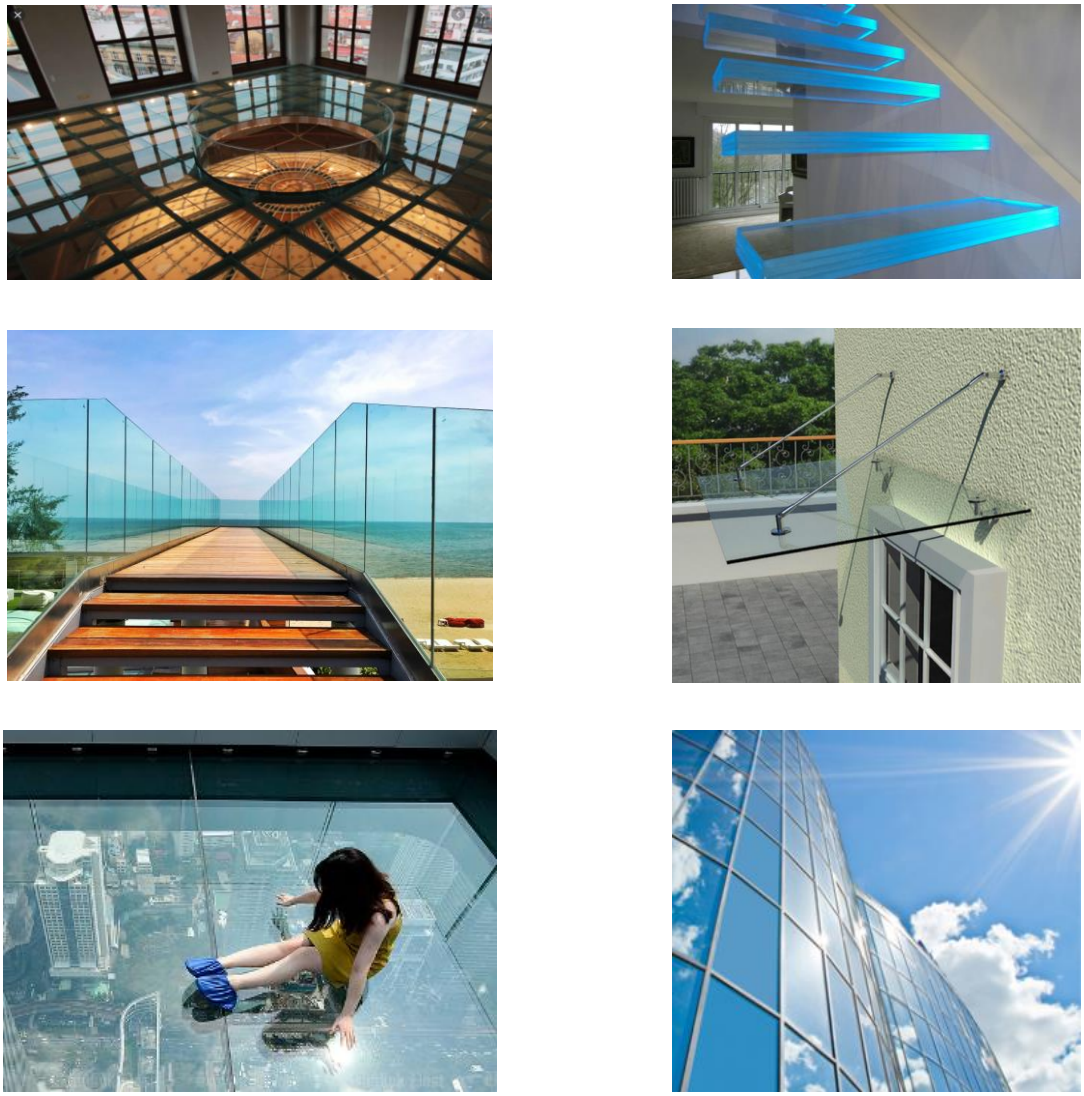

Fig. 11: Examples of structural members made of laminated glass [15], [16]

a) LG balustrade supported by U profile

b) Point fixing of LG roof panel supported by drilled “spider”

Fig. 12: Examples of structural connections between LG panel and supporting structure [17]

When LG panels are used as load bearing structural members in a real building, they must transmit, apart from self-weight, also variable loads such as live load, wind, snow, and temperature effects. Examples of these loads are shown in Fig. 13. The characteristic and design values of these loads are in engineering design of LG panels for structures in Europe determined according to European EN standards, e.g. EN 1991-1-1 [18]. Mechanical loads are applied on LG panels in the form of uniformly distributed load, line load, and locally concentrated load, see the examples in Fig. 14. Load in these cases acts out of plane and stresses LG panel with bending moments. When LG panel is, e.g., a part of a building façade, it is, in addition to mechanical loads, exposed to temperature changes. Moreover, mechanical loads applied on the panel are of different durations and can be applied at various temperatures. Fig. 13a) illustrates the example of horizontal short-term load (approx. 1 min) on the handrailing of LG panel. This panel is a part of balcony and is exposed to direct sunshine. Temperature of this panel may be over 50 °C. Contrary, LG roof panels in Fig. 13b) are subjected to snow load at -10 °C and duration of approx. 5 days. As it has been stated, these boundary conditions affect the stiffness of interlayer and, therefore, the overall bending stiffness of LG panel [8], [19]. Increase of shear strain of interlayer and vertical deflection of LG panel with increasing duration of static load and ambient temperature is schematically shown in Fig. 15. This figure reflects the decrease of interlayer´s shear stiffness G and the change of the state of the panel from “monolithic, fully shear coupled” to “laminated with limited shear coupling”. It has been shown in Fig. 6 that this fact is related to the stress-state of LG panel [9] whose precise determination not an easy task. Moreover, the loading history of LG panel may be miscellaneous. During its lifetime, the panel may be subjected to various variable loads of different durations and temperatures. Polymeric interlayer is a viscoelastic material which reacts with a delay to the applied load [20], therefore the previous loading case affects the current stress-state of LG panel [9] and the entire loading history of the panel should be considered in the precise analysis.

a) Horizontal live load on the hand railing

b) Snow load on the roof panel

Fig. 13: Examples of variable loads applied on LG panels, picture by author

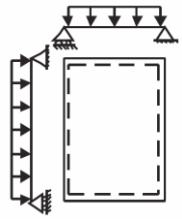

a) Floor LG panel loaded by self-weight

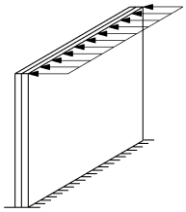

b) LG railing loaded by line load

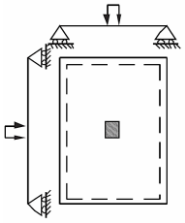

c) Floor LG panel loaded by locally concentrated load

Fig. 14: Examples of mechanical loads applied on LG panels in engineering design

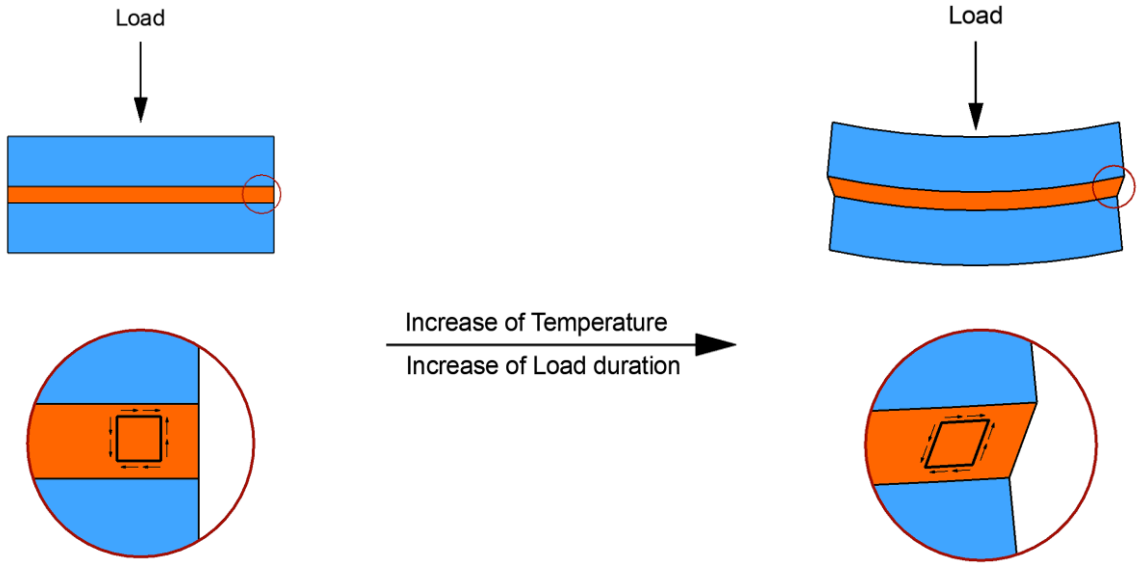

a) Low temperature and short-term load

b) Height temperatures and long-term load

Fig. 15: Schematic drawing pointing the growth of interlayer´s shear strain in LG panel with increasing temperature or duration of static load [21]

2.4. Polymeric interlayers in laminated glass

Safety requirements for load bearing glass structures postulate a prevention of an abrupt collapse. Glass fails by brittle fracture and structure users must immediately leave an endangered area within a few seconds. If a monolithic glass were used for roof panels or walk-on glazing, local peaks of stress would mean the brittle failure of the entire panel falling abruptly into the utility zone. Therefore, it is safer to bond the individual glass plies by polymeric interlayers to prevent this unfavourable effect. Useful properties of these materials are high strength to weight ratios, toughness, corrosion resistance, lack of conductivity, transparency, and colour. Many of these material properties are due to long chain molecular structure containing mostly atoms of carbon, hydrogen, oxygen, and nitrogen. Polymeric interlayers are at room temperature and atmospheric pressure in a solid state but they are usually processed in a liquid state at increased temperature and pressure. Long chain molecular structure of interlayers arises due to the manufacturing polymerization process in which the basic molecule (mer unit) is chained and forms a macromolecule (polymer) where mer unit repeats. Example of spatial structure of polyethylene macromolecule after polymerization process is shown in Fig. 16. The following subsections will further refer to general properties of polymers to understand the response of polymeric interlayers to the applied load.

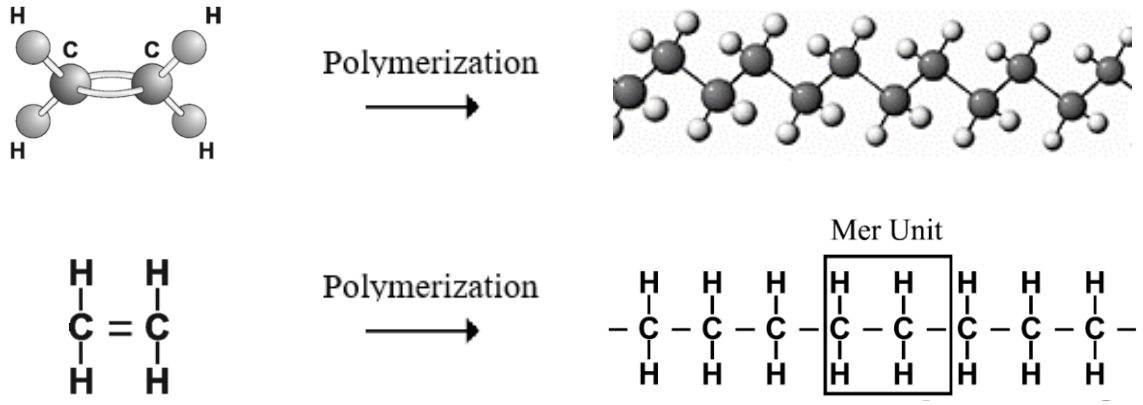

a) Ethylene molecule b) Macromolecule of polyethylene

Fig. 16: Formation of polyethylene macromolecule after polymerization in manufacturing process [22]

2.4.1. Classification of polymers and their response to the applied load

Chemical structure of polymers governs their response to the applied load [23]. This fact is especially attributed to atomic and molecular bonding in a material. There are, in general, two types of bonds: (i) primary or chemical bonds and (ii) secondary bonds [22]. Primary bonds in polymers are covalent when two atoms share electrons from their valence shells; and ionic bonds in which one atom donates an electron to another atom, e.g., $Na^{+}Cl^{-}$. Covalent bonds are present, e.g., in the polyethylene macromolecule, see Fig. 16. Secondary bonds are of great importance in polymers

and have significant impact on their molecular and bulk properties. These bonds are weaker than covalent bonds and are based on intermolecular electrostatic interactions. The level of these interactions is of various values and governs their designation, e.g., hydrogen, dipole, or van der Waals forces. To illustrate the level of above-mentioned atomic bonding, the dissociation energy values necessary to break the bonding and move the atoms and molecules far away from each other as well as interatomic distances are given in Tab. 3. One can see that the value of dissociation energy for secondary bonds is many times lower than that of primary bonds which will further assist in understanding the general classification of polymers.

Tab. 3: Comparison of primary and secondary bond distances and disassociation energies [22]

Bond type	**Interatomic distance [nm]**	**Dissociation energy [kcal/mole]**
Covalent (primary)	0.1-0.2	50-200
Ionic (primary)	0.2-0.3	10-20
Hydrogen (secondary)	0.2-0.3	3-7
Dipole (secondary)	0.2-0.3	1.5-3
van der Waals (secondary)	0.3-0.5	0.5-2

It has been said that polymers are typical for their long chain molecular structure. Bonding structure between the individual chains is the major aspect of their time and temperature response to the applied load [22]. From this point of view, polymers are classified as thermoplastics, thermosets, and thermoplastic elastomers. These groups can be further subdivided into smaller subgroups. General classification of polymers is shown in Fig. 17.

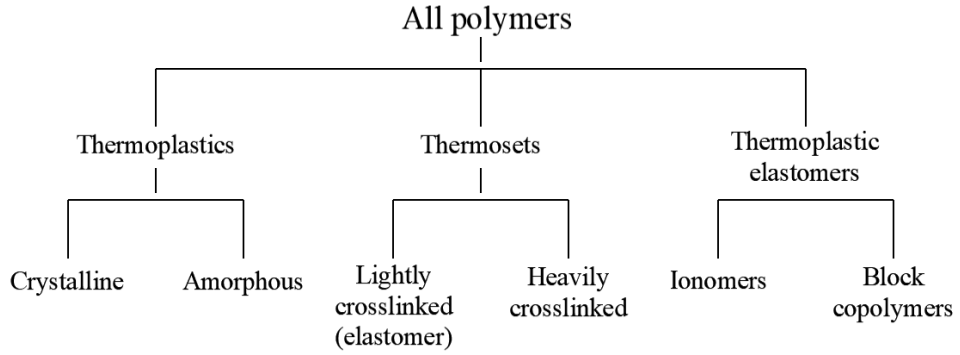

Fig. 17: Classification of polymers with respect to the intermolecular bonding [22]

Thermoplastics are typical for covalent intrachain bonds (bonds inside individual chains) and secondary interchain bonds (bonds between individual chains) and are denoted as “uncross-linked” polymers. Arrangement of long polymeric chains in thermoplastics governs their subdivision into crystalline and amorphous. In crystalline thermoplastics long polymeric chains are folded in regular formations. Amorphous thermoplastics are distinguished by nonregular, random structure of chains. The mixture of amorphous and crystalline regions is usual in many semicrystalline

thermoplastics, see the molecular structure of polyethylene (PE) in Fig. 18. The relative % amount of crystallinity has the effect on their physical properties [22]. For example, ultimate tensile strength and thermo-mechanical properties are improved with increasing % degree of crystallinity. Macromolecular structure enables softening and melting of thermoplastics when heated and return to the original configuration after subsequent cooling [22]. Therefore, these materials can be recycled. Example of thermoplastics are polyvinyl butyral (PVB) as a common material of polymeric interlayers [1], polyvinyl chloride (PVC), polycarbonate (PC), polyethylene (PE), etc.

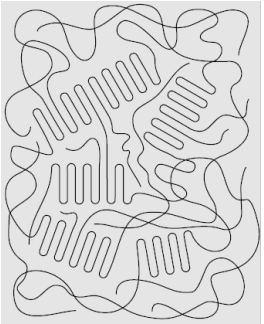

Fig. 18: Folded chains in crystalline regions tied together by amorphous regions in polyethylene [22]

Thermosets are characterized with covalent intrachain bonds, and both covalent and secondary interchain bonds. Right the presence of covalent interchain bonds, denoted as "chemical cross-link", differs thermosets from thermoplastics regarding time and temperature stiffness characteristics. These bonds arise in thermosets during their production process and processing (curing of thermosets in high temperatures even above 200 °C) usually by adding a cross-link initiator (often peroxide). The result is 3D cross-linked structure of thermosets. The exact procedure of production and processing of thermosets governs the density of cross-linking and their subsequent subdivision into elastomers (with lightly cross-linked structure) and network thermosets (heavily cross-linked), see Fig. 19. Covalent cross-linking in thermosets prevents the mutual displacement of the individual polymeric chains. It is subsequently not possible to melt thermosets after their curing since they chemically decompose before the melting point is achieved. Examples of thermosets are epoxy resin, acrylates, vulcanized rubber, etc. [10].

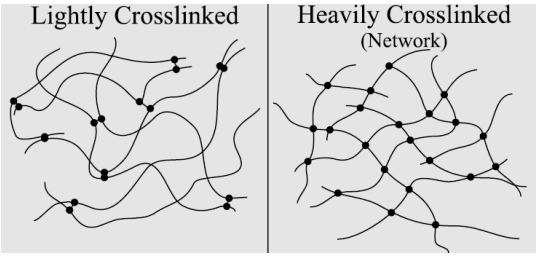

Fig. 19: Schematic cross-linked structure of thermosets [22]

Thermoplastic elastomers are typical for covalent intrachain bonds and "reversible interchain cross-link" which prevents the mutual displacement of polymeric chains under loading. Apart from thermosets, where covalent interchain cross-link is finally decomposed and lost when heated, reversible cross-link is reformed and active when the material is cooled back again [24]. Reversible cross-link exists in the form of noncovalent ionic bonding or block copolymer structure [24]. When reversible cross-link is active, thermoplastic elastomers are rather stiff (similar as thermosets). When the material is heated, reversible cross-links are broken, material softens and melts with subsequent cross-link formation when cooled back.

Ionic bonding, present in ionomers, is distinguished by polar ionic groups clustered together away from nonpolar polymer backbone chains [24]. These ionic groups lose their attractions for each other when heated and chains can move around freely, see Fig. 20. Example of this material is polyethylene-co-methacrylic acid ionomer.

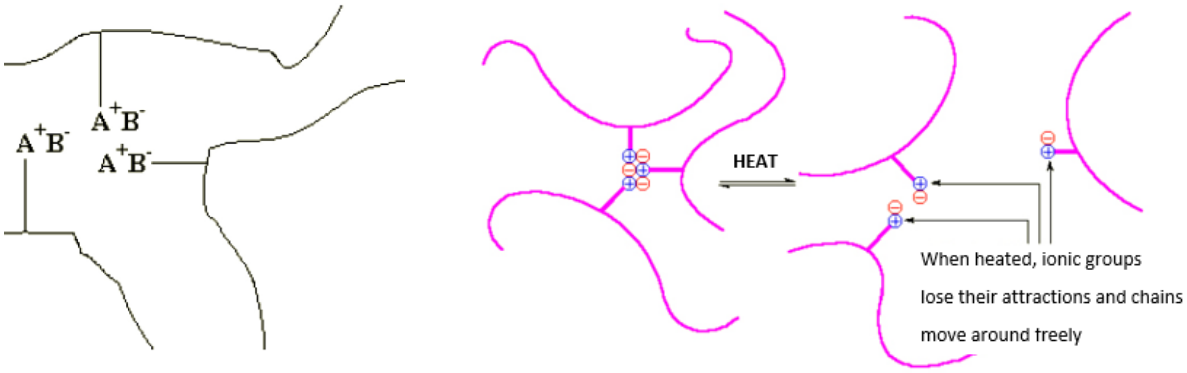

a) Polar ionic groups clustered from nonpolar chains

b) Reversible cross-link process when ionomer is heated or cooled

Fig. 20: Schematic chemical structure of ionomers [24]

Response of polymers to the applied load is characterized by three different types of deformation. All of them are associated with the change of molecular structure. These are:

a) elastic deformation as the consequence of angle changes of atomic chemical bonds (reversible deformation),
b) time dependent viscoelastic deformation as the consequence of polymeric chains extension (reversible deformation),
c) time dependent viscoplastic deformation as the consequence of mutual displacement of polymeric chains (non-reversible deformation).

Unlike for metals, response of polymeric materials under loading is strongly time dependent [23] as the consequence of molecular extensions and rearrangements. Total deformation of polymeric materials in time is the sum of the parts a) to c) mentioned above. Contribution of the individual parts into the total deformation depends on molecular structure of the certain polymer, especially on the type of interchain bonding [22]. Cross-linked polymers exhibit in time only

reversible deformations since the mutual displacement of polymeric chains is prevented. Uncross-linked polymers exhibit in time, in addition, also non-reversible deformations.

Important quantity governing the speed of molecular extensions and rearrangements in a polymer in time, is temperature. Increase of temperature accelerates these phenomena and vice versa [23]. More pronounced rearrangement in a chemical structure of polymer generally results in decrease of its stiffness.

2.4.2. Mechanical testing and time-temperature dependent mechanical properties of polymers

It has been stated that time and temperature are of major importance in task of polymers response to the applied load, and, that type of response is dependent on their intermolecular bonding. Mechanical properties of polymeric interlayers which are enormously important for use in load bearing LG applications, are shear stiffness and shear compliance, respectively. To find these quantities experimentally, (i) static creep or relaxation experiments in various temperatures and load durations [25] or (ii) dynamic mechanical thermal analysis (DMTA) [26] in various temperatures and frequencies can be performed. Mechanical tests are made on small samples of raw polymeric interlayers [27], on small scale specimens [28], or on large specimens [29]. Commonly used polymeric interlayers for LG applications are generally isotropic [30]. For these interlayers, the easiest method is an uniaxial tensile test in which the Young modulus is evaluated over time and the shear modulus is derived from it by means of expressions valid for isotropic linear elastic materials, as stated in European standard EN 16613 [30] aimed at determination of interlayer viscoelastic properties. In case of non-isotropic interlayers, direct shear or torsion tests are necessary. Illustrative examples of tensile test of a raw interlayer and shear tests of small-scale LG specimen are shown in Fig. 21.

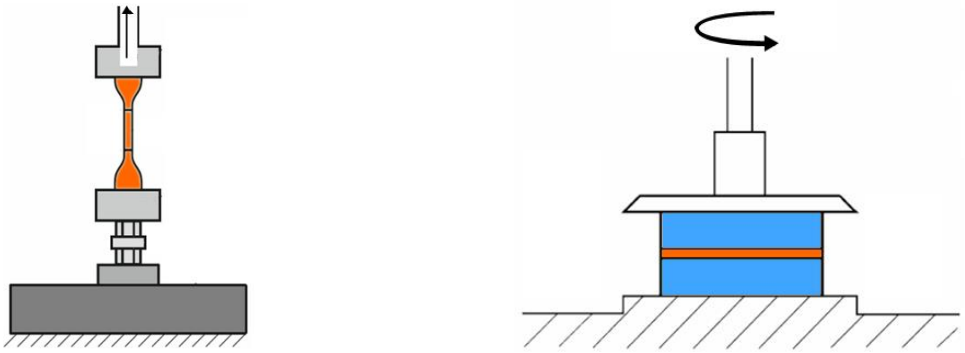

a) Tensile tests of a raw interlayer in hydraulic machine [27]

b) Torsion test on double LG small-scale specimen in rheometer [26]

Fig. 21: Examples of experimental testing of polymeric materials

The following text in this section holds for uniaxial tension/compression, shear, or even bulk compression as polymeric materials react to the applied load over time in the same fashion, regardless of the loading mode applied [23]. Only the notation changes depending on the loading mode considered. Throughout the entire thesis, stress, strain, and stiffness of a material (or its mechanical model) depending on the loading mode will be denoted as: $\{\sigma, \varepsilon, E\}$ for tension/compression; and $\{\tau, \gamma, G\}$ for shear. When polymeric material is subjected to constant stress σ_0 in time at constant temperature, its strain ε in time increases. This phenomenon is called creep. Part of the strain is instantaneous (elastic deformation ε_0), part is time delayed (viscoelastic or viscoplastic deformation). As said in the previous chapter, the ratio of these components in the total deformation depends on type of interchain bonding [23]. Crosslinked polymers attain, in a creep experiment, the equilibrium configuration ε_∞ when time $\rightarrow \infty$ and elastic plus viscoelastic strains occur in a material. Uncross-linked polymers attain, in addition, viscoplastic strains as the consequence of mutual displacement of polymeric chains. Therefore, the equilibrium configuration ε_∞ is not possible. Creep experiment for both types of polymers is shown in Fig. 22. Strain in time ε(t) induced by constant stress σ_0 can be expressed by Eq. (1). Compliance of a polymer in time J(t) is identical with measured strain in a creep test when $\sigma_0 = 1$.

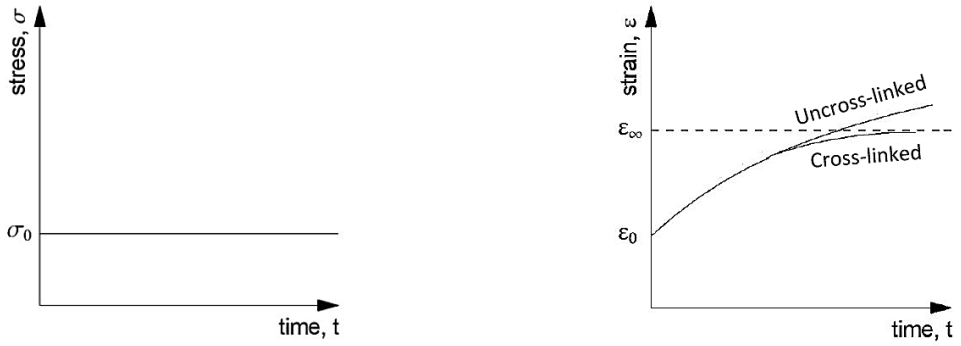

Fig. 22: Creep test of a polymeric material [23]

$$\sigma(t) = \sigma_0 \; ; \;\; \varepsilon(t) = \sigma_0 \cdot J(t) \tag{1}$$

When polymeric material is subjected to constant strain ε_0 in time at constant temperature, its stress σ in time decreases [23]. This phenomenon is called relaxation. Cross-linked polymers are typical for an equilibrium stress σ_∞ when time $\rightarrow \infty$, uncross-linked polymers do not attain any stress in long relaxation times. These phenomena are also related to the (non)presence of interchain bonding [23]. Secondary interchain bonds in uncross-linked polymers do not prevent the mutual movement of polymeric chains under long term load thus the stress completely disappears. Primary interchain bonds in cross-linked polymers serve as "added spring" and do not allow for complete rearrangement of chains in long relaxation times. Relaxation test for both types of polymers is shown in Fig. 23. Stress in time σ(t) induced in material by constant strain ε_0 is expressed by Eq. (2). Stiffness of polymer in time E(t) is identical with measured stress in relaxation test when $\varepsilon_0 = 1$.

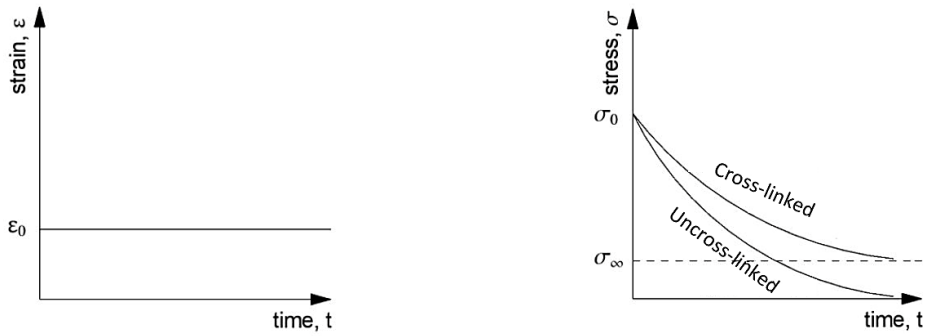

Fig. 23: Relaxation test of a polymeric material [23]

$$\varepsilon(t) = \varepsilon_0 \; ; \;\; \sigma(t) = \varepsilon_0 \cdot E(t) \tag{2}$$

Eqs. (1) and (2) of creep and relaxation tests of polymers assumed their compliance and stiffness being only time dependent. These polymers are called linear viscoelastic. Linearity of the constitutive response of a polymer requires the stiffness (compliance) response being independent of strain (stress) magnitude, i.e., $E(t) = \sigma(t)/\varepsilon_0$; $J(t) = \varepsilon(t)/\sigma_0$. Contrary, polymers whose stiffness (compliance) is, in addition, dependent on strain (stress) magnitude at relaxation (creep) tests, i.e., $E = f(t, \varepsilon_0)$; $J = f(t, \sigma_0)$, are non-linear viscoelastic [20]. To determine the linearity limits for polymers, their isochronous stress-strain curves from creep or relaxation tests at different times $t_1 \neq t_2$ can be plotted [31], see Fig. 24. For linear viscoelastic polymers, the isochronous response is linear, and the slope of isochronous curve decreases with time. As soon as linearity limits are exceeded, see the dashed line in Fig. 24, isochronous stress-strain curves begin to deviate from linearity. In literature, the limit of linear viscoelasticity for stiff polymers is given by shear strain of 1% [32]. For softer polymers, this limit can be much higher (to 50% or even more [22]). In intact LG panels, large deformation inducing non-linear viscoelastic behaviour of interlayers is not of importance and the theory of linear viscoelasticity can be applied [33]. Large deformation of polymeric interlayers occur in post-breakage phase of LG panel where interlayers show, in addition to time and temperature dependent behaviour, a non-linear relation between stress and strain that may be represented by some hyperelastic material model (e.g. Neo-Hooke, Mooney-Rivlin, etc.) [33]. It is then possible to consider a separable stiffness kernel as $E(t, \varepsilon) = E(t) \cdot f(\varepsilon)$ in which $E(t)$ is a time dependent part and $f(\varepsilon)$ is a strain dependent part [20]. Experiments also showed, that for a viscoelastic material the relaxation modulus and creep compliance are not generally reciprocals of each other, $E(t) \neq 1/J(t)$ [22], [23].

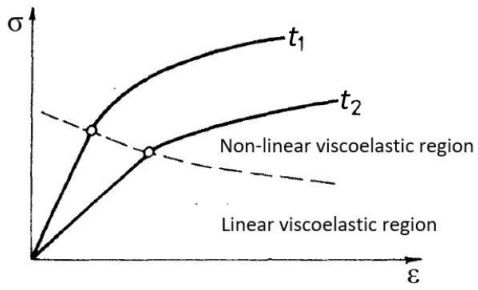

Fig. 24: Isochronous stress-strain curves with the border between (non)linear regions [31], time $t_2 > t_1$

Relaxation or creep effects in time may be accelerated or inhibited by the temperature of a polymeric material [22]. Increase of temperature accelerates the extension and rearrangement of polymeric chains and vice versa. It macroscopically results in changes of stiffness and compliance [23], [34]. There are generally three regions regarding temperature-stiffness dependence of polymers: (i) glassy region; (ii) rubbery region; and (iii) liquid flow region. In the glassy region, the behaviour of polymeric material is similar with an elastic material, short-term response to the applied load is very stiff, and viscoelasticity is inhibited. In the rubbery region, temperature accelerates extensions and rearrangements of polymeric chains, material softens, and acts as a flexible rubber. Flow region is characterized by continous slip of polymeric chains, material melts and its stiffness is very low [34].

Transition between the individual regions is characterized by "transition zones" with "glass transition temperature T_g" (between glassy and rubbery region), and "flow temperature T_f" (between rubbery and flow region). Temperature at which the polymer melts is called "melt temperature T_m". Transition zones usually cover wider temperature interval, they are characterized by pronounced change of stiffness and range of this interval depends on chemical composition of the certain polymer [19]. When the temperature of polymer is below the glass transition zone, it is assumed to be in "energy-elastic area". Temperature above glass transition zone and below flow region or degradation area means the polymer is in "entropy-elastic area" [9].

Regions of temperature-stiffness dependence of polymers characterized by short-term shear relaxation modulus, are shown in Fig. 25. Type of interchain bonding governs the temperature-stiffness dependence of the certain polymer [34]. Uncross-linked thermoplastics may exist in all three regions (i) to (iii), see Fig. 25, and go through both glass transition T_g and flow temperature T_f when heated. The lack of primary interchain bonds causes their melting when T_m is achieved and complete loss of stiffness. Interchain cross-links in thermosets do not allow the material to get to liquid flow region. At high temperatures, thermosets begin to physically degrade by compromising some of the cross-links that begin to break or reattach. This results in darkening and subsequent decomposition of a thermoset. It has been stated that covalent cross-link of thermosets is finally lost after decomposition and subsequent recycling is not possible. Highly cross-linked polymers (network thermosets) do not, in general theory, have any T_g and T_f [34], and they act as glass-like solids until they decompose. Contrary, lightly crosslinked polymers

(elastomers) attain considerable loss of stiffness in the glass transition region with defined T_g, get to the rubbery state, and may exist in both energy elastic and entropy elastic areas. Reversible cross-link present in thermoplastic elastomers enables, apart from thermosets, the material to melt and being further processed and recycled [24].

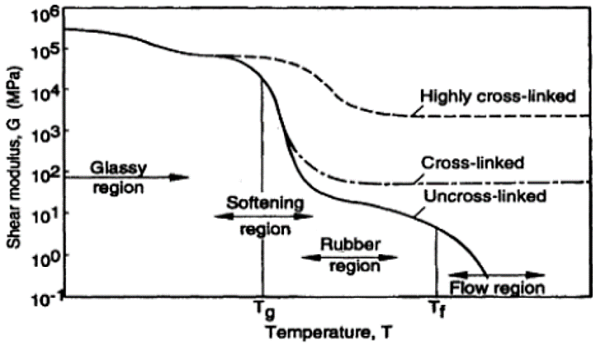

Fig. 25: General short-term shear stiffness-temperature relations of polymers [34]

More detailed shear modulus-temperature relations for the individual types of polymers are shown in Fig. 26. Amorphous thermoplastics attain significant decrease of stiffness in glass transition zone, rubbery plateau in entropy elastic area, and subsequent viscous flow and melt. Mixture of amorphous and crystalline regions in semicrystalline thermoplastics causes light decrease of stiffness in glass transition zone and sharp decrease of stiffness when "crystal melting temperature T_{cm}" is exceeded. They then quickly get to a low viscosity liquid and melt, see Fig. 26a). Elastomers as lightly cross-linked polymers with defined T_g attain a decrease of stiffness in glass transition zone and a pronounced stiffness plateau in the entropy elastic area with slight increase of stiffness at rising temperature before degradation at T_d, see Fig. 26b). Thermoplastic elastomers behave in a similar fashion as elastomers but their stiffness in the entropy elastic area continuously decreases and they subsequently melt at T_m.

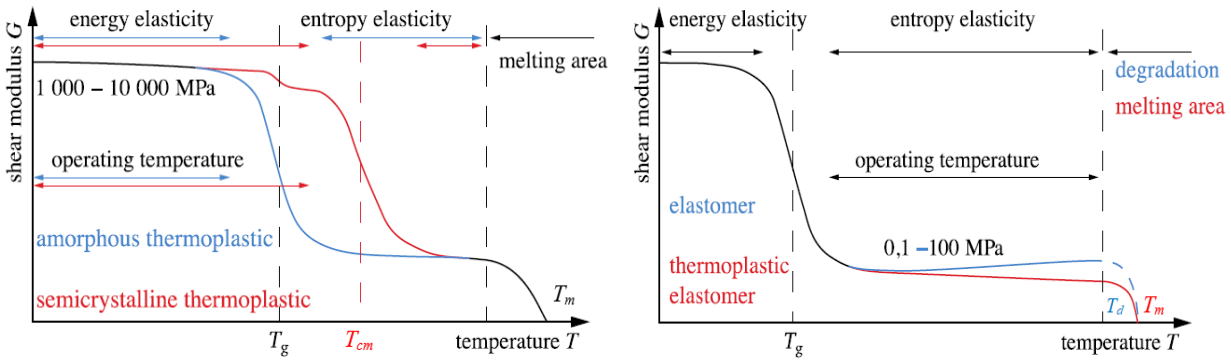

a) Uncross-linked polymers

b) Cross-linked polymers

Fig. 26: Shear stiffness-temperature relations of polymers regarding their intermolecular bonding [9]

Fig. 23 showed general dependence of polymers stiffness on time from relaxation tests while Fig. 25 illustrated this dependence on temperature. Leaderman in his studies [35] discusses time and temperature dependence of polymers. Results of creep tests of rubber at different temperatures by Kohlrausch [36] led him to notice the relation between time and temperature effects, i.e. creep curves at different temperatures are identical in shape but displaced relative to each other along the logarithmic time scale. Following Schwarzl [37], there is a thermodynamical correlation between temperature and time as relaxation processes of polymers are based on thermally activated molecular extensions and rearrangements. These findings mean that the creep or relaxation tests of polymers can be conducted in short time scale at multiple temperatures. Long term response at the certain temperature is then obtained by shifting the measured data at multiple temperatures to get smooth "Master Curve" which expresses the stiffness or compliance of tested polymer at certain temperature in broad time scale. This allows to map the long-term behaviour of the polymer out of short-time data. This procedure is called "Time Temperature Superposition Principle (TTSP)" as the outgrowth of kinetic theory of polymers [37]. Shifting the experimental stiffness data in multiple temperatures solely along the time scale assumes all relaxation times of the polymer are affected by the temperature in the same way (thermorheological simplicity). This approach has been found to hold for a vast array of polymers [22]. Some semi-crystalline thermoplastics may even require, in addition to horizontal shifts of experimental data, also their vertical shifts or rotations (thermorheologically complex polymers) to get the smooth Master Curve [38]. While the kinetic theory of polymers and subsequent TTSP is generally valid above the glass transition temperature T_g [23], the exact bottom limit is not generally defined. A guiding rule of thumb is that TTSP may be used below T_g as soon as the data is shiftable to form a smooth Master Curve [22]. Horizontal shift of illustrative data from shear relaxation test in the log. scale is shown in Fig. 27. Relaxation data at reference temperature T_{ref} was shifted horizontally along the log. time scale for the value of "horizontal temperature shift coefficient" $\log_{10}(a_T)$. This means the relation between shear relaxation modulus at reference temperature $G(\mathrm{T_{ref}})$ and extrapolated temperature $G(\mathrm{T})$ is given by Eq. (3) [19]. Relation between time t related to relaxation modulus at temperature T and time t_{ref} related to relaxation modulus at reference temperature T_{ref} using the shift coefficient $a_T(\mathrm{T})$ is in Eq. (4).

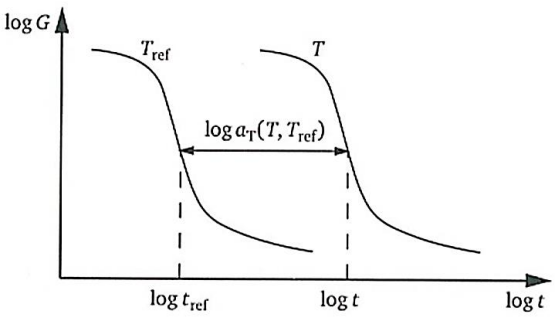

Fig. 27: Time-Temperature-Superposition Principle (TTSP) for thermorheologically simple polymers [19]

$$G(t,T) = G(t/a_T, T_{ref}) \tag{3}$$

$$\log_{10} a_T(T) = \log_{10} t - \log_{10} t_{ref} = \log_{10} \frac{t}{t_{ref}} \tag{4}$$

In literature, various functional forms for the dependency of horizontal temperature shift coefficient $\log_{10}(a_T)$ on the temperature T may be found. In the region of glass transition and entropy elastic area, Williams-Landel-Ferry (WLF) equation is mostly used [39], see the Eq. (5). In this equation, C_1 and C_2 are dimensionless constants which have to be determined by appropriate shifting techniques [38] to get a smooth Master Curve, and T_{ref} is chosen reference temperature. In the energy elastic area, the horizontal temperature shift coefficient may be determined using Arrhenius equation [38], see the Eq. (6), where R is the universal gas constant 8.3144621 [J/mol×K] and E_a [J/mol×K] is the activation energy of the polymer. Literature declares that adopting these two different models for the determination of horizontal temperature shift coefficient $\log_{10}(a_T)$ becomes necessary only if the tested temperature $T < T_g$ (then also Arrhenius equation should be considered), but the border temperature is not generally defined [22], [23]. The principle of TTSP using horizontal shifts of measured relaxation data in shear for the values of log a_T(T) and subsequent construction of Master Curve is schematically shown in Fig. 28a). Cartner et al. [40] constructed the Master Curve at 90 °C using TTSP for rubber toughened epoxy adhesive, see Fig. 28b), based on 10 min tensile relaxation tests from 70 °C to 120 °C which enabled him to get almost two years relaxation modulus at 90 °C. Time-temperature shifting generally enables to extend the range of measured data outside the range of experimental measurements but choosing reference temperatures T_{ref} out of testing temperatures may result in significant errors [22].

$$\log a_T(T) = \frac{-C_1 \cdot (T - T_{ref})}{C_2 + T - T_{ref}} \tag{5}$$

$$\log a_T(T) = -0.434 \cdot \frac{E_a}{R} \cdot \left(\frac{1}{T} - \frac{1}{T_{ref}}\right) \tag{6}$$

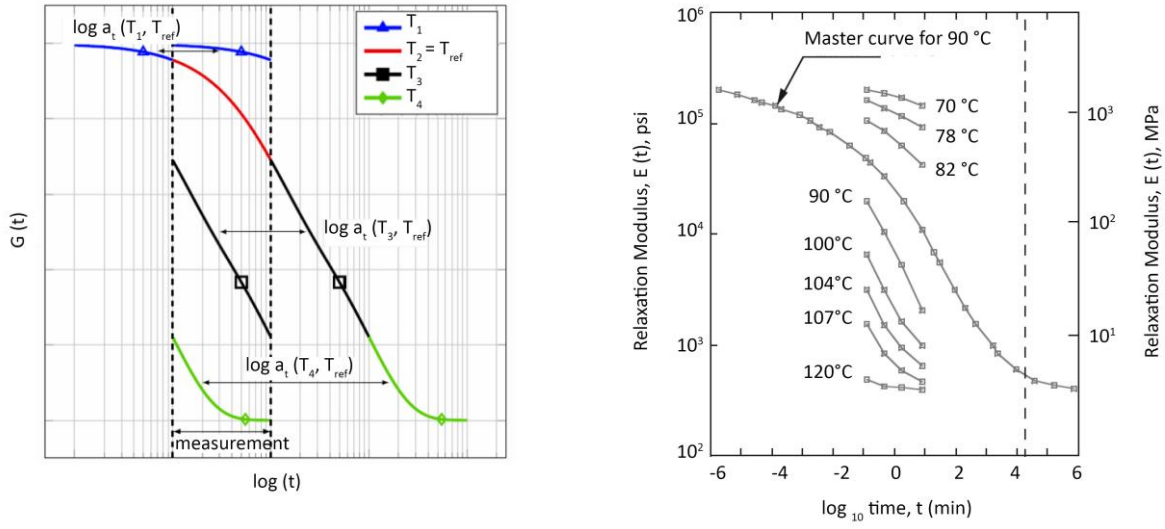

a) General TTSP technique from measured data [41], shear stiffness-time relations

b) Master Curve for rubber toughened epoxy adhesive [40], tensile stiffness-time relations

Fig. 28: Schematic construction of Master Curve out of short-time experimental relaxation data

2.4.3. Mechanical models of polymeric interlayers

It is practical to describe the experimental creep or relaxation data of polymers by discrete rheological mechanical models which can be further used in calculation of LG panels. Fig. 22 and Fig. 23 show that part of the response of polymer to the applied load is instantaneous and part time delayed. This means the combination of elastic springs and viscous dampers in mechanical models is appropriate, see Fig. 29. Elastic spring describes the instantaneous mechanical changes, viscous damper describes time dependent mechanical changes. Elastic spring is characterized by elastic modulus E [Pa], damper by viscosity η [Pa×s]. Even though all equations in this section 2.4.3 are formulated for uniaxial tension/compression, they also hold for shear loading mode. Instantaneous stress response σ of an elastic spring to applied strain ε is in Eq. (7). Stress response of a viscous damper is in Eq. (8) [23]. Time derivative of strain $\mathrm{d}\varepsilon/\mathrm{d}t$ in Eq. (8) causes time sensitivity of a damper. These elements can be appropriately combined to fit the experimental data.

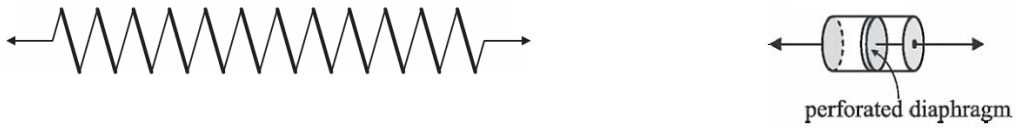

a) Elastic spring

b) Viscous damper

Fig. 29: Basic components of mechanical models for viscoelastic polymers [23]

$$\sigma = E \cdot \varepsilon \tag{7}$$

$$\sigma = \eta \cdot \frac{\mathrm{d}\varepsilon}{\mathrm{d}t} \tag{8}$$

To describe the response of a polymeric interlayer in a creep experiment, Kelvin-Voigt model may be used [42], see Fig. 30a). The ratio η/E is denoted as retardation time θ [s]. The differential equation of Kelvin-Voigt model relating stress σ and strain ε [23] becomes

$$\sigma = E \cdot \varepsilon + \eta \cdot \frac{\mathrm{d}\varepsilon}{\mathrm{d}t} \tag{9}$$

and compliance function J(t) of Kelvin-Voigt from the creep test when $\sigma_0 = 1$ then yields

$$J(t) = \frac{1}{E} \cdot [1 - \exp(-t/\theta)] \tag{10}$$

One Kelvin-Voigt model is not mostly sufficient to describe creep data accurately thus series of Kelvin-Voigt models, with added elastic spring E_0, are used to form Generalized Kelvin-Voigt model (GK-V) [22], see Fig. 30b). For cross-linked polymeric interlayers, all elastic moduli, in this model, are non-zero to attain an equilibrium configuration ε_∞ over long creep times. On the other hand, for uncross-linked interlayers, one spring in Kelvin-Voigt models in series is of zero stiffness so the entire model attains viscous flow in long creep times (Generalized Kelvin-Voigt model with a free damper) [22]. Ideal creep test is shown in Fig. 22 and the strain function ε(t) of Generalized Kelvin-Voigt model, suitable for cross-linked interlayers, describing the creep test is in Eq. (11) [22], where E_i is the stiffness of spring in i-th Kelvin-Voigt model, θ_i is the retardation time of i-th Kelvin-Voigt model, E_0 is the stiffness of added elastic spring, and σ_0 is the value of applied stress. Based on this, it is further possible to form the compliance of a cross-linked polymeric interlayer J(t) [1/Pa] in time, see Eq. (12). The effect of Kelvin-Voigt models addition in series on the correlation of generalized compliance function J(t) with experimental creep data of a viscoelastic material is shown in Fig. 31.

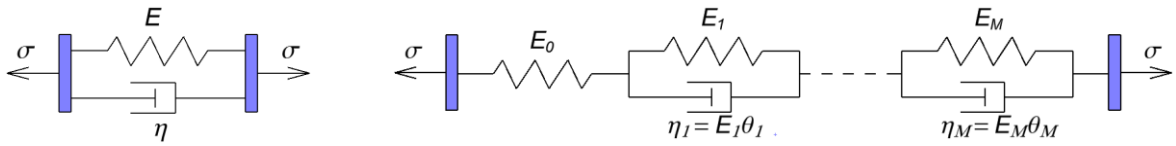

a) Kelvin-Voigt model b) Generalized Kelvin-Voigt (GK-V) model

Fig. 30: Kelvin-Voigt models with Prony series $\{E_0, E_i, \theta_i\}$ for the description of a creep test [22]

$$\sigma(t) = \sigma_0\,; \;\; \varepsilon(t) = \sigma_0 \cdot \tfrac{1}{E_0} + \sigma_0 \cdot \textstyle\sum_{i=1}^{M} \tfrac{1}{E_i} \cdot [1 - \exp(-t/\theta_i)] \tag{11}$$

$$J(t) = \frac{1}{E_0} + \sum_{i=1}^{M} \frac{1}{E_i} \cdot [1 - \exp(-t/\theta_i)] \tag{12}$$

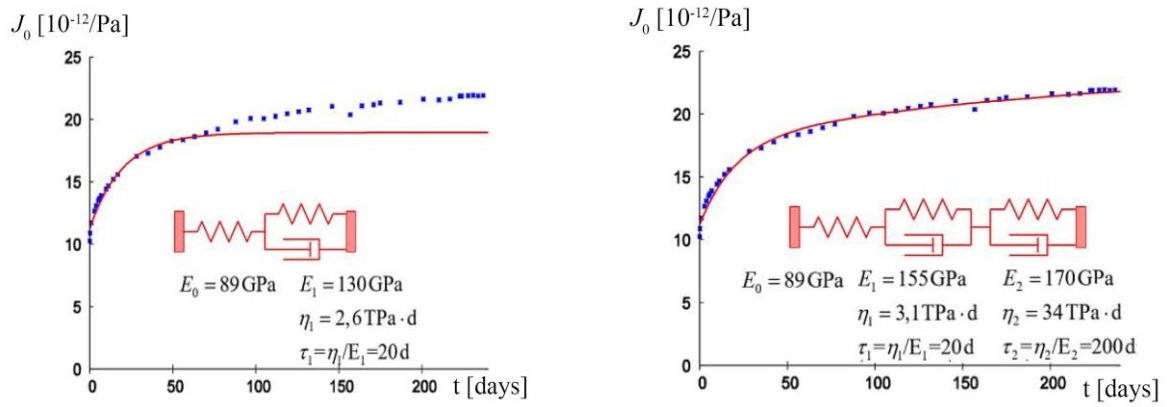

Fig. 31: Effect of GK-V model generalization on the correlation with experimental data of a viscoelastic material [43]

Relaxation function of a polymeric interlayer E(t) may be expressed by Maxwell model [42], see Fig. 32a). The ratio η/E is, in this model, denoted as relaxation time θ [s]. The differential equation of Maxwell model relating stress σ and strain ε [23] becomes

$$\sigma + \frac{\eta}{E} \cdot \frac{\mathrm{d}\sigma}{\mathrm{d}t} = \eta \cdot \frac{\mathrm{d}\varepsilon}{\mathrm{d}t} \tag{13}$$

and relaxation function E(t) of Maxwell model from the relaxation test when $\varepsilon_0 = 1$ then yields

$$E(t) = E \cdot \exp(-t/\theta). \tag{14}$$

Precise description of real relaxation data of the interlayer needs more Maxwell models in parallel with added elastic spring E_∞, see Fig. 32b). This model is called Generalized Maxwell model (GM model) or analogously Maxwell-Weichert model (M-W model) [22] and is suitable for cross-linked polymeric interlayers attaining the equilibrium stress σ_∞ in long relaxation times. Contrary, uncross-linked interlayers have zero equilibrium stress σ_∞ and can be described by Generalized Maxwell fluid model (GMF model) with no elastic spring E_∞ [22]. The illustration of an ideal relaxation test is shown in Fig. 23 and the stress function σ(t) of M-W model from the relaxation test is in Eq. (15) [22], where E_i is the stiffness of spring in i-th Maxwell model, E_∞ is the stiffness of added elastic spring, θ_i is the relaxation time of i-th Maxwell model, and ε_0 is the value of the applied strain. It is further possible to express the stiffness also called as relaxation function of cross-linked polymeric interlayer E(t) [Pa] in time, see Eq. (16). The value of E_∞ for uncross-linked interlayers should be zero. It cannot be generally said which model is more appropriate since it is possible to obtain analogous results using two or more different mechanical models. For example, to the Maxwell model it is possible to construct an analogous Kelvin model and vice versa [44]. However, most of commercial finite element software for calculations of LG is based on approximation of displacement field with implemented inputs of M-W Prony series $\{E_\infty, E_i, \text{and } \theta_i\}$, fitted to a certain polymeric interlayer which gives a preference to relaxation tests of interlayers [45].

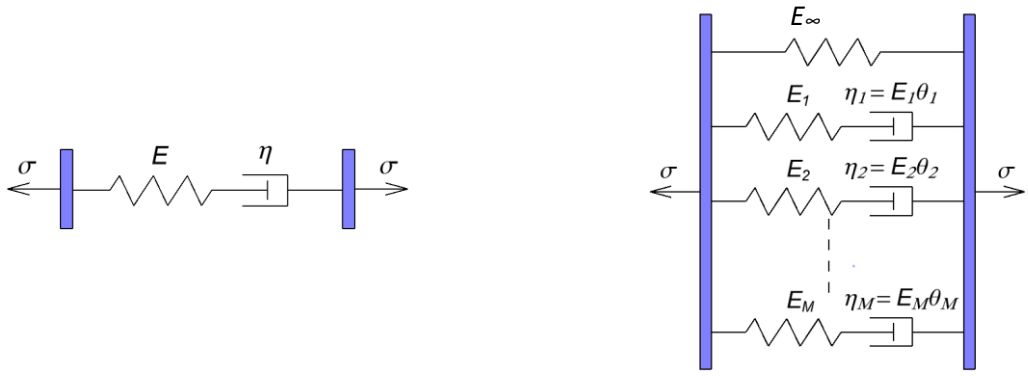

a) Maxwell model b) Maxwell-Weichert (M-W) model

Fig. 32: Maxwell model for the description of a relaxation test with Prony series $\{E_\infty, E_i, \theta_i\}$ [22]

$$\varepsilon(t) = \varepsilon_0 \; ; \;\; \sigma(t) = \varepsilon_0 \cdot [E_\infty + \textstyle\sum_{i=1}^{M} E_i \cdot \exp(-t/\theta_i)] \tag{15}$$

$$E(t) = E_\infty + \sum_{i=1}^{M} E_i \cdot \exp(-t/\theta_i) \tag{16}$$

Compliance function J(t) of Generalized Kelvin-Voigt model or relaxation function E(t) of Maxwell-Weichert model can be fitted to experimental creep or relaxation tests regardless of the loading mode applied since most interlayers for LG applications are isotropic [27], [30] with well-known relation

$$G = \frac{E}{2(1+\upsilon)} \; , \tag{17}$$

where G is an elastic shear modulus, E is Young modulus, and v is Poisson ratio of an interlayer. Since polymeric interlayers are assumed as nearly incompressible (v = 0.49; [30]), the approximate equality E(t) ≈ 3G(t) between Young relaxation modulus E(t) and shear relaxation modulus G(t) is justified, and results from uniaxial tensile and shear relaxation tests are interconvertible [23]. Polymeric interlayers are, in fact, a continuum, therefore their discrete rheological models are always an approximation. By choosing the infinite number of Maxwell models in parallel, it is possible to evaluate the relaxation function of a polymer precisely as

$$\begin{aligned} E(t) = \lim_{M\to\infty} \sum_{i=1}^{M} E_i \cdot \exp\left(-\frac{t}{\theta_i}\right) = \lim_{M\to\infty;\, \Delta\theta_i\to 0} \sum_{i=1}^{M} \frac{E_i}{\Delta\theta_i} \cdot \exp\left(-\frac{t}{\theta_i}\right) \cdot \Delta\theta_i = \\ = \int_0^\infty H(\theta) \cdot \exp\left(-\frac{t}{\theta}\right) \mathrm{d}\theta, \end{aligned} \tag{18}$$

where H(θ) is a continuous "relaxation spectrum" of the polymer [Pa/s], which is, for some polymers, available in literature [23].

Viscoelastic nature of polymeric interlayers means the material has "memory" and contemporary state of the interlayer may be affected by previous loading cases. Once the interlayer has been described by some rheological model with the certain differential equation (see, e.g., Eqs. (9) and (13)), its solution gives the response of the material to arbitrary strain or stress history. When the stiffness E(t) or compliance J(t) of the interlayer in time is defined, hereditary integral method by Boltzmann [20] can be used. It means that, the effect of a compound cause is the sum of the effects of the individual causes. This phenomenon is displayed in Fig. 33 where stress input in a creep test is varied.

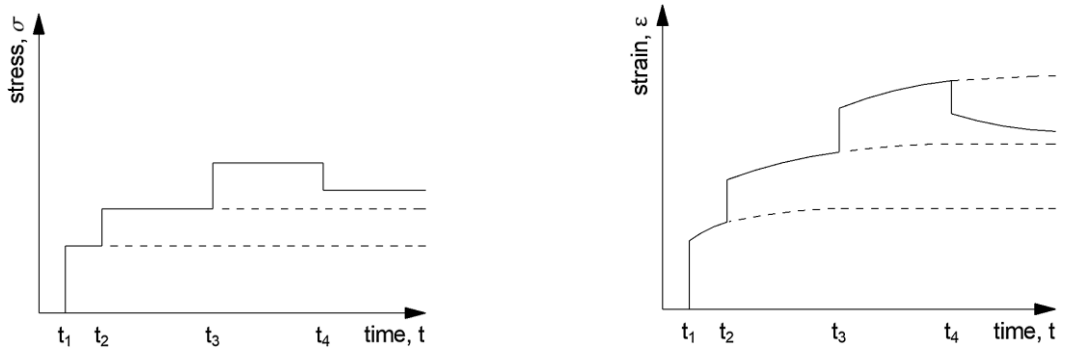

Fig. 33: Response of viscoelastic polymer to variable stress input in a creep test [20]

Formulas for strain (stress) output with variable stress (strain) input using Boltzmann superposition principle are shown in Eqs. (19) and (20) [20]

$$\varepsilon(t) = \int_0^t J(t - t') \cdot \frac{\mathrm{d}\sigma}{\mathrm{d}t'} \mathrm{d}t', \tag{19}$$

$$\sigma(t) = \int_0^t E(t - t') \cdot \frac{\mathrm{d}\varepsilon}{\mathrm{d}t'} \mathrm{d}t', \tag{20}$$

where t [s] is time in which the response of material is quantified, t' [s] is the exact time of the load increment in the interval $< 0; t >$, J(t) [1/Pa] is the compliance function of a material, and E(t) [Pa] is the relaxation function of a material. Since strain ε and stress σ induced at polymeric interlayers in intact LG panels are small, the interlayers are in viscoelastic regions and their compliance and stiffness are only time dependent [33]. This allows use their compliance or stiffness given by fitted Generalized Kelvin or Maxwell models as an input into Eqs. (19) and (20) to obtain strain ε(t) or stress σ(t) for variable load in time. For example, the response of M-W model subjected to constant strain rate dε/dt using Boltzmann superposition principle from Eq. (20) yields integral Eq. (21) with a solution given in Eq. (22).

$$\sigma(t) = \int_0^t E_\infty \cdot \frac{\mathrm{d}\varepsilon}{\mathrm{d}t'} + \sum_{i=1}^{M} E_i \cdot \exp\left[-(t - t')/\theta_i\right] \cdot \frac{\mathrm{d}\varepsilon}{\mathrm{d}t'} \mathrm{d}t' \tag{21}$$

$$\sigma(t) = \frac{\mathrm{d}\varepsilon}{\mathrm{d}t} \cdot E_\infty \cdot t + \frac{\mathrm{d}\varepsilon}{\mathrm{d}t} \cdot \sum_{i=1}^{M} E_i \cdot \theta_i \cdot [1 - \exp(-t/\theta_i)] \tag{22}$$

Widely used testing method of polymeric interlayers called Dynamic mechanical thermal analysis (DMTA) [26], [27] uses the sinusoidal strain input ε(t) applied on interlayer in various angular velocities ω [rad/s] and temperatures T [°C], see Eq. (23). Boltzmann superposition principle then yields Eq. (24)

$$\varepsilon(t) = \varepsilon_{max} \cdot \sin(\omega \cdot t), \tag{23}$$

$$\sigma(t) = \int_0^t E(t - t') \cdot \frac{\mathrm{d}\varepsilon}{\mathrm{d}t'} \mathrm{d}t' = \int_0^t E(t - t') \cdot \omega \cdot \varepsilon_{max} \cdot \cos(\omega \cdot t')\, \mathrm{d}t', \tag{24}$$

where ε_{max} [-] is the amplitude of applied dynamic strain and σ(t) [Pa] is the stress output. Evaluation of Eq. (24) yields Eq. (25) expressing the stress response of the viscoelastic material through the dynamic complex modulus E^* [Pa] with a real part (storage modulus E') and imaginary part (loss modulus E'') [23]. Graphical representation of these moduli is in Fig. 34 with a phase angle δ between stress and strain where tan $\delta = E''/E'$.

$$\sigma(t) = E^*(\omega) \cdot \varepsilon(t) = \varepsilon_{max} \cdot [E'(\omega) \cdot \sin(\omega \cdot t) + E''(\omega) \cdot \cos(\omega \cdot t)] \tag{25}$$

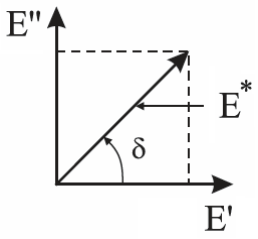

Fig. 34: Storage and loss moduli as components of the complex modulus, $E^* = E' + iE''$ [23]

Storage and loss moduli for M-W model loaded by sinusoidal strain input can be expressed using Eqs. (26) and (27) [23], where M is the number of Maxwell models in parallel. These moduli are important when Prony series $\{E_\infty, E_i, \text{ and } \theta_i\}$ of M-W model are to be fitted to experimental DMTA data which are given in the form of $E'(\omega)$ and $E''(\omega)$ moduli [26], [27].

$$E'(\omega) = E_\infty + \sum_{i=1}^{M} \frac{E_i \cdot \omega^2 \cdot \theta_i^2}{1 + \omega^2 \cdot \theta_i^2} \tag{26}$$

$$E''(\omega) = \sum_{i=1}^{M} \frac{E_i \cdot \omega \cdot \theta_i}{1 + \omega^2 \cdot \theta_i^2} \tag{27}$$

To introduce the effect of temperature into discrete M-W models of polymeric interlayers, all fitted relaxation times for reference temperature $\theta_i(T_{ref})$ can be multiplied by one common

temperature shift coefficient a_T(T), therefore relaxation times at extrapolated temperature θ_i(T) become [22]

$$\theta_i(T) = a_T(T) \cdot \theta_i(T_{ref}). \tag{28}$$

This formula presumes the material is thermorheologically simple which it has been found to hold for a vast array of polymers [22]. Following TTSP, it is then possible to write the relaxation function of fitted M-W model to DMTA results of tested polymer in both time and temperature domains by Eq. (29) which is schematically displayed in Fig. 35.

$$E(t,T) = E_\infty + \sum_{i=1}^{M} E_i \cdot \exp\left(-\frac{t}{a_T(T) \cdot \theta_i(T_{ref})}\right) \tag{29}$$

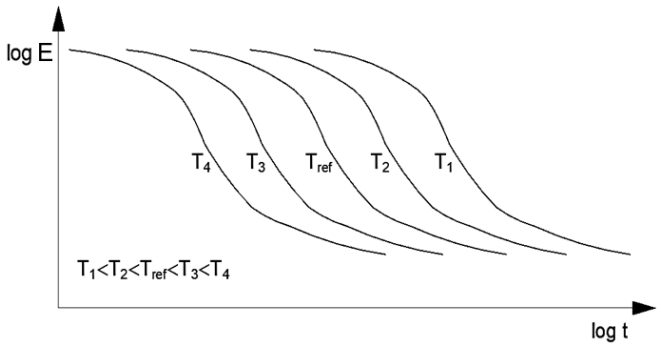

Fig. 35: Schematic relaxation function given by M-W model for thermorheologically simple polymers

2.4.4. Experimental mechanical data of polymeric interlayers from literature

This section refers to available experimental data from mechanical tests of interlayers. Due to a large spectrum of interlayers on the market, only representative samples are chosen.

Weller et. al [46] performed series of static small-scale single-lap shear tests, see Fig. 36, of polyvinyl butyral (PVB) and ethylene-vinyl acetate (EVA) interlayers in the temperature range -25 °C to 75 °C and strain rates 0.01, 0.1, and 1.0 [1/min]. PVB based interlayer exhibited significant softening between 10 °C and 25 °C when crossing the glass transition zone and viscous flow at 75 °C, see Fig. 37a). The effect of strain rate on the response of PVB at 25 °C is shown in Fig. 37b). Increase of strain rate from 0.01 [1/min] to 1.0 [1/min] meant increase of the initial shear modulus G_{init} from 0.4 MPa to 0.6 MPa. EVA based interlayer with the content of vinyl acetate 32% did not show any abrupt softening in the entire range of testing temperatures. The initial stiffness decreased gradually with increasing temperature, see Fig. 38a). This means the interlayer was not in the energy-elastic area since testing temperatures were above T_g of tested EVA ($T_{g,}$ = -43 °C [46]). The effect of strain rate on the initial shear modulus of EVA is shown in Fig. 38b) where G_{init} = 1.4 MPa at rate 0.01 [1/min] and G_{init} = 1.9 MPa at rate 1.0 [1/min].

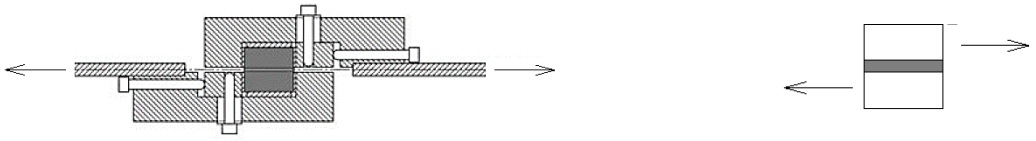

a) Test setup for shear test b) Single-lap testing specimen

Fig. 36: Test setup for single-lap shear test [46]

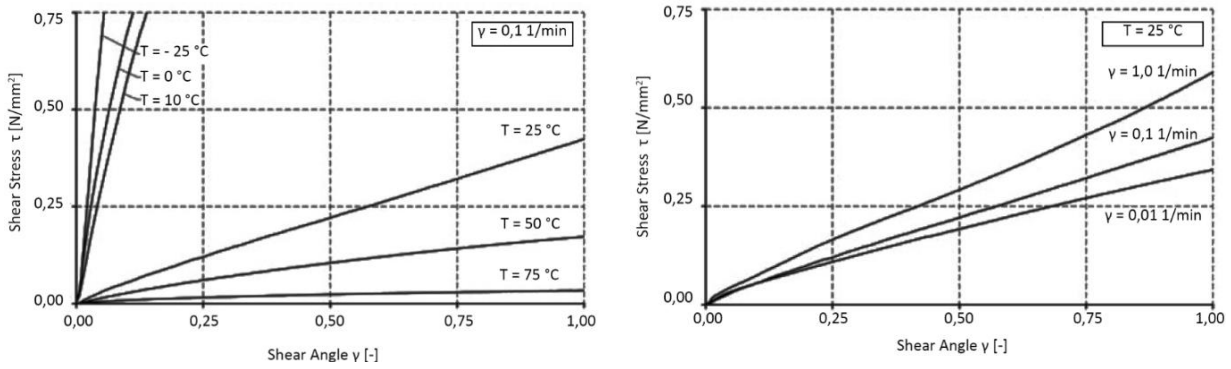

a) Effects of temperature at strain rate 0.1 [1/min] b) Effect of strain rate at +25 °C

Fig. 37: Engineering shear stress-strain relations of PVB [46]

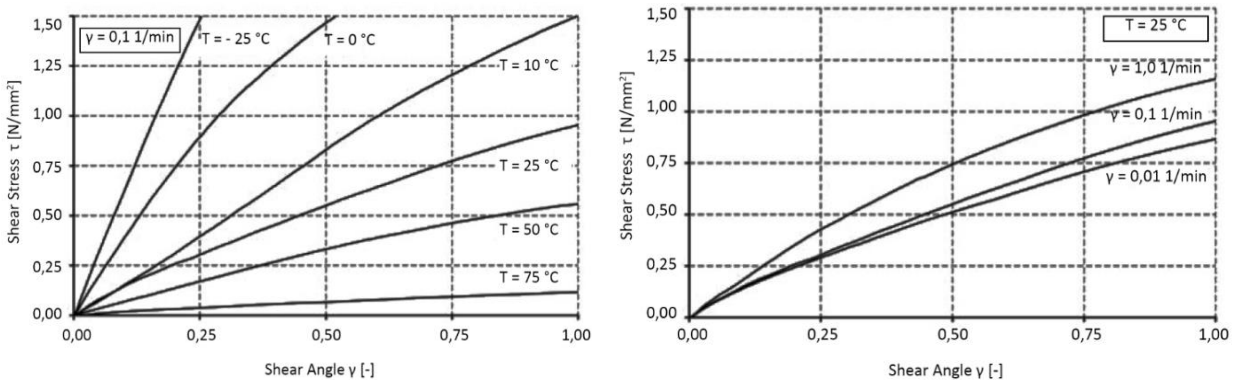

a) Effects of temperature at strain rate 0.1 [1/min] b) Effect of strain rate at +25 °C

Fig. 38: Engineering shear stress-strain relations of EVA [46]

Rühl et. al [47] performed static uniaxial tensile tests of a raw thermoplastic polyurethane (TPU) at room temperature and loading rates 8.3×10^{-5} m/s, 0.1 m/s, and 3.0 m/s using servo-hydraulic Zwick Roell HTM machine. Due to high elongation of TPU, Hencky´s strain vs. isochoric stress were evaluated. Strain was measured using Digital image correlation (DIC), see Fig. 39a). Results in Fig. 39b) show loading rate sensitive behaviour of TPU which is documented by the decrease of initial tensile stiffness modulus E_{init} varying between 100 MPa (at 3.0 m/s) and

20 MPa (at 8.3×10^{-5} m/s). TPU softens up to the value of Hencky´s strain 0.6. For higher strains, significant stiffening occurs at all loading rates.

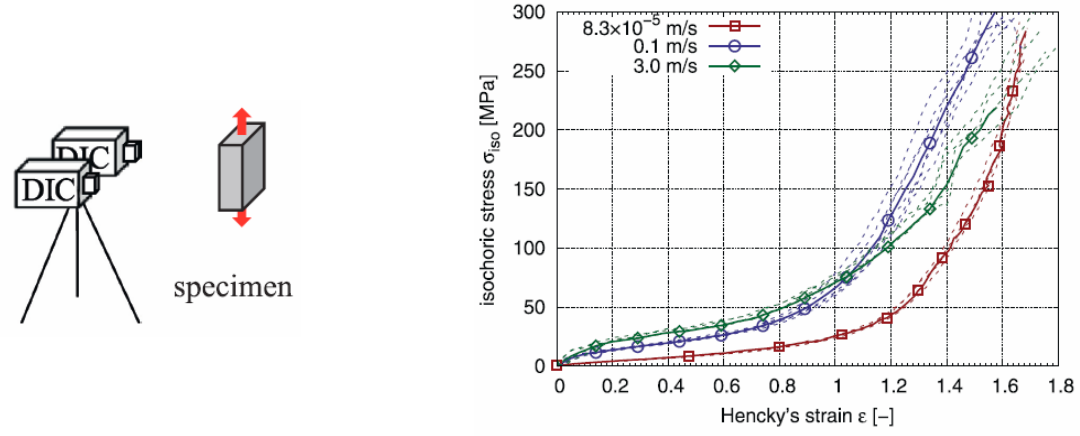

a) Experimental setup using DIC technology

b) Stress-strain relations: single experiments (dashed line), average curves (full line)

Fig. 39: Uniaxial tensile test of TPU [47]

Calleawaert et. al [48] conducted series of static long term three-point bending creep tests of large-scale double LG specimens laminated with ionomer interlayer SentryGlas® Plus. Two specimens of series B had dimensions of 1100 × 180 mm, and two specimens of series C had dimensions of 3000 × 360 mm. Nominal thickness of glass was 2 × 6 mm. To eliminate the effects of self-weight, the specimens were placed vertically, see Fig. 40. The specimens of series B (series C) were loaded at the midspan with force F = 150 N (F = 400 N) and midspan defection was measured by two LVDT´s, see results in Fig. 41. Analytical theory of Wölfel [49] then enabled to calculate the shear modulus G of Sentry Glas® Plus, see Fig. 42. Shear moduli decrease in time and are temperature sensitive. To illustrate, 10 s shear modulus G(t = 10 s) of SentryGlas® Plus at 60 °C is 10 MPa, and 12 days shear modulus G(t = 12 × 24 h) at 60 °C is 3.6 MPa. These 10 s and 12 days shear moduli at 65 °C are only 8.1 MPa and 2.1 MPa, respectively.

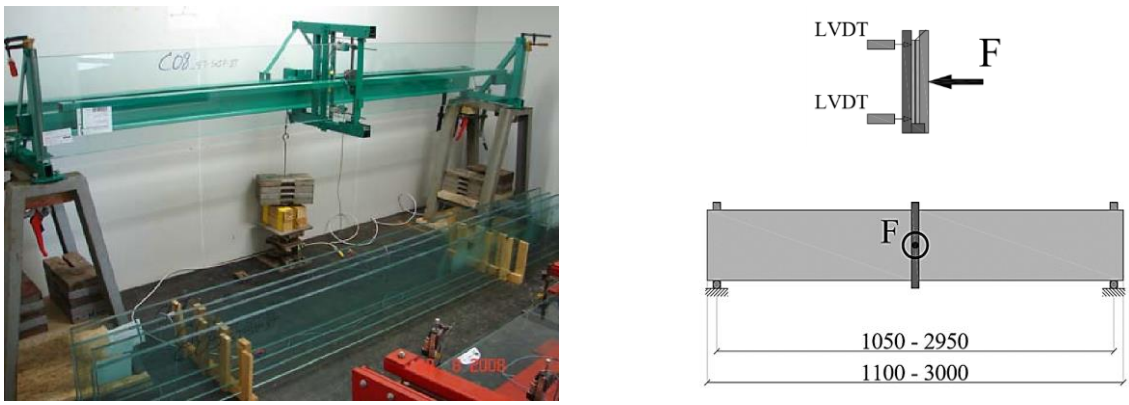

a) Real experiment of serie C specimens

b) Schematic bending test setup

Fig. 40: Test setup of three-point bending creep tests of double laminated glass specimens with ionomer interlayer [48]

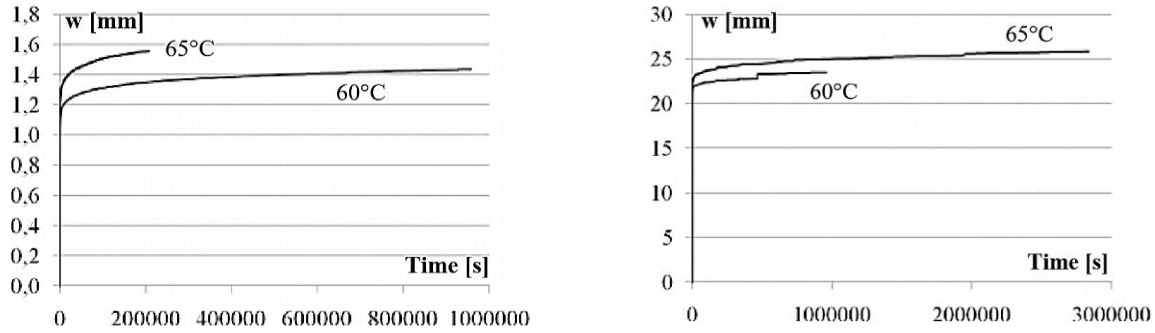

a) Specimens of series B

b) Specimens of series C

Fig. 41: Midspan deflection at three-point bending creep test measured by LVDT sensors [48]

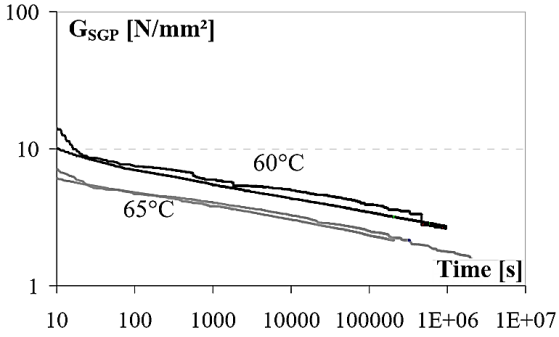

Fig. 42: Shear modulus of ionomer interlayer in time from three-point bending creep tests [48]

Andreozzi et. al [26] carried out strain controlled DMTA tests in rheometer using small-scale double LG specimens with PVB interlayer, see Fig. 43. Nominal thickness of glass was 2 × 8 mm. Specimens were tested in the range of temperatures < +30; +80 > °C and the range of frequencies < 10^{-4}; 10^{2} > Hz. Experimental shear storage G' and loss moduli G'' are plotted in Fig. 44.

By means of TTSP, the Master Curves of G' and G'' at reference temperature T_{ref} = 30 °C were constructed, see Fig. 45a). Assuming only horizontal shifts of experimental data, WLF constants at T_{ref} = 30 °C were determined as C_1 = 12.1 and C_2 = 82.0. By choosing an appropriate least squares optimization method to experimental Master Curve in Fig. 45a), Prony series of GMF model $\{G_i, \theta_i\}$ were fitted [26]. Using these series together with WLF constants C_1 and C_2 as inputs in Eq. (29), for shear, enabled to express PVB shear relaxation function G(t, T) in time and temperature domain, see Fig. 45b). Shear modulus decreases with increasing time and temperature. Assuming G_∞ = 0 MPa in GMF model means PVB behaves in long relaxation times as a typical uncross-linked polymer.

a) Schema of rheometer Anton Paar MCR 301 b) Specimen in a rheometer

Fig. 43: DMTA test setup of PVB in rheometer [26]

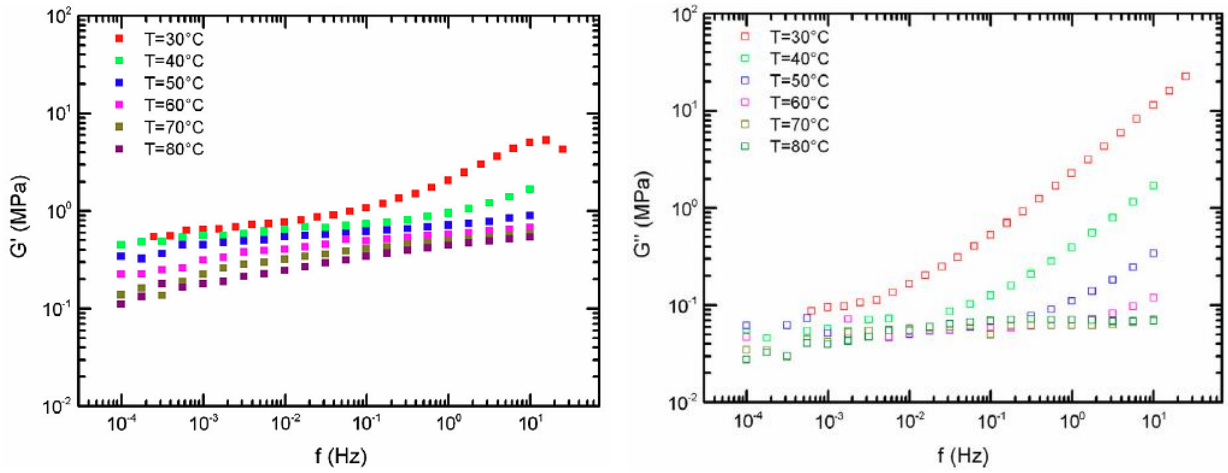

a) Shear Storage modulus G'(f) b) Shear Loss modulus G''(f)

Fig. 44: Raw DMTA data of PVB in rheometer [26]

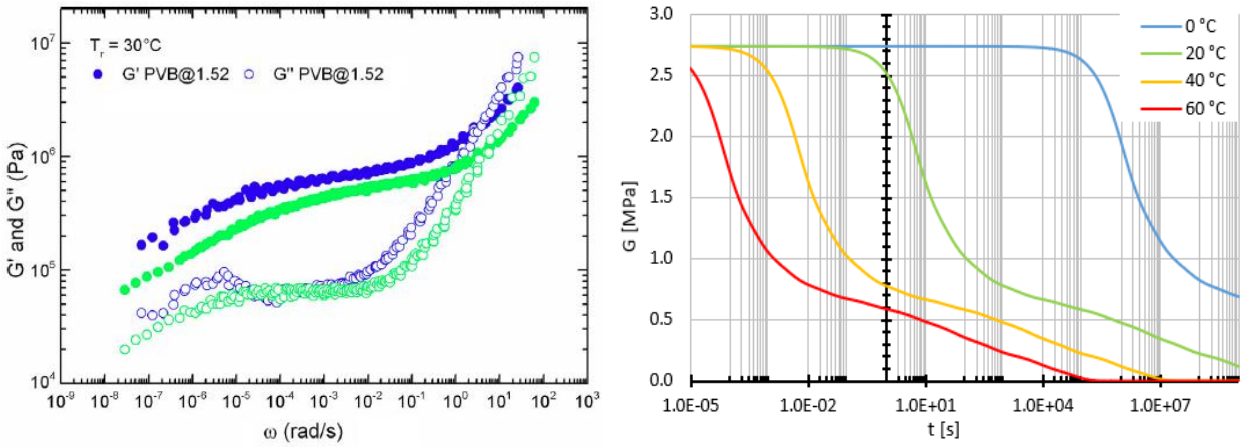

a) Master Curve at +30 °C b) Relaxation modulus at various temperatures

Fig. 45: DMTA results of PVB from shear tests in rheometer [26]

It is possible to find other DMTA results of common interlayers for LG applications in literature. Kuntsche et. al [19] provides complex dynamic shear modulus – temperature relations $G^*(T)$ of EVA, PVB, and ionomer interlayers from shear tests in the temperature range < +80; -60 > °C, Kraus et. al [33] performed series of DMTA in torsion of EVA strip and shows experimental shear storage G' and loss G'' moduli in the range of frequencies < 10^{-2}; 10^{1} > Hz including Master Curve at T_{ref} = -20 °C. Schuster et al. [38] performed series of DMTA in tension of EVA strip and illustrates the values of normal dynamic complex modulus E^* in the range of frequencies < 1; 50 > Hz as well as Master Curve at T_{ref} = -20 °C, etc.

2.5. Experimental data of laminated glass in bending from literature

When having the experimental data of a certain polymeric interlayer in hand, it is necessary to verify the performance of the entire glass panel laminated with this interlayer in out of plane loading. Under practical circumstances, glass structures need to be designed to resist bending stresses induced by out of plane loading. Four-point bending tests or uniform loading of LG panels are appropriate methods for the evaluation of their structural behaviour. These tests enable to monitor pre-breakage and post-breakage performance of LG panels, enable to compare their response to the applied load when laminated with various interlayers and enable to verify the mechanical properties of used interlayers. In scope of this, research is running.

Serafinavicius et. al [50] performed series of displacement controlled four-point bending tests of double LG panels (2 × 6 mm HTG) with dimensions of 360 × 1100 mm at room temperature according to EN 1288-3 [51] until failure. Panels were laminated with 1.52 mm thick PVB (trademark unspecified), 0.89 mm thick EVA (trademark unspecified), and 1.52 mm thick ionomer (SentryGlas® Plus) interlayers. Test setup is shown in Fig. 46. Midspan vertical displacement w and applied force F were measured. General force-displacement relationship is shown in Fig. 47a). When the peak of load F_{max} was reached (end of 1st loading phase), force F decreased abruptly, and

lower glass ply collapsed. In the 2nd loading phase, the upper ply was still active and allowed for further increase of force. As soon as residual load bearing capacity F_{res} was achieved, the entire panel collapsed (total failure).

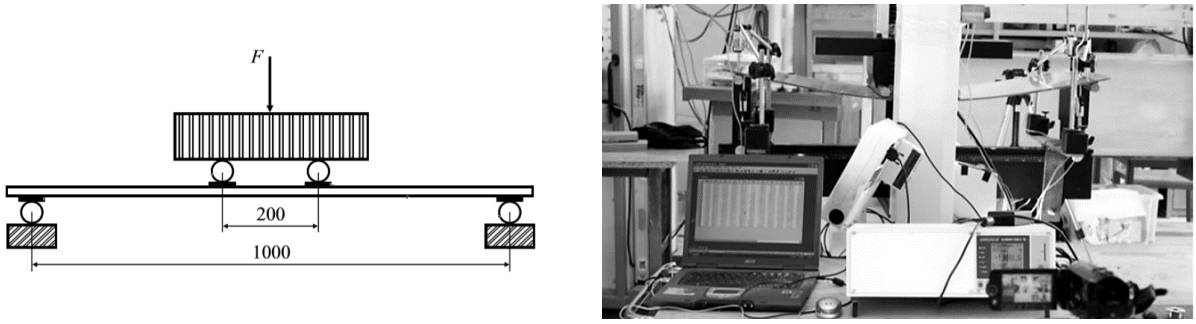

a) Static schema b) Real experiment

Fig. 46: Four-point bending tests of double LG panels with PVB, EVA, and ionomer interlayers [50], [51]

Experimental *F*-*w* relations of four-point bending tests by Serafinavicius et. al [50], plotted in Fig. 47b) to d), show the interlayers had limited time to relax and the relations were therefore almost linear. Material of used interlayer influenced the bending stiffness of LG panels, see various slopes of *F*-*w* relations, and their maximum load bearing capacity F_{max}.

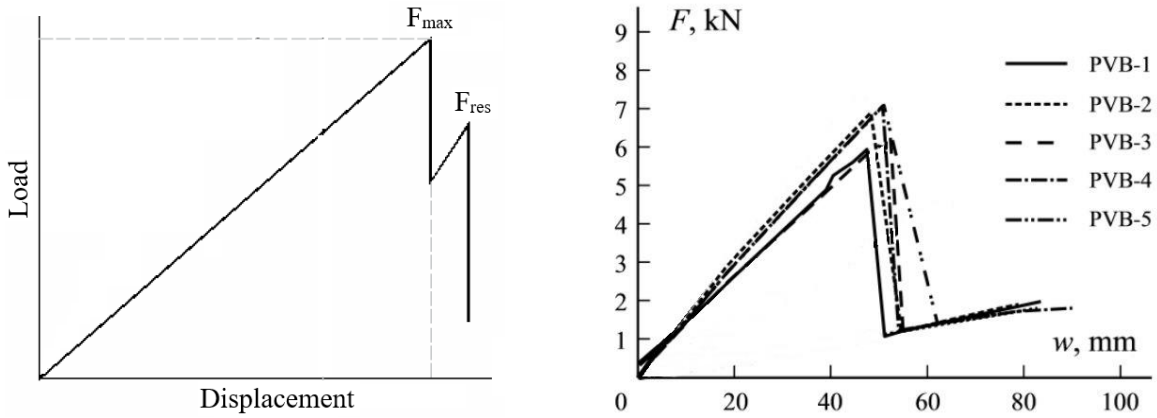

a) Schematic load-displacement schema b) Specimens with PVB

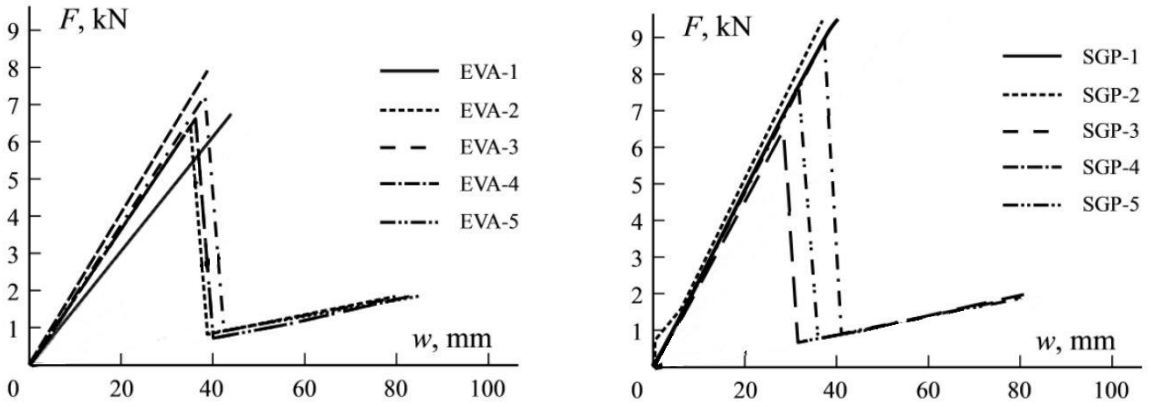

c) Specimens with EVA

d) Specimens with ionomer SentryGlas® Plus

Fig. 47: Experimental force-midspan vertical deflection relations of four-point bending tests of double LG panels laminated with various interlayers [50]

Sable et. al [11] performed series of four-point bending tests of double LG panels (2 × 5 mm FG) laminated with five 0.76 mm thick PVB and with nine 0.38 mm thick EVA interlayers at 25 °C until failure. The interlayers were of different trademarks. Static schema is shown in Fig. 48. Testing specimens had dimensions 500 × 100 mm. Tests were displacement controlled with the vertical cross-head loading rate 6 mm/min. Midspan vertical displacement w and applied force F were measured. These tests showed that the trademark of used PVB or EVA interlayer had the influence on the bending stiffness of the panel and on the maximum load bearing capacity F_{max}, see Fig. 49. LG Panel with PVB® DG 41 was found to be the stiffest from all PVB specimens whereas LG panel with EVA® Crystal was found to be the most compliant from all EVA specimens. Results from four-point bending tests of LG panels can be further modelled by numerical finite element (FE) analysis to verify material models of used interlayer [52].

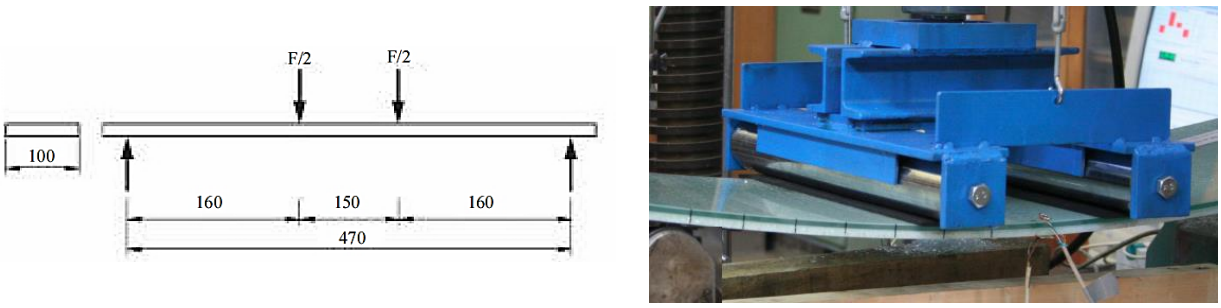

a) Static schema

b) Real experiment

Fig. 48: Four-point bending tests of double LG panels laminated with various PVB and EVA interlayers [11]

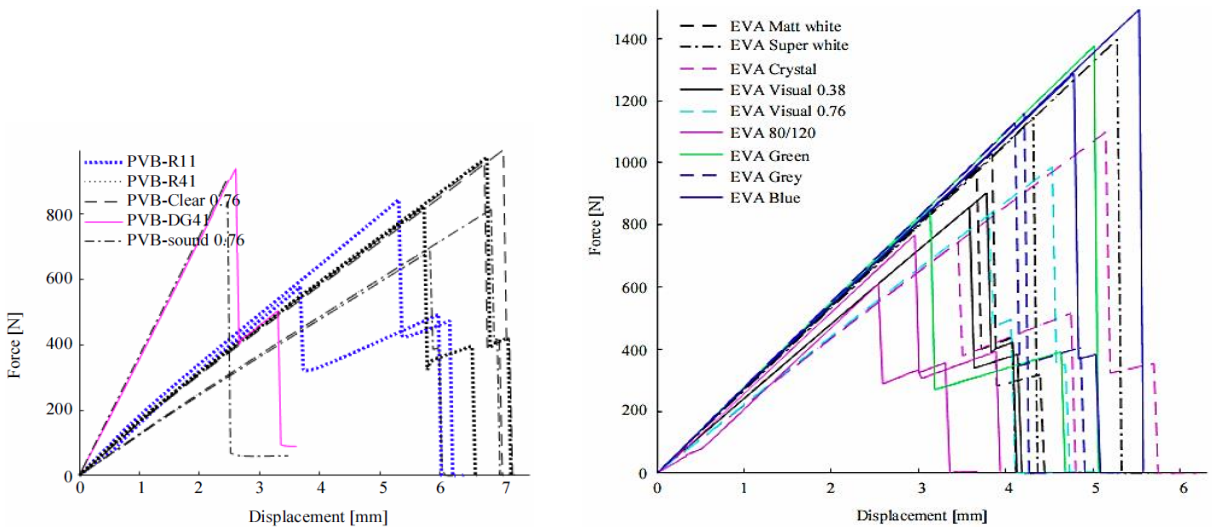

a) Various types of PVB interlayers

b) Various types of EVA interlayers

Fig. 49: Experimental force-midspan vertical deflection relations from four-point bending tests of double LG panels [11]

Serafinavicius et. al [53] performed series of four-point bending creep tests of double LG panels made of FG with dimensions 360 × 1100 mm and glass thickness 2 × 6 mm in the climatic chamber. Static and loading schema was made according to EN 1288-3 [51], see Fig. 46a). Panels were laminated with PVB (trademark unspecified), EVA (trademark unspecified), and ionomer (SentryGlas®Plus) interlayers. All interlayers were of the same thickness 1.52 mm, 3 specimens of each interlayer. Tests were performed at three temperatures: 20 °C, 30 °C, and 40 °C. Every test took 24 hours at constant temperature, one full experiment took 72 hours in total. Constant vertical force F applied on the panel, including self-weight, was 0.512 kN. Midspan vertical deflections and normal tensile stress on the lower surface of the specimen were monitored, see Fig. 50. Results show increase of measured quantities with increasing time and temperature as the consequence of decreasing shear modulus of interlayers, see illustration in Fig. 15. Time and temperature effects were significant in case of PVB with maximum increase of deflections (for 2 mm) and normal stress (for 4 MPa) after 72 h. Contrary, specimens with ionomer SGP were almost time and temperature insensitive with increase of deflections only for 0.5 mm and normal stress for 0.5 MPa after 72 h. It is also possible to find other experimental results of LG panels in literature. Representative example is given by Bennison et. al [54] and his loading tests of all sides supported double LG panels of rectangular shape laminated with PVB and SGP where the effect of applied load on maximal principal stress was studied.

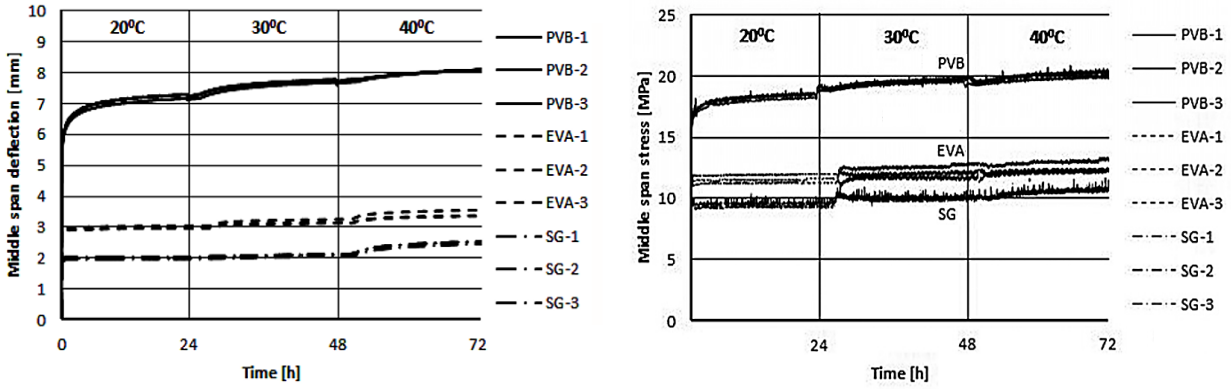

a) Midspan vertical deflections in time b) Midspan tensile stress on lower surface in time

Fig. 50: Experimental relations from four-point bending creep tests of double LG panels laminated with various interlayers [53]

2.6. Calculation methods of laminated glass in bending

An engineer in practice must deal with the design of load bearing LG structure loaded in certain boundary conditions. There are, in general, (i) analytical and (ii) numerical methods possible. Each method can be further assumed as elastic or viscoelastic regarding material properties of interlayer, see the general division in Fig. 51. In elastic solution, glass and interlayer are considered as linear elastic materials. Interlayer is characterized by one certain value of shear modulus G, glass by Young modulus E. Response of LG using an elastic solution is calculated to the current loading case. Contrary, viscoelastic solution includes the entire loading history of LG panel and is based on the Boltzmann superposition principle which requires complete knowledge of interlayer´s shear relaxation modulus in time (and temperature) domain G(t, T).

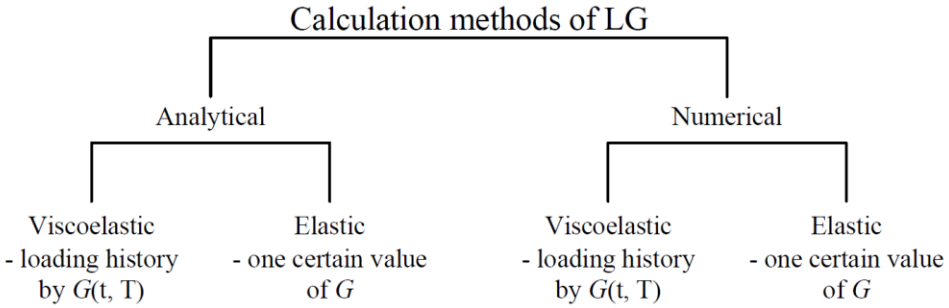

Fig. 51: General distribution of LG calculation methods in bending with respect to shear stiffness of interlayer G

2.6.1. Analytical methods

Analytical linear elastic (LE) methods are mostly preferred simple methods. It is possible to neglect the shear coupling by putting $G = 0$ for interlayer and to calculate the elastic response of the individual plies of LG panel to proportionally lowered load. This method has been incorporated into German standard DIN 18008 [5]. More sophisticated linear elastic methods assuming interlayer´s shear elastic modulus $G \neq 0$ are, e.g., Wölfel-Bennison method (W-B) or Enhanced Effective Thickness method (EET). Both are based on the so-called "Effective Thickness" which means the thickness of glass monolith with bending properties equivalent to the *i*-th glass ply of investigated laminated panel in terms of stress or deflection. Effective Thickness of the monolith depends on the level of shear forces transfer between glass plies in bending.

W-B method, incorporated into American standards ASTM [55], was originally intended for the calculation of sandwich structures consisting of two external layers with sufficient axial stiffness and the soft-core layer providing shear stiffness only. Wölfel´s method [49] was later extended by S. J. Bennison for the determination of the Effective Thickness of 1D double LG panels depending on the coefficient of shear forces Γ. This coefficient represents a measure of the shear forces transfer through the interlayer, it varies from 0 to 1 [56] and can be expressed as

$$\Gamma = \frac{1}{1 + \beta \cdot \frac{tE}{bGl^2} \cdot \frac{A_1 A_2}{A_1 + A_2}}, \tag{30}$$

where t is thickness of the interlayer [mm], E is Young modulus of glass [MPa], G is one certain value of interlayer´s shear modulus [MPa]; l is span of the panel [mm], b is the width of cross section [mm], A_i denotes the area of the individual glass ply in the cross section [mm^2], and β [-] is the coefficient related to boundary conditions of LG panel. This coefficient is in Wölfel´s theory suggested as $\beta = 9.6$ only for uniformly loaded simply supported 1D LG panels but civil engineers often use this value in calculations of double LG panels loaded in various loading and boundary conditions, even for 2D problems [57]. Input parameters for W-B method are displayed in Fig. 52.

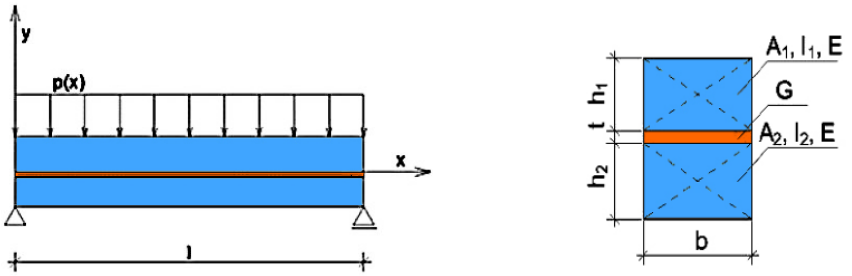

Fig. 52: Input parameters for the calculation of Effective Thickness of double LG panel by W-B [58]

The Effective Thickness for vertical deflection $h_{ef,w}$ and for normal stress of *i*-th glass ply in double LG panel $h_{i,ef,\sigma}$ ($i \in \{1, 2\}$) are calculated according to the Eqs. (31) and (32) [58]

$$h_{ef,w} = \sqrt[3]{h_1^3 + h_2^3 + 12 \cdot \Gamma \cdot I_s} \ , \tag{31}$$

$$h_{1,ef,\sigma} = \sqrt{\frac{h_{ef,w}^3}{h_1 + 2 \cdot \Gamma \cdot h_{s,2}}} \ , \qquad h_{2,ef,\sigma} = \sqrt{\frac{h_{ef,w}^3}{h_2 + 2 \cdot \Gamma \cdot h_{s,1}}} \ , \tag{32}$$

where h_1, resp. h_2 is the thickness of glass ply [mm], Γ is coefficient of shear forces [-], I_s refers to baricentrical inertia of two glass plies [mm^3], and $h_{s,i}$ are modified values of cross section thickness [mm]. Relations for I_s and $h_{s,i}$ may be found in literature by Galuppi et al. [58].

EET method, already incorporated into Italian standards CNR-DT [59], was recently proposed by Galuppi et al. [60]. The main idea of this method consists in finding the best approximation of the deflected shape of LG panel by minimizing the value of strain energy functional. The shape function of vertical deflection is, by default, assumed in the form of an elastic curve of a monolithic panel with the constant cross section under the same loading and boundary conditions of the problem. The model assumes geometrical linearity and all materials to be linear elastic. EET method was originally suggested for 1D problems of double LG panels, e.g., two-sides simply supported narrow roof panel [60], and it was later extended for 2D problems [61] designed even as multi-laminated elements. Input parameters for 1D or 2D double LG panels are shown in Fig. 53.

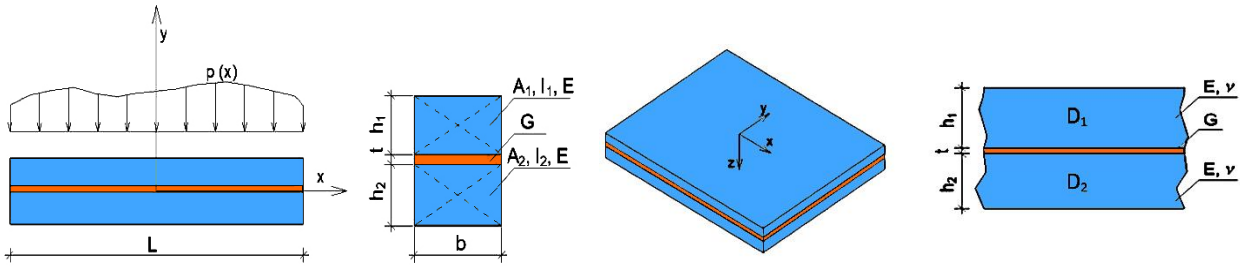

a) Input parameters for 1D laminated panels b) Input parameters for 2D laminated panels

Fig. 53: Input parameters for the calculation of Effective Thickness of double LG panel by EET method

Using the same notation as in case of W-B method, the Effective Thickness for vertical deflection $h_{ef,w}$ and for normal stress of i-th glass ply $h_{i,ef,\sigma}$ ($i \in \{1, 2\}$) for both 1D and 2D double LG panels are calculated according to Eqs. (33) and (34) [60]

$$h_{ef,w} = 1/\sqrt[3]{\frac{\eta}{h_1^3 + h_2^3 + 12 I_s} + \frac{1 - \eta}{h_1^3 + h_2^3}} , \tag{33}$$

$$h_{1,ef,\sigma} = 1/\sqrt[2]{\frac{2\eta\, h_{s,2}}{h_1^3 + h_2^3 + 12 I_s} + \frac{h_1}{h_{ef,w}^3}} , \qquad h_{2,ef,\sigma} = 1/\sqrt[2]{\frac{2\eta\, h_{s,1}}{h_1^3 + h_2^3 + 12 I_s} + \frac{h_2}{h_{ef,w}^3}} , \tag{34}$$

where the baricentrical inertia of two glass plies I_s and other variables are noted in the same way as in W-B method [58]. Minimization of the strain energy given by deflected shape of double

LG panel under various loading and boundary conditions enables to determine the coefficient of shear forces η (analogous to Γ in W-B) lying in range < 0; 1 > and, therefore, makes the method universal. Its notation for 1D and 2D problems is expressed using Eqs. (35) and (36), respectively.

$$\eta = 1/(1 + \frac{tE}{bG} \cdot \frac{I_1 + I_2}{I_{tot}} \cdot \frac{A_1 A_2}{A_1 + A_2} \cdot \Psi) \tag{35}$$

$$\eta = 1/(1 + \frac{t}{G} \cdot \frac{D_1 + D_2}{D_{tot}} \cdot \frac{12 D_1 D_2}{D_1 h_2^2 + D_2 h_1^2} \cdot \Psi) \tag{36}$$

In these equations, E is Young modulus of glass [MPa], G is one certain value of interlayer´s shear modulus [MPa], I_{tot} (D_{tot}) are the moment of inertia (flexural rigidity) of the monolithic 1D (2D) panel in [mm^4, (Nmm)], I_i is the moment of inertia of i-th 1D glass ply [mm^4], and D_i is the flexural rigidity of i-th 2D glass ply [Nmm]. Designation of other variables is shown in Fig. 53. The shape coefficient ψ [mm^{-2}] captures loading and boundary conditions and is tabulated in literature [58].

When the loading history is assumed, it is possible to express the response of LG panel analytically over the entire time interval. The equilibrium differential equations are based on Boltzmann superposition principle and can be hardly solved without use of numerical methods. Example of such viscoelastic method is Full Viscoelastic Solution (FVS) suggested by Galuppi et al. [62] as a representative of a linear viscoelastic (LVE) approaches.

2.6.2. Numerical solution and practical examples of calculations

Numerical solution of static problems in mechanics of solids is based on Newton´s principle of zero force resultant of volume forces $\{X\}$ and surface forces $\{p\}$ of a problem given by Eq. (37).

$$\iiint_V \{X\} \mathrm{d}V + \iint_A \{p\} \mathrm{d}A = \{0\} \tag{37}$$

Most of commercial software (Mepla®, ANSYS®, etc.) is based on approximation of displacement field $\{u\}$ in the panel which fulfils the Principle of virtual displacement (PVD) in static analysis [31] as an equivalent to Newton´s principle in Eq. (37). PVD is given by Eq. (38).

$$\iiint_V \{\delta\varepsilon\}^T \{\sigma\} \mathrm{d}V = \iiint_V \{\delta u\}^T \{X\} \mathrm{d}V + \iint_A \{\delta u\}^T \{p\} \mathrm{d}A \tag{38}$$

Eqs. (37) and (38) are noted as: $\{\sigma\}$ is the equilibrium symmetric stress tensor in the panel of volume V in Voigt notation, $\{X\}$ is the vector of volume forces, $\{p\}$ is the vector of forces acting on panel´s surface A, $\{\delta u\}$ ($\{\delta\varepsilon\}$) is the vector (tensor in Voigt notation) of kinematically possible virtual displacement (strain) of the panel. Assuming the displacement vector $\{u\}$ is approximated using the displacement of discrete nodes of the panel $\{r\}$, the following equation for static analysis must be computationally solved [31]

$$[K]\{r\} = \{f\}, \tag{39}$$

where $[K]$ is the stiffness matrix of the panel and $\{f\}$ refers to the applied load vector in discrete nodes of the panel $\{r\}$. Since deflections of LG panels may be large and interlayer is a viscoelastic

material, the problem may become nonlinear $[K] = [K(\{r\},t)]$ and it must be solved using an iterative algorithm, e.g., Newton-Raphson method [31]. Discrete nodes are grouped into finite elements (FE) stored in software library. LG can be conveniently modelled by a layered shell element but most of commercial codes do not have such elements in their library [58]. Contrary, 3D analysis is time consuming. An example is given by Molnár et al. [52] who modelled the response of rectangular simply supported uniformly loaded 6 + 10 mm thick double LG panel using ANSYS®, see Fig. 54. He meshed the individual plies using one hexahedron element SOLID 45 in a vertical sense. FE model enables to plot the distribution of normal stress over the panel´s cross section and draw the isolines over the surface, see Fig. 55.

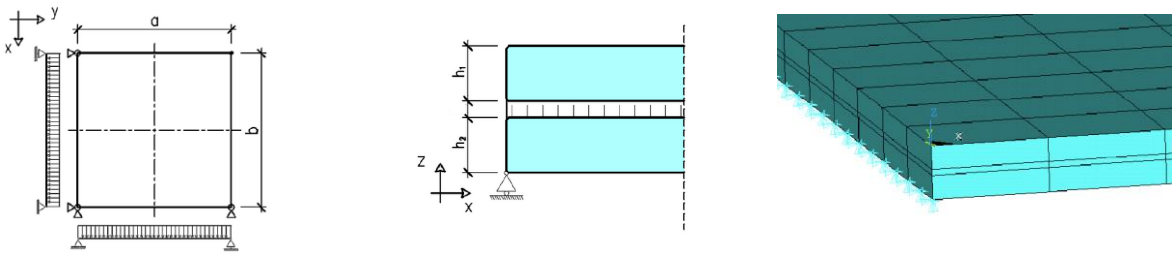

a) Static schema of the panel b) Detail of support c) Detail of FE mesh

Fig. 54: Rectangular double LG panel (6 + 10 mm) under uniform load modelled in ANSYS® [52]

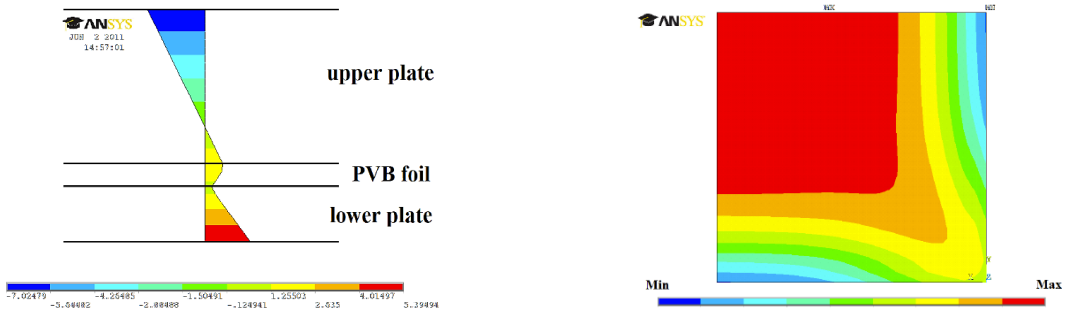

a) Distribution of normal stress over the cross section b) Principal stress on the ¼ of lower glass ply - izolines

Fig. 55: Numerical results using FE software for double LG panel (6 + 10 mm) in bending [52]

Moreover, FE models enable to validate the analytical methods. Galuppi et. al [58] investigated rectangular double LG panels (2 × 10 mm, interlayer 0.76 mm) under various loading and boundary conditions and calculated the values of Effective Thickness given by analytical W-B and EET methods and numerical 1st order FE numerical solution in Mepla®. Models assumed both materials as linear elastic. The panel had dimensions of a = 3000 mm and b = 2000 mm and was uniformly loaded by 0.75 kN/m^2. For such cases, W-B coefficient β = 9.6 [57], was used. Fig. 56 illustrates the % error on the evaluation of Effective Thickness using both W-B and EET in comparison to numerical results while changing the ratio of panel´s dimensions and keeping the

interlayer´s shear modulus *G* fixed. It is evident that results by W-B are close to EET when the ratio of dimensions *a*/*b* >> 1 and vice versa.

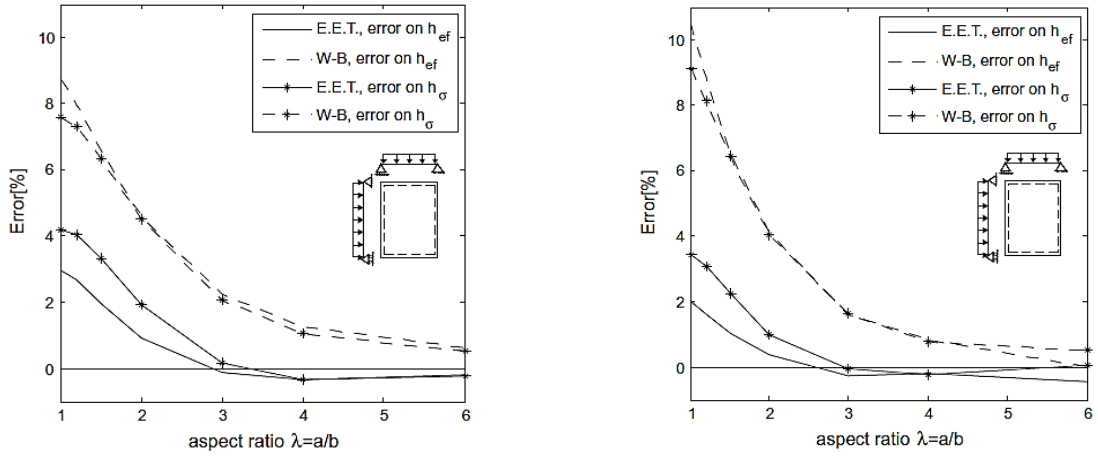

a) Panel´s edge a = 3 m b) Panel´s edge a = 2 m

Fig. 56: Error on evaluation of Effective Thickness for stress and for deflection in different ratios of panel´s dimensions using W-B and EET methods [58]

Since both linear elastic W-B and EET methods are used in practice for various boundary conditions, Galuppi et al. [58] investigated the effect of interlayer´s shear modulus *G* on the values of Effective Thickness of three sides simply supported rectangular double LG panels, see Fig. 57. Under this condition, both analytical methods give consistent results with numerical calculation over the entire interval of interlayer´s shear modulus $G \in \langle 0.01; 10 \rangle$ MPa.

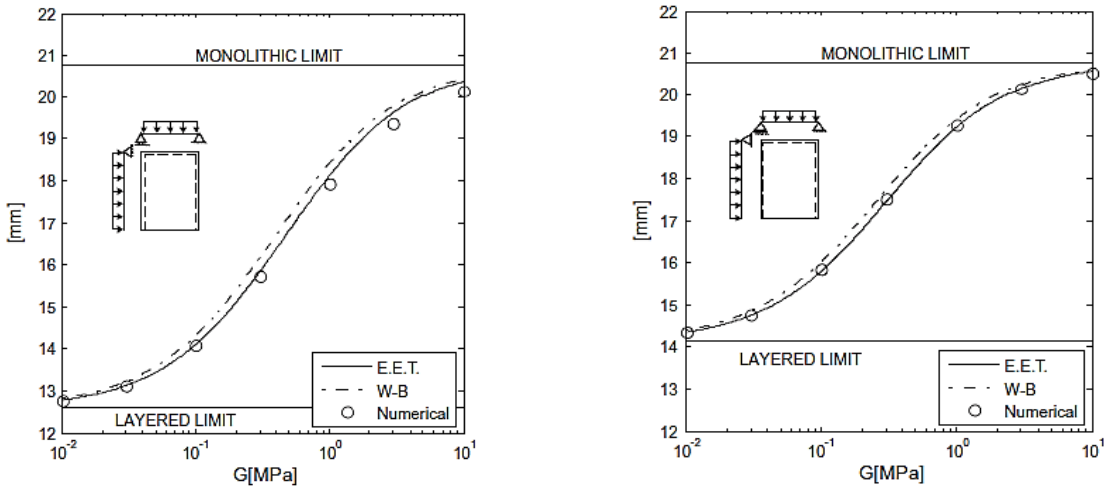

a) Effective Thickness for deflection b) Effective Thickness for stress

Fig. 57: Simply supported double LG panel 3000 × 2000 mm, comparison of Effective Thickness by W-B, EET, and numerical LE solution for certain value of interlayer´s shear modulus [58]

Numerical as well as analytical solution can be performed using both linear elastic (LE) and linear viscoelastic (LVE) approaches, see Fig. 51. To remind, LE solution requires one discrete value of interlayer´s shear modulus *G* and LVE solution requires complete knowledge of *G* in time and temperature domain *G*(t, T). Examples of discrete and continuous inputs of shear moduli *G* are shown in Fig. 58.

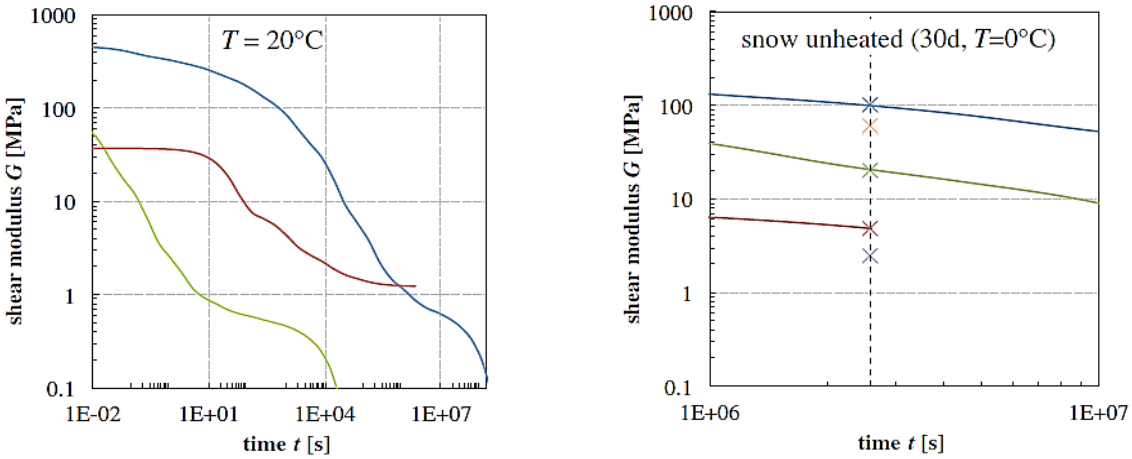

a) Continuous shear moduli b) Continuous shear moduli with discrete values

Fig. 58: Shear relaxation moduli in time at certain temperature for various interlayers [9]

The main difference between LE and LVE numerical solutions consists in the characteristic stress-strain relation of the interlayer. Whereas this relation for LE solution is linear, see Eq. (40) for 3D analysis in Voigt matrix notation, LVE solution uses the integral Boltzmann formula and, therefore, makes the solution time dependent. This is shown by matrix notation of 3D analysis in Eq. (41) where $\{\sigma\}$ is the stress tensor of interlayer in Voigt notation, $[E(t)]$ is time dependent elastic stiffness matrix of interlayer, $\{\varepsilon\}$ is the strain tensor of interlayer in Voigt notation, and t' is the exact time of strain increment from the interval < 0; t >.

$$\{\sigma\} = [E]\{\varepsilon\} \tag{40}$$

$$\{\sigma(t)\} = \int_0^t [E(t-t')] \frac{\mathrm{d}\{\varepsilon\}}{\mathrm{d}t'} \mathrm{d}t' \tag{41}$$

The comparison of LE and LVE solutions conducted on the example of two-sides simply supported double LG panel, with 0.76 mm PVB interlayer Saflex® DG as a part of vertical glazing, was performed by Kuntsche et. al [9]. This panel made of 2 × 6 mm FG, as a part of vertical glazing, was loaded by uniform load 2.3 kN/m^2 at 25 °C for 10 min. M-W Prony series of Saflex® DG were taken from Z-70.3-230 [63] for LVE analysis. Discrete value of interlayer´s shear modulus given by this M-W model, used in LE analysis, was *G*(t = 10 min, 25 ° C) = 2.9 MPa. Both LE and LVE solutions were carried out using small displacement theory in ANSYS®. Boundary conditions and maximum principal stress in time are shown in Fig. 59. Results show that

maximum principal stress from LE solution is constant whereas that given by LVE increases over the entire time interval. Important notice is that stress given by LE in time is higher than that by LVE and their difference in 10 min is negligible (11.7 MPa vs. 11.2 MPa). Kuntsche et al. [9] illustrated by this example that using the LE solution may simplify the assessment of LG panel loaded by static load.

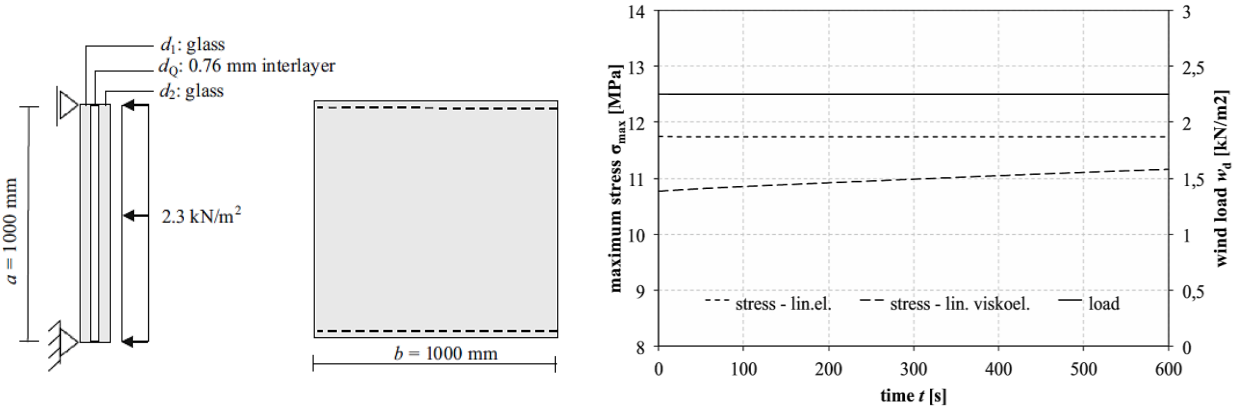

a) Geometry and load b) Comparison of maximum principal stress

Fig. 59: Double LG façade panel loaded by wind at +25 °C and 10 min of load duration [9]

2.7. State of art – conclusion

Literature survey illustrates the dependence of macroscopic mechanical properties of various polymeric interlayers on temperature and duration of static load. This phenomenon becomes important in response of LG panels under static out of plane loading. Material of used interlayer in lamination process is, therefore, important. Whether the glass plies shear coupling is considered in the design of LG panel in bending, time and temperature effects together with loading and boundary conditions must be considered. When stiffness of the certain interlayer is specified, attention should be paid to the selected computational method of laminated glass in bending since each method is appropriate to certain boundary conditions and cost-effectiveness of the design.

3. Scope and main goals of doctoral thesis

The subject of author´s research are time and temperature dependent stiffness characteristics of polymeric interlayers and the role of these interlayers in laminated glass loaded by out of plane loading.

The goals of the thesis consisted in (i) the description of time and temperature dependent shear stiffness of selected polymeric interlayers used in laminated glass and (ii) the effect of shear stiffness of studied interlayers on the performance of laminated glass panels in bending, see Fig. 60. The former was based on small-scale static and dynamic single-lap shear tests, the latter was based on static four-point bending tests of large-scale double LG specimens. Both experimental campaigns were supported by analytical and numerical studies.

a) Polymeric interlayer b) Laminated glass in bending

Fig. 60: Main subjects of author´s research, picture by author

Experimental part includes:

- static and dynamic single-lap shear tests of small-scale specimens laminated with studied interlayers at various temperatures and loading rates in the climatic chamber,
- four-point bending destructive tests of large-scale specimens with studied interlayers at various loading rates and room temperature,
- four-point bending creep tests of large-scale specimens with studied interlayers at various temperatures in the climatic chamber.

Theoretical part includes:

- creation of mechanical models of studied interlayers and their verification using experimental results,
- verification of experimental initial shear moduli of studied interlayers given by small-scale static single-lap shear tests using analytical and numerical calculations of large-scale four-point bending destructive tests,
- parametric study regarding the effect of interlayer´s shear modulus G on the value of the Effective Thickness of double laminated glass panel loaded in various boundary conditions,
- practical analytical calculation of load effects acting on double laminated glass façade and roof panel according to EN 16612.

4. General layout and individual stages of the thesis solution

General layout of the thesis is structured into (i) state of art, (ii) experimental part, (iii) analytical part, (iv) numerical part, and (v) parametric study. Research and the entire experimental campaign were structured into the following partial phases:

1) literature study and state of art completion,
2) selection of studied polymeric interlayers and manufacture of testing specimens,
3) performance of static single-lap shear tests of small-scale double LG specimens at various temperatures and loading rates,
4) performance of dynamic single-lap shear tests of small-scale double LG specimens at various temperatures and frequencies,
5) performance of four-point bending destructive tests of large-scale double LG specimens at room temperature and various loading rates,
6) performance of four-point bending creep tests of large-scale double LG specimens in the climatic chamber,
7) verification of initial shear moduli of selected interlayers given by static single-lap shear tests using analytical and numerical calculations of four-point bending destructive tests,
8) construction of mechanical models of selected polymeric interlayers and their verification by performed experiments,
9) creation of parametric studies mapping the effect of interlayer´s shear modulus G on the value of Effective Thickness of double LG panels in bending loaded in various conditions,
10) evaluation of achieved results and their impact on engineering practice.

5. Selection of appropriate interlayers and manufacture of testing specimens

5.1. Selected interlayers for experimental investigation

The choice of interlayers was governed by their proportional presence in existing structures and by type of interchain bonding. Commonly used materials for LG applications are polyvinyl butyral (PVB) and ethylene-vinyl acetate (EVA). Interlayers made of ionomer and thermoplastic polyurethane (TPU) are less common but get currently extended due to their specific molecular structure. Each material can be included into one appropriate category regarding the type of intermolecular bonding plotted in Fig. 17.

Polyvinyl butyral (PVB) is an amorphous thermoplastic polymer. Chemical formula of PVB is shown in Fig. 61a). Chemical structure is formed by random arrangement of polymeric chains with secondary interchain bonds. To regulate the stiffness, producers add additives and plasticizers into this material. The glass transition temperature T_g of PVB lies between 12 °C and 20 °C [46], [64]. Benefitable properties are high transparency and high tearing strength.

Ethylene-vinyl acetate (EVA) is a thermoplastic material which is produced during the copolymerization of ethylene and vinyl acetate. Chemical formula is shown in Fig. 61b). Depending on the content of vinyl acetate (usually between 5% and 50%), the mechanical properties of this material, e.g., temperature dependent stiffness, are modified. For example, Weller et al. [46] declares $T_{g,\,EVA}$ = -43 °C for a 32% content of vinyl acetate. Although EVA is an uncross-linked thermoplastic, it may be, in contrast to PVB, converted into a cross-linked thermoset during the lamination process [65]. This process taking place in small laminators keeping the vacuum and temperature process controlled, transforms free “soup of flowing molecules” into the mass of cross-linked thermoset. The density of covalent chemical cross-link depends on the certain conditions of lamination (temperature, time of lamination, cross-link initiator, etc.) [66]. The difference in chemical structure between PVB and EVA after the lamination process is schematically shown in Fig. 62.

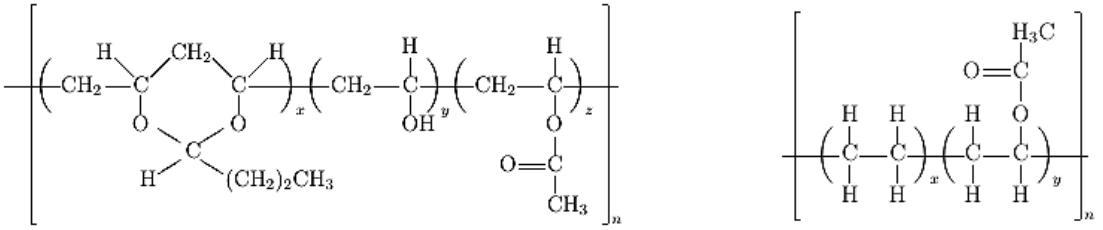

a) Polyvinyl butyral (PVB) b) Ethylene-vinyl acetate (EVA)

Fig. 61: Chemical formulas of tested PVB and EVA materials

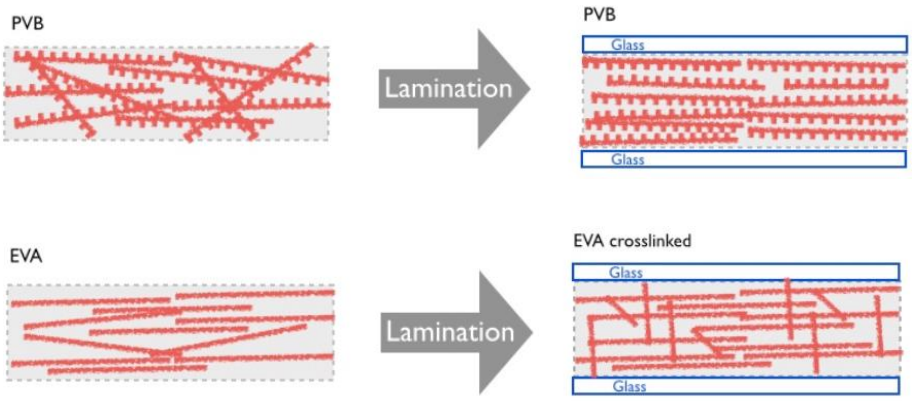

Fig. 62: Difference in chemical structure between PVB and EVA after lamination process [65]

Thermoplastic polyurethane (TPU) belongs among thermoplastic elastomers and consists of hard diisocyanate and soft polyol block copolymers, see its chemical formula in Fig. 63b). The glass transition temperature T_g of TPU is a wide range value [67]. TPU interlayers, originally produced in the USA, are relatively new on the European market and their production extends due to hydrolysis resistance and UV stability.

Ionomer interlayers as thermoplastic elastomers contain nonionic repeat units as well as a small amount of ion repeat units. An example of such material is polyethylene-co-methacrylic acid neutralized with NaOH. This product is the sodium salt called "Surlyn", see Fig. 63a). Ion cross-link is in this case formed by grouped clusters of Na^+O^-. The presence of reversible ion cross-link in the base material causes relatively high tensile stiffness of these interlayers and high glass transition temperature, around 50 °C [29].

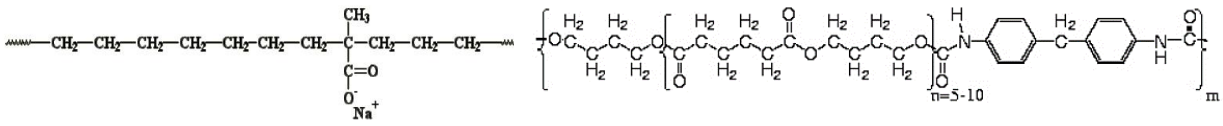

a) Poly(ethylene-co-methacrylic acid) ionomer neutralized with NaOH

b) Thermoplastic polyurethane (TPU)

Fig. 63: Chemical formulas of tested ionomer and TPU materials

Each producer denotes each interlayer with a specific trademark. Since PVB and EVA are the most common materials, two interlayers of each trademark were studied. Representative PVB interlayers were **Trosifol® BG R20** and **Trosifol® Extra Strong** (both by Kuraray™). Representative EVA interlayers were **Evalam® 80/120** (by Pujol™) and **Evasafe®** (by Bridgestone™). TPU interlayer was represented by **Krystalflex® PE399** (by Huntsman™), and finally **SentryGlas® 5000** (by Kuraray™) as "Surlyn" ionomer. Some trademarks of interlayers have already been changed. This applies to Trosifol® BG R20 currently named as

Trosifol® UltraClear and Trosifol® Extra Strong currently named as Trosifol® Extra Stiff. For both renamed interlayers, the chemical composition was not modified. Studied interlayers will be, throughout the entire thesis, denoted in abbreviation as:

- Trosifol® BG R20 = Trosifol BG (or only BG)
- Trosifol® Extra Strong = Trosifol ES (or only ES)
- Evalam® 80/120 = EVA L,
- Evasafe® = EVA S,
- SentryGlas® 5000 = SG 5000,
- Krystalflex® PE399 = TPU KF.

All interlayers were of non-aged structure. Interlayers are stored in big roles and can be even coloured, see Fig. 64. Representative technical data of studied interlayers are shown in Tab. 4. Trosifol BG and Trosifol ES as representatives of PVB were chosen intentionally since they differ in the amount of plasticizer added into PVB. Trosifol ES is less plasticized than Trosifol BG but details are not available. EVA L and EVA S as representatives of EVA material differ in the cross-link density as the consequence of their different conditions at lamination: EVA L – only 3% (very lightly cross-linked), EVA S – 88% (heavily cross-linked 3D structure). This was the reason of their choice. Specific values of T_g and tensile strength of SG 5000 and TPU KF governed the choice of these thermoplastic elastomers.

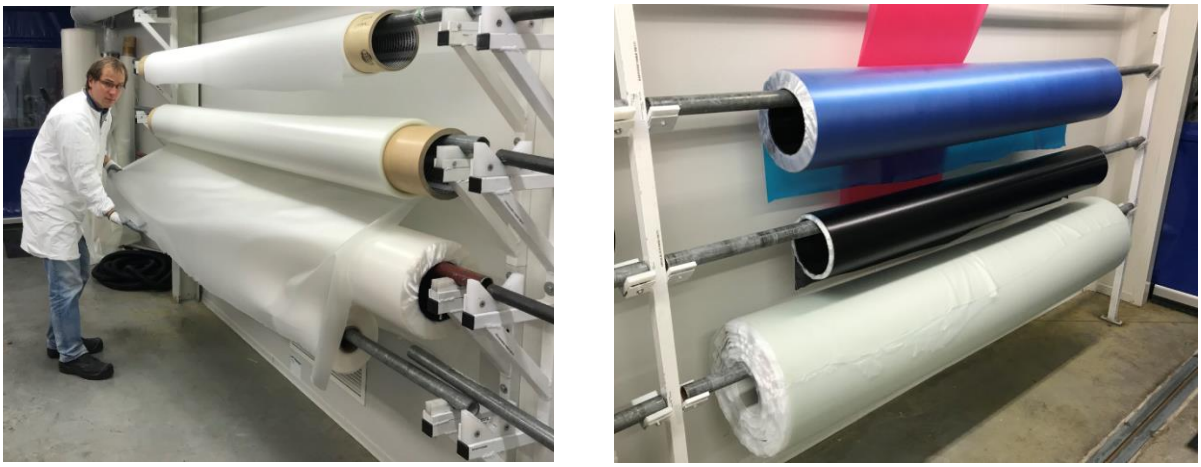

Fig. 64: Storage of interlayers in big roles before lamination

Tab. 4: Representative technical data of tested interlayers

Property	EVA S	Trosifol BG	Trosifol ES	SG 5000	TPU KF	EVA L
Density [g/cm^3]	xxx	1.065	1.081	0.95	xxx	xxx
Thermal conductivity [W/mK]	xxx	0.20	0.152	0.246	xxx	xxx
Tensile strength [MPa]	26	>23.0	xxx	34.5	45.0	13.9
Usual nominal thickness [mm]	0.4; 0.8	0.76; 1.52	0.76	0.89; 1.52	0.76; 1.25	0.38; 0.76
Hardness [Shore]	82	xxx	xxx	xxx	80	67-70
Melting point [°C]	+79	xxx	xxx	+94	+80	xxx
Glass transition temperature [°C]	-28	+26	+41	+52	-36	xxx

Note: Complete set of technical data for studied interlayers is in their technical sheets, see attachment of this thesis.

5.2. Manufacture and details of testing specimens

For experimental investigation, double LG specimens were used. These were made of FG, HSG, and HTG. Manufacturer declared the nominal thickness of one glass ply as 10 mm. Nominal declared thickness of interlayers was: Trosifol BG – 0.76 mm and 1.52 mm, Trosifol ES – 0.76 mm, EVA L – 0.76 mm, EVA S – 0.8 mm, SG 5000 – 0.89 mm, and TPU KF – 0.76 mm. Nominal plane dimensions of one glass ply for small-scale experiments were 150 × 50 mm and for large scale experiments were 360 × 1100 mm. General schema of lamination process is shown in Fig. 10. At first, the interlayer needs to be embedded between glass plies, see the manufacture of specimens in Fig. 65.

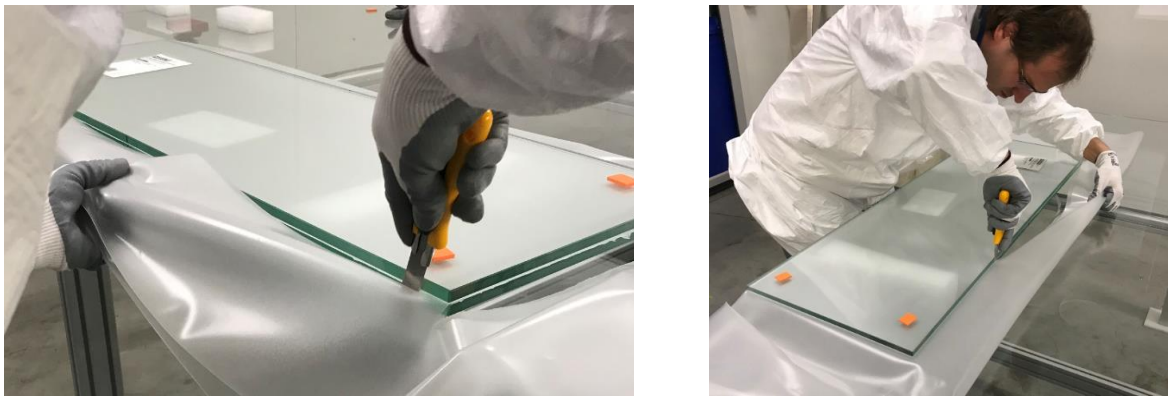

Fig. 65: Manual lamination of testing specimens by author

As soon as the manual lamination is completed, the automatic lamination process to ensure an absolute transparency and adhesiveness of interlayer to glass, begins. This may be done in huge autoclave or in small laminator, see Fig. 66, at elevated temperature. When the interlayer has low adhesion to glass, lamination needs to be performed in autoclave where the pressure is applied on the laminated panel. Lamination is technologically complicated process and influences the

mechanical properties of LG panel. EVA specimens were laminated in laminator. They were individually sealed with plastic vacuum bags and heated – EVA L to 78 °C for 210 min and EVA S to 135 °C for 60 min with added peroxide as a cross-link initiator. As stated, different conditions at lamination result in different cross-link density of EVA interlayers (EVA L 3%, EVA S 88%). Specimens with remaining interlayers were laminated in autoclave: Trosifol BG and Trosifol ES specimens – pressure 12 bar at 145 °C for 4 hours, SG 5000 specimens – pressure 12 bar at 130 °C for 4.5 hours, and TPU KF – pressure 5 bar at 120 °C for 5 hours.

a) Autoclave b) Laminator

Fig. 66: Automatic machines for lamination

After the completion of lamination process, manufactured double LG testing specimens were transported to CTU for experiments. The shape of specimens is shown in Fig. 67. Specimens were supplied by companies IZOS® and OGB®.

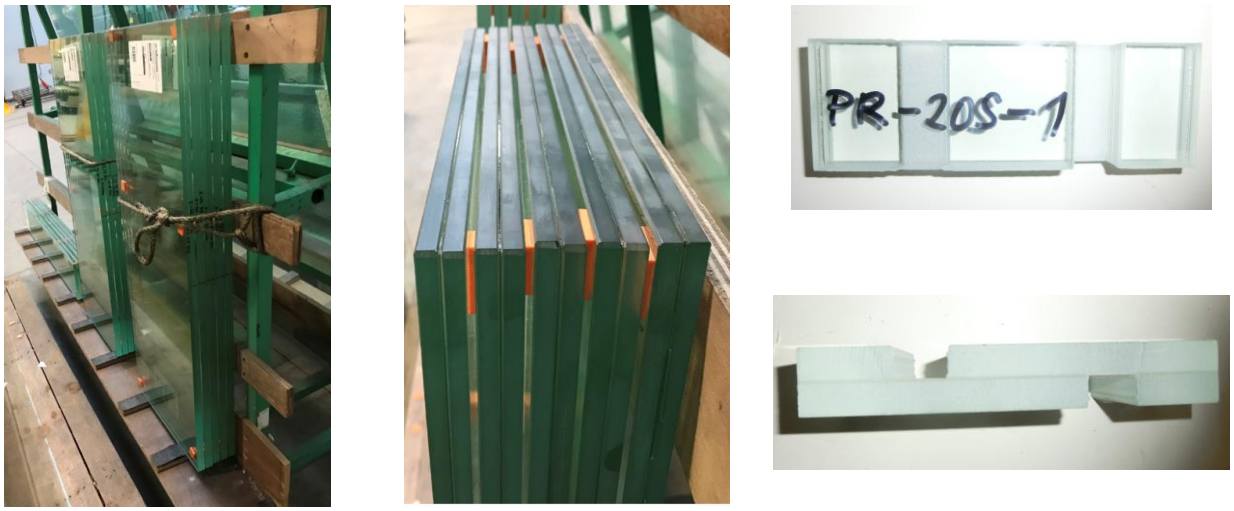

a) Large-scale specimens b) Small-scale specimens

Fig. 67: Testing specimens after completion of lamination process

Fig. 68 shows the dimensions of testing specimens in detail. Large-scale LG specimens had plane dimensions of 360 × 1100 mm and small-scale LG specimens had plane dimensions of 150 × 50 mm. To enable the shear tests of small-scale specimens, water jet cut the specimens into required shape, see Fig. 68b). The nominal thickness of glass plies was identical for both types of LG specimens (2 × 10 mm). Illustrated dimensions of specimens in Fig. 68 are documented by real specimens in Fig. 67. General amounts of testing specimens with an appropriate interlayer are stated in Tab. 5. Declared nominal thickness of glass 10 mm was verified by twenty measurements using caliper. Average measured value was 9.95 mm with standard deviation 0.01 mm.

Tab. 5: General amounts of testing specimens with appropriate interlayer for author´s research

Small-scale specimens		Large-scale specimens	
Interlayer	Amount	Interlayer	Amount
Trosifol BG	100	Trosifol BG	20
Trosifol ES	90		
EVA L	90	EVA L	20
EVA S	90		
SG 5000	90	SG 5000	15
TPU KF	90		

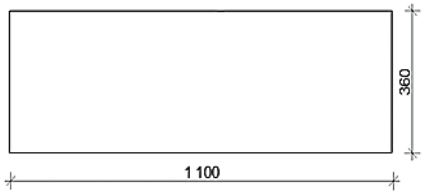

a) Plane dimensions of large-scale specimen - top view

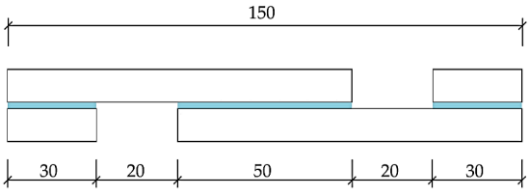

b) Plane dimensions of small-scale specimen side view

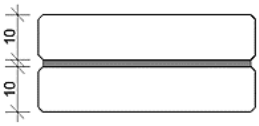

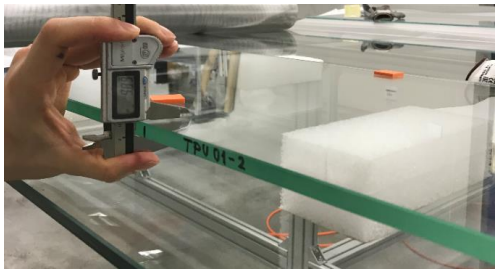

c) Cross section of all testing specimens and nominal thickness of glass verified by caliper

Fig. 68: Nominal values of dimensions

6. Experimental part of the thesis

Experimental part of the thesis aims at most important experimental results as an essential source of data.

6.1. Static single-lap shear tests of small-scale specimens

To get the basic understanding of temperature-stiffness characteristics of selected interlayers, small-scale static single-lap shear tests were performed at first. The tests were aimed at the initial shear modulus – temperature and loading rate sensitivity. Shear stress and shear strain of tested interlayers are herein assumed as engineering values.

6.1.1. Test setup and evaluation of results

In these tests, the specimens were put into the metal jaws of the testing device TEMPOS, with the climatic chamber TIRA TEST T250/1. The tests were controlled by TEMPOS cross-head vertical displacement inducing mutual displacement of metal jaws with glass plies, see the real experiment in Fig. 69. Resulting tensile force *F* in steel rods was measured by load cell HBM U9B 20kN. To measure the mutual displacement of glass plies *u*, potentiometric linear transducers, Megatron MMR 1011 were stuck directly to the glass, see Fig. 69a) and Fig. 70. Temperature in the chamber was measured by Pt 1000 sensor.

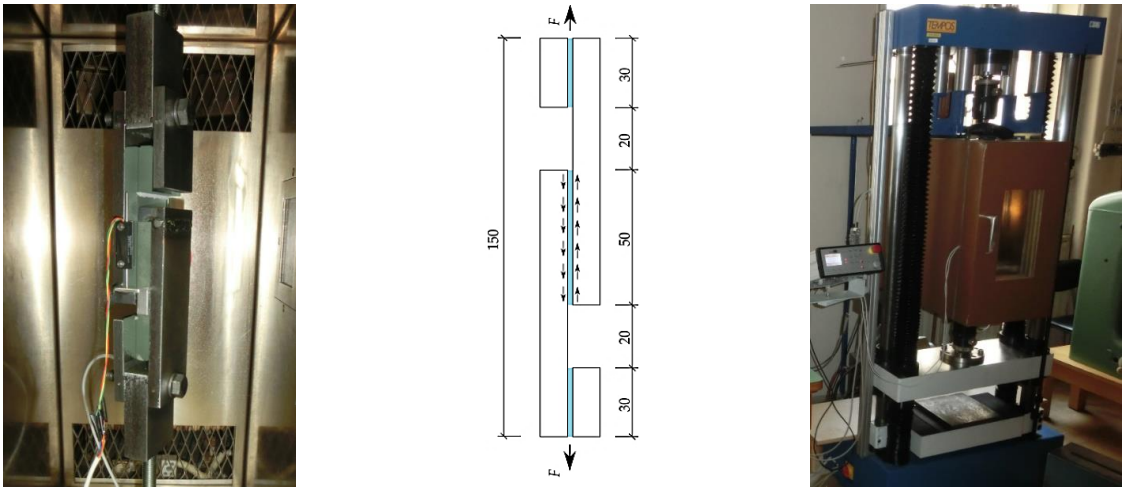

a) Specimen in metal jaws b) Direction of acting force c) Running test

Fig. 69: Specimen in the testing device TEMPOS with the climatic chamber

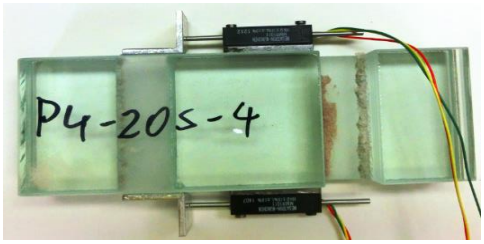

a) Specimen with mounted transducers

b) Detail of transducer

Fig. 70: Testing specimen with transducers Megatron MMR 1011

Since the exact thickness of interlayer was important for results, three points along its length of ten representative specimens from each interlayer were measured using microscope and average value was then used in evaluation of results. Representative points are shown in Fig. 71. TEMPOS cross-head connected with steel rods having metal jaws with the specimen in the end, was set on three loading rates of vertical displacement as: 2.0 mm/min, 0.5 mm/min, 0.125 mm/min. Climatic chamber was tempered at 0 °C, 20 °C, 40 °C, or 60 °C. Each specimen was loaded at one constant cross-head loading rate of displacement and constant temperature until failure. Summary of testing specimens used for static tests with average thickness of interlayer and loading conditions is shown in Tab. 6.

a) Trosifol BG

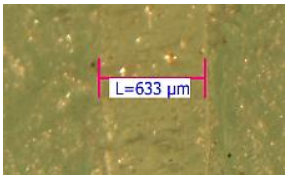

b) EVA L

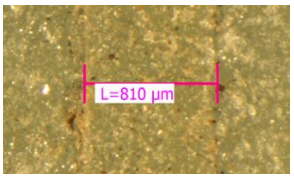

c) EVA S

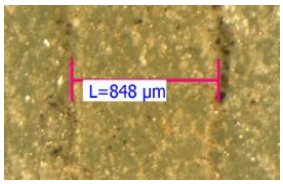

d) Trosifol ES

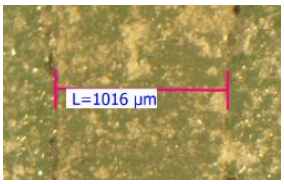

e) SG 5000

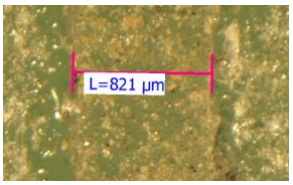

f) TPU KF

Fig. 71: Microscope images of all interlayers at representative points

Tab. 6: Summary of testing specimens, average thickness of interlayer, loading conditions

Type	Tempe-rature [°C]	Loading rate [mm/min]	Number of specimens	Average thickness (standard deviation) [mm]	Type	Tempe-rature [°C]	Loading rate [mm/min]	Number of specimens	Average thickness (standard deviation) [mm]
Trosifol BG	0	2.0	4	1.50 (0.03)	EVA S	0	2.0	4	0.81 (0.04)
		0.5	7				0.5	7	
	+20	2.0	8			+20	2.0	10	
		0.5	5				0.5	5	
		0.125	10				0.125	10	
	+40	2.0	10			+40	2.0	10	
		0.5	5				0.5	0	
		0.125	10				0.125	9	
	+60	2.0	10			+60	2.0	10	
		0.5	5				0.5	0	
		0.125	10				0.125	10	
Trosifol ES	0	2.0	4	0.85 (0.03)	TPU KF	0	2.0	4	0.82 (0.05)
		0.5	7				0.5	7	
	+20	2.0	10			+20	2.0	10	
		0.5	5				0.5	10	
		0.125	10				0.125	10	
	+40	2.0	10			+40	2.0	10	
		0.125	9				0.125	10	
	+60	2.0	10			+60	2.0	10	
		0.125	10				0.125	10	
EVA L	0	2.0	10	0.63 (0.02)	SG 5000	0	2.0	4	1.01 (0.05)
		0.5	5				0.5	7	
	+20	2.0	10			+20	2.0	10	
		0.5	5				0.5	5	
		0.125	10				0.125	10	
	+40	2.0	10			+40	2	10	
		0.125	10				0.125	10	
	+60	2.0	10			+60	2	10	
		0.125	10				0.125	10	

The mutual vertical displacement of steel rods with metal jaws induced tensile force F as the resultant of shear stress τ acting on the interlayer, see Fig. 69b). The value of shear stress was calculated using Eq. (42), where A is the area of stressed interlayer between glass plies 50 × 50 mm. Shear stress τ caused shear strain of interlayer γ that was calculated as an engineering value from the mutual slippage of glass plies u and average thickness of interlayer p according to Eq. (43). Theoretical shear strain input in time by TEMPOS cross-head displacement and stress-strain outputs measured on the interlayer are displayed in Fig. 72. Stress-strain relation was basically nonlinear. To quantify the results of experiments, the initial shear modulus G_{init} was evaluated for each specimen. The procedure of G_{init} evaluation from experimental stress-strain relations is schematically shown in Fig. 72c). The value of shear stress τ_{init} for the evaluation of G_{init} was chosen with respect to corresponding values of engineering strain γ_{init} to be, if possible, higher than those in intact LG panels (shear strains are usually low, to 1% [33]). Based on this request, τ_{init} was chosen as 0.4 MPa for all interlayers, except for Trosifol BG which did not achieve the value of 0.4 MPa at 60 °C. Therefore, the values of all G_{init} for Trosifol BG were evaluated using τ_{init} = 0.2 MPa.

$$\tau = F/A \tag{42}$$

$$\gamma \approx \tan\gamma = u/p \tag{43}$$

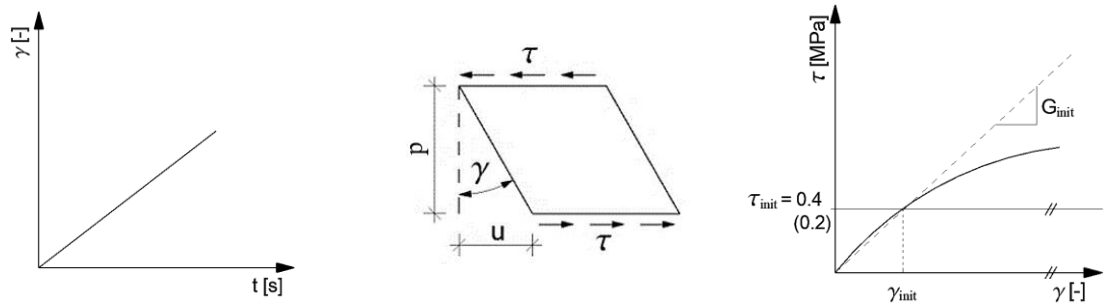

a) Theoretical shear strain applied on interlayer γ in time

b) Shear strain of interlayer

c) Measured stress-strain relation and initial shear modulus G_{init}

Fig. 72: Prescribed shear strain input and measured shear stress-strain relation of the interlayer

6.1.2. Representative experimental relations and summary of results

Charts in Fig. 73 show representative shear stress-strain relations of all tested interlayers. Complete set is in the attachment. It is shown all interlayers react to the ambient temperature and loading rate.

Stress-strain relations of both EVA interlayers are nonlinear and temperature sensitive, see Fig. 73a) and b). Both act as a flexible rubber, but more detailed comparison shows that EVA S interlayer is stiffer. To give the example, at 20 °C and shear stress 1.0 MPa: $\gamma_{EVA\,S}$ = 0.2 and $\gamma_{EVA\,L}$ = 0.5, and at 40 °C and shear stress 2.0 MPa: $\gamma_{EVA\,S}$ = 1.2 and $\gamma_{EVA\,L}$ = 3.5. This phenomenon is attributed to different cross-link density of both interlayers (EVA L 3% and EVA S 88%). Low cross-link density of EVA L is well documented at 60 °C and loading rate 0.125 mm/min where this interlayer, apart from EVA S, gets to viscous flow.

Experimental relations of both PVB based interlayers are plotted in Fig. 73c) and d). At 0 °C, the interlayers act as glass-like solid. As the temperature further increases, both interlayers show loading rate sensitivity and reduction of stiffness. Even though both are made of polyvinyl butyral, producers add a certain amount of plasticizer into the base material. Trosifol ES is less plasticized than Trosifol BG but certain numbers are not available. This results in their different response to the applied load. At 20 °C, Trosifol ES is still in the glassy region but Trosifol BG already approaches the rubbery state. As the temperature further increases, Trosifol BG softens gradually and gets to viscous flow at 60 °C which is typical for uncross-linked polymers. Trosifol ES drastically softens between 20 °C and 40 °C and gets also to the viscous flow at 60 °C.

Relations of SG 5000 interlayer are plotted in Fig. 73e). Noncovalent ion-crosslink causes stiff glass-like behaviour to 40 °C, therefore the curves at 0 °C to 40 °C are not well recognizable in a

plotted range of shear strains. As the temperature exceeds 50 °C, the material softens and gets to the rubbery state. SG 5000 still shows a certain shear stiffness even at 60 °C and clearly recognizable stress-strain relations well document material viscoelasticity.

Experimental relations of TPU KF are shown in Fig. 73f). Smooth increase of stress-strain nonlinearity and softening between 0 °C and 60 °C reflects gradual changes in the molecular structure of this thermoplastic elastomer. At 0 °C, the stress-strain relations are almost linear but at 60 °C, the nonlinearity well documents the molecular movement in the material. TPU KF even at 60 °C shows a certain load resistance at small strains but for shear strain $\gamma > 2.0$, the viscous flow occurs.

Fig. 73 also illustrates significant softening of the materials when crossing their glass transition temperature. This is well recognizable in case of both PVB´s and SG 5000 interlayers.

To illustrate the response of "stiff" interlayers SG 5000 and Trosifol ES at 0 °C and 20 °C in detail, Fig. 74 is provided. Since both interlayers are in the glassy region, the viscoelasticity is inhibited (SG 5000 is completely elastic, Trosifol ES shows certain signs of loading rate sensitivity at 20°C).

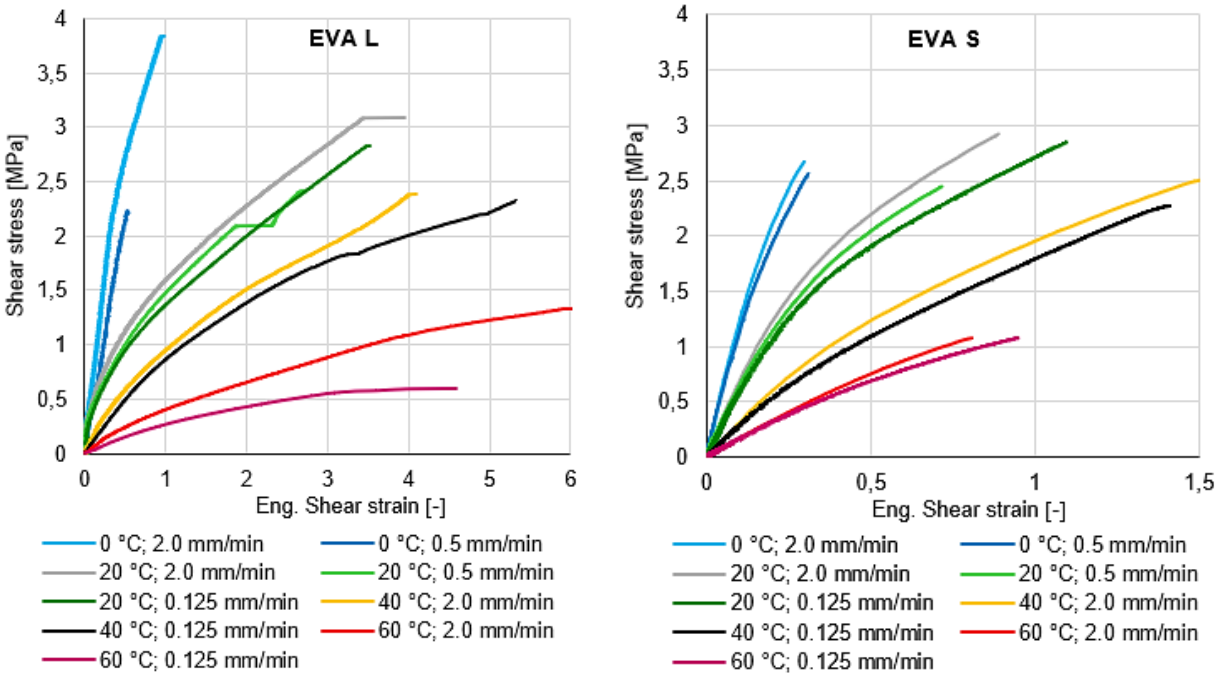

a) Evalam® 80/120 b) Evasafe®

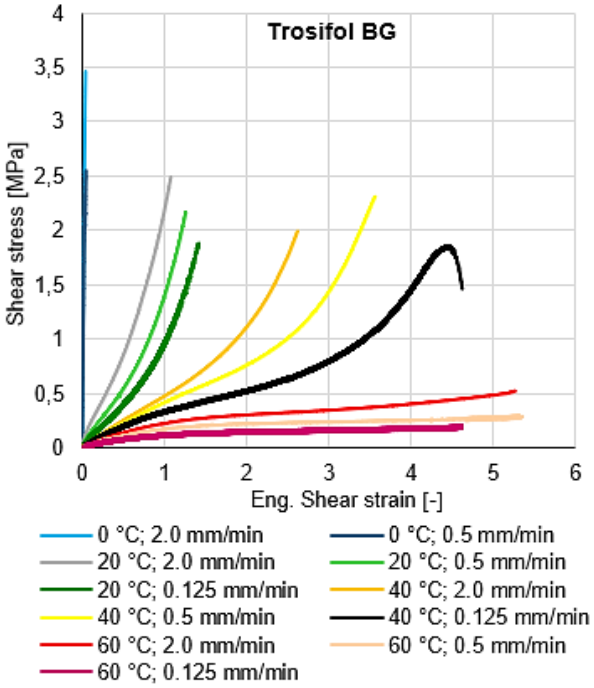

c) Trosifol® BG R20

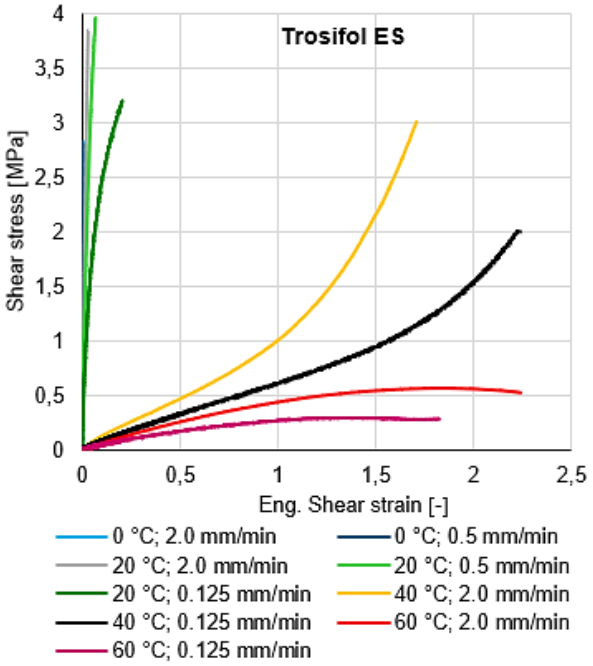

d) Trosifol® Extra Strong

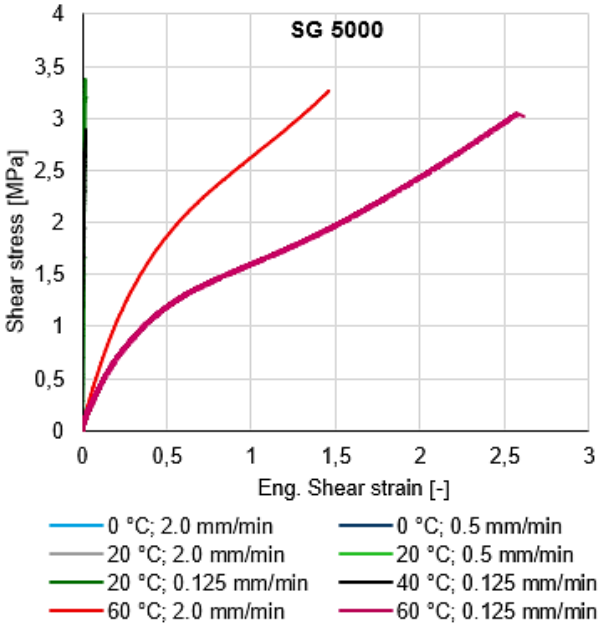

e) SentryGlas® 5000

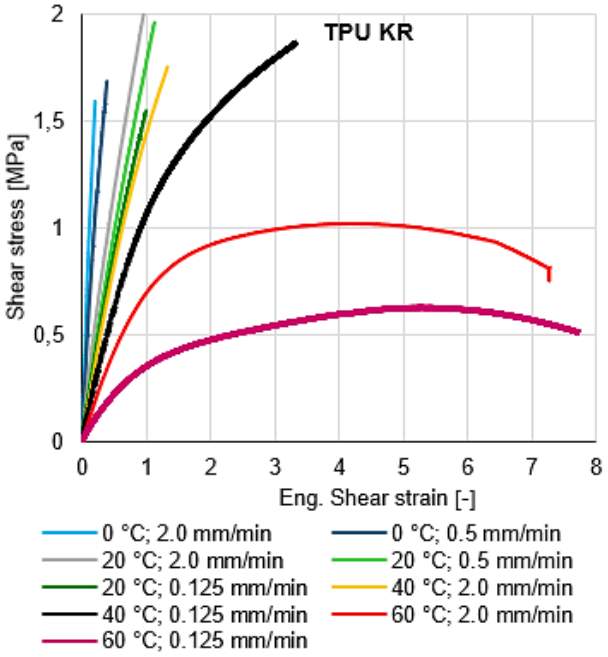

f) Krystalflex® PE399

Fig. 73: Representative shear stress-strain relations of all tested interlayers at prescribed TEMPOS cross-head loading rate of vertical displacement in [mm/min]

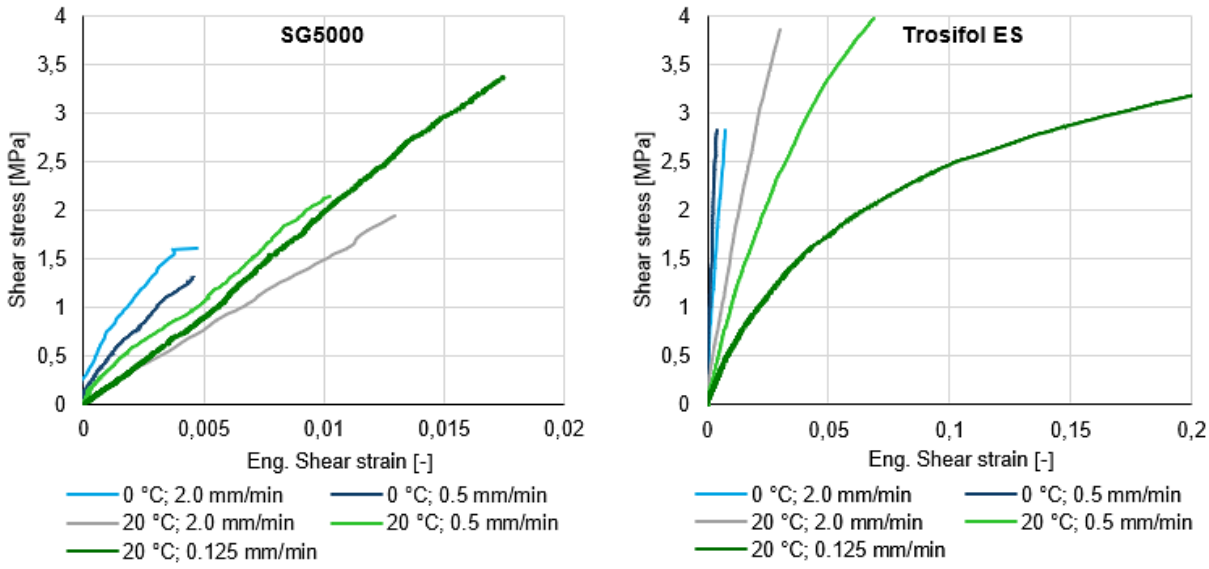

a) SentryGlas® 5000 b) Trosifol® Extra Strong

Fig. 74: Representative shear stress-strain relations of "stiff" interlayers at prescribed TEMPOS cross-head loading rate of vertical displacement in [mm/min]

Average values of initial shear stiffness G_{init} of all interlayers with standard deviations are shown in Tab. 7. Seeing these values, general statement can be made: the initial shear stiffness of interlayer is temperature and loading rate sensitive. Increase of temperature or decrease of loading rate results in reduction of the initial shear stiffness.

Even though both PVB based interlayers are pretty stiff at 0 °C (e.g. $G_{init,ES}$ = 1887 MPa) and attain noteworthy drop of the initial shear stiffness between 0 °C and 20 °C, they differ in the content of plasticizers which results in absolutely different values of G_{init} at these temperatures. At 40 °C and 60 °C, both PVB´s attain low values of G_{init} and get to viscous flow, e.g., $G_{init,BG}$ = 0.12 MPa at 60 °C. Stiff response of Trosifol ES at 0 °C and 20 °C disabled to measure its initial shear stiffness precisely as the values of standard deviations in Tab. 7 indicate.

The highest value of $G_{init,\ EVA\ S}$ = 13.2 MPa at 0 °C and smooth decrease of $G_{init,\ EVA}$ with increasing temperature indicates both EVA interlayers were in the rubbery state at all testing temperatures. Higher cross-link density of EVA S results, in comparison to EVA L, in higher initial shear moduli at all temperatures, e.g., $G_{init,EVA\ S}$ = 6.8 MPa vs. $G_{init,EVA\ L}$ = 4.1 MPa (both at 20 °C and at loading rate 2.0 mm/min). At 60 °C, EVA L got to viscous flow, but EVA S was still able to resist the load with the initial stiffness of approx. 1.5 MPa.

The values of $G_{init,\ TPU\ KF}$ were similar with $G_{init,EVA\ L}$. The initial stiffness also decreased smoothly with increasing temperature reflecting the rubbery response of TPU KF.

Experimental testing of SG 5000 was on the limit of testing device since this interlayer acted as glass like solid to 40 °C, see the values of $G_{init,\ SG\ 5000}$ standard deviations in Tab. 7. Significant

decrease of $G_{init,\ SG\ 5000}$ was measured between 40 °C and 60 °C, when crossing its T_g, from approx. 145 MPa to 6 MPa. SG 5000 showed the highest initial stiffness at 60 °C from all tested interlayers.

Tab. 7: Average moduli and standard deviations of the initial shear stiffness G_{init}

Type	Tempe-rature [°C]	Loading rate [mm/min]	Average value of G_{init} [MPa]	Standard deviation [MPa]	Type	Tempe-rature [°C]	Loading rate [mm/min]	Average value of G_{init} [MPa]	Standard deviation [MPa]
Trosifol BG	0	2.0	144.13	20.73	EVA S	0	2.0	13.26	0.08
		0.5	103.32	22.59			0.5	13.28	0.97
	+20	2.0	1.71	0.12		+20	2.0	6.86	0.39
		0.5	1.09	0.02			0.5	6.39	0.40
		0.125	0.80	0.03			0.125	6.22	0.31
	+40	2.0	0.46	0.05		+40	2.0	3.43	0.27
		0.5	0.45	0.03					
		0.125	0.31	0.05			0.125	3.09	0.29
	+60	2.0	0.27	0.04		+60	2.0	1.64	0.05
		0.5	0.15	0.03					
		0.125	0.12	0.01			0.125	1.44	0.11
Trosifol ES	0	2.0	1887.94	430.21	TPU KF	0	2.0	10.51	0.49
		0.5					0.5	6.85	0.68
	+20	2.0	225.47	56.97		+20	2.0	2.96	0.62
		0.5	105.23	8.58			0.5	2.22	0.09
		0.125	61.31	12.73			0.125	1.85	0.12
	+40	2.0	0.90	0.10		+40	2.0	1.77	0.12
		0.125	0.61	0.03			0.125	1.62	0.65
	+60	2.0	0.47	0.02		+60	2.0	0.82	0.27
		0.125	0.37	0.16			0.125	0.40	0.13
EVA L	0	2.0	7.46	3.06	SG 5000	0	2.0	684.65	362.61
		0.5	6.52	3.38			0.5	290.83	155.95
	+20	2.0	4.13	1.91		+20	2.0	245.60	99.88
		0.5	2.93	1.41			0.5	206.21	61.06
		0.125	2.37	0.74			0.125	214.23	45.43
	+40	2.0	0.84	0.23		+40	2.0	not spec.	not spec.
		0.125	0.98	0.18			0.125	144.49	55.51
	+60	2.0	0.44	0.11		+60	2.0	9.45	3.65
		0.125	0.21	0.02			0.125	5.44	2.30

6.1.3. Experimental failure modes

Failure of testing specimens occurred in two modes: brittle fracture of glass or delamination of the interlayer. The crucial factor affecting the type of failure was temperature. At temperatures 0 °C and 20 °C, all interlayers were stiff enough, therefore the specimens were strained by pronounced bending moment and fractured near the lap joint. At 60 °C, all interlayers, besides SG 5000, delaminated. EVA S and Trosifol BG specimens failed in both failure modes at 40 °C: 60% of EVA S specimens fractured and 40% delaminated, and 60% of Trosifol BG specimens delaminated while 40% fractured. Loading rate did not have, in general, any effect on the type of failure. Both failure modes of EVA S at 40 °C are presented in Fig. 75.

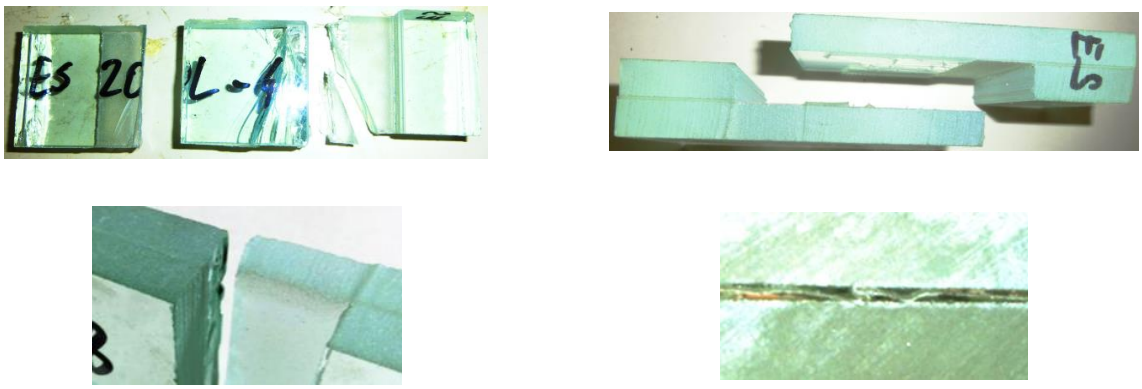

a) Specimen after brittle fracture b) Detail of delamination

Fig. 75: Failure modes of EVA S interlayer at 40 °C

In practice, the loss of interlayer´s adhesion to glass at high temperatures may occur. Average values of engineering shear strains at failure γ_{fail} are shown in Tab. 8. Strains at delamination are safely above 1% but it should be noted that small-scale experiments are not able to introduce size-effects and construction details resulting in a sudden delamination of LG in a real structure. Extreme shear stiffness of Trosifol ES at 0 °C resulted in the lowest γ_{fail} values at brittle fracture, 0.01, see Fig. 74b). On the other hand, TPU KF at 60 °C achieved the highest γ_{fail} values at delamination, 7.71, see Fig. 73f). The standard deviation values of γ_{fail} mostly increase with increasing temperature as the failure mode changed from brittle fracture to delamination.

Tab. 8: Average values of shear strain at failure with standard deviations, failure modes

Type	Tempe-rature [°C]	Average value of γ_{fail} [-]	Standard deviation [-]	Failure mode	Type	Tempe-rature [°C]	Average value of γ_{fail} [-]	Standard deviation [-]	Failure mode
Trosifol BG	0	0.029	0.01	B.F.	EVA S	0	0.320	0.02	B.F.
	+20	1.437	0.80	B.F.		+20	0.813	0.12	B.F.
	+40	3.457	0.62	B.F./DEL.		+40	1.393	0.12	B.F./DEL.
	+60	4.827	1.10	DEL.		+60	0.839	0.06	DEL.
Trosifol ES	0	0.010	0.01	B.F.	TPU KF	0	0.261	0.05	B.F.
	+20	0.094	0.08	B.F.		+20	0.979	0.17	B.F.
	+40	1.895	0.36	B.F.		+40	1.799	0.67	B.F.
	+60	1.894	0.70	DEL.		+60	7.711	1.39	DEL.
EVA L	0	0.794	0.27	B.F.	SG 5000	0	0.040	0.09	B.F.
	+20	3.453	0.91	B.F.		+20	0.014	0.01	B.F.
	+40	5.406	0.78	B.F.		+40	0.016	0.01	B.F.
	+60	6.493	2.30	DEL.		+60	1.367	0.99	B.F.

Note: B.F. = Brittle fracture of glass; DEL. = Delamination of the interlayer

6.2. Dynamic single-lap shear tests of small-scale specimens

To express the shear stiffness of interlayers in time and temperature domain using TTSP, series of Dynamic mechanical thermal analysis (DMTA) of small-scale specimens in shear were carried out. The word "dynamic" has in this context no relation with inertia effects. Shear stress and strain of the interlayer are herein assumed as engineering values.

6.2.1. Test setup and evaluation of results

DMTA was performed using identical specimens and testing equipment as in static single-lap shear tests, including load assembly, metal jaws, climatic chamber, etc. An exception makes the loading device MTS 500B which enabled the cyclic loading of interlayer and two temperature sensors Pt 100 glued directly to the glass surface for precise monitoring of specimen´s temperature. Testing equipment is in Fig. 76. To apply low temperatures in the chamber, liquid nitrogen stored in Dewar vessel was blown directly into the chamber, see the running DMTA test in Fig. 77b). Numbers of testing specimens with testing conditions are shown in Tab. 9. Frequency and temperature range were governed by the limits of testing device and by the stiffness of the interlayer.

Tab. 9: Summary of testing specimens and loading conditions of DMTA

Interlayer	Thickness [mm]	Total number of specimens	Temperature range [°C]	Frequency [Hz]
Trosifol BG	1.50	6	< -5; +40 >	< 0.05; 4.95 >
Trosifol ES	0.85	3	< +25; +45 >	< 0.05; 4.95 >
EVA L	0.63	6	< -10; +50 >	< 0.05; 4.95 >
EVA S	0.81	6	< -5; +50 >	< 0.05; 4.95 >
SG 5000	1.01	6	< +25; +70 >	< 0.05; 4.95 >
TPU KF	0.82	6	< -5; +50 >	< 0.05; 4.95 >

a) Hydraulic MTS 500B device

b) Temperature sensor Pt 100

c) Climatic chamber with metal jaws

d) MTS loading cylinder

e) Temperature in the chamber (red) and on the specimen (black) during DMTA

f) Detail of testing specimen with the temperature sentors Pt 100

Fig. 76: Testing equipment used for DMTA testing

a) Specimen in metal jaws

b) Specimen in the climatic chamber and Dewar vessel with nitrogen

Fig. 77: DMTA of small-scale specimens

As soon as the specimen was fixed into the metal jaws, it was tempered at the testing temperature and prestressing tensile force F_s in the range of 1.2 kN to 1.5 kN was applied. The value of prestressing force assured the specimen not to fall out from jaws during cycling. The individual cycling was displacement controlled. Applied frequency of cycling was gradually increasing from 0.05 Hz to 4.95 Hz with a step of 0.05 Hz. Duration of prestressing force between the individual cycles was 10 s, totally 99 cycles at constant temperature were applied. Loading schema of cycling in time is shown in Fig. 78. As soon as all 99 cycles were over, the temperature was shifted upwards for 5 °C, the specimen was sufficiently tempered (for at least 10 min), and new set of cycling at new shifted temperature was launched.

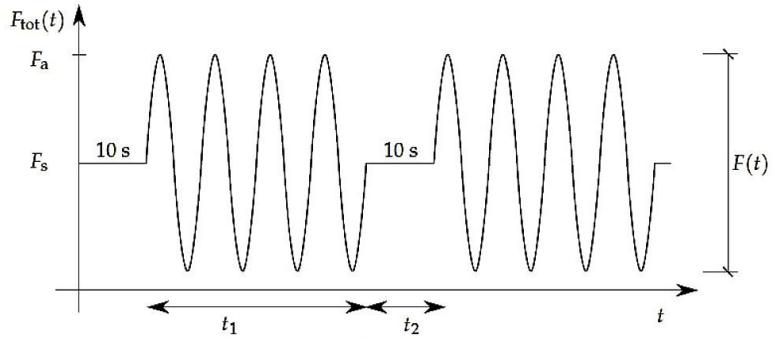

Fig. 78: Time course of DMTA: time t_1 – displacement controlled one loading cycle at one certain constant frequency, time t_2 – force controlled experiment between the individual cycles

The amplitude of MTS loading cylinder displacement during cycling u_{max} was set in the range of 0.17 mm - 0.20 mm. The prestressing force and displacement of the loading cylinder caused total shear strain γ_{tot} and shear stress τ_{tot} of the interlayer (see performance of interlayer in loading Fig. 72b)) written as

$$\gamma_{tot}(t) = \gamma(t) + \gamma_s\,, \tag{44}$$

$$\tau_{tot}(t) = \tau(t) + \tau_s\,, \tag{45}$$

where γ(t) and τ(t) represent the dynamic shear strain and stress. They are related to cylinder displacement. The static shear strain γ_s and stress τ_s are related to prestressing force F_s. In each cycle, the dynamic shear strain of the interlayer induced by loading cylinder, was prescribed as

$$\gamma(t) = \gamma_{max}\ \cdot \sin(\omega \cdot t)\,, \tag{46}$$

where ω [rad/s] is the loading angular velocity, t [s] is the instantaneous time in each cycle, and γ_{max} is the amplitude of the dynamic shear strain caused by amplitude of MTS cylinder displacement u_{max}. The corresponding dynamic shear stress of interlayer follows

$$\tau(t) = F(t)/A\,, \tag{47}$$

where A is the shear area of 50 × 50 mm, and F(t) is measured dynamic force, see Fig. 78.

To express the dynamic shear stress output from dynamic shear strain input, Boltzmann principle was applied, see Eq. (24). The evaluation of this integral Eq. (24) for shear yields [20]

$$\begin{aligned}\tau(t) &= \int_0^t G(t-t')\cdot\omega\cdot\gamma_{max}\cdot\cos(\omega\cdot t')\,dt' = \\ &= G^*(\omega)\cdot\gamma(t) = \gamma_{max}\cdot[G'(\omega)\cdot\sin(\omega\cdot t) + G''(\omega)\cdot\cos(\omega\cdot t)] = \tau_{max}\ \cdot\sin(\omega\cdot t+\delta)\,,\end{aligned} \tag{48}$$

where G^* is the dynamic complex shear modulus [Pa] with the real part (stored energy in cycle – storage modulus G') and imaginary part (loss of energy in cycle – loss modulus G''), see Fig. 34. Eq. (48) shows there is a certain phase shift δ between stress τ(t) and strain γ(t) which expresses the rate of material viscosity (δ = 0 means elastic material, $\delta = \pi/2$ means purely viscous material).

The dynamic shear stress-strain relation of one cycle is plotted through the viscoelastic loop in Fig. 79a).

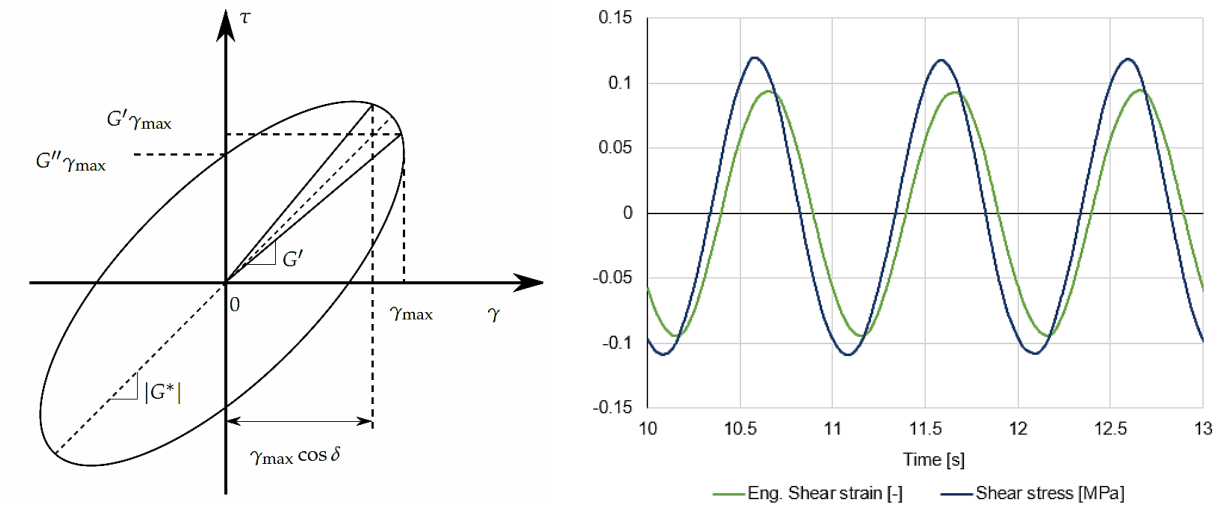

a) Viscoelastic stress-strain loop of one loading cycle

b) Time course of shear stress and shear strain, Trosifol BG (frequency 1 Hz, +40 °C)

Fig. 79: Viscoelastic loop and time course of stress and strain from DMTA for Trosifol BG, dynamic parts

Viscoelastic loop shows important points which serve for the evaluation of dynamic complex shear modulus G^* with storage and loss moduli G' and G'' which were, in the next part of thesis, used for evaluation of interlayer´s shear modulus $G(t, T)$. The slope of the loop indicates the value of G^*. When $\omega \cdot t = \pi/2$, γ_{max} is achieved, see Eq. (46), then $\tau(t = \pi/2\omega) = G' \cdot \gamma_{max}$. When $t = 0$, shear strain $\gamma = 0$ and $\tau(t = 0) = G'' \cdot \gamma_{max}$. Moduli $G^*(\omega)$, $G'(\omega)$, and $G''(\omega)$ were evaluated from each viscoelastic loop. Representative viscoelastic loops for all interlayers tested at 40 °C and 1 Hz are in Fig. 80. The example of dynamic shear strain input and stress output in time during DMTA of Trosifol BG loaded at 40 °C by 1 Hz is shown in Fig. 79b). It can be seen, there is a certain time shift Δt between both quantities, $|\Delta t| = |\delta/\omega|$, which documents the viscoelastic nature of the interlayer and correctness of Eq. (48).

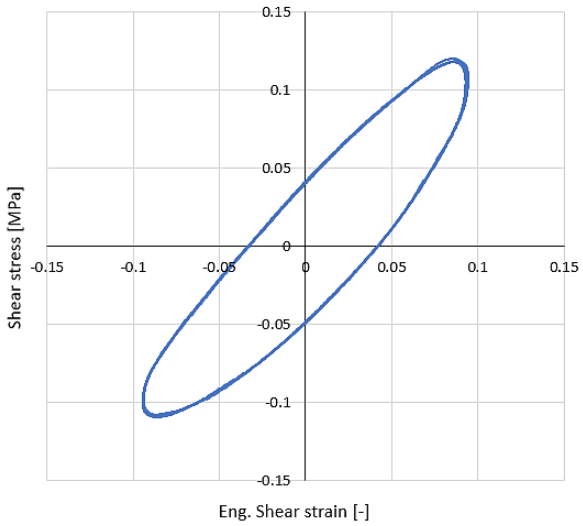

a) Trosifol BG

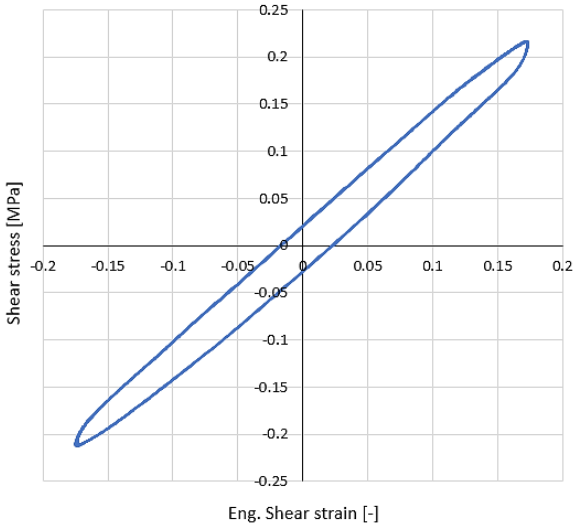

b) EVA L

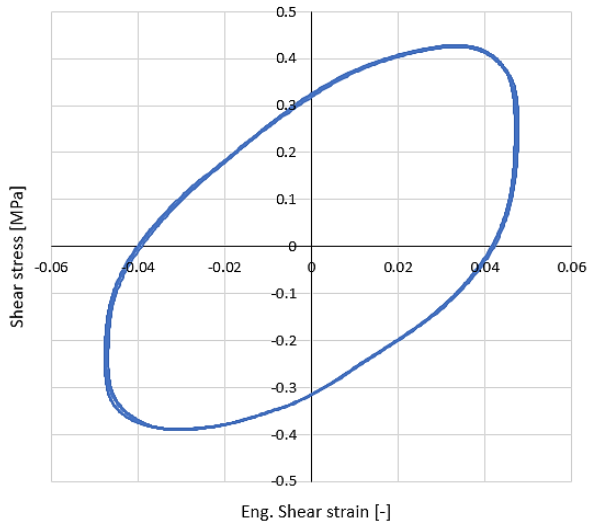

c) Trosifol ES

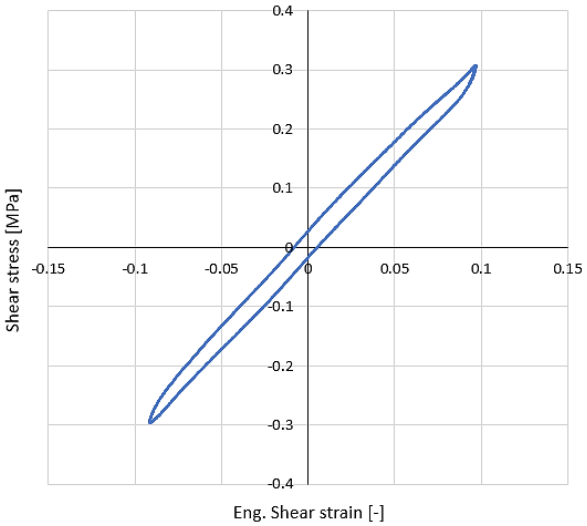

d) EVA S

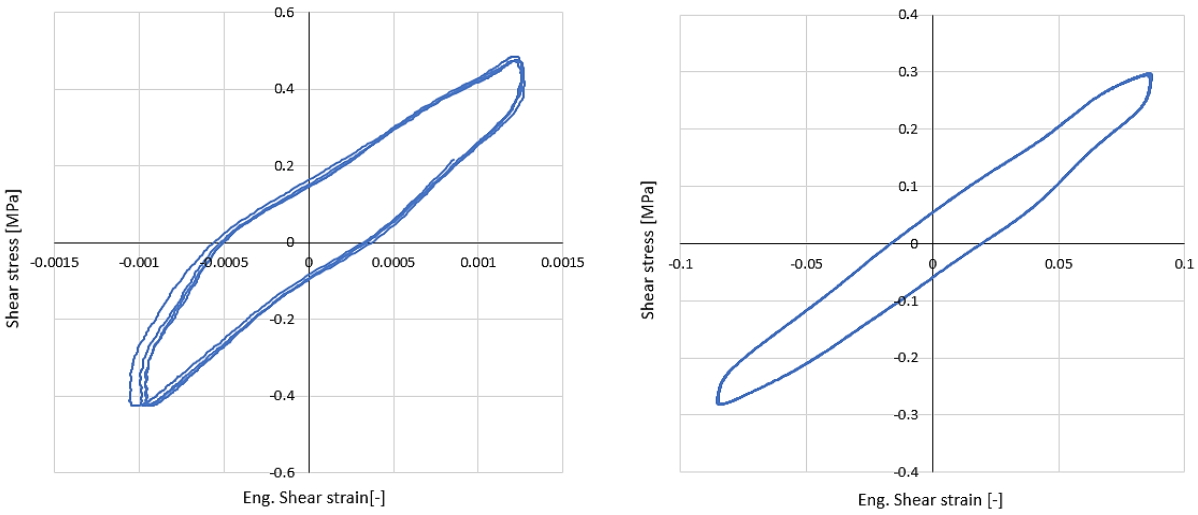

e) SG 5000 f) TPU KF

Fig. 80: Experimental viscoelastic loops from DMTA of all tested interlayers at 1 Hz and +40 °C

6.2.2. Validation of linear viscoelasticity

Prior to DMTA testing, the legitimacy of the theory of linear viscoelasticity was verified. Since the experimental results were, in the sequel, used for M-W Prony series identification, it was necessary to verify the linear viscoelastic limit of strain loaded interlayer was not exceeded, meaning its shear modulus G(t, T) given by M-W model being independent of strain amplitude γ_{max}. Shear storage and loss moduli of M-W model, see section 2.4.3, loaded by sinusoidal shear strain input in Eq. (46), are then [26]

$$G'(\omega) = G_\infty + \sum_{i=1}^{M} \frac{G_i \cdot \omega^2 \cdot \theta_i^2}{1 + \omega^2 \cdot \theta_i^2}, \tag{49}$$

$$G''(\omega) = \sum_{i=1}^{M} \frac{G_i \cdot \omega \cdot \theta_i}{1 + \omega^2 \cdot \theta_i^2}, \tag{50}$$

where $\{G_\infty, G_i,$ and $\theta_i\}$ are shear M-W Prony series, and M is the number of Maxwell models in parallel. Both storage and loss moduli in Eqs. (49) and (50) are only angular velocity dependent and the values of G_∞ and G_i are constants. This means both moduli G' and G'' were derived using Boltzmann principle for a linear system and, therefore, fitted M-W model holds for a linear viscoelastic region. Following Kraus et al. [33], the specimen was at constant frequency of 1 Hz and at constant temperature loaded by oscillatory loading where the amplitude of cylinder displacement u_{max} was varied from 0.05 mm to 0.25 mm with a step of 0.01 mm which covers the experimental range. Prestressing force F_s between the cycles was still in range of 1.2 kN and 1.5 kN. As soon as the slope of experimental viscoelastic loop remains constant while increasing u_{max}, the dynamic complex shear modulus G^*, with G' and G'' moduli, is only frequency dependent and the interlayer is in the linear viscoelastic region [33]. Experimental relations G^* vs. u_{max} for all interlayers at representative temperatures are shown in Fig. 81. Testing temperature was governed

by T_g of tested interlayers. The choice $T > T_g$ at DMTA ignited potential presence of viscoelastic nonlinearity [33].

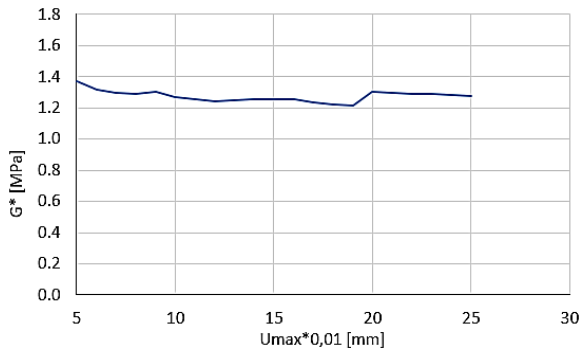

a) Trosifol BG +40 °C

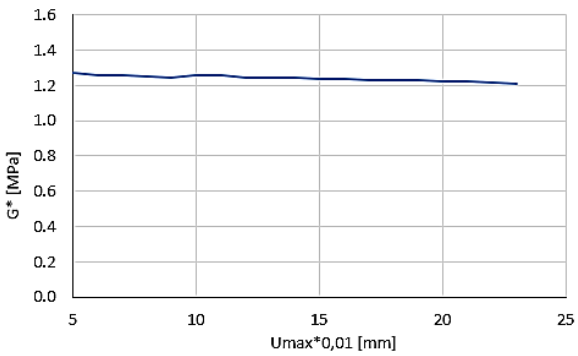

b) EVA L +45 °C

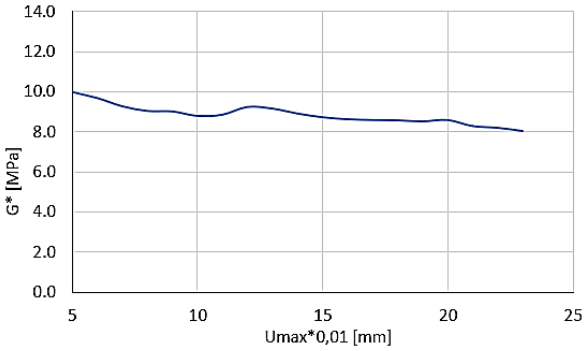

c) Trosifol ES +40 °C

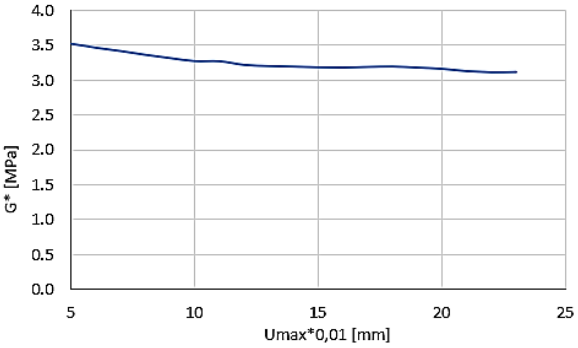

d) EVA S +45 °C

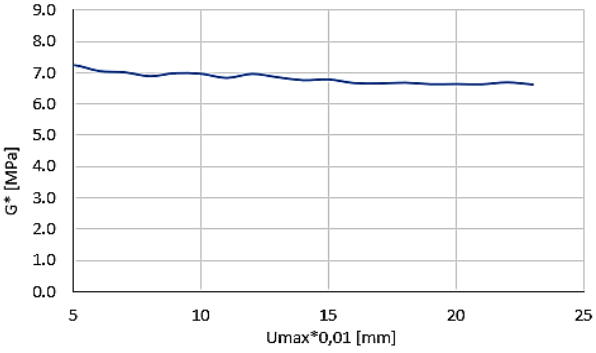

e) SG 5000 +65 °C

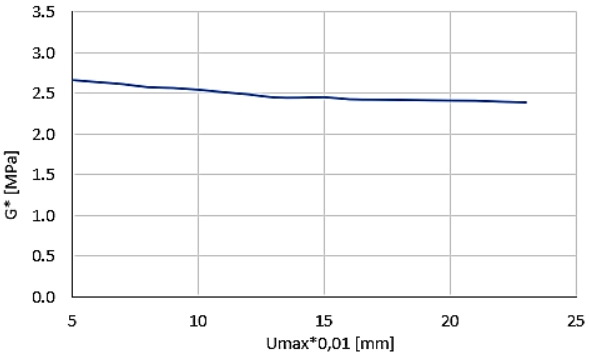

f) TPU KF +50 °C

Fig. 81: Check on linear viscoelasticity for plotted amplitudes of cylinder displacement u_{max} at 1 Hz and at representative temperatures, dynamic shear modulus G^* vs. MTS cylinder displacement amplitude u_{max}

Seeing G^* vs. u_{max} relations, dynamic shear modulus remains almost constant in tested interval of u_{max} for all interlayers. Hence, it is assumed the linear viscoelastic limit was not exceeded and DMTA results can be used for the Prony series identification of M-W model in a linear viscoelastic region.

6.2.3. Representative experimental relations and summary of results

Experimental complex dynamic shear modulus G^* - frequency f relations in the range of testing temperatures, for one representative specimen of each interlayer, are plotted in Fig. 82. As stated before, plotted values of G^* in graphs and tables indicate the slope of viscoelastic stress-strain loop at frequency f in Fig. 79a). Complete sets are in the attachment. Relations for all interlayers have one common phenomenon – the value of G^* increases with decreasing temperature or increasing frequency input. Considering frequency input being proportional to the loading rate and temperature affecting the molecular rearrangement of the polymer, DMTA results are, in the sense of stiffness, analogous with results from static shear shear tests in section 6.1. If one considers the approximate relation between shear storage modulus and relaxation modulus suggested by Schwarzl [37] $G'(f) \sim G(t = 1/f)$ and equation $G^* = G' + iG''$, all DMTA experimental relations meet the assumption of decreasing shear stiffness modulus G while temperature or time of static load increase.

Significant growth of stiffness for Trosifol BG was recorded between 25 °C and 10 °C and for Trosifol ES between 40 °C and 25 °C, when crossing their glass transition zones. Testing temperature below T_g, see Tab. 4, meant stiff response of both PVB´s meaning the noise of the data, see Fig. 82a) and b). When these two figures get overlapped, one can see that Trosifol ES responded in a stiffer manner than Trosifol BG. Narrow interval of testing temperatures for Trosifol ES was governed by sudden delamination at 45 °C and stiff glass-like response at 25 °C meaning no sense of testing at lower temperatures.

Average measured numerical values of G^*, G', and G'' for both PVB´s are shown in Tab. 10 and in Tab. 11. Shear storage modulus G' in both cases forms major part of complex modulus and the loss of interlayer´s internal energy as a heat in each cycle, given by G'', was suppressed. Taking the stress-strain phase angle δ as a rate of material viscosity and relation $\tan \delta = G''/G'$ [23], the elastic behaviour predominates over viscous for both PVB´s. Assuming phase angle δ being proportional to the "width" of viscoelastic loop [20] means Trosifol BG showed "more rate of elasticity" than Trosifol ES, e.g., at 40 °C and 1 Hz: $\delta_{BG,\ 40\ °C} = 0.002$ and $\delta_{ES,\ 40\ °C} = 0.004$, see Fig. 80a) and c).

Experimental relations of both EVA based interlayers illustrate gradual growth of stiffness with decreasing temperature which means both were in the rubbery state. Whether comparing their representative experimental relations and their average numerical values of $G^*(f)$ plotted in Tab. 12 and Tab. 13, it becomes noteworthy, EVA S was stiffer than EVA L. Since both acted as a flexible rubber, no data noise was recorded, see Fig. 82c) and d). Average numerical values of

G^*, G', and G'' for both EVA´s plotted in Tab. 12 and Tab. 13 show, shear storage modulus was dominant over loss modulus meaning low rate of material viscosity.

TPU KF stiffened considerably between 5 °C and -5 °C with a noise of the data for frequency above 1 Hz meaning the glass transition zone has been entered, see Fig. 82e). Since $T_{g,TPU\ KF}$ = -36 °C, the experiment shows the glass transition zone is a wide range interval. Average numerical values in Tab. 14 show the dominancy of shear storage modulus G' over loss modulus G'' at certain testing conditions and increasing rate of material viscosity with increasing temperature. This is illustrated, e.g., by increase of average phase angle $\delta_{-5\ °C}$ = 0.004, $\delta_{40\ °C}$ = 0.007, $\delta_{50\ °C}$ = 0.009.

Testing of SG 5000 in Fig. 82f) was specific by the temperature range. Since $T_{g,\,SG\,5000}$ = 52 °C, the tests were conducted up to 70 °C until delamination. Bottom limit of temperature range 25 °C was governed by stiff glass-like response of SG 5000 causing the noise of the data. Seeing the values of G^* stated in Tab. 15, significant loss of stiffness was recorded between 40 °C and 55 °C, when crossing the value of T_g, and the subsequent rubbery response up to 70 °C. Also, in this case, the value of storage modulus G' makes major part of dynamic complex shear modulus G^* meaning low rate of material viscosity which increases with temperature (e.g., $\delta_{25\ °C}$ = 0.005, $\delta_{70\ °C}$ = 0.007).

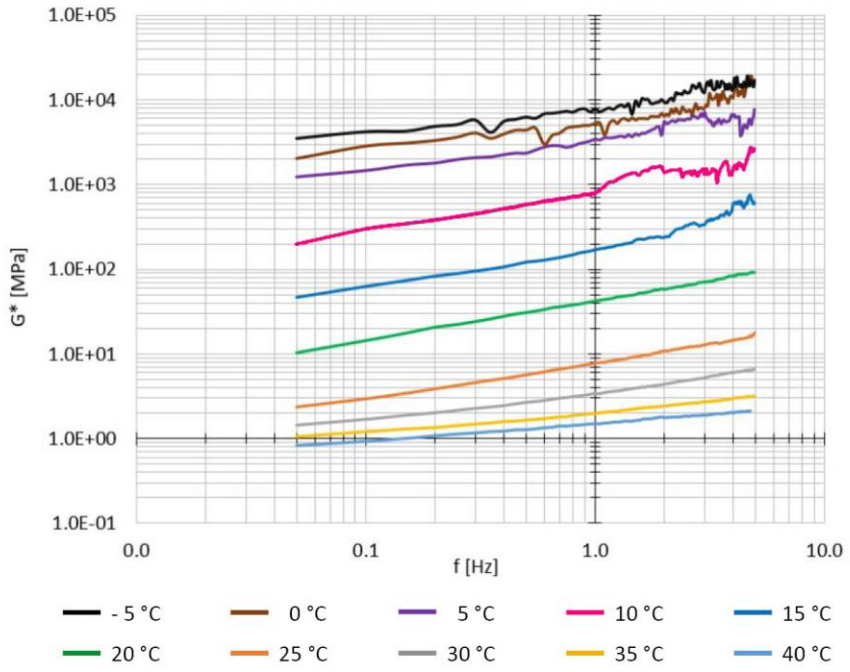

a) Trosifol BG

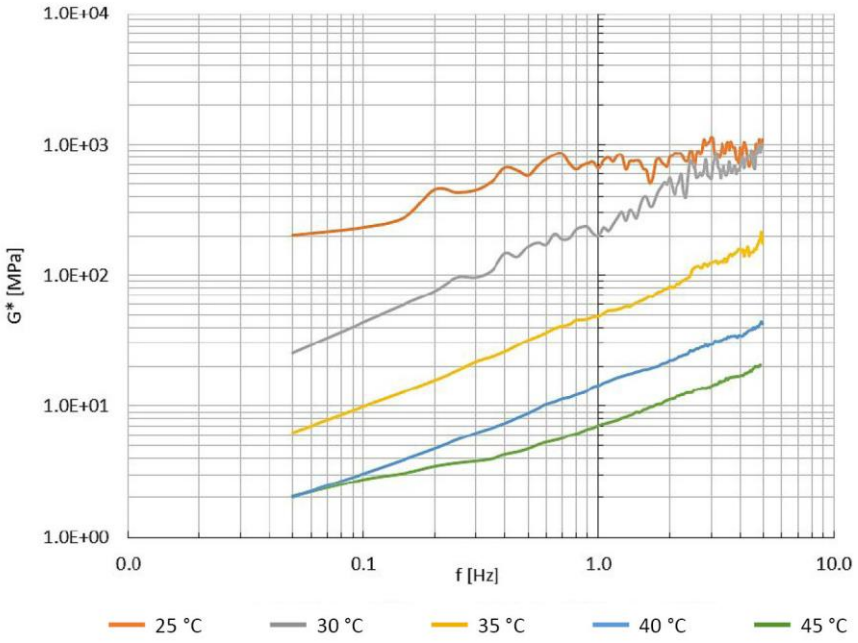

b) Trosifol ES

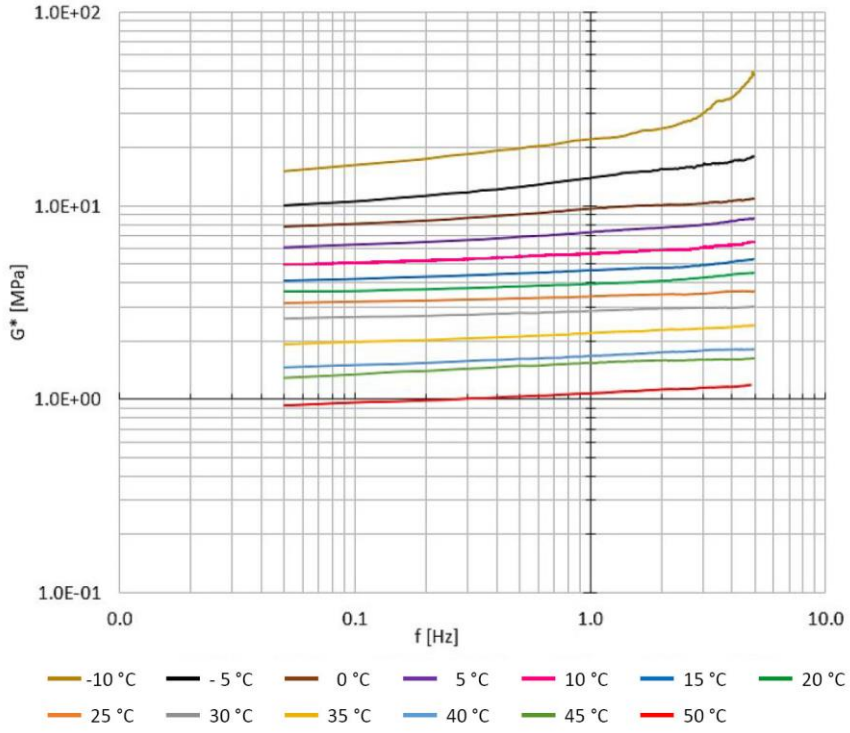

c) EVA L

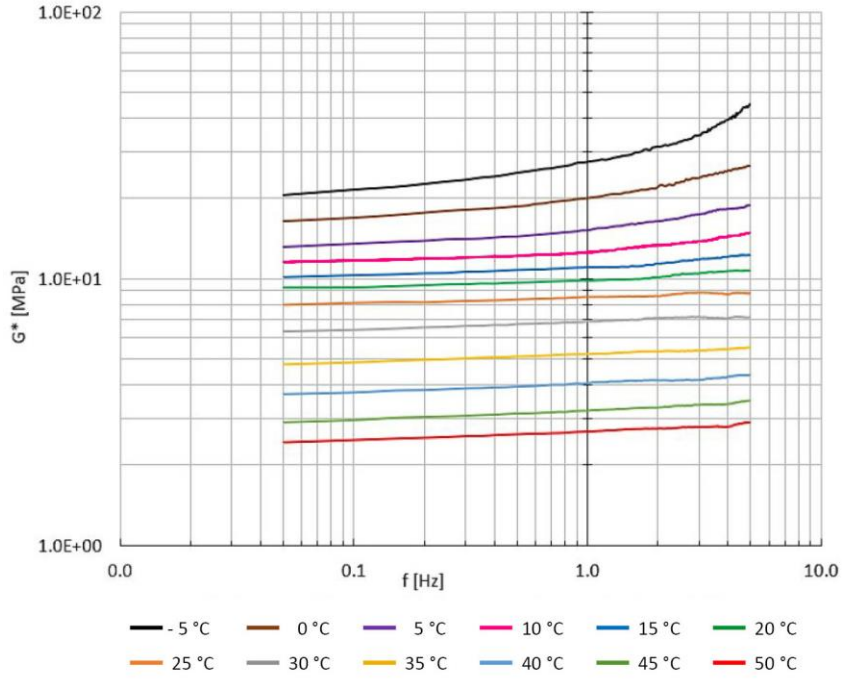

d) EVA S

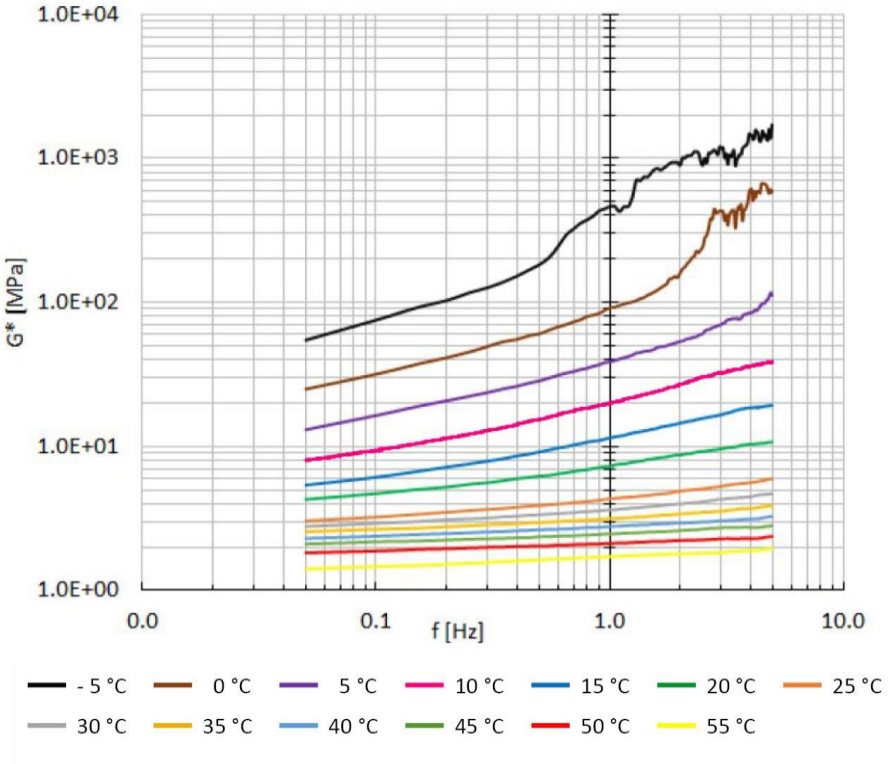

e) TPU KF

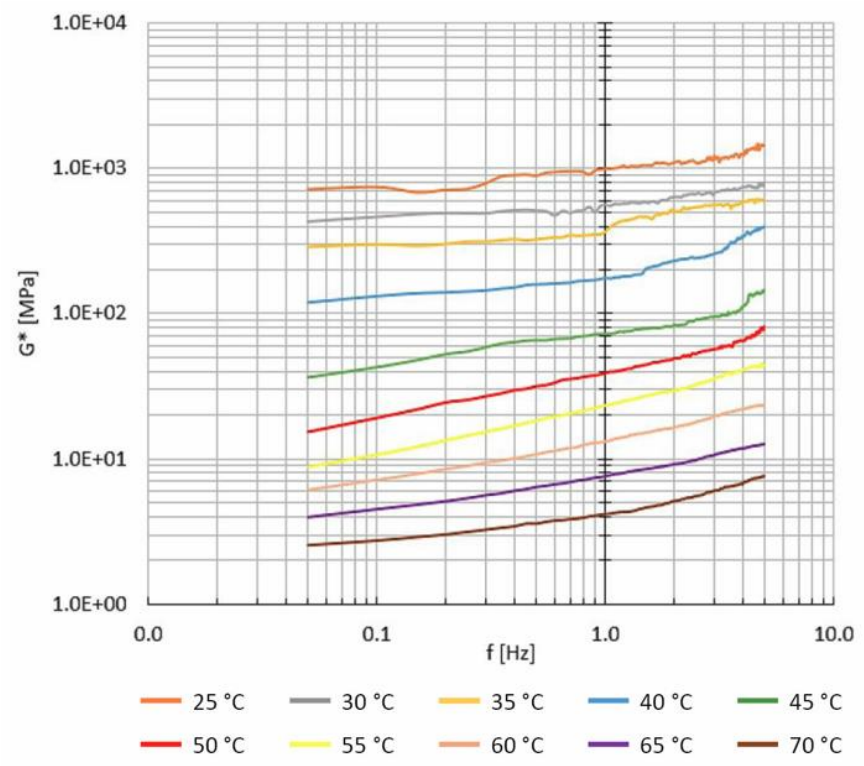

f) SG 5000

Fig. 82: DMTA experimental complex dynamic shear modulus – frequency relations of one representative specimen

Tab. 10: Average experimental values of shear dynamic complex, storage, and loss moduli of Trosifol BG

	-5 °C			0 °C			+5 °C			+10 °C		
f	G*	G'	G"	G*	G'	G"	G*	G'	G"	G*	G'	G"
[Hz]	[MPa]	[MPa]	[MPa]	[MPa]	[MPa]	[MPa]	[MPa]	[MPa]	[MPa]	[MPa]	[MPa]	[MPa]
0.05	3507.55	3507.55	1.33	2033.44	2033.44	0.44	1230.95	1230.95	0.11	136.16	136.16	0.02
0.5	6244.25	6244.23	14.96	4390.49	4390.49	1.91	2344.92	2344.92	2.17	330.40	330.40	0.69
1	7733.89	7733.87	18.13	5275.46	5275.44	15.13	3431.67	3431.61	19.00	425.94	425.93	2.63
2.5	12127.85	12127.27	117.98	7216.12	7215.79	68.51	5928.15	5927.84	61.19	820.53	820.47	7.45
4.95	17048.23	17040.76	504.56	16329.65	16327.8	240.7	7695.87	7690.74	280.9	1546.3	1545.7	42.61

	+15 °C			+20 °C			+25 °C			+30 °C		
f	G*	G'	G"	G*	G'	G"	G*	G'	G"	G*	G'	G"
[Hz]	[MPa]	[MPa]	[MPa]	[MPa]	[MPa]	[MPa]	[MPa]	[MPa]	[MPa]	[MPa]	[MPa]	[MPa]
0.05	41.30	41.30	0.01	8.80	8.80	0.00	2.56	2.56	0.00	1.50	1.50	0.00
0.5	99.11	99.11	0.07	25.85	25.85	0.07	5.93	5.93	0.01	2.75	2.75	0.01
1	132.36	132.36	0.59	34.53	34.53	0.12	8.01	8.01	0.02	3.46	3.46	0.02
2.5	226.27	226.25	2.76	52.21	52.21	0.55	12.02	12.02	0.15	4.81	4.81	0.04
4.95	369.95	369.85	8.42	71.45	71.44	1.55	16.59	16.59	0.36	6.41	6.41	0.16

	+35 °C			+40 °C		
f	G*	G'	G"	G*	G'	G"
[Hz]	[MPa]	[MPa]	[MPa]	[MPa]	[MPa]	[MPa]
0.05	1.13	1.13	0.00	0.80	0.80	0.00
0.5	1.77	1.77	0.00	1.20	1.20	0.00
1	2.12	2.12	0.01	1.38	1.38	0.01
2.5	2.73	2.73	0.02	1.67	1.67	0.02
4.95	3.32	3.32	0.06			

Tab. 11: Average experimental values of shear dynamic complex, storage, and loss moduli of Trosifol ES

	+25 °C			+30 °C			+35 °C			+40 °C		
f	G*	G'	G"	G*	G'	G"	G*	G'	G"	G*	G'	G"
[Hz]	[MPa]	[MPa]	[MPa]	[MPa]	[MPa]	[MPa]	[MPa]	[MPa]	[MPa]	[MPa]	[MPa]	[MPa]
0.05	127.93	127.93	0.01	23.19	23.19	0.00	6.21	6.21	0.00	2.25	2.25	0.00
0.5	295.47	295.47	0.66	70.16	70.16	0.17	27.87	27.87	0.04	8.06	8.06	0.01
1	339.68	339.68	1.65	98.18	98.18	0.17	42.30	42.30	0.13	12.46	12.46	0.03
2.5	490.63	490.58	5.46	143.99	143.98	1.24	76.41	76.41	0.82	21.15	21.15	0.19
4.95	611.78	611.52	17.80	346.57	346.47	8.17	121.5	121.5	2.23	31.70	31.69	0.61

	+45 °C		
f	G*	G'	G"
[Hz]	[MPa]	[MPa]	[MPa]
0.05	2.11	2.11	0.00
0.5	4.73	4.73	0.01
1	7.16	7.16	0.03
2.5	13.26	13.26	0.12
4.95	20.58	20.58	0.32

Tab. 12: Average experimental values of shear dynamic complex, storage, and loss moduli of EVA L

	-10 °C			-5 °C			0 °C			+5 °C		
f	G*	G'	G"	G*	G'	G"	G*	G'	G"	G*	G'	G"
[Hz]	[MPa]	[MPa]	[MPa]	[MPa]	[MPa]	[MPa]	[MPa]	[MPa]	[MPa]	[MPa]	[MPa]	[MPa]
0.05	15.03	15.03	0.01	10.02	10.02	0.00	7.58	7.58	0.00	6.03	6.03	0.00
0.5	20.27	20.27	0.03	12.59	12.59	0.03	8.84	8.84	0.02	6.78	6.78	0.02
1	22.89	22.89	0.12	13.97	13.97	0.05	9.44	9.44	0.06	7.15	7.15	0.03
2.5	28.07	28.07	0.26	16.45	16.45	0.17	10.39	10.39	0.13	7.74	7.74	0.09
4.95	41.25	41.24	0.61	19.43	19.42	0.50	11.14	11.14	0.28	8.18	8.18	0.16

	+10 °C			+15 °C			+20 °C			+25 °C		
f	G*	G'	G"	G*	G'	G"	G*	G'	G"	G*	G'	G"
[Hz]	[MPa]	[MPa]	[MPa]	[MPa]	[MPa]	[MPa]	[MPa]	[MPa]	[MPa]	[MPa]	[MPa]	[MPa]
0.05	4.96	4.96	0.00	4.16	4.16	0.00	3.67	3.67	0.00	3.33	3.33	0.00
0.5	5.43	5.43	0.02	4.53	4.53	0.01	3.94	3.94	0.01	3.59	3.59	0.01
1	5.64	5.64	0.03	4.69	4.69	0.02	4.06	4.06	0.02	3.70	3.70	0.02
2.5	5.99	5.99	0.08	4.90	4.90	0.04	4.25	4.24	0.08	3.92	3.92	0.05
4.95	6.37	6.37	0.20	5.25	5.25	0.15	4.50	4.49	0.11	4.15	4.15	0.12

	+30 °C			+35 °C			+40 °C			+45 °C		
f	G*	G'	G"	G*	G'	G"	G*	G'	G"	G*	G'	G"
[Hz]	[MPa]	[MPa]	[MPa]	[MPa]	[MPa]	[MPa]	[MPa]	[MPa]	[MPa]	[MPa]	[MPa]	[MPa]
0.05	2.66	2.66	0.00	2.06	2.06	0.00	1.57	1.57	0.00	1.29	1.29	0.00
0.5	2.87	2.87	0.01	2.26	2.26	0.01	1.75	1.75	0.01	1.47	1.47	0.00
1	2.97	2.97	0.02	2.35	2.35	0.01	1.82	1.82	0.01	1.53	1.53	0.00
2.5	3.10	3.10	0.05	2.46	2.46	0.03	1.91	1.91	0.02	1.59	1.59	0.02
4.95	3.26	3.26	0.07	2.66	2.66	0.05	1.93	1.93	0.06	1.65	1.65	0.07

	+50 °C		
f	G*	G'	G"
[Hz]	[MPa]	[MPa]	[MPa]
0.05	1.08	1.08	0.00
0.5	1.25	1.25	0.00
1	1.31	1.31	0.01
2.5	1.37	1.37	0.02
4.95	1.54	1.54	0.05

Tab. 13: Average experimental values of shear dynamic complex, storage, and loss moduli of EVA S

	-5 °C			0 °C			+5 °C			+10 °C		
f	G*	G'	G"	G*	G'	G"	G*	G'	G"	G*	G'	G"
[Hz]	[MPa]	[MPa]	[MPa]	[MPa]	[MPa]	[MPa]	[MPa]	[MPa]	[MPa]	[MPa]	[MPa]	[MPa]
0.05	20.17	20.17	0.01	16.45	16.45	0.00	13.58	13.58	0.00	11.77	11.77	0.00
0.5	24.06	24.06	0.04	18.62	18.62	0.04	14.84	14.84	0.04	12.51	12.51	0.03
1	26.30	26.30	0.05	19.81	19.81	0.11	15.55	15.55	0.07	12.87	12.87	0.06
2.5	30.37	30.37	0.27	22.23	22.23	0.23	16.97	16.96	0.20	13.79	13.79	0.14
4.95	40.33	40.32	0.64	25.96	25.95	0.52	18.84	18.84	0.43	15.04	15.04	0.40

	+15 °C			+20 °C			+25 °C			+30 °C		
f	G*	G'	G"	G*	G'	G"	G*	G'	G"	G*	G'	G"
[Hz]	[MPa]	[MPa]	[MPa]	[MPa]	[MPa]	[MPa]	[MPa]	[MPa]	[MPa]	[MPa]	[MPa]	[MPa]
0.05	10.23	10.23	0.00	9.25	9.25	0.00	8.16	8.16	0.00	6.39	6.39	0.00
0.5	10.89	10.89	0.04	9.60	9.60	0.02	8.56	8.56	0.01	6.79	6.79	0.02
1	11.15	11.15	0.07	9.78	9.78	0.04	8.75	8.75	0.04	6.94	6.94	0.04
2.5	11.70	11.70	0.22	10.21	10.21	0.09	8.99	8.99	0.10	7.23	7.23	0.09
4.95	12.22	12.21	0.33	10.51	10.51	0.16	9.09	9.09	0.16	7.39	7.39	0.21

	+35 °C			+40 °C			+45 °C			+50 °C		
f	G*	G'	G"	G*	G'	G"	G*	G'	G"	G*	G'	G"
[Hz]	[MPa]	[MPa]	[MPa]	[MPa]	[MPa]	[MPa]	[MPa]	[MPa]	[MPa]	[MPa]	[MPa]	[MPa]
0.05	4.96	4.96	0.00	3.81	3.81	0.00	3.03	3.03	0.00	2.47	2.47	0.00
0.5	5.28	5.28	0.01	4.05	4.05	0.01	3.25	3.25	0.00	2.64	2.64	0.01
1	5.40	5.40	0.03	4.14	4.14	0.03	3.32	3.32	0.01	2.71	2.71	0.02
2.5	5.57	5.57	0.07	4.30	4.30	0.07	3.45	3.45	0.04	2.81	2.81	0.03
4.95	5.65	5.65	0.15	4.40	4.40	0.09	3.55	3.55	0.11	2.91	2.91	0.08

Tab. 14: Average experimental values of shear dynamic complex, storage, and loss moduli of TPU KF

	-5 °C			0 °C			+5 °C			+10 °C		
f	G*	G'	G"	G*	G'	G"	G*	G'	G"	G*	G'	G"
[Hz]	[MPa]	[MPa]	[MPa]	[MPa]	[MPa]	[MPa]	[MPa]	[MPa]	[MPa]	[MPa]	[MPa]	[MPa]
0.05	46.89	46.89	0.01	21.98	21.98	0.00	12.21	12.21	0.00	7.58	7.58	0.00
0.5	130.02	130.02	0.13	48.52	48.52	0.11	24.55	24.55	0.06	14.25	14.25	0.05
1	247.49	247.49	1.01	68.21	68.21	0.20	31.86	31.86	0.12	17.71	17.71	0.09
2.5	524.11	524.07	6.74	142.10	142.09	1.57	48.35	48.35	0.43	25.22	25.21	0.35
4.95	1062.73	1062.63	12.73	409.38	409.28	9.24	85.44	85.42	1.46	35.25	35.24	0.80

	+15 °C			+20 °C			+25 °C			+30 °C		
f	G*	G'	G"	G*	G'	G"	G*	G'	G"	G*	G'	G"
[Hz]	[MPa]	[MPa]	[MPa]	[MPa]	[MPa]	[MPa]	[MPa]	[MPa]	[MPa]	[MPa]	[MPa]	[MPa]
0.05	5.34	5.34	0.00	4.16	4.16	0.00	3.12	3.12	0.00	2.84	2.84	0.00
0.5	8.82	8.82	0.02	6.09	6.09	0.02	4.02	4.02	0.01	3.43	3.43	0.01
1	10.81	10.81	0.06	7.12	7.12	0.03	4.50	4.50	0.02	3.73	3.73	0.01
2.5	14.25	14.25	0.18	8.99	8.99	0.15	5.32	5.32	0.04	4.25	4.25	0.05
4.95	17.92	17.92	0.34	10.77	10.77	0.23	6.10	6.10	0.17	4.79	4.79	0.15

	+35 °C			+40 °C			+45 °C			+50 °C		
f	G*	G'	G"	G*	G'	G"	G*	G'	G"	G*	G'	G"
[Hz]	[MPa]	[MPa]	[MPa]	[MPa]	[MPa]	[MPa]	[MPa]	[MPa]	[MPa]	[MPa]	[MPa]	[MPa]
0.05	2.60	2.60	0.00	2.39	2.39	0.00	2.19	2.19	0.00	1.89	1.89	0.00
0.5	3.04	3.04	0.01	2.73	2.73	0.00	2.46	2.46	0.01	2.11	2.11	0.01
1	3.25	3.24	0.01	2.88	2.88	0.02	2.57	2.57	0.01	2.19	2.19	0.02
2.5	3.59	3.59	0.05	3.12	3.12	0.06	2.76	2.76	0.01	2.32	2.32	0.03
4.95	3.99	3.99	0.11	3.40	3.40	0.08	2.94	2.94	0.09	2.44	2.44	0.05

	+55 °C		
f	G*	G'	G"
[Hz]	[MPa]	[MPa]	[MPa]
0.05	1.41	1.41	0.00
0.5	1.63	1.63	0.01
1	1.72	1.72	0.00
2.5	1.82	1.81	0.03
4.95	1.96	1.96	0.04

Tab. 15: Average experimental values of shear dynamic complex, storage, and loss moduli of SG 5000

	+25 °C			+30 °C			+35 °C			+40 °C		
f	G*	G'	G"	G*	G'	G"	G*	G'	G"	G*	G'	G"
[Hz]	[MPa]	[MPa]	[MPa]	[MPa]	[MPa]	[MPa]	[MPa]	[MPa]	[MPa]	[MPa]	[MPa]	[MPa]
0.05	763.89	763.89	0.14	523.85	523.85	0.02	303.43	303.43	0.09	159.06	159.06	0.03
0.5	966.25	966.25	2.29	664.57	664.56	1.86	402.24	402.24	0.59	247.61	247.61	0.68
1	1059.16	1059.14	6.02	710.97	710.97	2.74	437.78	437.77	1.31	296.88	296.88	1.60
2.5	1194.03	1193.92	16.05	826.88	826.81	10.45	566.55	566.54	2.89	459.13	459.09	5.51
4.95	1321.67	1321.18	34.96	1015.07	1014.72	24.25	691.83	691.51	20.57	903.19	903.03	14.99

	+45 °C			+50 °C			+55 °C			+60 °C		
f	G*	G'	G"	G*	G'	G"	G*	G'	G"	G*	G'	G"
[Hz]	[MPa]	[MPa]	[MPa]	[MPa]	[MPa]	[MPa]	[MPa]	[MPa]	[MPa]	[MPa]	[MPa]	[MPa]
0.05	36.80	36.80	0.00	15.56	15.56	0.00	9.16	9.16	0.00	5.89	5.89	0.00
0.5	68.06	68.06	0.15	32.44	32.44	0.07	18.98	18.98	0.03	10.78	10.78	0.03
1	80.11	80.11	0.39	40.21	40.21	0.18	24.03	24.03	0.11	13.30	13.30	0.06
2.5	117.34	117.33	1.33	54.58	54.58	0.35	33.04	33.04	0.28	18.10	18.09	0.31
4.95	195.17	195.12	3.91	87.26	87.23	2.26	45.67	45.66	0.86	23.30	23.30	0.46

	+65 °C			+70 °C		
f	G*	G'	G"	G*	G'	G"
[Hz]	[MPa]	[MPa]	[MPa]	[MPa]	[MPa]	[MPa]
0.05	3.83	3.83	0.00	2.72	2.72	0.00
0.5	6.31	6.31	0.02	3.91	3.91	0.01
1	7.70	7.70	0.04	5.07	5.07	0.03
2.5	10.27	10.27	0.13	6.54	6.54	0.08
4.95	13.12	13.11	0.35	8.44	8.44	0.24

6.3. Four-point bending destructive tests of large-scale specimens at one loading rate

To verify the performance of large-scale double LG panels with selected PVB and EVA interlayers using different types of glass, series of four-point bending tests according to EN 1288-3 [51] were performed. Large-scale specimens are shown in Fig. 67a).

6.3.1. Test setup

Four-point bending destructive tests using 100kN MTS testing machine were performed. Numbers of testing specimens with nominal dimensions are plotted in Tab. 16. Static schema of the test is shown in Fig. 83a). All experiments were controlled with constant MTS cross-head loading rate of vertical displacement 1.8 mm/min. Midspan vertical deflections *w* were measured by two displacement sensors (DS I, DS II), see Fig. 83b). Further, six strain gauges (SG) LY 11-10/120 were glued on the glass at the midspan, see Fig. 84. Applied force *F*, normal stress in glass σ, and vertical deflections *w* were monitored during the experiment.

Tab. 16: Numbers of specimens with certain type of glass laminated with PVB or EVA interlayer

Type of glass	0.76 mm Trosifol BG R20	0.76 mm Evalam 80/120
2×10 mm Float glass (FG)	5	5
2×10 mm Heat strengthened (HSG)	2	2
2×10 mm Heat toughened (HTG)	3	2

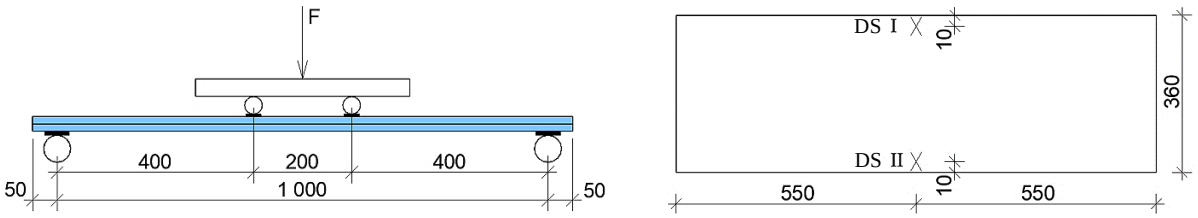

a) Static schema of the test b) Position of displacement sensors on the specimen

Fig. 83: Four-point bending tests – test schema

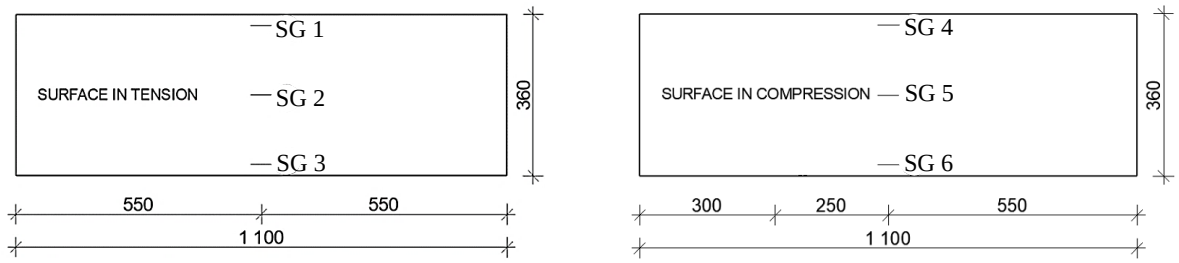

a) Lower glass ply, lower surface b) Upper glass ply, upper surface

Fig. 84: Positions of the strain gauges LY 11-10/120 on the specimen

Prior to testing, it was necessary to glue to all 114 strain gauges on the testing specimens, set the displacement sensors on the marked points, get the MTS device ready, and put the testing specimen on the supports according to schemas in Fig. 83 and Fig. 84. Pictures catching the preparation of the experiments are shown in Fig. 85. As soon as the specimen was put on the supports and all sensors were offset, the specimen was always loaded with prescribed MTS cross-head loading rate 1.8 mm/min as follows: 1st loading phase until breakage of the lower glass ply (reaching maximal force F_{max}). The specimen was then unloaded, sensors were offset, and 2nd loading phase was launched in terms of residual load bearing capacity F_{res} measurement. Temperature of glass was measured by non-contact thermometer, see Fig. 85, and was during the tests recorded in range of 19 °C to 23 °C.

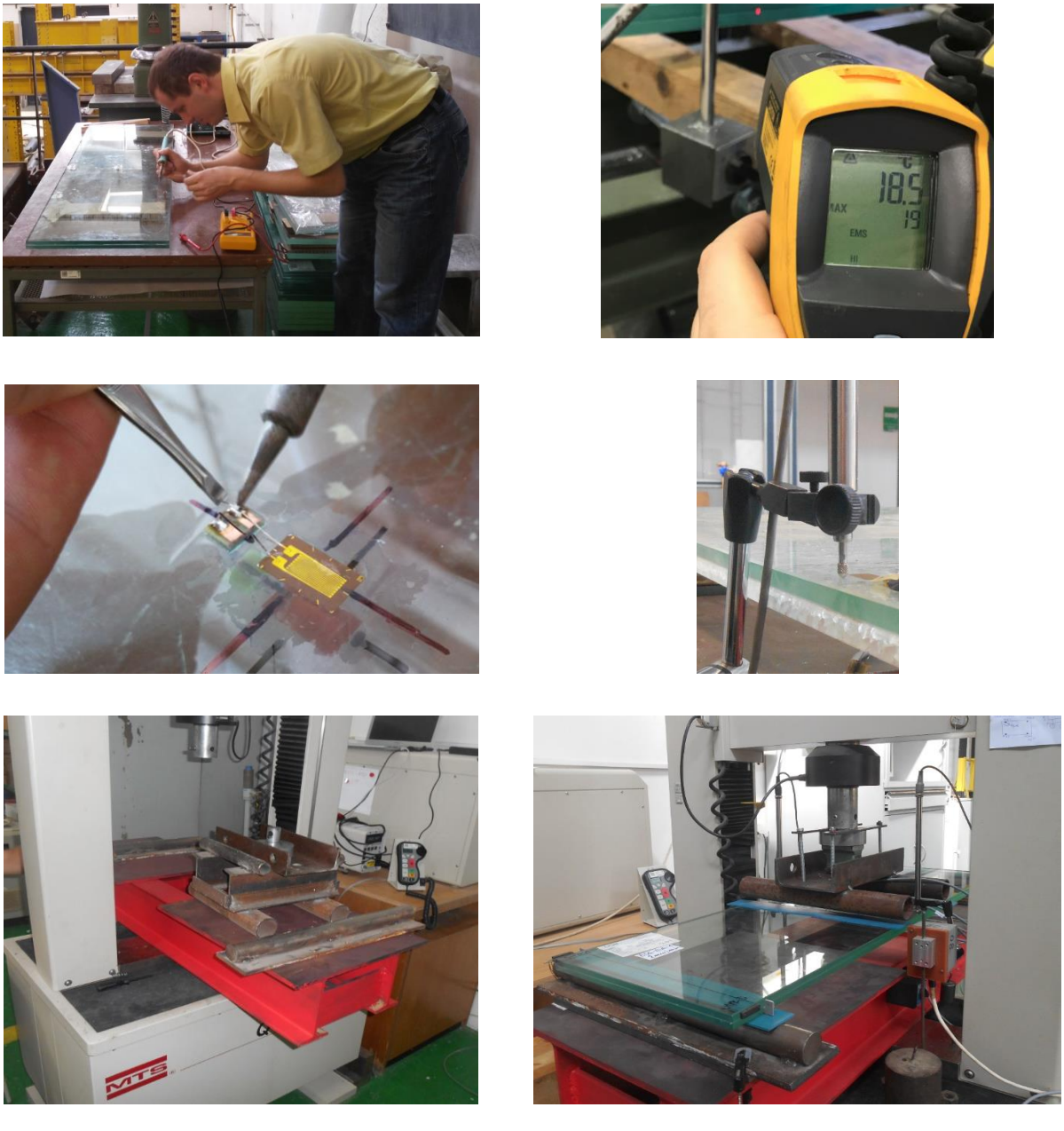

Fig. 85: Preparation of four-point bending tests

6.3.2. Summary of results – 1st loading phase

Representative experimental relations are displayed in Fig. 86. Complete set is enclosed in the attachment. These relations compare the response of HTG and FG specimens laminated with EVA L and Trosifol BG. In particular, normal stress measured by strain gauges 1 and 4 (SG 1, SG 4) and vertical deflections (average measured by displacement sensors DS I and DS II) are plotted. Seeing these charts, the interlayers did not have enough time to relax meaning almost linear experimental relations. EVA L panels were of higher bending stiffness k than panels with Trosifol BG meaning lower achieved vertical deflections at a certain value of force, e.g., $k_{HTG\text{-}EVA\ L}$ = 0.60 kN/mm and $k_{HTG\text{-}BG}$ = 0.35 kN/mm. Attributing these differences to the shear stiffness of interlayer [8], EVA L was stiffer than Trosifol BG. This fact correlates with the comparison of their initial shear moduli G_{init} at 20 °C measured on small-scale specimens in Tab. 7. Distribution of normal stress over the width of the cross section at the end of 1st loading phase for the same representative specimens plotted in Fig. 86, is shown in Fig. 87. One can see that normal stress is neither uniformly distributed along the width of the cross section, nor over the thickness of the panel. Tensile stress attains higher values near the edge of lower glass ply (SG 1, SG 3) than in the centre (SG 2). More interesting fact is that, for all specimens in Fig. 87, this tensile stress (by SG 1, SG 3) was in absolute value higher than compressive stress measured by opposite strain gauges (by SG 4, SG 6) which means glass plies were not fully shear coupled and the shear stiffness of both interlayers was probably lower than 10 MPa [68] which would also correlate with measured values of G_{init} at 20 °C in Tab. 7.

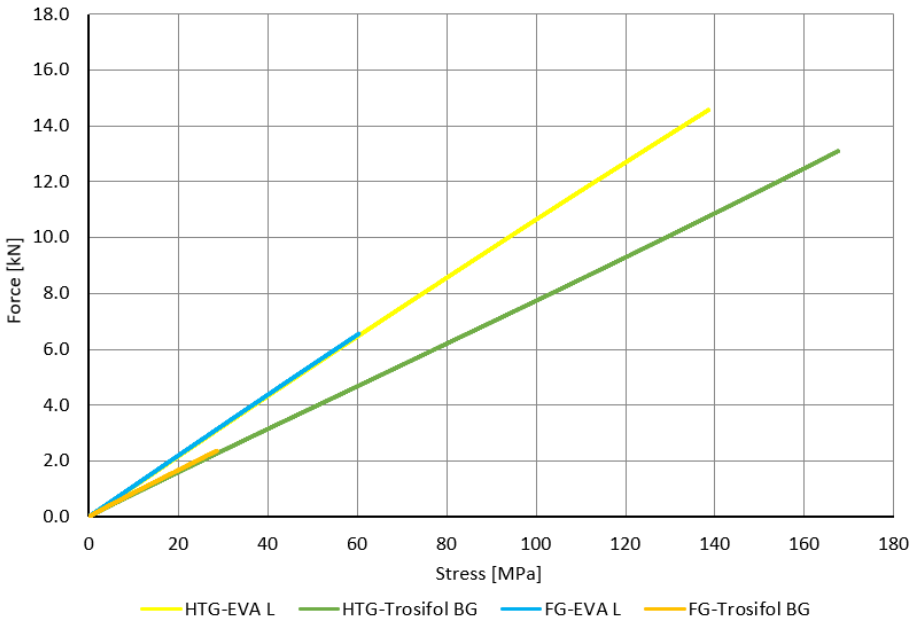

a) Normal tensile stress measured by SG 1

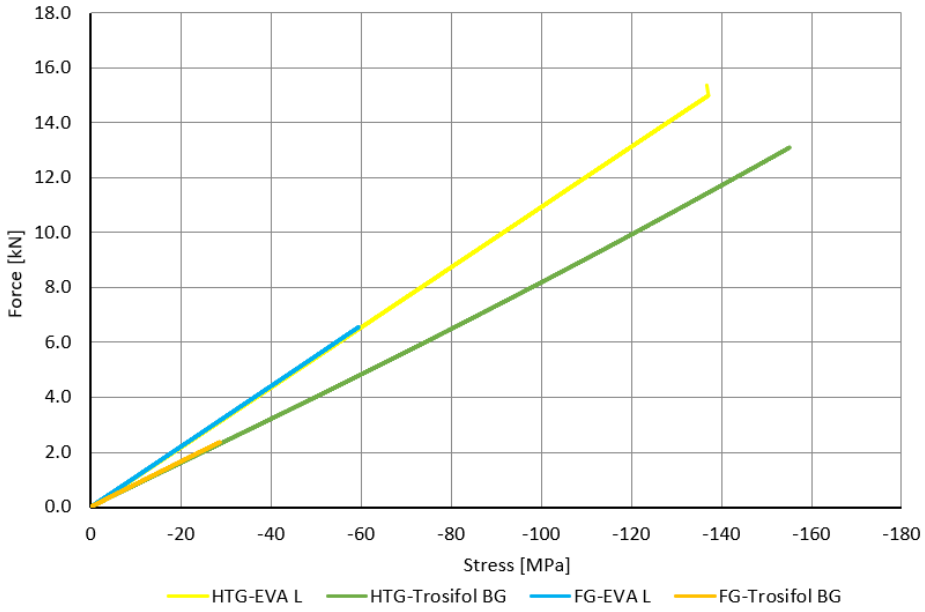

b) Normal compressive stress measured by SG 4

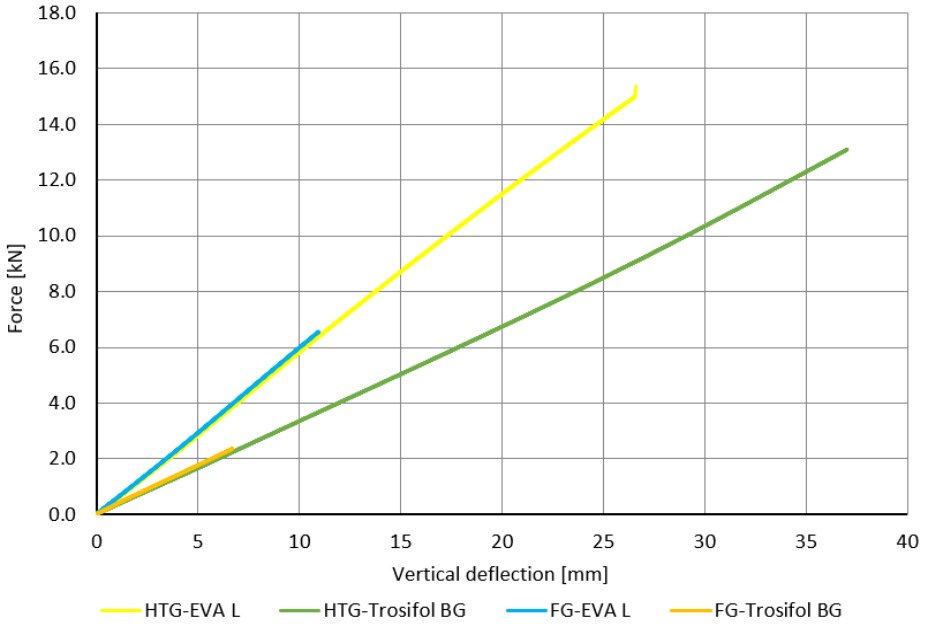

c) Vertical deflection (average by DS I and DS II)

Fig. 86: Representative experimental relations of 1st loading phase for Trosifol BG and EVA L specimens

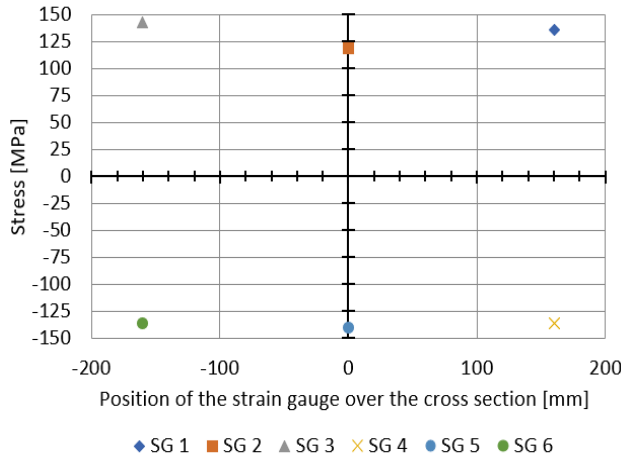

a) HTG – EVA L

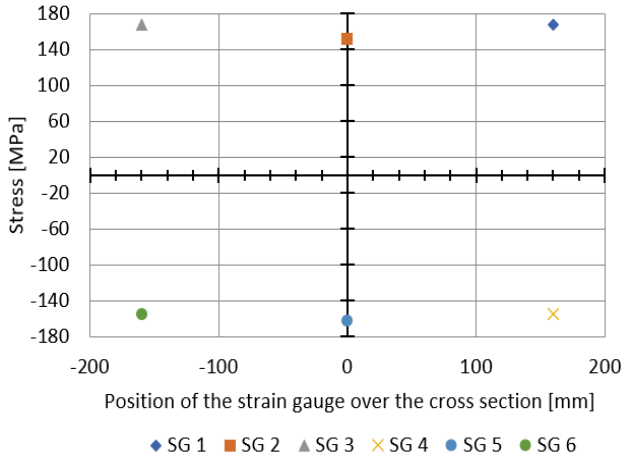

b) HTG – Trosifol BG

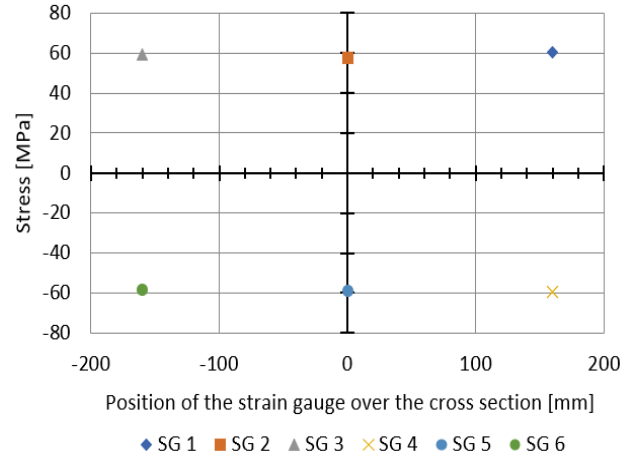

c) FG – EVA L

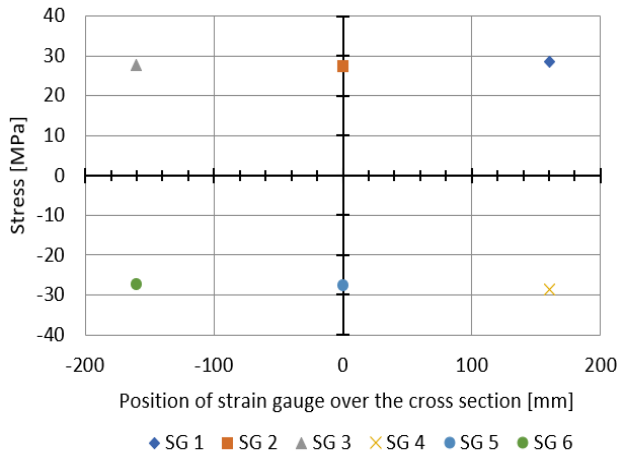

d) FG – Trosifol BG

Fig. 87: Distribution of normal stress over the specimen´s cross section at the end of 1st loading phase

Note: Bold horizontal axis displayed in these charts represents the width of the cross section (horizontal main axis of inertia), bold vertical axis then represents the vertical main axis of inertia.

Summary of average measured quantities with standard deviations at the end of 1st loading phase supplemented with bending stiffness of all specimens, shown in Tab. 17, confirms previous statements. EVA L specimens were, in average, of higher bending stiffness than specimens with Trosifol BG. This is well documented, e.g., by lower absolute values of normal stress and deflections of EVA L measured at higher applied force in comparison to Trosifol BG specimens made of HTG, see the values in bold in Tab. 17. This means EVA L interlayer was stiffer than Trosifol BG [8]. Different average values of normal stress measured by opposite strain gauges over the thickness of the cross section mean the glass plies were not fully shear coupled. This fact becomes more pronounced with increasing force. Increased tensile strength of glass caused by heat treatment is, in Tab. 17, well documented by the growth of average maximum applied force F_{max}

for various types of glass with either PVB or EVA. Details of specimen´s breakage after 1st loading phase for FG and HTG are shown in Fig. 88. All pictures show glass shards are adhered to the interlayer, upper ply is still intact, and the panel warns when overloaded. This is the proof of safety.

Tab. 17: Average values and standard deviations of measured quantities at the end of 1st loading phase

Specimen	Force F [kN]	Stress SG 1 [MPa]	Stress SG 2 [MPa]	Stress SG 3 [MPa]	Stress SG 4 [MPa]	Stress SG 5 [MPa]	Stress SG 6 [MPa]	Deflection [mm]	Bending stiffness [kN/mm]
HTG-EVA L	**16.9**	**147.9**	**118.6**	**143.1**	**-136.8**	**-154.0**	**-149.0**	**29.0**	0.582
HSG-EVA L	9.4	88.2	85.9	87.3	-88.2	-87.3	-87.4	16.5	
FG-EVA L	5.5	50.5	48.8	50.0	-49.8	-48.7	-49.2	9.3	
HTG-Trosifol BG	**12.8**	**162.3**	**147.5**	**160.2**	**-149.9**	**-156.0**	**-147.0**	**35.3**	0.352
HSG-Trosifol BG	7.4	94.0	87.5	94.8	-89.1	-89.8	-88.8	21.6	
FG-Trosifol BG	4.0	43.5	46.8	43.1	-48.8	-47.9	-47.4	11.6	

Specimen	F √Var [kN]	SG 1 √Var [MPa]	SG 2 √Var [MPa]	SG 3 √Var [MPa]	SG 4 √Var [MPa]	SG 5 √Var [MPa]	SG 6 √Var [MPa]	Deflection √Var [mm]
FG-EVA L	1.10	9.94	9.55	10.12	9.82	9.63	9.77	1.73
HTG-Trosifol BG	0.34	5.30	4.39	5.74	4.65	6.45	5.39	1.43
FG-Trosifol BG	1.15	9.81	13.82	10.22	14.46	14.77	14.23	3.54

Note: Standard deviations are stated for at least 3 specimens in the certain category, bending stiffness $k = F_{max}/w_{max}$

a) Testing specimen made of FG laminated with Trosifol BG, shards are adhered to the interlayer

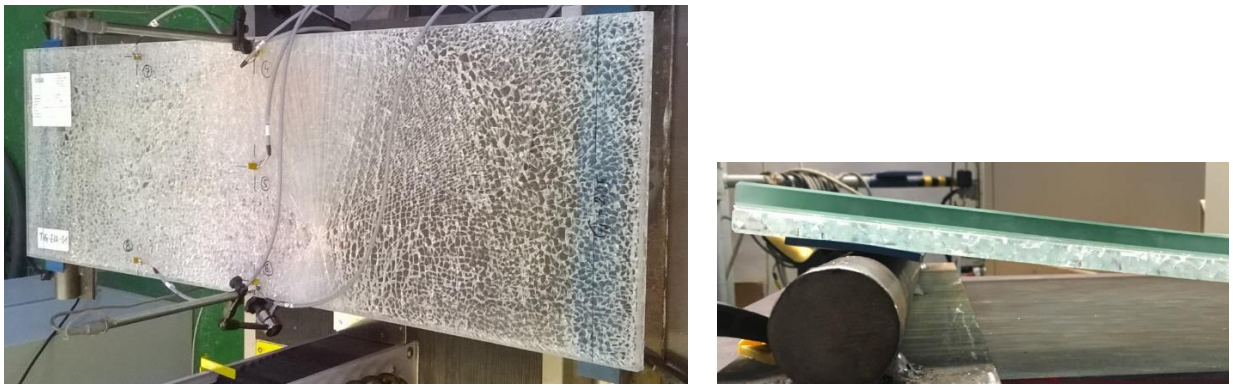

b) Testing specimen made of HTG laminated with EVA L, shards are adhered to the interlayer

Fig. 88: Large-scale specimens after breakage of lower glass ply, end of 1st loading phase

6.3.3. Summary of results – 2nd loading phase

Both EVA and PVB interlayers enabled to load all specimens in the 2nd loading phase. Compressive normal stress measured by strain gauge SG 4 and vertical deflections (average measured by displacements sensors DS I and DS II) in relation to the applied load, for the same specimens plotted in section 6.3.2, are shown in Fig. 89. There is not almost any difference in bending stiffness of specimens with respect to the type of interlayer since the load is carried solely by the upper glass ply, see Fig. 7 – 2nd phase. The main difference consists in total values of residual load bearing capacity F_{res} which is governed by the type of glass as documented by average values of F_{res} in Tab. 18. In addition, type of used glass influences the warning effects. Thermal toughening of glass means HTG achieves much higher, visible deflections than FG, see the comparison of deflections before total failure in Fig. 90.

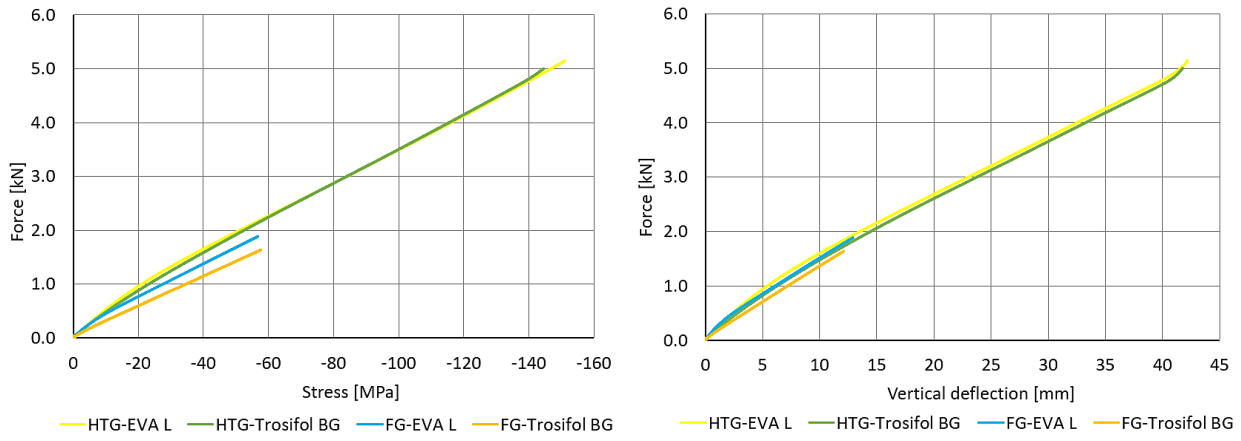

a) Normal stress by SG 4 b) Vertical deflection (average by DS I and DS II)

Fig. 89: Midspan relations of the same representative specimens as in section 6.3.2, 2nd loading phase

Tab. 18: Average values and standard deviations of residual load bearing capacity for certain type of glass

Type of glass	Residual load bearing capacity F_{res} [kN]	Standard deviation √Var [kN]
HTG	6.3	1.52
HSG	3.8	0.98
FG	1.9	0.41

a) FG right before total failure, no warning effects given by deflection

b) HTG right before total failure warns with visible deflections

Fig. 90: Comparison of warning effects before total failure regarding the type of glass

The behaviour of the specimen after total failure was governed by the type of glass. FG and HSG broke into large shards being able to resist the compressive stress. Interlayer was active in tension and upper ply in compression, see Fig. 7 – 3rd phase, therefore the specimens did not fall down the supports, see Fig. 91a) and b). HTG broke into very small shards in the entire volume. This fact, in combination with negligible flexural stiffness of interlayers, meant HTG specimens fell down the supports, see Fig. 91c). Both Trosifol BG and EVA L interlayers after total failure kept the shards adhered in a similar fashion without significant loss of shards mass.

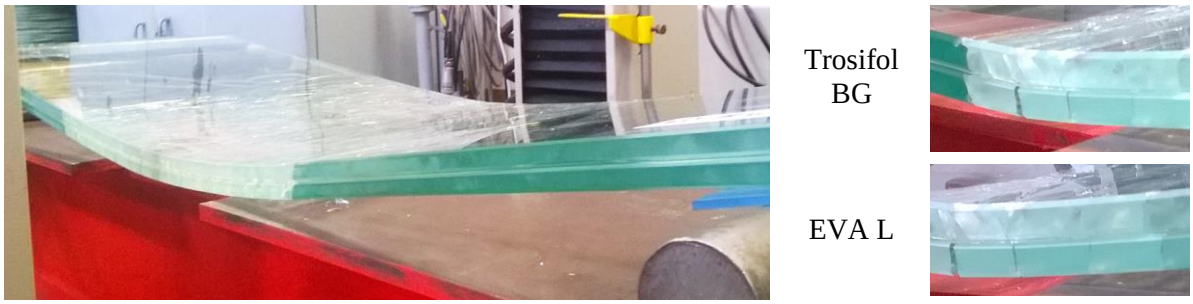

a) Float glass (FG), specimen still on the support after total failure

b) Heat strengthened glass (HSG), specimen still on the support after total failure

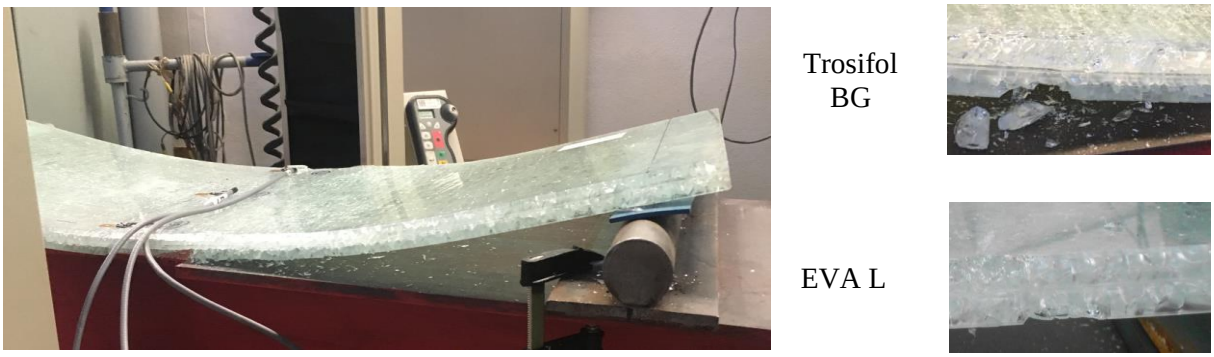

c) Heat toughened glass (HTG), specimen fell down the support after total failure

Fig. 91: Comparison of specimen´s behaviour after total failure using different types of glass

6.4. Four-point bending destructive tests of large-scale specimens at various loading rates

To verify the influence of the loading rate on the response of large-scale specimens and to compare the performance of EVA, PVB, and ionomer interlayers after total failure of the specimen, series of their four-point bending destructive tests in 3 various loading rates were performed. For that purpose, all specimens were made of heat toughened glass (HTG).

6.4.1. Test setup

All tests were performed using identical testing equipment as in four-point bending destructive tests in section 6.3. Static and loading schema, positions of displacement sensors (DS I, DS II) and strain gauges (SG 1 – SG 6) were also the same as in section 6.3. Tested specimens were laminated with Trosifol BG, EVA L, and SG 5000 interlayers. Tests were controlled with MTS cross-head vertical displacement. Load was again applied in two loading phases: 1st phase until breakage of lower glass ply (then unloaded) and 2nd phase until total failure of the specimen. The main aspect of these tests was MTS cross-head vertical displacement prescribed, in 1st phase, in three various loading rates such as 2.0 mm/min, 0.5 mm/min, and 0.125 mm/min. These loading rates were chosen the same as in case of small-scale static single-lap shear tests in section 6.1. Loading rate was kept constant during the entire loading phase. Applied force F, normal stress σ, and vertical deflection w at the midspan were monitored. Temperature of glass was during the tests recorded by non-contact thermometer between 19 °C and 24 °C. Numbers of specimens with nominal dimensions and with prescribed loading rates in 1st loading phase are shown in Tab. 19.

Tab. 19: Numbers of testing specimens tested in certain loading rates of cross-head vertical displacement

Type of interlayer	Type of glass	2.0 mm/min	0.5 mm/min	0.125 mm/min
0.76 mm Trosifol BG	2×10 mm HTG	3	3	3
0.76 mm EVA L	2×10 mm HTG	3	3	3
0.89 mm SG 5000	2×10 mm HTG	3	4	4

6.4.2. Summary of results – 1st loading phase

Experimental relations, particularly tensile stress by strain gauge SG 3 and vertical deflection (average given by displacement sensors DS I and DS II) of representative specimens, are shown in Fig. 92. Decrease of the loading rate enabled relaxation of PVB and EVA interlayers. It resulted in the growth of vertical deflections and tensile stress in glass at certain value of force. Relaxation effects were the most pronounced in case of Trosifol BG specimens where the experimental relations are well recognizable, see Fig. 92a). Contrary, SG 5000 specimens were loading rate insensitive, the interlayer did not relax by the change of the loading rate and the experimental relations almost overlap, see Fig. 92c). To show the effect of loading rate on measured quantities, Tab. 20 is provided. Left part shows midspan tensile stress and vertical deflections for the certain value of force. The growth of tensile stress and vertical deflections for Trosifol BG specimens loaded by 10 kN, to 35%, illustrates the relaxation effects of this interlayer were significant. EVA L specimens showed less apparent relaxation effects by lower increase of both measured quantities at 12 kN, to 8%. In case of SG 5000 specimens, no increase of stress and deflections by change of the loading rate was recorded. Above mentioned facts are supported by the average values of maximal force, maximal deflections, and bending stiffness of all specimens from one certain loading rate category in right part of Tab. 20. The experiments proved the load duration (loading rate) as an important aspect in case of Trosifol BG specimens by change of these quantities, whereas low relaxation of SG 5000 interlayer meant that average maximal force, maximal deflection, and bending stiffness, were loading rate insensitive.

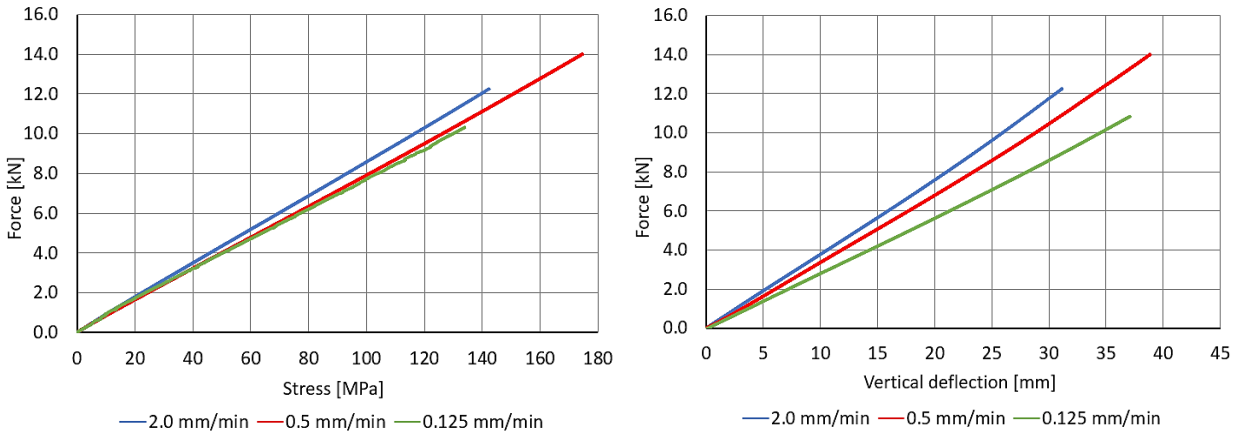

a) Trosifol BG: normal stress by SG 3 and vertical deflection (average by DS I and DS II)

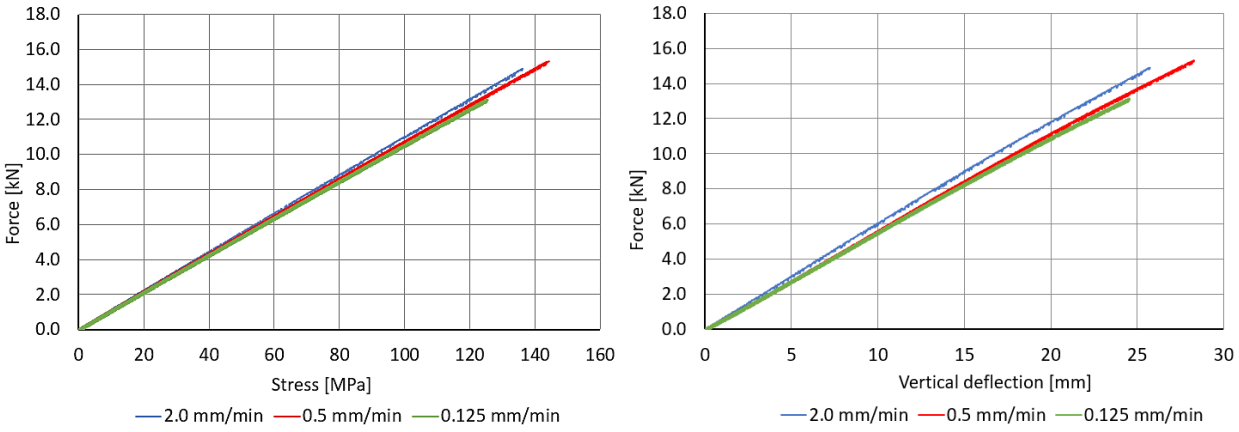

b) EVA L: normal stress by SG 3 and vertical deflection (average by DS I and DS II)

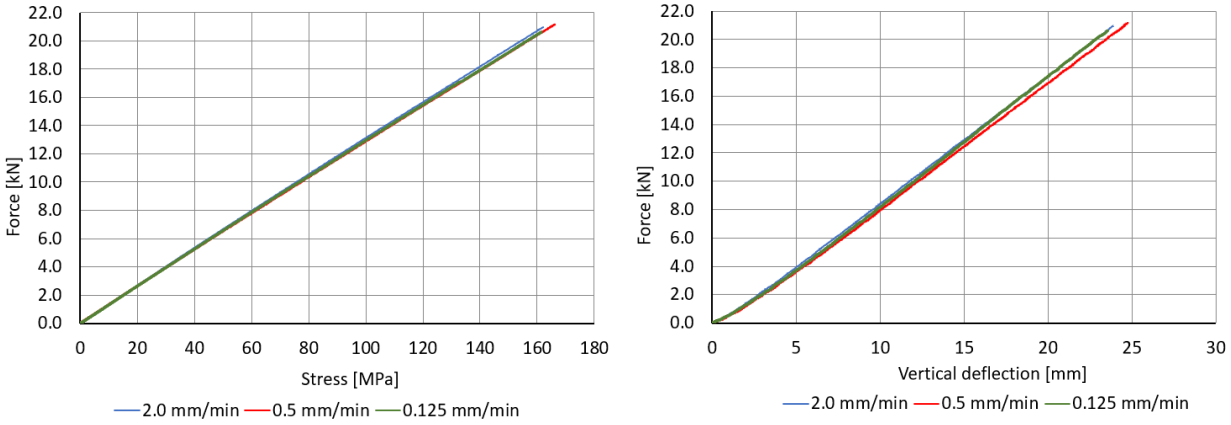

c) SG 5000: normal stress by SG 3 and vertical deflection (average by DS I and DS II)

Fig. 92: Experimental relations of representative specimens loaded in various MTS cross-head loading rates of vertical displacement in [mm/min]

Tab. 20: Summary of measured values for certain force, average measured values of entire category

Specimen	Loading rate	Stress SG3	Deflection	Max force	Max deflection	Bending stiffness	Standard deviation
VALUES FOR CERTAIN LEVEL OF APPLIED FORCE				AVERAGE VALUES OF ENTIRE CATEGORY			
[kN]	[mm/min]	[MPa]	[mm]	[kN]	[mm]	[kN/mm]	[kN/mm]
10 kN							
Trosifol BG 01	2.0	116.6	25.95				
Trosifol BG 02	2.0	117.0	25.93	13.2	33.5	0.394	0.003
Trosifol BG 03	2.0	120.7	26.79				
Trosifol BG 04	0.5	126.2	28.83				
Trosifol BG 05	0.5	126.8	29.60	12.1	35.1	0.315	0.005
Trosifol BG 06	0.5	126.3	30.05				
Trosifol BG 07	0.125	129.8	35.01				
Trosifol BG 08	0.125	130.6	36.48	10.8	38.2	0.276	0.005
Trosifol BG 09	0.125	129.8	36.10				

Specimen	Loading rate	Stress SG3	Deflection	Max force	Max deflection	Bending stiffness	Standard deviation
VALUES FOR CERTAIN LEVEL OF APPLIED FORCE				AVERAGE VALUES OF ENTIRE CATEGORY			
[kN]	[mm/min]	[MPa]	[mm]	[kN]	[mm]	[kN/mm]	[kN/mm]
12 kN							
EVA L 01	2.0	109.5	20.47				
EVA L 02	2.0	109.9	20.77	15.8	27.9	0.565	0.009
EVA L 03	2.0	111.3	21.11				
EVA L 04	0.5	112.4	21.66				
EVA L 05	0.5	115.8	21.56	15.1	27.7	0.545	0.001
EVA L 06	0.5	110.8	21.36				
EVA L 07	0.125	116.1	22.00				
EVA L 08	0.125	xxx	21.31	13.3	25.1	0.532	0.004
EVA L 09	0.125	114.9	22.36				
20 kN							
SG 5000 01	2.0	155.58	23.15				
SG 5000 02	2.0	154.43	22.86	21.1	23.5	0.872	0.008
SG 5000 03	2.0	156.43	22.87				
SG 5000 04	0.5	156.79	23.44				
SG 5000 05	0.5	156.88	23.01	20.5	23.9	0.857	0.008
SG 5000 06	0.5	157.84	23.28				
SG 5000 11	0.5	156.08	23.68				
SG 5000 07	0.125	156.47	22.83				
SG 5000 08	0.125	20 kN not achieved		19.9	23.0	0.865	0.009
SG 5000 09	0.125	155.72	23.13				
SG 5000 10	0.125	152.75	22.95				

Note: Stated deflections of each specimen were determined as average values obtained from DS I and DS II, bending stiffness of each specimen was calculated as: $k = F_{max}/w_{max}$

As already stated, specimens with SG 5000 were loading rate insensitive. Moreover, experiments showed this interlayer ensured full shear coupling of glass plies since the normal stress in glass measured by opposite strain gauges was, in absolute values, nearly identical during the entire loading phase. This is well illustrated by the values of normal stress given by SG 3 and SG 6 measured at specimen loaded at MTS cross-head loading rate 2.0 mm/min, see Fig. 93.

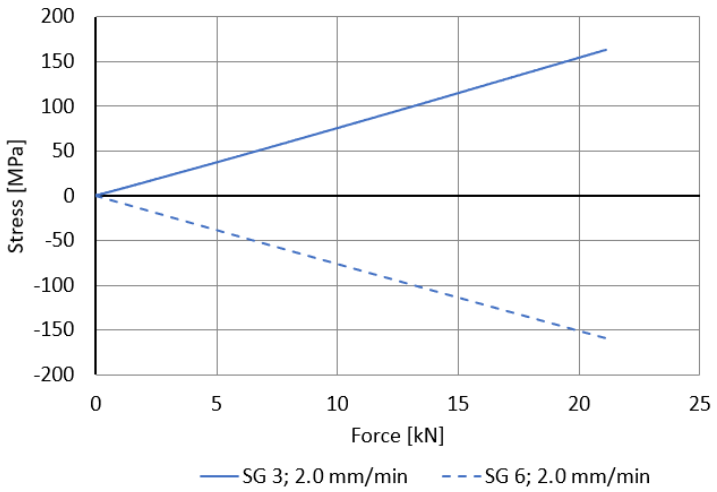

Fig. 93: Comparison of tensile and compressive normal stress in glass measured by opposite strain gauges for specimen laminated with SG 5000, specimen loaded at MTS cross-head loading rate 2.0 mm/min

6.4.3. Summary of results – 2nd loading phase

Specimens made of HTG in section 6.3.3 fell down the supports after total failure which is not desirable in a real structure. The purpose of 2nd loading phase, in this section, was to study the influence of used interlayers on the performance of HTG specimens after total failure. In scope of this, MTS cross-head loading rate, for all specimens, was prescribed as 2.0 mm/min. Comparison of specimens laminated with studied interlayers after total failure is documented in Fig. 94. Specimens with Trosifol BG fell down the support but the surface was flat with no transverse cracks. EVA L specimens also fell down the support and, in addition, the massive transverse cracks caused by tearing of EVA L were other undesirable signs of low post-breakage safety. SG 5000 specimens were rather specific. Although SG 5000 dropped noticeable mass of shards, extreme stiffness of this interlayer meant the panel was able to carry itself and even added arm load after total failure. Due to this, HTG specimens with SG 5000 after total failure were found to be much safer than those with Trosifol BG and EVA L.

a) Trosifol BG: specimens fell down the support, no transverse cracks are present

b) EVA L: specimen fell down the support with massive transverse crack over the specimen

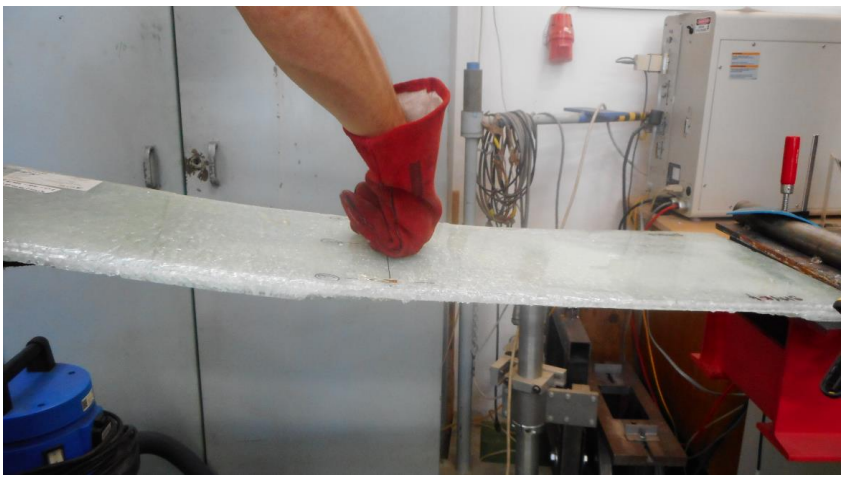

c) SG 5000: specimen stayed on the support being stiff enough to carry itself and added arm load

Fig. 94: Comparison of specimens laminated with studied interlayers after total failure

6.5. Four-point bending creep tests of large-scale specimens in the climatic chamber

To study time and temperature relaxation effects of large-scale specimens laminated with studied interlayers, sets of four-point bending creep tests in the climatic chamber, following Serafinavicius et al. [53], were performed.

6.5.1. Test setup

For creep tests, totally three large-scale specimens were used. Static and loading schema, position and marking of strain gauges as well as displacement sensors were the same as in four-point bending destructive tests in section 6.3. In addition, four temperature sensors Pt 100 glued directly on the glass, see Fig. 95a) and b), temperature compensating strain gauge to eliminate disturbing temperature effects, see Fig. 95f), and climatic chamber in Fig. 95h) were used. Total force F applied on the specimens using steel bars was 1.12 kN, see the experiment in Fig. 95c) to e). The level of load was chosen with respect to prevention of glass breakage during the test. Self-weight of the specimen was 20 kg. The specimen on the supports was conditioned in the closed chamber for at least 24 hours at testing temperature before applying the load. The chamber was then opened and the load in the form of steel bars was quickly applied. The load then acted in the closed chamber in the range of 117 h to 310 h depending on the interlayer. After unloading, the residual normal stress σ by strain gauges SG 1 – SG 6 and vertical deflections w by displacement sensors DS I and DS II were still monitored for at least 24 h. Detailed summary of testing specimens with nominal dimensions and testing conditions is plotted in Tab. 21. Testing temperature in the chamber was kept constant during the entire creep experiment, see the record of glass temperature in Fig. 95g).

Tab. 21: Summary of testing specimens tested in the creep tests in the climatic chamber

Type of interlayer	Type of glass	Number of specimens	Load duration [h]	Tested temperature [°C]
0.76 mm Trosifol BG	2×10 mm HTG	1	< 117; 163 >	+30; +40; +50
0.76 mm EVA L	2×10 mm HTG	1	< 145; 210 >	+30; +40; +50
0.89 mm SG 5000	2×10 mm HTG	1	< 145; 310 >	+30; +40; +50; +60

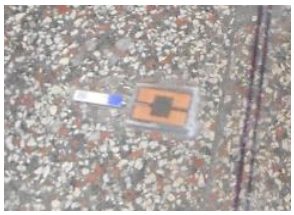

a) Pt 100 temperature sensor glued on the glass

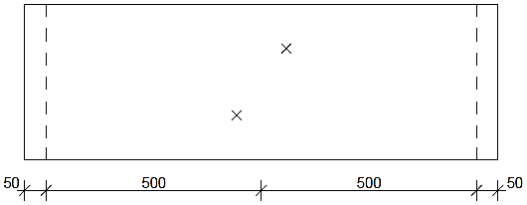

b) Position of Pt 100 sensors glued opposite to each other on both surfaces of the specimen

c) Testing apparatus in the climatic chamber

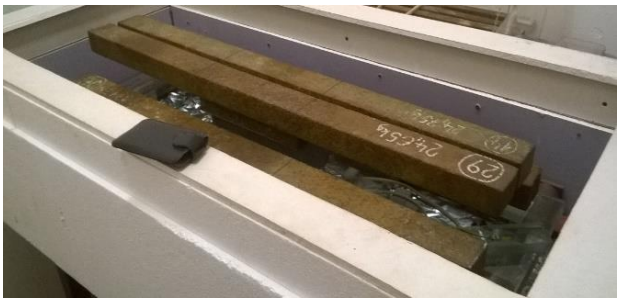

d) Real experiment in the climatic chamber

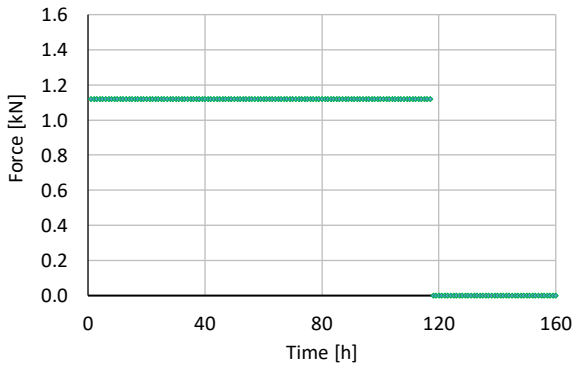

e) Example of applied load in time, Trosifol BG loaded at +40 °C

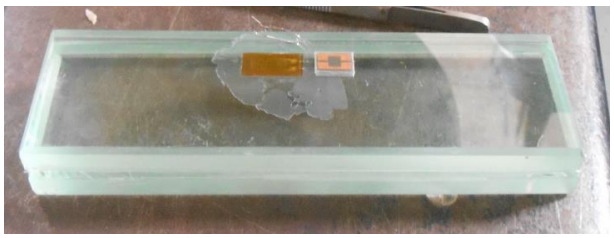

f) Compensating strain gauge glued on unloaded small-scale specimen

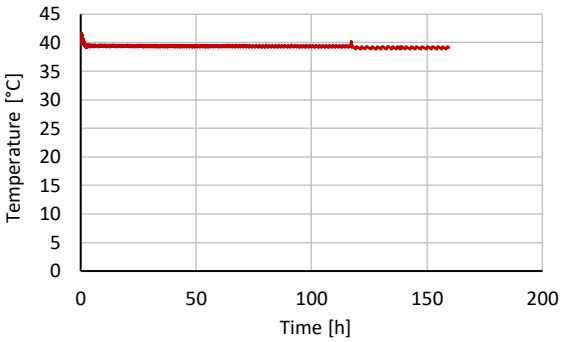

g) Temperature of glass measured by Pt 100, Trosifol BG loaded at +40 °C

h) Closed climatic chamber for creep tests ensures climatic conditions, test is running

Fig. 95: Testing equipment used for creep tests

6.5.2. Experimental results

All experimental relations from creep tests are shown in Fig. 96, particularly midspan tensile stress in glass and deflections in time. All specimens showed one common phenomenon: stress and vertical deflection increased with the load duration and with elevated temperature. This is attributed to the relaxation effects of interlayers. Comparison of stress and deflections values in time for all interlayers shows that Trosifol BG specimen attained the highest values of stress and deflections at certain fixed time and temperature. Contrary SG 5000 specimen was the stiffest with the lowest values of both quantities. Attributing these findings to the shear moduli of interlayers [8], they are ordered as follows: $G_{BG}(t, T) < G_{EVA\,L}(t, T) < G_{SG\ 5000}(t, T)$ in the tested time and temperatures range.

Measured stress and deflections of Trosifol BG have rising tendency at 30 °C and 40 °C. At 50 °C, there is an asymptotic course in time. It seems the relaxation process at 50 °C had passed completely after approx. 80 h and the shear stiffness was then negligible. Specimen at all testing temperatures achieved residual stress and deflections after unloading which is attributed to viscoplastic strains present in this thermoplastic interlayer.

EVA L specimen showed rising stress and deflections during the entire loading phase meaning continuous relaxation of interlayer. Very low 3% cross-link density of EVA L caused the occurrence of residual stress and deflections due to viscoplastic strains of EVA.

Time relations of SG 5000 specimens at loading phase at 30 °C and 40 °C were asymptotic. Author attributes this phenomenon to ion cross-link of this interlayer not allowing for the development of viscoplastic strains. Noticeable growth of both stress and deflections was recorded between 40 °C and 50 °C when crossing the glass transition zone of SG 5000. Unloading at 30 °C and 40 °C is characterized by both stress and deflection approaching zero asymptote due to ion cross-link contribution. Unloading at 60 °C was not recorded due to the collapse of the specimen caused by nickel-sulphide inclusion, see Fig. 97. This is typical for HTG without Heat Soak Test.

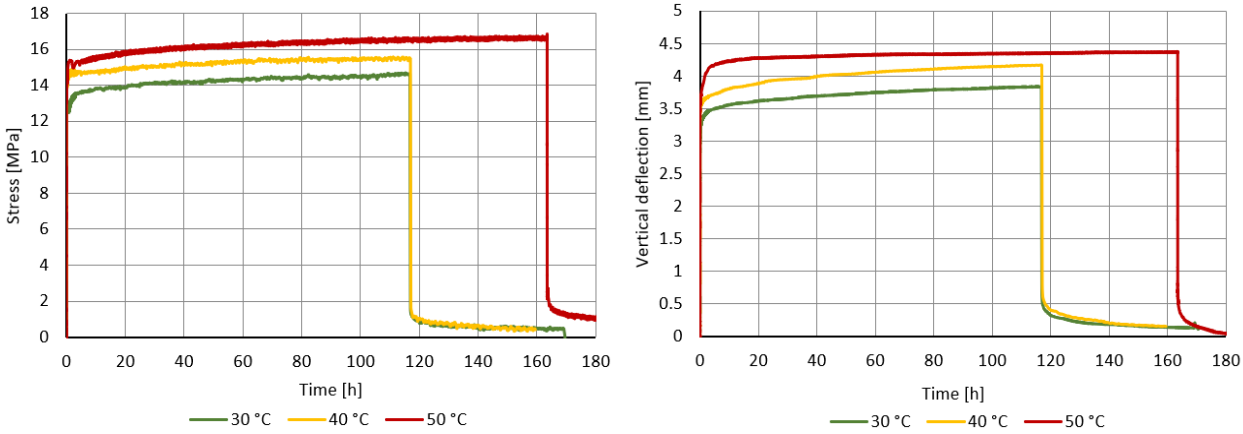

a) Trosifol BG: normal stress measured by SG 2 and deflection measured by DS I

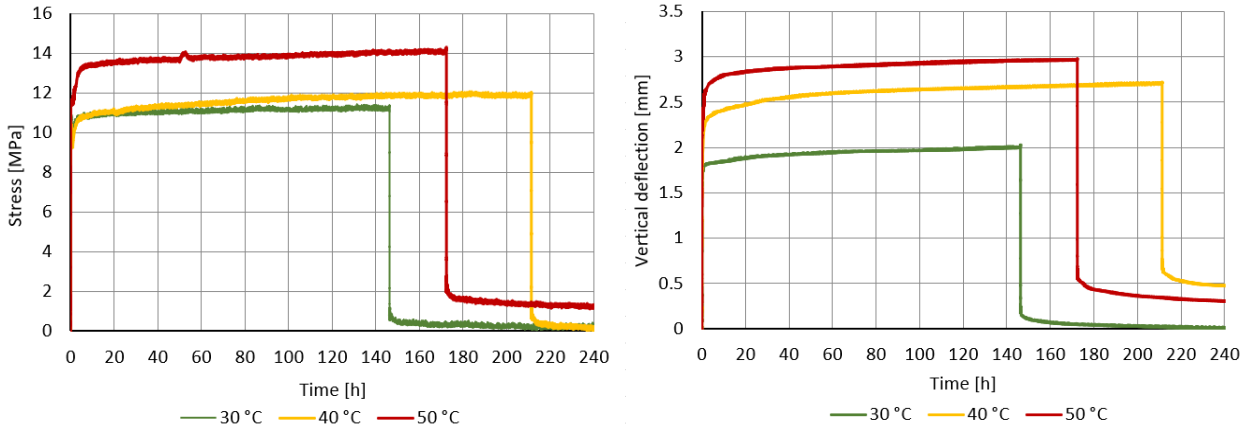

b) EVA L: normal stress measured by SG 2 and deflection measured by DS I

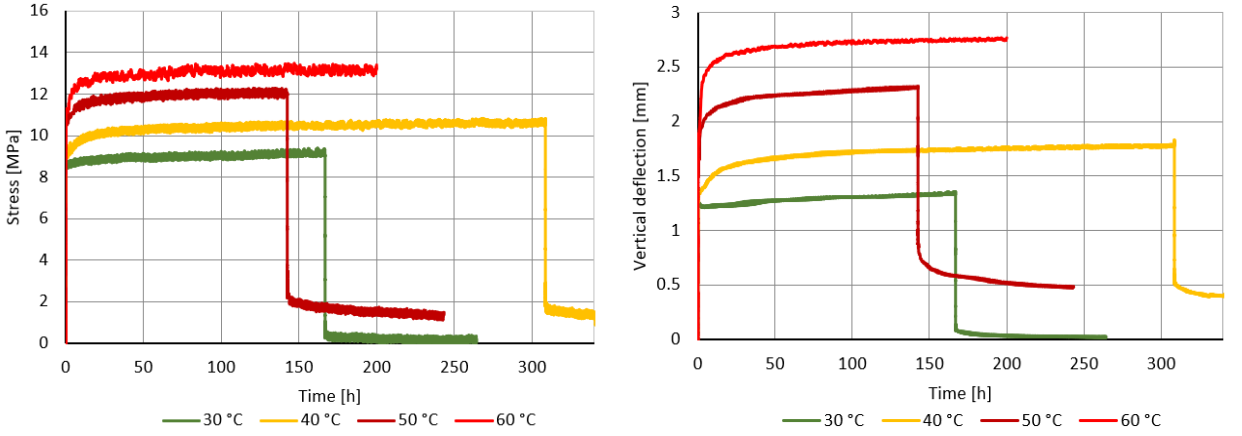

c) SG 5000: normal stress measured by SG 2 and deflection measured by DS I

Fig. 96: Experimental tensile stress and vertical deflections measured in time at creep tests

a) Abrupt collapse during the test b) Detail of nickel sulphide inclusion

Fig. 97: Abrupt collapse of loaded SG 5000 specimen at +60 °C caused by nickel sulphide inclusion

6.6. Experimental part – conclusions

In this part of the thesis, numbers of experiments with small-scale and large-scale double LG specimens were performed and evaluated. The specimens were laminated with the following interlayers: **Evalam® 80/120** and **Evasafe®** (ethylene-vinyl acetate), **Trosifol® BG R20** and **Trosifol® Extra Strong** (polyvinyl butyral), **Krystalflex® PE399** (thermoplastic polyurethane), and **SentryGlas® 5000** (ionomer based). Special attention was paid to the effect of temperature, loading rate, and load duration on the shear stiffness of studied interlayers. The main findings from experiments are concluded below.

a) Small scale single-lap shear tests

- Temperature and loading rate influence the response of all interlayers to the applied load. In particular, initial shear stiffness G_{init} decreases as the temperature increases or the load is applied more slowly. Analogously, dynamic complex shear modulus of interlayers G^* decreases with increasing temperature or decreasing frequency input.
- Shear storage modulus G' was the major component of dynamic complex shear modulus G^* of all interlayers.
- Although both EVA L and EVA S interlayers are of the same chemical base, their shear stiffness at identical loading conditions is different. The same applies for Trosifol BG and Trosifol ES interlayers.
- Delamination of interlayer at 60 °C was dominant failure mode observed at static tests.

b) Large-scale four-point bending tests

- Midspan normal stress in glass of tested EVA L and Trosifol BG specimens in destructive bending tests at room temperature was not uniformly distributed over the thickness of the cross section. In these cases, the shear coupling of glass plies was limited. Contrary, specimens with SG 5000 showed this interlayer ensured glass plies being fully shear coupled.
- The type of used interlayer in destructive tests did not influence the value of residual load bearing capacity F_{res} of the specimen in accidental situation (one glass ply broken). This value was affected solely by the type of used glass. Heat toughened glass (HTG) specimens attained the highest values of F_{res} and warned with visible deflections before total failure.
- Performance of the specimen after total failure at room temperature was influenced by the type of used glass and interlayer. Float glass (FG) and heat strengthened glass (HSG) specimens stayed on the supports regardless of the type of interlayer. Extreme stiffness of SG 5000 meant HTG panel even after total failure still had certain bending stiffness and stayed on the supports. On the other hand, HTG panels laminated with Trosifol BG and EVA L fell down the supports. Therefore, in practice, supporting structure of HTG panels laminated with these interlayers must be designed with respect to this unfavourable effect.
- Trosifol BG specimens were in destructive tests the most loading rate sensitive. Contrary, SG 5000 specimens did not show any loading rate sensitivity. This finding applies for the room temperature.
- Comparison of average bending stiffness of specimens with EVA L, Trosifol BG, and SG 5000 loaded at destructive tests at certain testing cross-head loading rate is the following: $k_{SG\,5000} > k_{EVA\,L} > k_{BG}$. Their shear moduli at room temperature can be then sorted as: $G_{SG\,5000} > G_{EVA\,L} > G_{BG}$. It meets the comparison of their initial shear moduli G_{init} from small-scale static shear experiments.
- Creep tests of specimens laminated with Trosifol BG, EVA L, and SG 5000 interlayers at 30 °C, 40 °C, and 50 °C showed the following inequalities of their shear moduli: $G_{SG\,5000} > G_{EVA\,L} > G_{BG}$. This applies for the loading time up to 120 h and stated temperatures.

At selection of tested interlayers, attention was paid to their chemical structure, particularly to the intermolecular bonding as the main aspect of stiffness in time and temperature domain. Static single-lap shear tests enabled to get the basic understanding of temperature and loading rate sensitivity of studied interlayers but the shear stiffness investigation in time and temperature domain was enabled by DMTA experiments. Performance of selected interlayers in LG was then verified by series of four-point bending tests of large-scale specimens. Small-scale experiments showed that identical chemical base of two interlayers does not predetermine identical stiffness in identical loading conditions. Large-scale experiments revealed the interlayer may even ensure full shear coupling of individual glass plies in the panel.

7. Analytical part of the thesis

This part of the thesis aims at use of obtained experimental data for the determination of shear stiffness of selected interlayers. Particularly, Maxwell-Weichert (M-W) Prony series of Trosifol BG, Trosifol ES, EVA L, and EVA S are determined, and these constructed models are verified. Moreover, initial shear moduli G_{init} of Trosifol BG, EVA L, and SG 5000 at 20 °C, are used as an input into analytical calculation of large-scale specimens tested in four-point bending destructive tests using Wölfel-Bennison (W-B) and Enhanced Effective Thickness (EET) methods.

7.1. Construction of Maxwell models for selected interlayers based on DMTA results

Polymeric interlayers are, in the sense of mechanics, a continuum with the theoretical continuous relaxation spectrum $H(\theta)$. To work with polymers using mechanical models, relaxation times of the polymer are considered as discrete values and relaxation function of the polymer $G(t)$ is then expressed in the sense of Eq. (16). As already stated in section 2.4.3, the series of Maxwell models in parallel forming M-W model or GMF model, are commonly used mechanical models which approximate the mechanical response of strain loaded polymers. This model needs discrete Prony series input $\{G_\infty, G_i, \text{and } \theta_i\}$ for approximation of shear stiffness of a polymer.

Assuming TTSP for thermorheologically simple polymers with the relaxation function $G(t, T)$ expressed in the sense of Eq. (3) having all relaxation times $\theta_i(T)$ affected in the same notation as

$$\theta_i(T) = a_T(T) \cdot \theta_i\left(T_{ref}\right), \tag{51}$$

where $a_T(T)$ is the temperature shift coefficient, it is possible to create Master Curve at reference temperature T_{ref} from DMTA experimental data $G^*(f, T)$ or $G^*(\omega, T)$ of the polymer [22], [38] loaded by sinusoidal strain input in Eq. (46), using Eq. (52) as

$$G^*(\omega, T) = G^*\left(\omega \cdot a_T, T_{ref}\right), \tag{52}$$

where ω is the angular velocity input [rad/s]. The same applies for frequency input f [Hz] assuming $\omega = 2 \cdot \pi \cdot f$. Graphical representation of Eq. (52) is displayed in Fig. 98. Horizontal temperature shift coefficient $\log_{10} a_T(T)$ will be, in the sequel, for all interlayers, considered in the form of WLF equation for all tested temperatures given by Eq. (5).

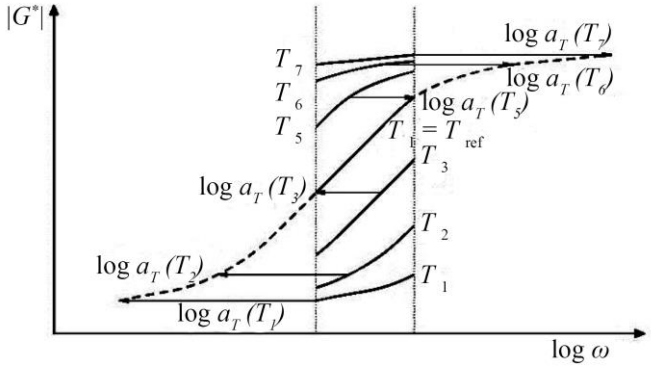

Fig. 98: Horizontal shift of measured relations in DMTA and construction of Master Curve at T_{ref}

Supposing the thermorheological simplicity of tested interlayers [22] and DMTA data in shear being fitted by M-W model loaded by sinusoidal shear strain input in linear viscoelastic region, its dynamic complex shear modulus is then analytically expressed by Eq. (53), where *i* refers to *i*-th Maxwell model, *M* denotes the number of Maxwell models in parallel, and "i" is a complex unit.

$$G^*(\omega,T) = G_\infty + \sum_{i=1}^{M} \frac{G_i \cdot \omega^2 \cdot \theta(T_{ref})_i^2 \cdot a_T(T)^2}{1+\omega^2 \cdot \theta(T_{ref})_i^2 \cdot a_T(T)^2} + \mathrm{i} \cdot \sum_{i=1}^{M} \frac{G_i \cdot \omega \cdot \theta\left(T_{ref}\right)_i \cdot a_T(T)}{1+\omega^2 \cdot \theta(T_{ref})_i^2 \cdot a_T(T)^2} \quad (53)$$

7.1.1. Maxwell models based on DMTA results of single-lap shear tests

This section refers to construction of M-W models based on DMTA in section 6.2. A technique of WLF constants and Prony series evaluation for all interlayers, in this section, combined the TTSP incremental horizontal shift procedure with a least square algorithm [38] followed by Kuntsche method [69] implemented in Matlab®. To construct the Master Curve of Trosifol BG, DMTA results of one representative specimen at all temperatures were chosen, see G'(f) relations in Fig. 99. Considering the experimental inequalities G'(f, T) >> G''(f, T), TTSP was applied at G'(f, T) relations, and Master Curve at T_{ref} = 20 °C was constructed, see Fig. 100. Fitting Prony series of M-W model to experimental Master Curve means non-linear optimization problem with 2*M*+1 parameters. According to Kuntsche [69], unknown parameters can be reduced to *M*+1 by choosing at least one Maxwell model per frequency decade and, therefore, fixing the relaxation times. Kuntsche fitting procedure consists in minimization of the objective function given in the form of Eq. (54) [69] which is the error sum of squares between model and experimental data.

$$F(\{G_i\}, G_\infty) = \sum_{j=1}^{m} (\log(G'(\omega_j)) - \log(G_j'))^2 + 10 \cdot (\log(G''(\omega_j)) - \log(G_j''))^2 \quad (54)$$

In Eq. (54), G_j' and G_j'' are experimental storage and loss moduli at angular velocity ω_j and temperature *T*; $G'(\omega_j)$ with $G''(\omega_j)$ are the storage and loss moduli given by fitted M-W model at angular velocity ω_j and temperature *T*; and *m* is the number of measurements. By choosing 30 Maxwell models with relaxation times in the range < 10^{-10}; 10^{19} > [s] covering the range of Master

Curve frequency decades, M-W Prony series using global optimization in Eq. (54), were obtained. These are shown in Tab. 22.

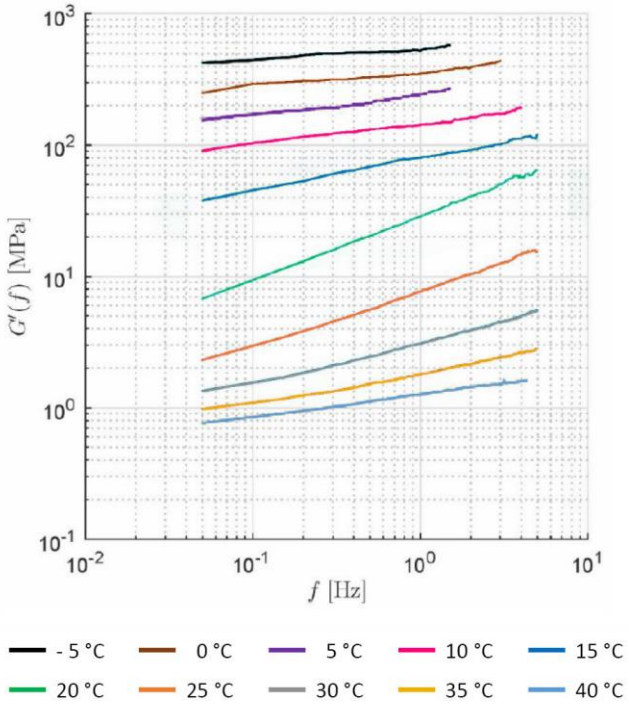

Fig. 99: Measured storage modulus G'(f) of representative specimen with Trosifol BG

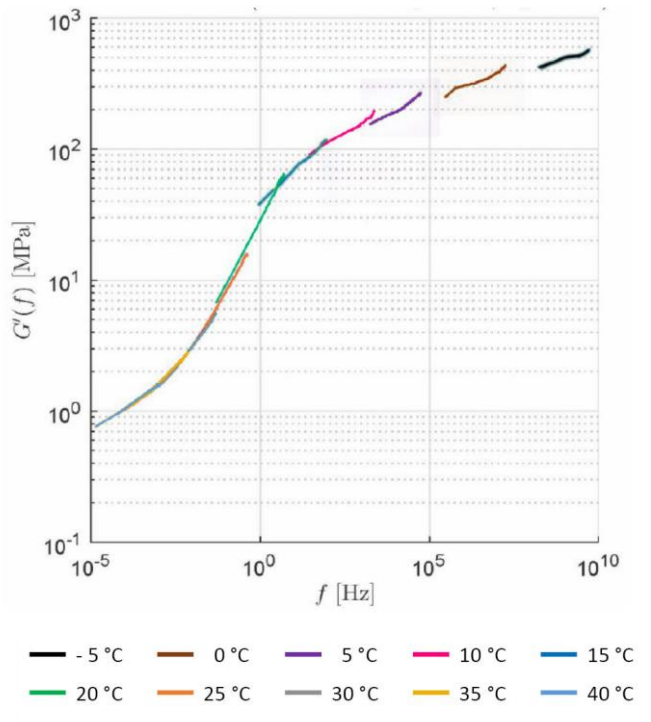

Fig. 100: Master Curve of representative Trosifol BG specimen at T_{ref} = +20 °C, C_1 = 15.0; C_2 = 64.3

Tab. 22: Viscoelastic WLF and Prony series of Trosifol BG

WLF model at T_{ref} = +20 °C			
C_1	15.0	C_2	64.3
Maxwell-Weichert model at T_{ref} = +20 °C			
G_∞ = 0.01326 MPa			
θ_i [s]	G_i [MPa]	θ_i [s]	G_i [MPa]
1.000E-10	6.862E+01	1.000E+05	1.907E-01
1.000E-09	6.214E+01	1.000E+06	8.083E-02
1.000E-08	6.214E+01	1.000E+07	5.753E-02
1.000E-07	6.214E+01	1.000E+08	4.696E-02
1.000E-06	5.077E+01	1.000E+09	4.025E-02
1.000E-05	5.077E+01	1.000E+10	3.510E-02
1.000E-04	4.403E+01	1.000E+11	3.075E-02
1.000E-03	4.323E+01	1.000E+12	2.690E-02
1.000E-02	4.323E+01	1.000E+13	2.340E-02
1.000E-01	4.129E+01	1.000E+14	2.013E-02
1.000E+00	1.087E+01	1.000E+15	1.702E-02
1.000E+01	2.816E+00	1.000E+16	1.400E-02
1.000E+02	9.297E-01	1.000E+17	1.096E-02
1.000E+03	4.327E-01	1.000E+18	7.635E-03
1.000E+04	2.993E-01	1.000E+19	3.207E-03

Fitted value of G_∞ = 0.013 MPa captures well the uncross-linked structure of tested interlayer. G'(f) relations by fitted M-W model at 20 °C and the corresponding shear relaxation functions G(t, T) by Eq. (55), are shown in Fig. 101. G'(f) relations match well with the experiment. Relaxation functions meet the viscoelastic nature of polymers – decreasing shear stiffness in time and elevated temperature. The model predicts the equilibrium shear stiffness G_∞ at 60 °C achieved after 10^{14} s which is not practically possible. The interlayer theoretically ensures only limited shear coupling of glass plies in bended LG panel at 20 °C, 40 °C, and 60 °C because the value of shear relaxation modulus G(t) < 10 MPa [68]. Other important values of Trosifol BG are instantaneous shear stiffness $G_{inst} = \sum G_i + G_\infty$ = 544.3 MPa, and short-term shear relaxation moduli G(t = 10 s): 240 MPa at 0 °C, 3.2 MPa at 20 °C, 0.5 MPa at 40 °C, and 0.3 MPa at 60 °C.

$$G(t,T) = G_\infty + \sum_{i=1}^{M} G_i \cdot \exp\left(-\frac{t}{a_T(T) \cdot \theta_i(T_{ref})}\right) \tag{55}$$

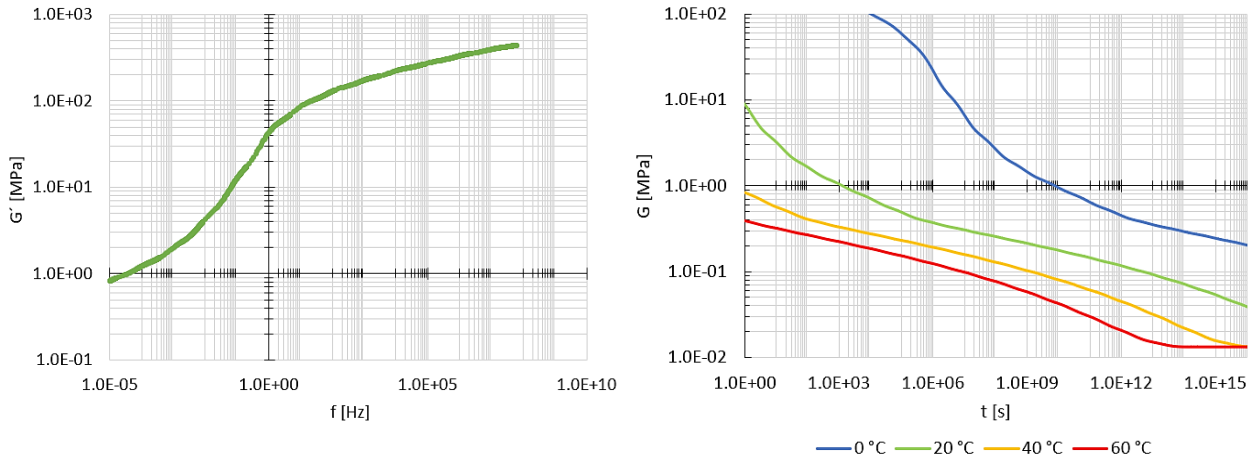

a) Shear storage modulus $G'(f, T = +20\ °C)$ b) Shear relaxation functions $G(t, T)$

Fig. 101: Analytical relations given by fitted M-W model of Trosifol BG from Tab. 22

To construct the Master Curve of Trosifol ES, DMTA relations $G'(f)$ of one representative specimen were chosen, see Fig. 102. Inequality $G'(f, T) >> G''(f, T)$ allowed to apply TTSP only at $G'(f)$ relations and Master Curve at T_{ref} = 20 °C was constructed, see Fig. 103. This figure also plots, for comparison, the Master Curve of Trosifol BG. By choosing 40 Maxwell models with relaxation times in the range $< 10^{-11}; 10^{10} >$ [s] covering Master Curve frequency decades, M-W Prony series were fitted, see Tab. 23.

$G'(f)$ relations by fitted M-W model at 20 °C and the corresponding shear relaxation functions $G(t, T)$ by Eq. (55), are shown in Fig. 104. Relaxation functions decrease in time and elevated temperature. At 60 °C, Trosifol ES gets to equilibrium shear stiffness G_∞ = 1.27 MPa at 10^4 s. At 0 °C, the equilibrium stiffness is reached after 10^{12} s which is not practically possible. Other important values of Trosifol ES are instantaneous shear stiffness $G_{inst} = \sum G_i + G_\infty$ = 5968 MPa, and short-term shear relaxation moduli $G(t = 10\ s)$: 3259 MPa at 0 °C, 321 MPa at 20 °C, 1.9 MPa at 40 °C, and 1.5 MPa at 60 °C.

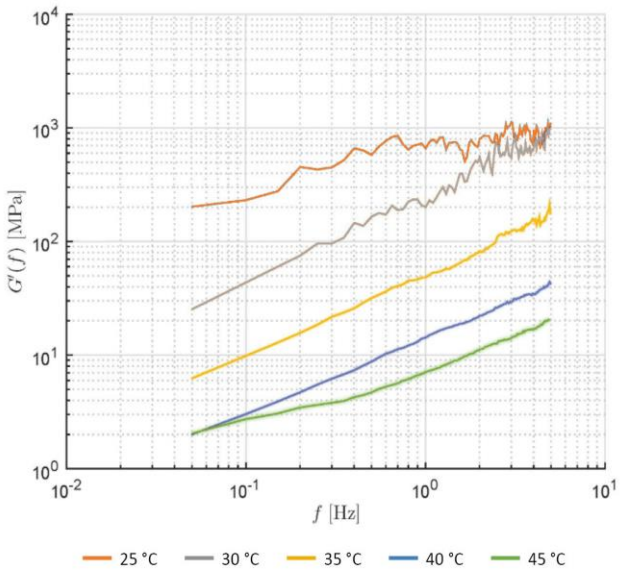

Fig. 102: Measured storage modulus G'(f) of representative specimen with Trosifol ES

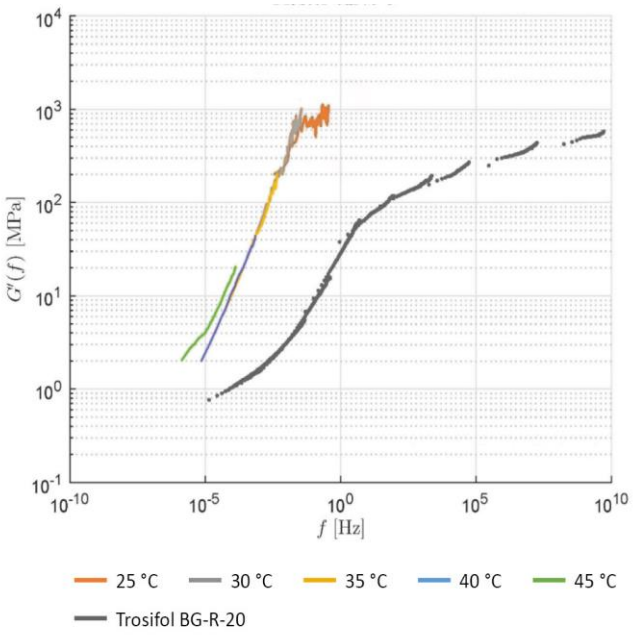

Fig. 103: Master Curve of representative Trosifol ES specimen at T_{ref} = +20 °C, C_1 = 18.4; C_2 = 75.6

Tab. 23: Viscoelastic WLF and Prony series of Trosifol ES

WLF model at T_{ref} = +20 °C			
C_1	18.4	C_2	75.6
Maxwell-Weichert model at T_{ref} = +20 °C			
G_∞ = 1.270 MPa			
θ_i [s]	G_i [MPa]	θ_i [s]	G_i [MPa]
1.000E-11	3.249E+02	3.039E+03	5.126E+00
5.298E-11	3.248E+02	1.610E+04	5.126E+00
2.807E-10	3.248E+02	8.532E+04	2.030E-01
1.487E-09	3.248E+02	4.520E+05	8.275E-02
7.880E-09	3.248E+02	2.395E+06	8.274E-02
4.175E-08	3.247E+02	1.269E+07	8.273E-02
2.212E-07	3.247E+02	6.723E+07	8.272E-02
1.172E-06	3.247E+02	3.562E+08	8.270E-02
6.210E-06	3.247E+02	1.887E+09	8.267E-02
3.290E-05	3.247E+02	1.000E+10	8.262E-02
1.743E-04	3.246E+02	1.425E+05	5.290E-06
9.237E-04	3.246E+02	4.924E+05	4.960E-06
4.894E-03	3.246E+02	1.701E+06	4.649E-06
2.593E-02	3.246E+02	5.878E+06	4.319E-06
1.374E-01	3.246E+02	2.031E+07	3.961E-06
7.279E-01	3.246E+02	7.017E+07	3.566E-06
3.857E+00	3.246E+02	2.424E+08	3.122E-06
2.043E+01	3.246E+02	8.377E+08	2.603E-06
1.083E+02	1.061E+02	2.894E+09	1.954E-06
5.736E+02	5.126E+00	1.000E+10	9.787E-07

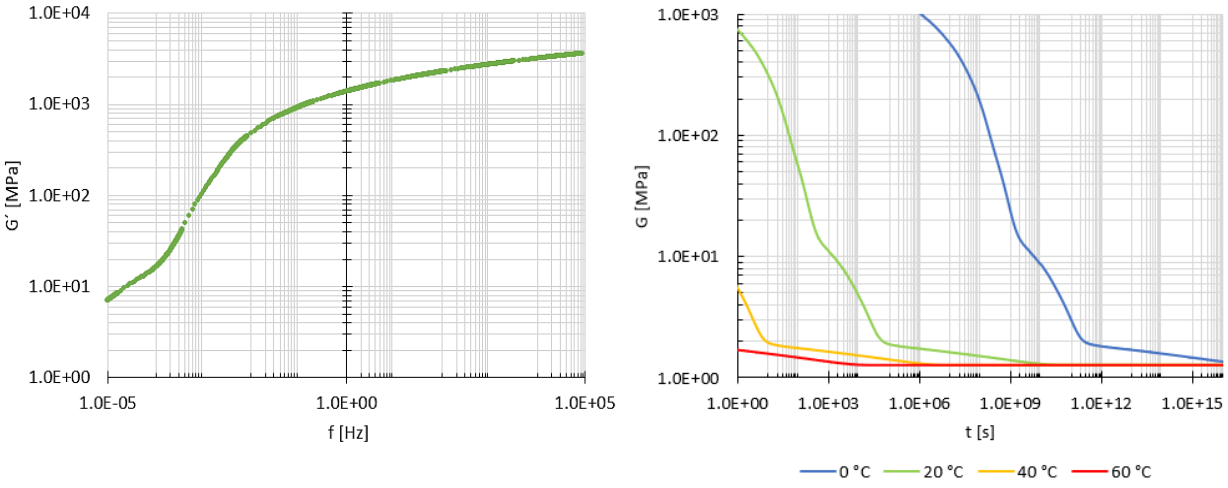

a) Shear storage modulus G'(f, T = +20 °C)

b) Shear relaxation functions G(t, T)

Fig. 104: Analytical relations given by fitted M-W model of Trosifol ES from Tab. 23

Also, in case of EVA S, the shear storage modulus was dominant over loss modulus and TTSP was applied only at G'(f) relations. By doing so, G'(f) relations of one representative specimen were chosen, see Fig. 105, and the corresponding Master Curve at T_{ref} = 20 °C plotted in Fig. 106,

was constructed. For M-W Prony series fit, 22 relaxation times in the range $<10^{-09}$; $10^{12}>$ [s] including frequency range of Master Curve were chosen and the fitted series are shown in Tab. 24. Equilibrium shear stiffness $G_\infty = 0.36$ MPa meets the cross-link structure of this interlayer. Relations $G'(f)$ at 20 °C and subsequent shear relaxation functions $G(t, T)$ of EVA S, given by its M-W using Eq. (55), are shown in Fig. 107. At 60 °C, EVA S gets to equilibrium shear stiffness G_∞ already after 10^4 s whereas 0 °C means no equilibrium configuration within 10^{12} s. Instantaneous shear stiffness of this interlayer $G_{inst} = \sum G_i + G_\infty = 38.1$ MPa is much lower than in case of both PVB´s, and its short-term shear relaxation moduli $G(t = 10\ s)$ are: 10.8 MPa at 0 °C, 6.7 MPa at 20 °C, 2.9 MPa at 40 °C, and 1.9 MPa at 60 °C.

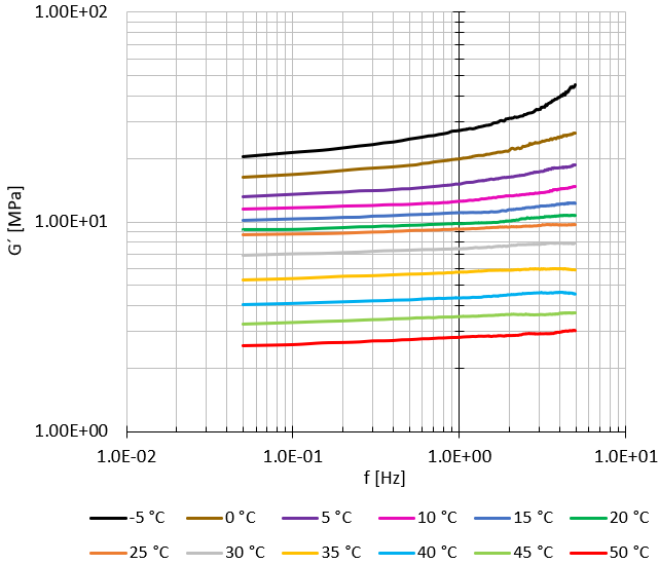

Fig. 105: Measured storage modulus $G'(f)$ of representative specimen with EVA S

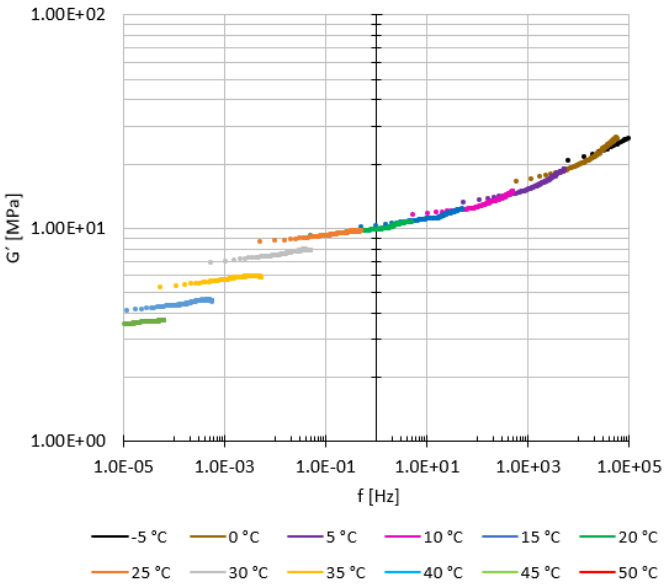

Fig. 106: Master Curve of representative EVA S specimen at T_{ref} = +20 °C, C_1 = 230.0; C_2 = 1150.1

Tab. 24: Viscoelastic WLF and Prony series of EVA S

WLF model at T_{ref} = +20 °C			
C_1	230.0	C_2	1150.1
Maxwell-Weichert model at T_{ref} = +20 °C			
G_∞ = 0.362 MPa			
θ_i [s]	G_i [MPa]	θ_i [s]	G_i [MPa]
1.00E-09	5.899	1.00E+02	1.322
1.00E-08	2.882	1.00E+03	0.653
1.00E-07	0.789	1.00E+04	1.260
1.00E-06	0.136	1.00E+05	1.003
1.00E-05	1.412	1.00E+06	0.159
1.00E-04	17.767	1.00E+07	0.194
1.00E-03	0.071	1.00E+08	0.220
1.00E-02	0.365	1.00E+09	0.060
1.00E-01	1.670	1.00E+10	0.985
1.00E+00	0.063	1.00E+11	0.141
1.00E+01	0.284	1.00E+12	0.396

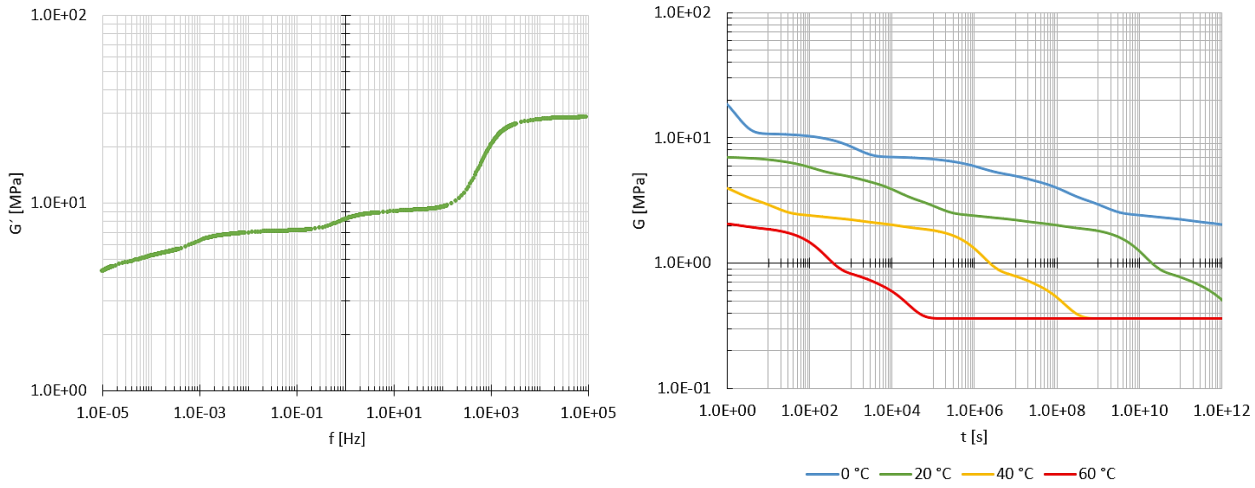

a) Shear storage modulus G'(f, T = +20 °C) b) Shear relaxation functions G(t, T)

Fig. 107: Analytical relations given by fitted M-W model of EVA S from Tab. 24

7.1.2. Maxwell models based on combined DMTA results of single-lap shear tests and tests in rheometer

This part shows that the experimental testing of interlayer in various modes may deliver different results. In the sequel, experimental results of Trosifol BG and EVA L given by DMTA of single-lap shear tests in MTS performed by author and of torsion tests in rheometer performed by Schmidt et al. [70] will be shown and compared. Moreover, M-W Prony series and WLF constants based on combined results from both testing modes will be presented. Testing modes are displayed in Fig. 108.

In rheometer HAAKE MARS, cylindrical specimens 5 mm + 0.76 mm + 5 mm with EVA L and Trosifol BG were tested in a stress-controlled regime in the range of frequencies

< 0.001; 50 > Hz and temperatures < +10; +60 > °C with a step of 10 °C. Four Trosifol BG and seven EVA L specimens were tested in total. Check on linearity in rheometer was also performed. Experimental relations of shear storage modulus against angular velocity $G'(\omega)$ for representative Trosifol BG and EVA L specimens are plotted in Fig. 109. Closer look shows, there is a variability of obtained results at certain temperature regarding the experimental method.

a) DMTA in single-lap shear mode, MTS

b) DMTA in torsion mode, rheometer [70]

Fig. 108: Various DMTA testing modes of Trosifol BG and EVA L

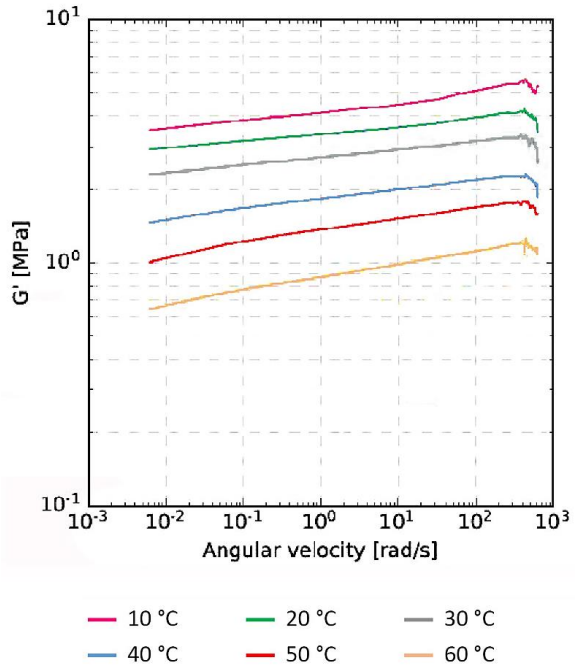

a) EVA L, torsion in rheometer

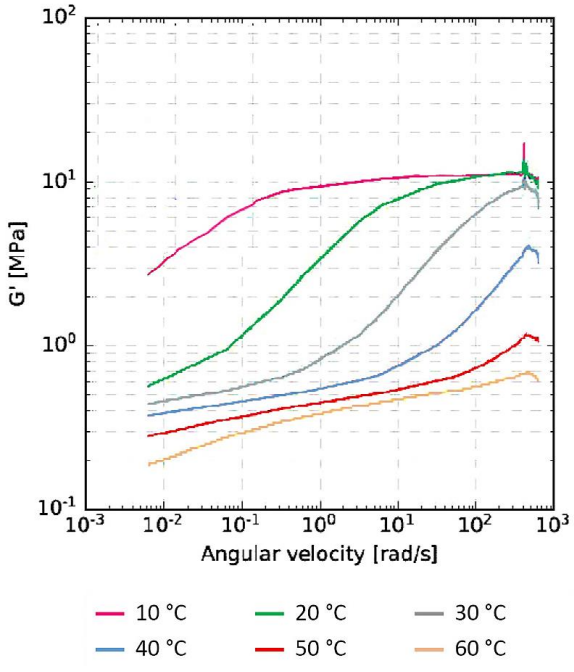

b) Trosifol BG, torsion in rheometer

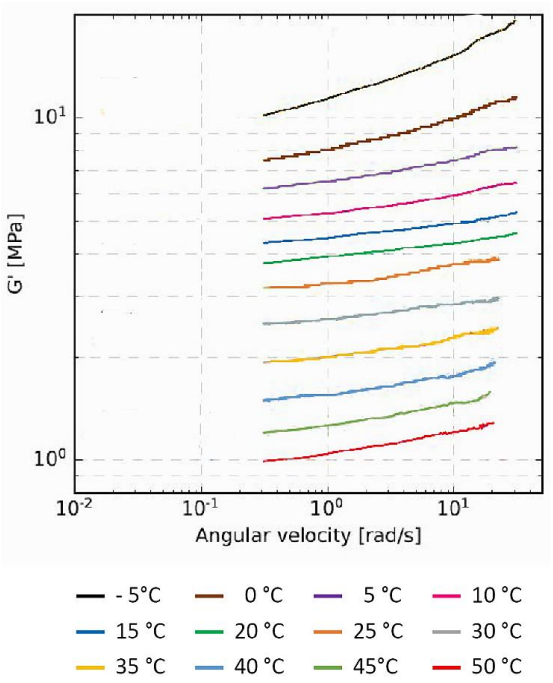

c) EVA L, single-lap shear test in MTS

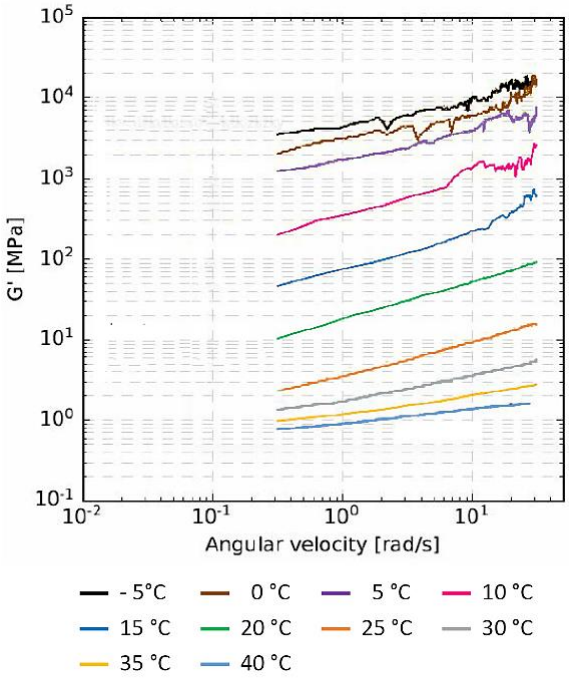

d) Trosifol BG, single-lap shear test in MTS

Fig. 109: Storage modulus-angular velocity relations for representative Trosifol BG and EVA L specimens

In the next step, Master Curving process and M-W Prony series fit using DMTA data of representative specimens in Fig. 109 were performed. WLF constants using TTSP and Prony series were, in this section, fitted simultaneously. This is noted as global fit procedure. Denoting ω_r as prescribed angular frequency and T_r as prescribed temperature of measurement r, the experimental data are given in the form $[\hat{G}_r', \hat{G}_r'', \omega_r, T_r]$ and data by M-W model in the form $[G'(\omega_r, T_r); G''(\omega_r, T_r)]$. Considering Eqs. (5), (51), (53), WLF constants $\{C_1, C_2\}$ and M-W Prony series $\{G_\infty, G_i, \theta_i\}$ minimizing the objective function in Eq. (56) were searched.

$$F(\{G_i\}, G_\infty, C_1, C_2) = \sum_{r=1}^{R} [(G'(\omega_r, T_r)) - (\hat{G}_r')]^2 + [(G''(\omega_r, T_r)) - (\hat{G}_r'')]^2 \qquad (56)$$

The procedure exploits the fact both $G'(\omega_r, T_r)$ and $G''(\omega_r, T_r)$ from Eqs. (49), (50) are linear in $\boldsymbol{G} = \{G_1, G_2, \ldots G_i, G_\infty\}^T$. The sum of squares in Eq. (56) can be then in matrix notation written as

$$F(\boldsymbol{G}, C_1, C_2) = \left(\boldsymbol{X}(C_1, C_2)\boldsymbol{G} - \hat{\mathrm{G}}\right)^T \left(\boldsymbol{X}(C_1, C_2)\boldsymbol{G} - \hat{\mathrm{G}}\right), \qquad (57)$$

where $\hat{\mathrm{G}} = \{\hat{G}_1' \ldots \hat{G}_R', \hat{G}_1'' \ldots \hat{G}_R''\}^T$ stores experimental storage and loss moduli, and the components of the matrix $\boldsymbol{X}(C_1, C_2) = [\boldsymbol{X}', \boldsymbol{X}'']^T$ are in Eq. (58)

$$X'_{r,i} = \frac{\omega_r^2 \cdot \theta_i^2(T_r)}{1 + \omega_r^2 \cdot \theta_i^2(T_r)}, \qquad X''_{r,i} = \frac{\omega_r \cdot \theta_i(T_r)}{1 + \omega_r^2 \cdot \theta_i^2(T_r)}, \qquad (58)$$

where i denotes i-th Maxwell model. The dependence of $\boldsymbol{X}(C_1, C_2)$ results from Eq. (51) and WLF Eq. (5). Least squares method in Eq. (56) than gives by minimization the optimal set $\boldsymbol{G}$ in matrix notation as

$$\boldsymbol{G}(C_1, C_2) = \left(\boldsymbol{X}^{\boldsymbol{T}}\boldsymbol{X}\right)^{-1}\boldsymbol{X}^{\boldsymbol{T}}\hat{\mathrm{G}}. \tag{59}$$

Substituting these optimal values back to Eq. (57), the objective function is written in matrix notation as follows

$$F(C_1, C_2) = \left(\boldsymbol{X}\left(\boldsymbol{X}^{\boldsymbol{T}}\boldsymbol{X}\right)^{-1}\boldsymbol{X}^{\boldsymbol{T}}\hat{\mathrm{G}} - \hat{\mathrm{G}}\right)^{T}\left(\boldsymbol{X}\left(\boldsymbol{X}^{\boldsymbol{T}}\boldsymbol{X}\right)^{-1}\boldsymbol{X}^{\boldsymbol{T}}\hat{\mathrm{G}} - \hat{\mathrm{G}}\right), \tag{60}$$

which depends only on WLF parameters. To find the optimal values C_1 and C_2 of the objective function $F(C_1, C_2)$, Nelder-Mead method was employed [71] advantaged by no necessity of gradient F to be known. Trosifol BG or EVA L data Master Curves at 20 °C for experimental data in Fig. 109 with $G'(\omega)$ relations given by fitted M-W models using the above algorithm, are shown in Fig. 110. The experimental data at Master Curves in Fig. 110 are, for a clarity, a bit diluted. It is obvious that for one representative specimen tested by one experimental method, the fitting algorithm constructs the resulting data Master Curve being well described by corresponding M-W model. But Master Curves given by both experimental methods do not overlap. Assuming the approximate equality $G'(f) \sim G(t = 1/f)$ [37], the relaxation functions $G(t,\ T = 20\ °C)$ of one interlayer based on DMTA in either shear or in torsion, would be different. This is not physically possible. Moreover, Fig. 111 of experimental $G'(\omega)$ relations at 20 °C and 40 °C shows, the variability of data is not only between shear and torsion mode but also between the individual specimens at a certain temperature tested by one certain method. Given the results in Fig. 110 and Fig. 111, the final Master Curve was constructed from all available data sets. It means, all measured $G'(\omega)$ and $G''(\omega)$ moduli given by both experimental methods were used simultaneously is an input in the above fitting algorithm. Final Master Curves of experimental data $G'(\omega)$ at T_{ref} = 20 °C and $G'(\omega)$ relations by fitted M-W models of Trosifol BG and EVA L interlayers are shown in Fig. 112.

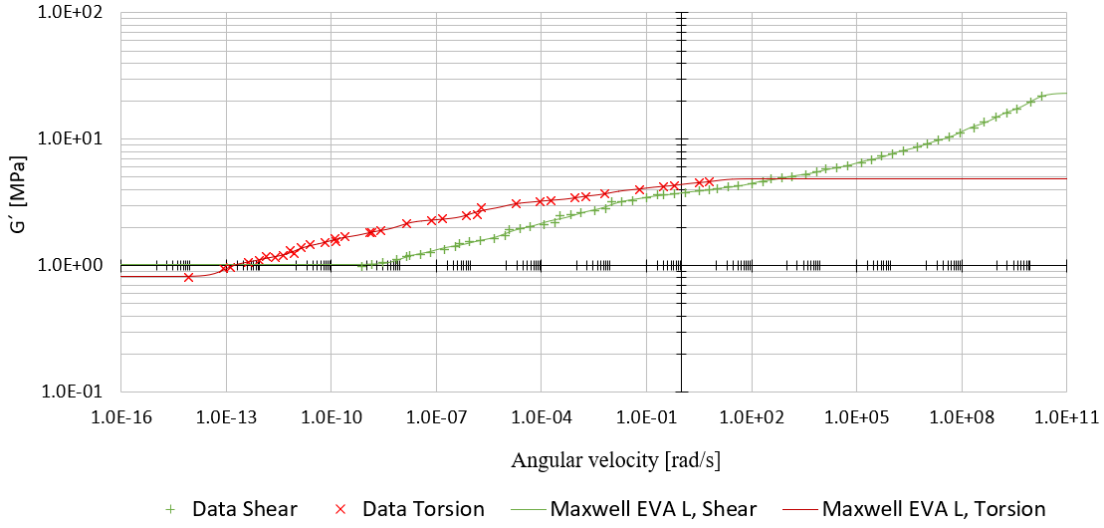

a) Master Curve of EVA L at T_{ref} = +20 °C, Shear: C_1 = 193.8, C_2 = 642.8; Torsion: C_1 = 55.9, C_2 = 148.2

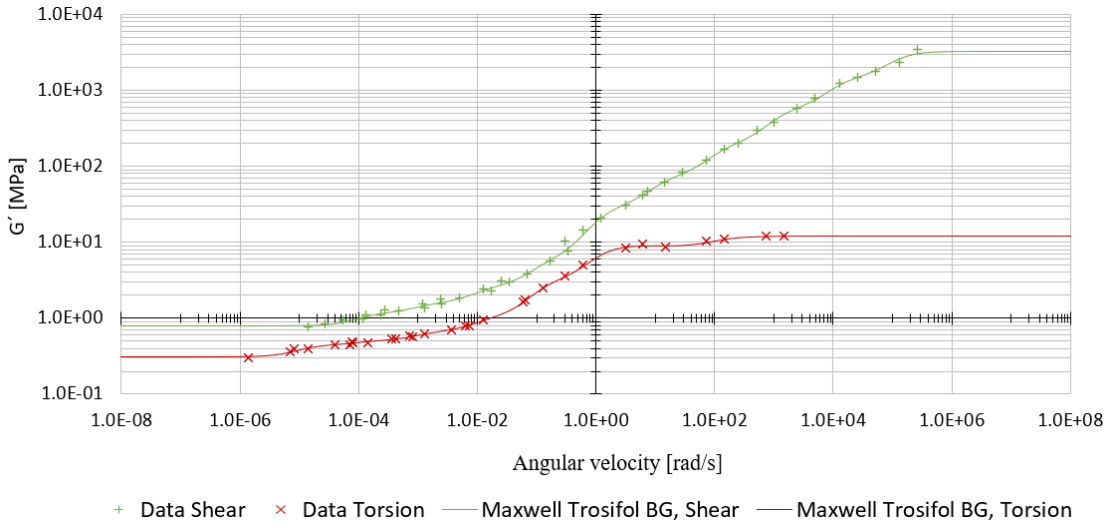

b) Master Curve of Trosifol BG at T_{ref} = +20 °C, Shear: C_1 = 25.8, C_2 = 98.5; Torsion: C_1 = 11.2, C_2 = 57.0

Fig. 110: Representative Master Curves of Trosifol BG and EVA L given by individual DMTA methods

It is obvious in Fig. 112 that, due to the variability of measured data, the deviation of optimal Master Curves given by fitted M-W models from the data points is higher than in cases where the data series of only one representative specimen were considered. This is the disadvantage of M-W Prony fit to all data sets against fit to one data set, compare Fig. 110 and Fig. 112. To illustrate, the sum of squared relative errors is 2.63 and 4.51 for EVA L and Trosifol BG, respectively, using the fit to all experimental data sets. Contrary, fitting the model to one representative data set in Fig. 110 gives squared relative errors as: EVA L (0.15 in shear; 0.12 in torsion) and Trosifol BG (0.44 in shear; 0.15 in torsion).

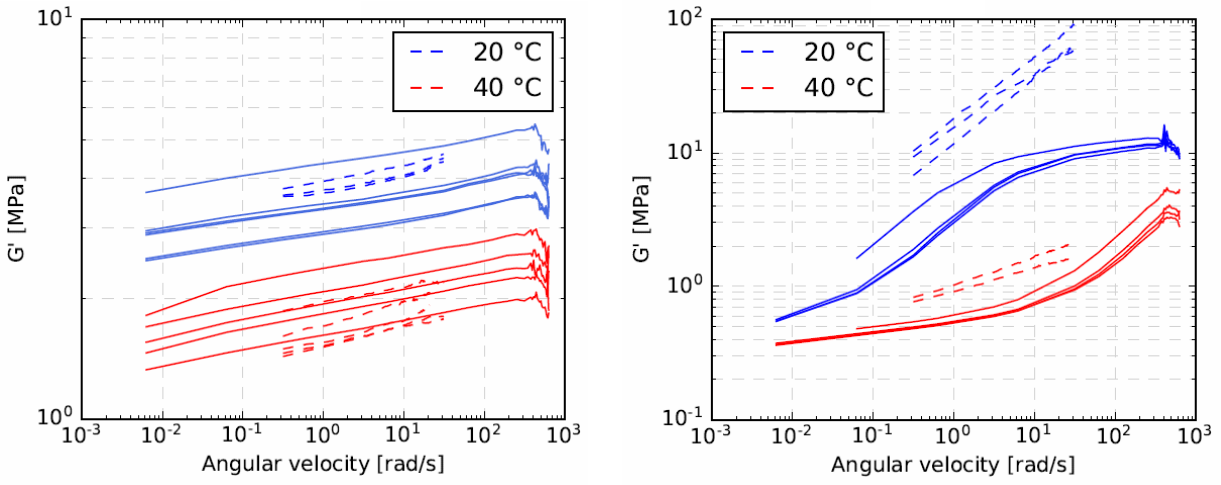

a) $G'(\omega)$ relations of EVA L

b) $G'(\omega)$ relations of Trosifol BG

Fig. 111: Comparison of shear (dashed) and torsion (full) DMTA results plotted for individual specimens

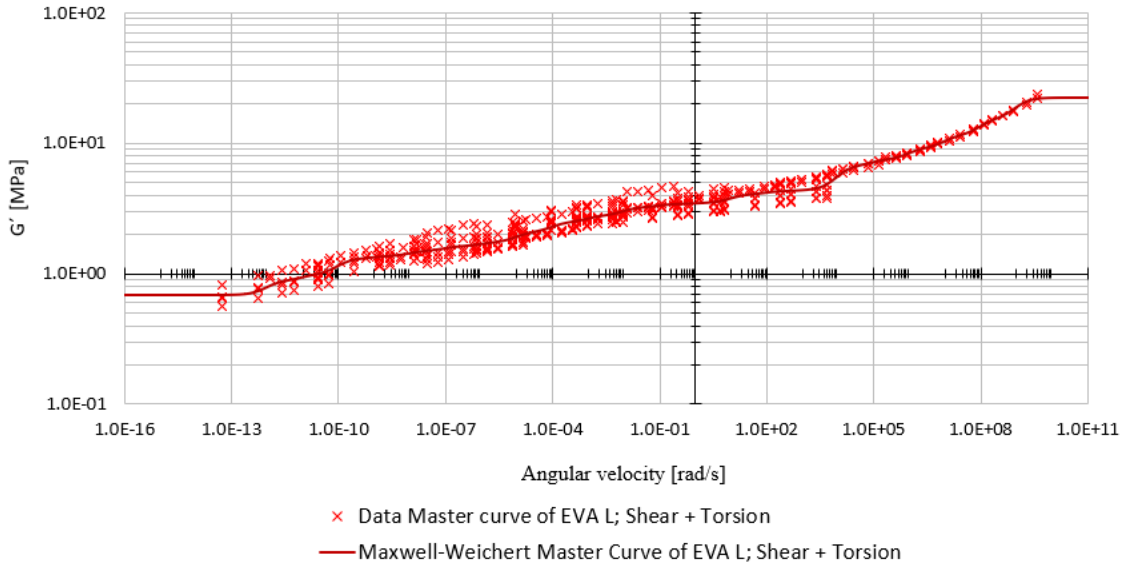

a) Master Curve of EVA L by global fit at T_{ref} = +20 °C; C_1 = 339.1, C_2 = 1185.8

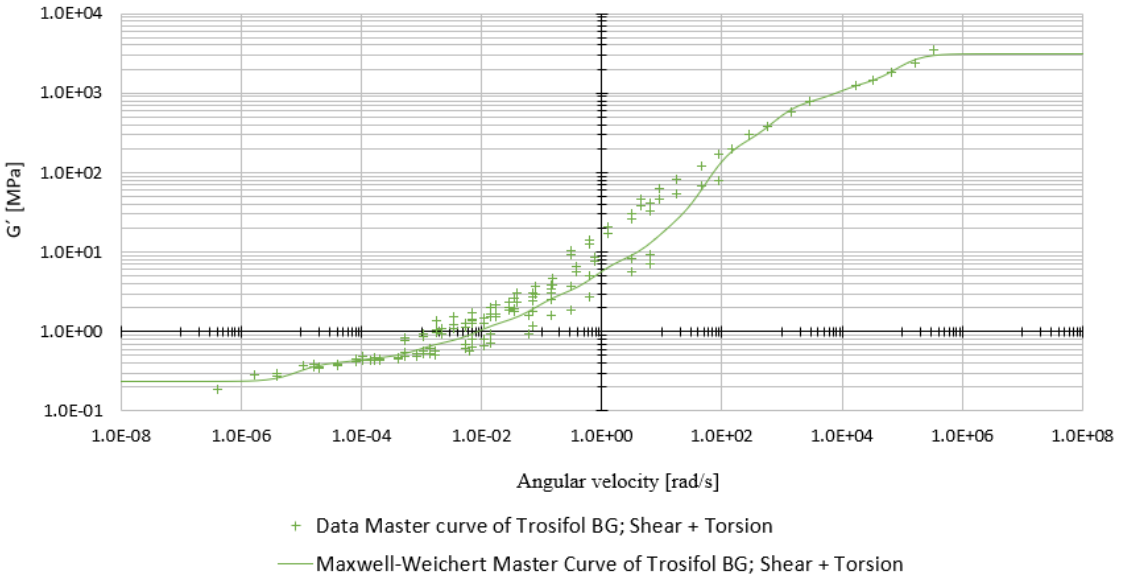

b) Master Curve of Trosifol BG by global fit at T_{ref} = +20 °C; C_1 = 8.63, C_2 = 42.42

Fig. 112: Master Curve fitted to all combined experimental data given by DMTA in shear + torsion modes

WLF constants and M-W Prony series at T_{ref} = 20 °C of EVA L and Trosifol BG based on global fit to all combined experimental data are shown in Tab. 25. For EVA L, 22 relaxation times in the range $< 10^{-09}; 10^{12} >$ [s], and for Trosifol BG, 11 relaxation times in the range $< 10^{-05}; 10^{05} >$ [s] were chosen in order to provide one Maxwell model per frequency decade. Equilibrium shear stiffness of Trosifol BG $G_{\infty,BG}$ = 0.232 MPa is higher than in case of two-step fit at one data set from DMTA in shear ($G_{\infty,BG}$ = 0.013 MPa, see section 7.1.1). Shear relaxation

functions of both interlayers using M-W Prony series from Tab. 25 as an input into Eq. (55), are shown in Fig. 113. All decrease in time and elevated temperature. Both interlayers attain an equilibrium shear stiffness G_∞ at 60 °C relatively quickly, within 10^2 s, whereas 0 °C means their shear stiffness decreases continuously by 10^{12} s. M-W models of both interlayers predict G(t, T = 20 °C, 40 °C, 60 °C) < 10 MPa which mostly ensures only limited shear coupling of glass plies in bending [68]. EVA L is of instantaneous shear stiffness $G_{inst} = \sum G_i + G_\infty$ = 22.3 MPa and short-term shear moduli G(t = 10 s): 6.6 MPa at 0 °C, 3.2 MPa at 20 °C, 1.6 MPa at 40 °C, and 0.7 MPa at 60 °C. Trosifol BG attains instantaneous shear stiffness $G_{inst} = \sum G_i + G_\infty$ = 3085 MPa and short-term shear moduli G(t = 10 s): 3051 MPa at 0 °C, 1.9 MPa at 20 °C, 0.4 MPa at 40 °C, and 0.3 MPa at 60 °C.

Tab. 25: WLF and Prony series of Trosifol BG and EVA L based on global fit to all combined DMTA data sets in shear + torsion modes

WLF and Maxwell-Weichert models at T_{ref} = +20 °C			
Trosifol BG			
C_1 [-]	8.635	C_2 [-]	42.422
G_∞ [MPa]	0.232	T_{ref} [°C]	+20
EVA L			
C_1 [-]	339.102	C_2 [-]	1185.816
G_∞ [MPa]	0.682	T_{ref} [°C]	+20

	Trosifol BG	EVA L		Trosifol BG	EVA L
θ_i [s]	G_i [MPa]	G_i [MPa]	θ_i [s]	G_i [MPa]	G_i [MPa]
1.00E-09	--	6.934	1.00E+02	0.587	0.445
1.00E-08	--	3.899	1.00E+03	0.260	0.300
1.00E-07	--	2.289	1.00E+04	0.064	0.402
1.00E-06	--	1.673	1.00E+05	0.168	0.348
1.00E-05	1782.124	0.762	1.00E+06	--	0.112
1.00E-04	519.209	2.401	1.00E+07	--	0.127
1.00E-03	546.177	0.065	1.00E+08	--	0.138
1.00E-02	216.893	0.248	1.00E+09	--	0.051
1.00E-01	13.618	0.576	1.00E+10	--	0.323
1.00E+00	4.988	0.056	1.00E+11	--	0.100
1.00E+01	1.664	0.189	1.00E+12	--	0.200

Note: The range of testing temperatures < -5; +60 > °C and frequencies < 0.001; 50.0 > Hz affected the interval of angular velocities covered by data Master Curve and, subsequently, the relaxation function covered by fitted M-W model. To improve the range of applicability of presented mechanical models, the range of testing temperatures and frequencies would have to be extended calling for subsequent refit of the model.

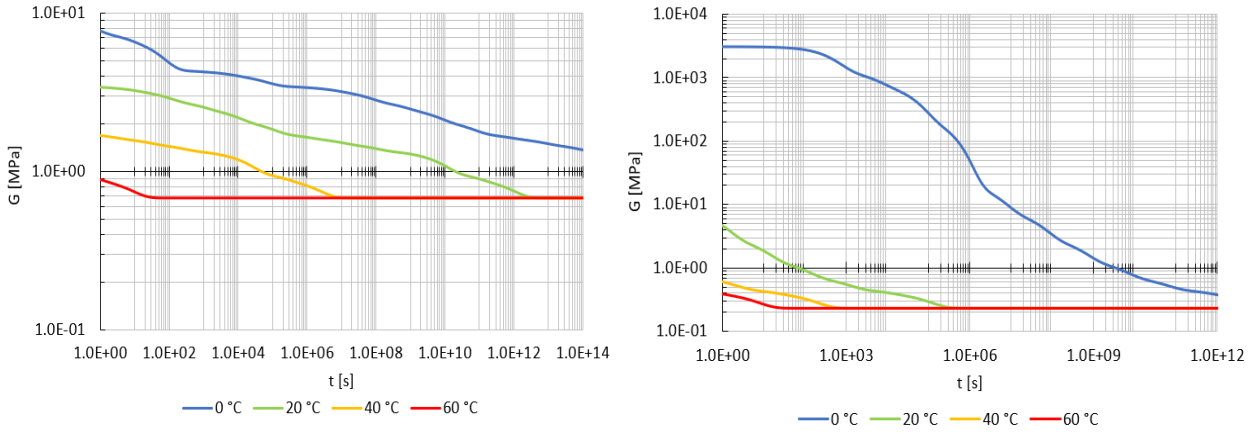

a) EVA L b) Trosifol BG

Fig. 113: Shear relaxation functions by M-W models based on all combined DMTA data in shear + torsion modes from Tab. 25

Important notice results from comparison of relaxation functions of both PVB based and EVA based interlayers. EVA S is generally stiffer than EVA L when neglecting their values of G_∞. This fact is attributed to different cross-link density. Concomitantly, Trosifol ES is stiffer than Trosifol BG which documents different content of plasticizers added into PVB. These facts are illustrated by comparison of their shear moduli $G(t)$ at representative temperatures 20 °C and 40 °C in Fig. 114. This finding corresponds to mentioned inequalities of G_{init} from static single-lap shear tests for both PVB and EVA interlayers plotted in Tab. 7 at certain temperature and loading rate.

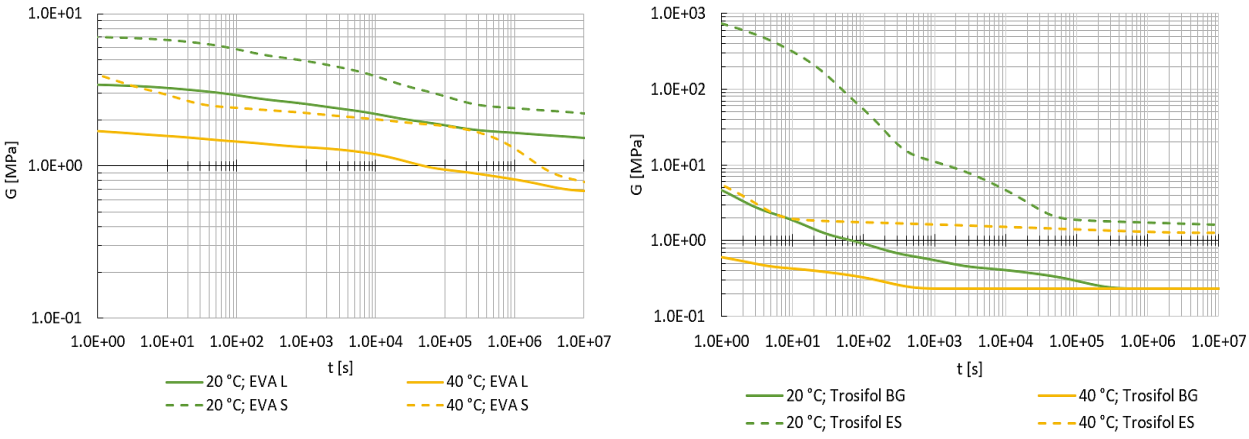

a) EVA S: shear, EVA L: shear + torsion b) Trosifol ES: shear, Trosifol BG: shear + torsion

Fig. 114: Comparison of shear relaxation functions of both PVB and EVA interlayers given by presented M-W models based on DMTA in various testing modes

7.2. Response of constructed Maxwell models to various strain rate inputs at various temperatures

To check the temperature sensitivity of fitted M-W models, their shear stress output τ(t, T) in time t to various constant shear strain rate inputs dγ/dt at tested temperatures T was analytically calculated using Eq. (61) as an analogy to Eq. (22) based on Boltzmann principle. In this equation, M is the number of Maxwell models and $\{G_\infty, G_i, \theta_i\}$ are shear M-W Prony series. Shear strain rate input applied on constructed M-W models from section 7.1, was identical with the theoretical shear strain rate applied on the interlayers in static single-lap shear tests in section 6.1, which is calculated as dγ/dt = du/dt·(1/p), where du/dt is the prescribed TEMPOS cross-head rate of vertical displacement and p is the thickness of interlayer from Tab. 6. Effect of temperature is included into Eq. (61) in the form of relaxation times modification according to Eq. (51) noting the temperature shift coefficient a_T in the form of WLF Eq. (5). Having the M-W model of interlayer, its response to the applied strain rate, see Fig. 115, should approach the experimental data in Fig. 73. The summary of strain rates dγ/dt applied at fitted models of studied interlayers is shown in Tab. 26. Shear stress and shear strain are, in this section, stated as engineering values.

$$\tau(t,T) = \frac{\mathrm{d}\gamma}{\mathrm{d}t} \cdot G_\infty \cdot t + a_T \cdot \frac{\mathrm{d}\gamma}{\mathrm{d}t} \cdot \sum_{i=1}^{M} G_i \cdot \theta_i(T_{ref}) \cdot [1 - \exp(-\frac{t}{a_T(T) \cdot \theta_i(T_{ref})})] \qquad (61)$$

Tab. 26: Loading rates applied on fitted M-W models from section 7.1

Interlayer	Thickness [mm]	Loading rate du/dt [mm/min]	Loading rate du/dt [mm/s]	Loading rate dγ/dt [1/s]
EVA L	0.63	2.000	0.0333	0.053
		0.500	0.0083	0.013
		0.125	0.0021	0.003
EVA S	0.81	2.000	0.0333	0.041
		0.500	0.0083	0.010
		0.125	0.0021	0.003
Trosifol BG	1.50	2.000	0.0333	0.022
		0.500	0.0083	0.006
		0.125	0.0021	0.001
Trosifol ES	0.85	2.000	0.0333	0.039
		0.500	0.0083	0.010
		0.125	0.0021	0.002

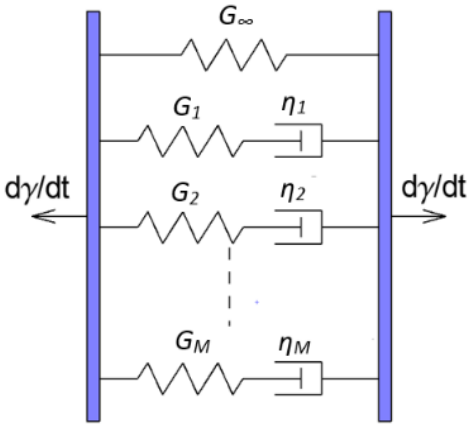

a) Testing frame of single-lap shear tests

b) Strain rate loaded M-W model of interlayer

Fig. 115: Static single-lap shear tests of interlayers modelled by analytical response of their M-W models

Analytically calculated shear stress τ against shear strain γ given by M-W models at certain time t and testing temperatures T together with experimental τ-γ relations of EVA L, EVA S, Trosifol BG, and Trosifol ES, are shown in Fig. 116. All analytical relations correlate with those by experiments in terms of temperature and loading rate sensitivity. Analytically determined shear stiffness of all interlayers decreases with increasing temperature or decreasing loading rate which respects the viscoelastic nature of polymers.

Going further into comparison of numerical values, M-W models provided τ-γ relations consistent with experimental data to shear strains of approx. 30% in case of EVA L, EVA S, and Trosifol BG. This is satisfactory foundation since shear strain in intact LG panels in bending is lower in practice [33]. Higher shear strains resulted in stiffer response of M-W models, probably, due to exceeding the limit of linear viscoelasticity (then Schapery integral equation or a hyperelastic model of elastic springs hold better for stress output [72]) or due to lower real shear strain rate of the interlayer caused by TEMPOS frame stiffness, see Fig. 115a). Analytical relations of Trosifol ES show pronounced deviations from experimental relations even for low values of shear strains calling for M-W Prony series modification.

Although WLF equation of the temperature shift coefficient a_T(T) was used for all testing temperatures, with no distinction between entropy elastic or energy elastic areas, stiffening of both PVB´s when crossing their T_g, is well captured by their M-W models, see Fig. 116f) h) j). Analytical τ-γ relations of both EVA´s also well capture their rubbery state with gradual loss of initial shear stiffness at increasing temperature.

Comparison of analytical response given by M-W models of Trosifol BG with experiments shows both models are well temperature and loading rate sensitive, noting that one based on combined DMTA results in shear + torsion fits better to experimental data than that based only on DMTA in shear, compare Fig. 116f) and h).

Plotted analytical relations illustrate that constructed M-W models of PVB and EVA interlayers show stiffer response of Trosifol ES and EVA S than that of Trosifol BG and EVA L, respectively. This fact is consistent with experimental results.

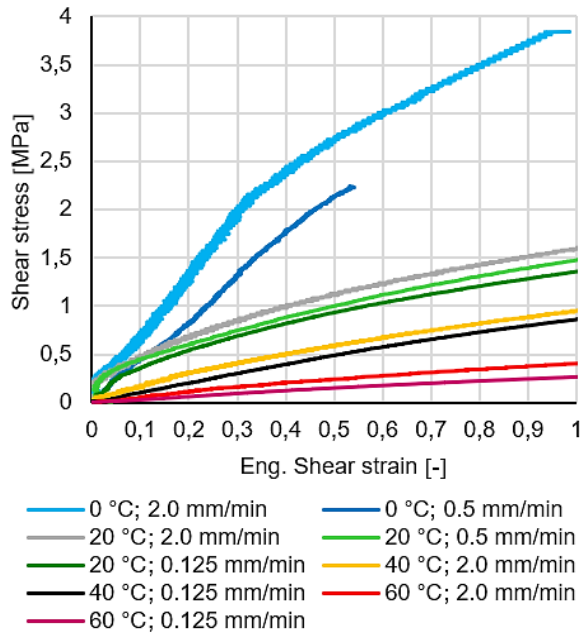

a) EVA L: static single-lap shear test

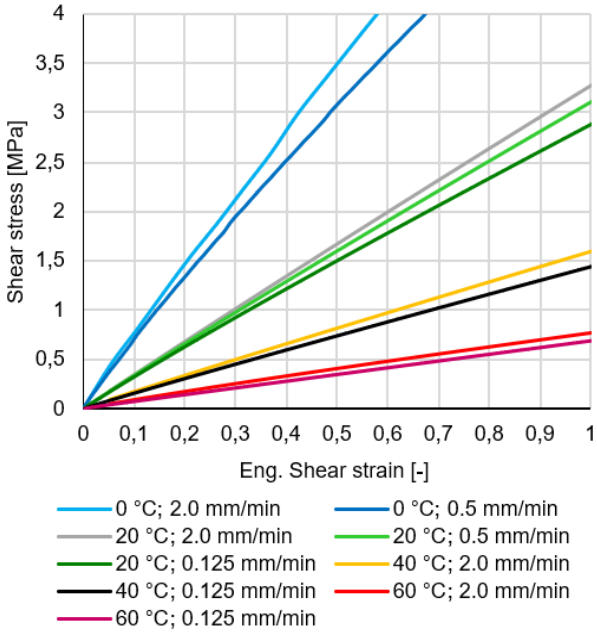

b) EVA L: M-W model, Prony input in Tab. 25

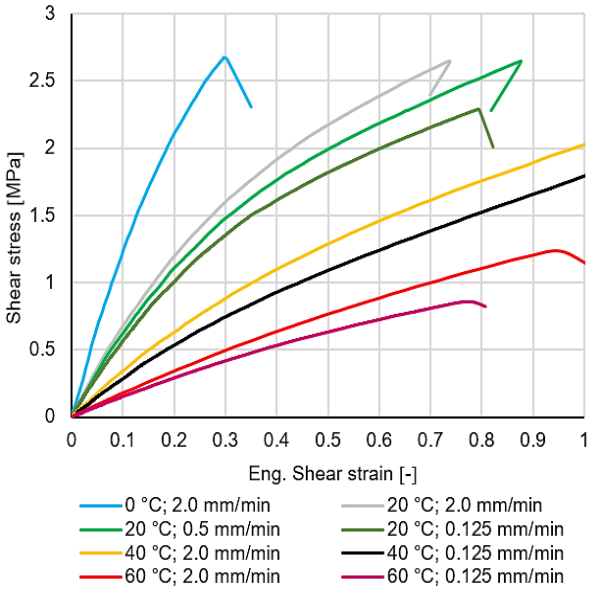

c) EVA S: static single-lap shear test

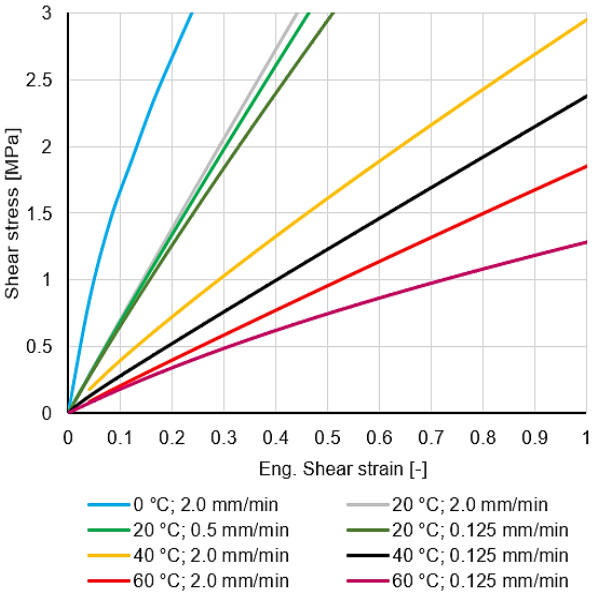

d) EVA S: M-W model, Prony input in Tab. 24

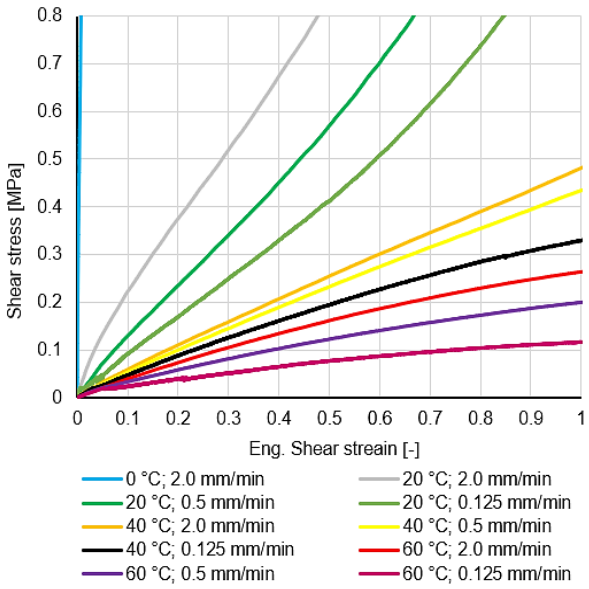

e) Trosifol BG: static single-lap shear test

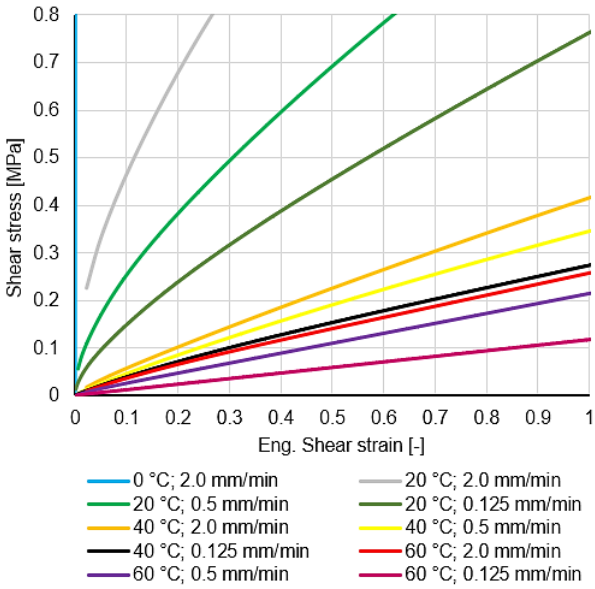

f) Trosifol BG: M-W model, Prony input in Tab. 25

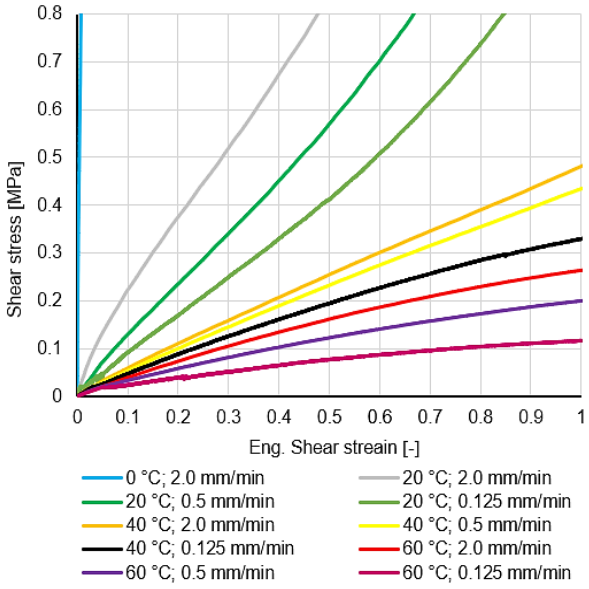

g) Trosifol BG: static single-lap shear test

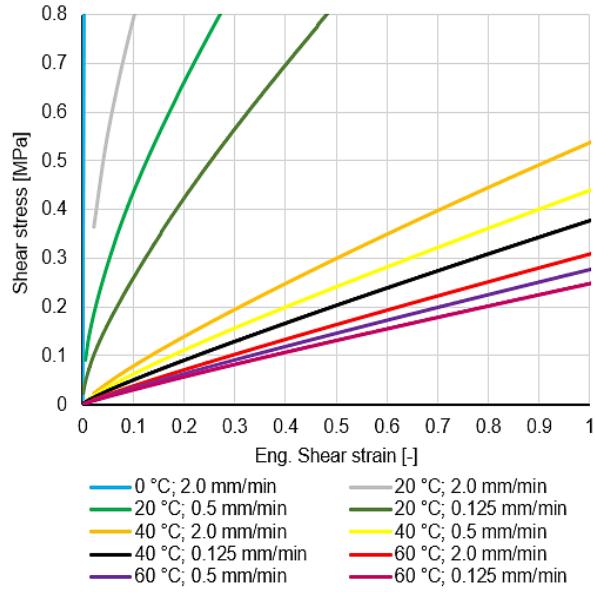

h) Trosifol BG: M-W model, Prony input in Tab. 22

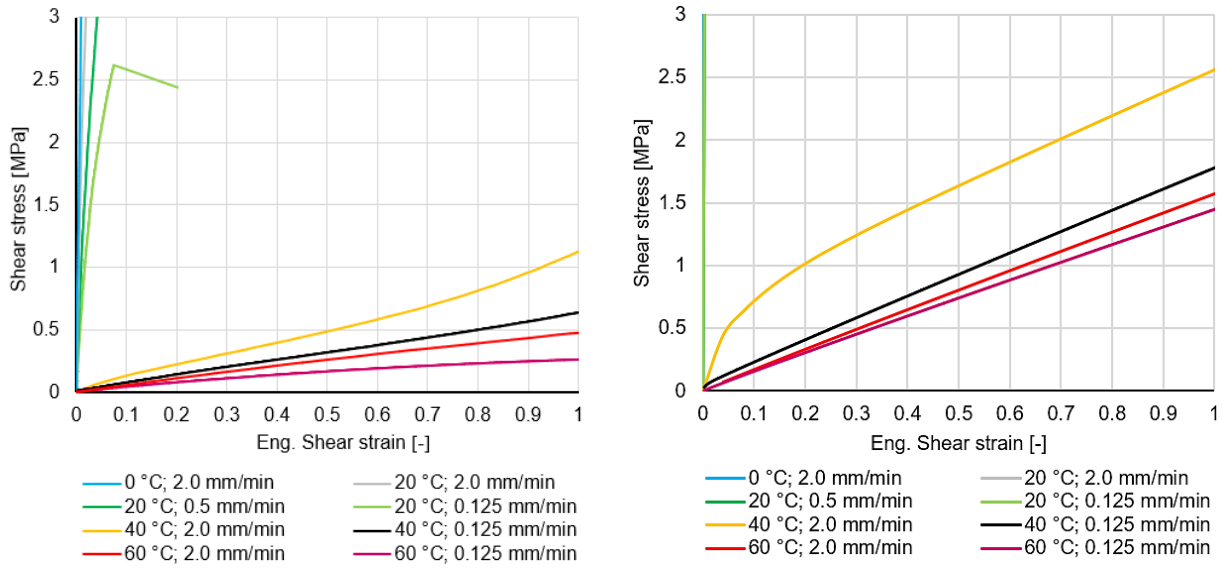

i) Trosifol ES: static single-lap shear test j) Trosifol ES: M-W model, Prony input in Tab. 23

Fig. 116: Comparison of experimental and analytical stress-strain relations of studied interlayers

Experimental and analytical τ-γ relations of Trosifol ES in Fig. 116 i) and j) are not consistent even for low values of shear strains with a need of M-W Prony series modification. Author attributes this need to measurement inaccuracies caused by stiff response of Trosifol ES in DMTA ($T_{g,\,ES}$ = 41 °C) or to omitted implementation of Arrhenius Eq. (6) into exact determination of temperature shift coefficient a_T(T). To get a better correlation with experiment, shear stiffness of elastic springs was 30% reduced and a new set of viscoelastic parameters was obtained, see Tab. 27. Using these parameters as an input in Eq.(61), analytical shear stress-strain relations were drawn in Fig. 117.

Tab. 27: Viscoelastic WLF and modified Prony series of Trosifol ES based on correlation with static small-scale single-lap shear tests in section 6.1

WLF model at T_{ref} = +20 °C			
C_1	18.4	C_2	75.6
Maxwell-Weichert model at T_{ref} = +20 °C			
G_∞ = 0.9 MPa			
θ_i [s]	G_i [MPa]	θ_i [s]	G_i [MPa]
1.000E-11	2.27E+02	3.039E+03	3.59E+00
5.298E-11	2.27E+02	1.610E+04	3.59E+00
2.807E-10	2.27E+02	8.532E+04	1.42E-01
1.487E-09	2.27E+02	4.520E+05	5.79E-02
7.880E-09	2.27E+02	2.395E+06	5.79E-02
4.175E-08	2.27E+02	1.269E+07	5.79E-02
2.212E-07	2.27E+02	6.723E+07	5.79E-02
1.172E-06	2.27E+02	3.562E+08	5.79E-02
6.210E-06	2.27E+02	1.887E+09	5.79E-02
3.290E-05	2.27E+02	1.000E+10	5.78E-02
1.743E-04	2.27E+02	1.425E+05	3.70E-06
9.237E-04	2.27E+02	4.924E+05	3.47E-06
4.894E-03	2.27E+02	1.701E+06	3.25E-06
2.593E-02	2.27E+02	5.878E+06	3.02E-06
1.374E-01	2.27E+02	2.031E+07	2.77E-06
7.279E-01	2.27E+02	7.017E+07	2.50E-06
3.857E+00	2.27E+02	2.424E+08	2.19E-06
2.043E+01	2.27E+02	8.377E+08	1.82E-06
1.083E+02	7.43E+01	2.894E+09	1.37E-06
5.736E+02	3.59E+00	1.000E+10	6.85E-07

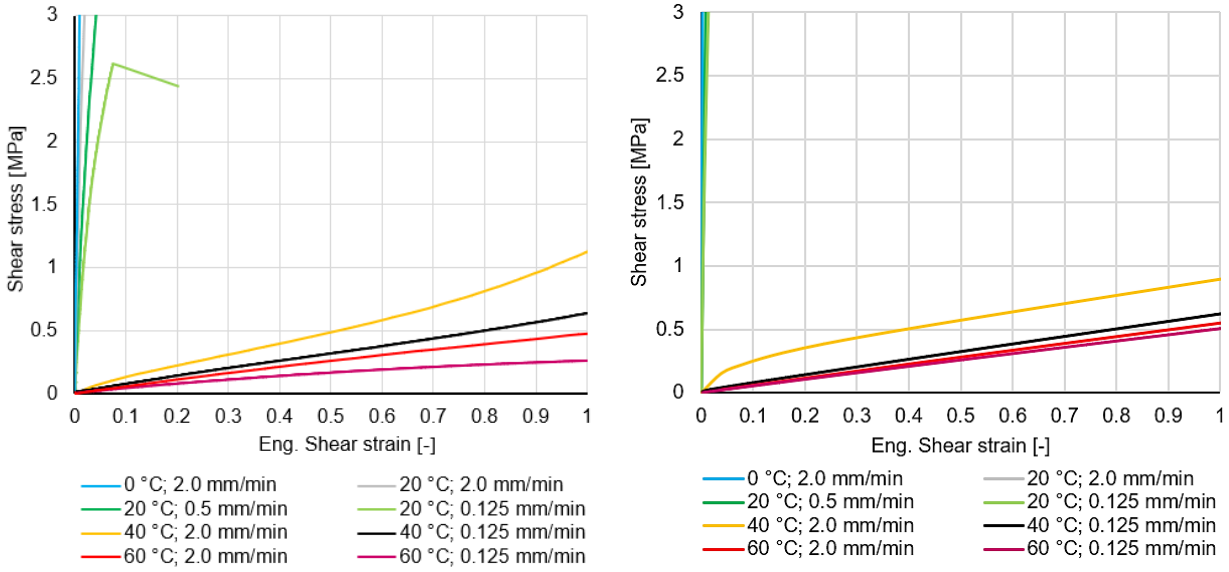

a) Trosifol ES: static single-lap shear test b) Trosifol ES: M-W model, Prony input in Tab. 27

Fig. 117: Comparison of experimental and analytical relations by modified M-W model of Trosifol ES

Modified M-W model already gives similar values of the initial shear stiffness with those measured by experiment. An agreement is also apparent for analytical stress-strain relations of shear strain to approx. 30%.

Shear relaxation functions $G(t, T)$ of Trosifol ES given by modified M-W model using Eq. (55) are shown in Fig. 118a). Trosifol ES is still stiffer than Trosifol BG, see the comparison of their relaxation functions in Fig. 118. Relaxation functions $G(t, T)$ of Trosifol BG in Fig. 118b) and c) based on various DMTA methods do not overlap. Hence, there is still a need to verify fitted relaxation functions by real experiments. Modified short-term shear moduli of Trosifol ES are the following: $G(t = 10\ s)$: 2281 MPa at 0 °C, 224 MPa at 20 °C, 1.3 MPa at 40 °C, and 1.1 MPa at 60 °C.

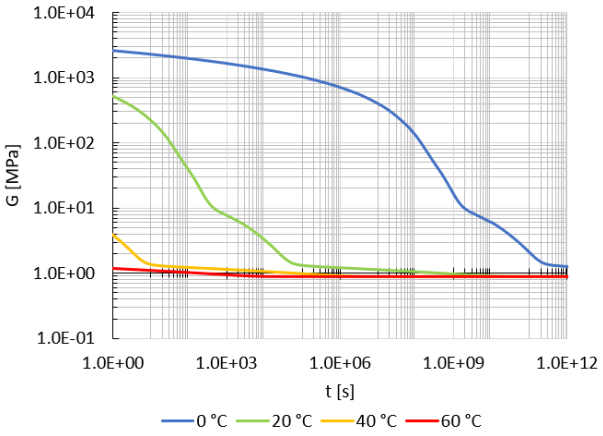

a) Trosifol ES: M-W Prony input from Tab. 27 (from DMTA results in shear)

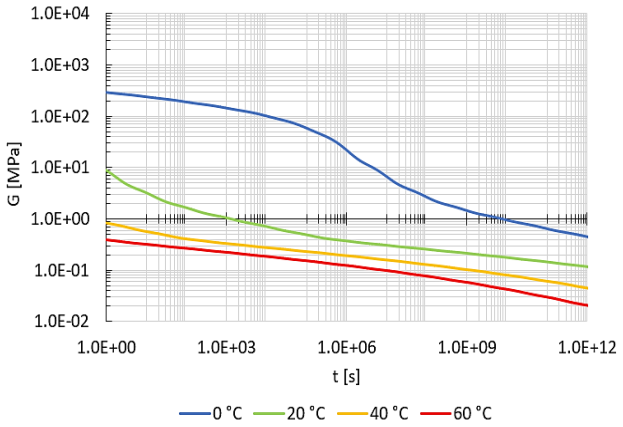

b) Trosifol BG: M-W Prony input from Tab. 22 (from DMTA results in shear)

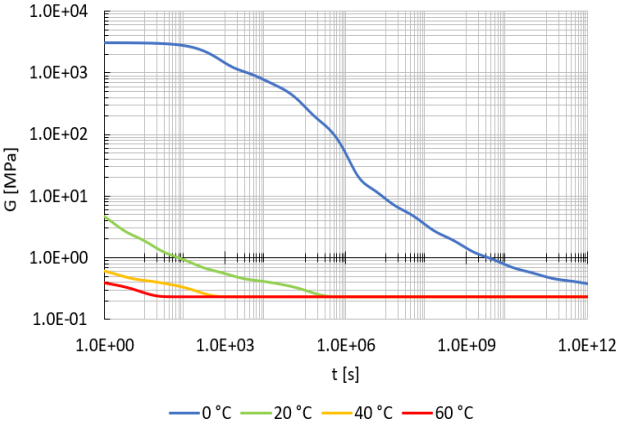

c) Trosifol BG: M-W Prony input from Tab. 25 (from combined DMTA results in shear + torsion)

Fig. 118: Shear relaxation functions of tested PVB interlayers given by various M-W models

7.3. Relation of experimental initial shear moduli of selected interlayers with four-point bending destructive tests

The linearity of experimental relations measured at four-point bending destructive tests of large scale Trosifol BG and EVA L specimens at cross-head loading rate 1.8 mm/min in section 6.3, and SG 5000 specimens at cross-head loading rate 2.0 mm/min in section 6.4, with relatively short duration of experiments (for HTG to 15 min), showed limited relaxation of interlayers during the 1st loading phase. This evoked the idea to calculate the response of the specimens in four-point bending destructive tests analytically (by W-B and EET methods) using the value of interlayers initial shear moduli G_{init} input from static single-lap shear tests in section 6.1 and verify the suitability of this input for short-term loaded 1D panels. Since four-point bending destructive tests were performed at room temperature and shear strain rate $\mathrm{d}\gamma/\mathrm{d}t$ of the interlayer in those tests was lower than that in static single-lap shear tests, the values of G_{init} from static shear tests in form of G_{init}(loading rate 0.125 mm/min, T = 20 °C) were used in analytical calculations. It means inputs in form: $G_{init,\,BG}$ = 0.8 MPa, $G_{init,EVA\,L}$ = 2.4 MPa and $G_{init,SG\,5000}$ = 206.0 MPa, see Tab. 7. Nominal dimensions of glass and interlayers were used, see Tab. 21. Plane dimensions were 360 × 1100 mm and the span l of the panel was 1000 mm, see static schema in Fig. 83a).

The example of Effective Thickness analytical calculations will be illustrated for Trosifol BG using both mentioned methods in [mm, MPa]. W-B method assumes boundary coefficient β = 9.6 [57] and the shape coefficient ψ [mm^{-2}] in EET will be considered in the form $\psi = 10/l^2$ for midspan loaded panel [58]. Notation of geometrical variables is shown in Fig. 52 and Fig. 53a).

W-B

Coefficient of shear forces Γ:

$$\Gamma = \frac{1}{1+\beta\cdot\frac{tE}{bGl^2}\cdot\frac{A_1A_2}{A_1+A_2}} = \frac{1}{1+9.6\cdot\frac{0.76\cdot 70000}{360\cdot 0.8\cdot 1000^2}\cdot\frac{3600\cdot 3600}{3600+3600}} = 0.24 \tag{62}$$

Effective Thickness for deflection:

$$h_{ef,w} = \sqrt[3]{h_1^3 + h_2^3 + 12\Gamma I_s} = \sqrt[3]{10^3 + 10^3 + 12\cdot 0.24\cdot 578.9} = 15.4 \text{ mm} \tag{63}$$

Effective Thickness for stress:

$$h_{1,ef,\sigma} = h_{2,ef,\sigma} = \sqrt{\frac{h_{ef,w}^3}{h_1 + 2\Gamma h_s}} = \sqrt{\frac{15.4^3}{10 + 2\cdot 0.24\cdot 5.4}} = 17.0 \text{ mm} \tag{64}$$

EET

Coefficient of shear forces η:

$$\eta = \frac{1}{1+\frac{tE}{bG}\cdot\frac{I_1+I_2}{I_{tot}}\cdot\frac{A_1A_2}{A_1+A_2}\cdot\Psi} = \frac{1}{1+\frac{0.76\cdot 70000}{360\cdot 0.8}\cdot\frac{2\cdot 30000}{268399}\cdot\frac{3600\cdot 3600}{3600+3600}\cdot 10^{-5}} = 0.57 \tag{65}$$

Effective Thickness for deflection:

$$h_{ef,w} = \frac{1}{\sqrt[3]{\frac{\eta}{h_1^3 + h_2^3 + 12I_s} + \frac{1-\eta}{h_1^3 + h_2^3}}} = \frac{1}{\sqrt[3]{\frac{0.57}{10^3 + 10^3 + 12 \cdot 578.9} + \frac{1-0.57}{10^3 + 10^3}}} = 15.3 \text{ mm} \tag{66}$$

Effective Thickness for stress:

$$h_{1,ef,\sigma} = h_{2,ef,\sigma} = \frac{1}{\sqrt{\frac{2\eta h_s}{h_1^3 + h_2^3 + 12I_s} + \frac{h_1}{h_{ef,w}^3}}} = \frac{1}{\sqrt{\frac{2 \cdot 0.57 \cdot 5.4}{10^3 + 10^3 + 12 \cdot 578.9} + \frac{10}{15.3^3}}} = 16.9 \text{ mm} \tag{67}$$

Note, both glass plies are of the same thickness 10 mm meaning their identical value of Effective Thickness for stress. Analytical calculation of Effective Thickness of EVA L and SG 5000 specimens was made using the same procedure with appropriate values of *G*, results are shown in Tab. 28. Both analytical methods delivered similar values of Effective Thicknesses for certain interlayer. The value of Effective Thickness decreases with decreasing shear stiffness *G* which is correct.

Using these values of Effective Thicknesses in the analytical calculation of four-point bending destructive tests enabled to determine the midspan normal stress and vertical deflection of lower glass ply for certain value of force by converting this task into 1D problem with $h_{ef,w}$ and $h_{ef,\sigma}$ respecting Navier bending hypothesis of slender beams, i.e., 1st order LE calculation of the monolithic beam in four-point bending (under the same loading and boundary conditions) defined by $h_{ef,w}$ and $h_{ef,\sigma}$. Analytical results are plotted in Fig. 119, and the values for certain force are numbered in Tab. 29. Experimental results in Fig. 119 are stated for the same testing specimens plotted in sections 6.3.2 (Fig. 86 – Trosifol BG and EVA L) and 6.4.2 (Fig. 92c – SG 5000).

Tab. 28: Parameters in analytical calculation of four-point bending destructive tests using W-B and EET

Trosifol BG: G = 0.8 [MPa]					
	W-B			EET	
Γ	$h_{ef,w}$	$h_{ef,\sigma}$	η	$h_{ef,w}$	$h_{ef,\sigma}$
[-]	[mm]	[mm]	[-]	[mm]	[mm]
0.24	15.40	17.00	0.57	15.30	16.90

EVA L: G = 2.4 [MPa]					
	W-B			EET	
Γ	$h_{ef,w}$	$h_{ef,\sigma}$	η	$h_{ef,w}$	$h_{ef,\sigma}$
[-]	[mm]	[mm]	[-]	[mm]	[mm]
0.48	17.48	18.76	0.79	17.36	18.70

SG 5000: G = 206 [MPa]					
	W-B			EET	
Γ	$h_{ef,w}$	$h_{ef,\sigma}$	η	$h_{ef,w}$	$h_{ef,\sigma}$
[-]	[mm]	[mm]	[-]	[mm]	[mm]
1.0	20.82	20.86	0.99	20.75	20.80

Closer look at Fig. 119 shows W-B is in coincidence with EET for all interlayers. Analytical results match well with experiment for EVA L and for SG 5000. Less favourable analytical relations are given for Trosifol BG where both experimental quantities, at certain force, are underestimated by both W-B and EET (deviation of EET from experiment is to 10% for stress). All statements are documented in Tab. 29. From an engineering point of view, stated deviations are satisfactory and show the suitability of G_{init} input from static single-lap shear tests into analytical calculations of short-term loaded 1D double LG panels at room temperature (to max 15 min as revealed by experiment) laminated with Trosifol BG, EVA L, and SG 5000 interlayers.

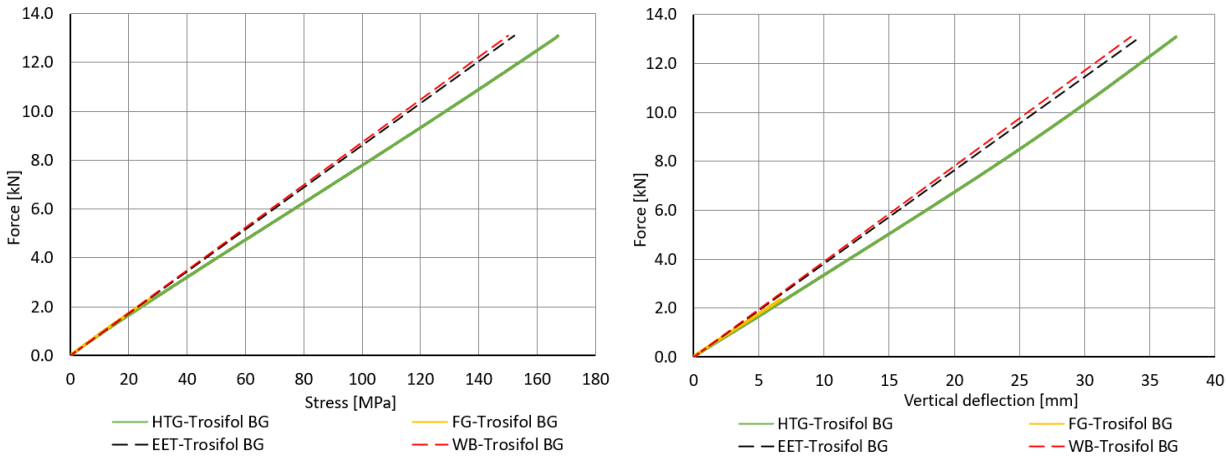

a) Trosifol BG: normal stress by SG 3 and vertical deflection (average by DS I and DS II)

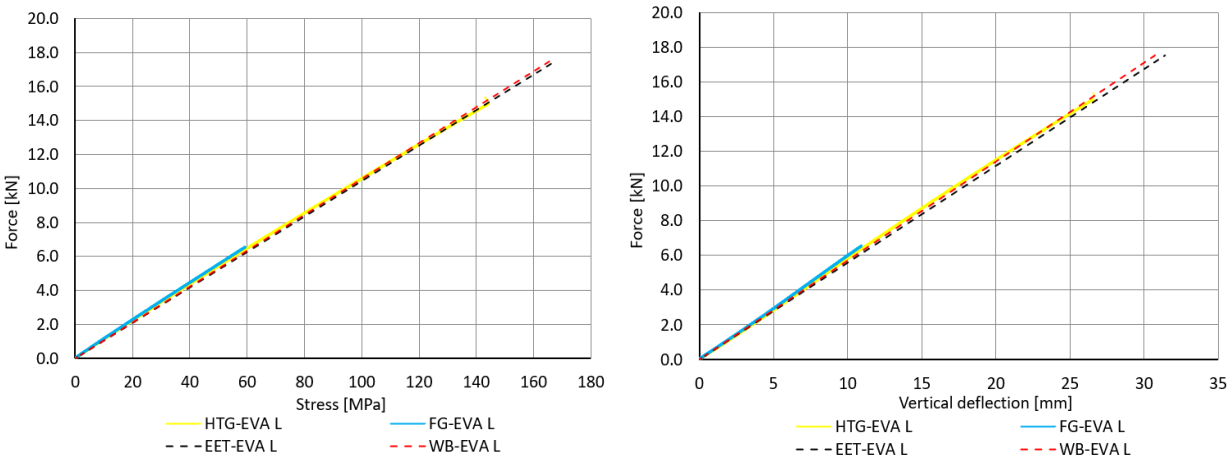

b) EVA L: normal stress by SG 3 and vertical deflection (average by DS I and DS II)

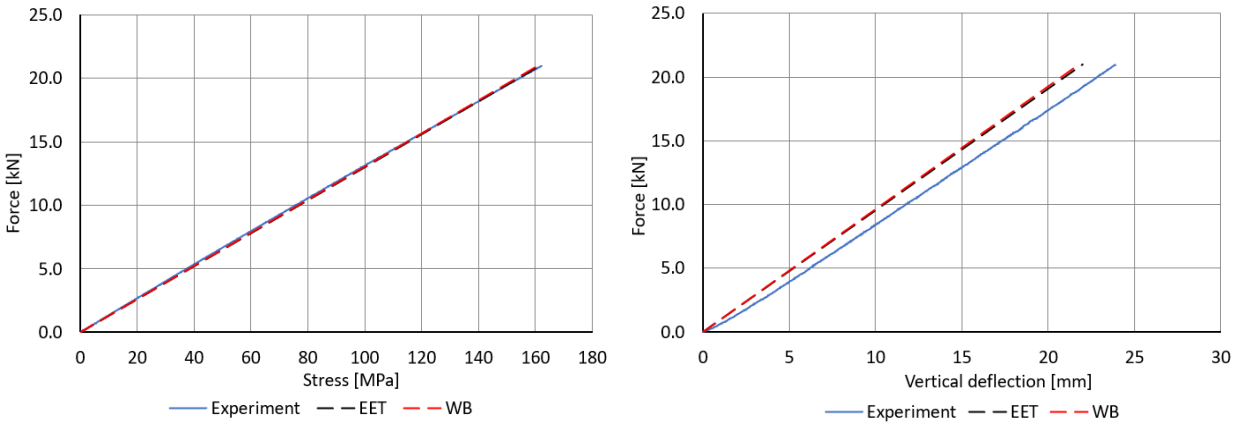

c) SG 5000: normal stress by SG 3 and vertical deflection (average by DS I and DS II)

Fig. 119: Comparison of four-point bending experimental relations at +20 °C for specimens plotted in sections 6.3.2 (Trosifol BG and EVA L) and 6.4.2 (SG 5000) with analytical relations by W-B and EET

Tab. 29: Comparison of experimental midspan normal stress in glass and vertical deflections with those by analytical W-B and EET methods using G_{init}(20 °C) inputs

Interlayer	Force F [kN]	Stress SG3 [MPa]	Deflection (average by DS I and DS II) [mm]	Stress EET [MPa]	Deflection EET [mm]	Stress W-B [MPa]	Deflection W-B [mm]
Trosifol BG	12.0	153.8	34.2	138.8	31.3	136.9	30.6
EVA L	14.0	134.2	24.6	133.6	25.0	132.1	24.4
SG 5000	18.0	138.6	20.7	138.2	18.8	137.6	18.6

7.4. Analytical part – conclusions

In this part of the thesis, experimental DMTA data of Trosifol BG, Trosifol ES, EVA L, and EVA S was used to fit their WLF constants C_1 and C_2 of temperature shift coefficient a_T(T) using Time Temperature Superposition Principle (TTSP) and to construct their optimal data Master Curves fitted by M-W models. To obtain the optimal set of M-W Prony series {G_∞, G_i, and θ_i} of each interlayer, optimizations in Matlab® by Kuntsche method [69] or by Nelder-Mead method [71] were employed. Fitting procedures were based on (i) DMTA data of Trosifol BG, Trosifol ES, and EVA S from shear tests in MTS and (ii) combined DMTA data of Trosifol BG and EVA L from shear tests in MTS + torsion tests in rheometer. Constructed M-W models were further loaded by strain rate input $d\gamma/dt$, identical with that theoretical one applied on the interlayers in static single-lap shear tests in section 6.1. The response of M-W models to the applied strain rate $d\gamma/dt$ was compared with experimental results. Moreover, the relation between $G_{init,EVA\ L}$, $G_{init,BG}$ and $G_{init,SG\ 5000}$ (from static single-lap shear tests in section 6.1) and results from four-point bending destructive tests in sections 6.3 and 6.4, was illustrated. The main findings of this part are concluded below.

- There is a variability between DMTA experimental data for specific temperature and frequency given by certain testing mode (if shear or torsion mode is used). Selected DMTA testing mode, therefore, influences fitted relaxation function.
- Keeping the variability of DMTA data obtained by different testing modes in mind, global fit of Master Curve and M-W Prony series including all measured and combined DMTA data equally, with the same weight, is appropriate. But the deviation of this optimal Master Curve given by the so fitted M-W model from combined experimental data is higher in comparison to that one fitted to one specimen tested by one certain DMTA method only. Therefore, the relaxation function of interlayer based on certain testing mode(s) still needs to be verified by real experiment.
- Different relaxation functions of both studied PVB based and EVA based interlayers mean identical chemical base of two interlayers does not predetermine identical shear stiffness. Exact chemical structure and composition of interlayer as well as lamination process are other important factors governing the final stiffness of a certain product. Hence, specific trademark of interlayer is important.
- Strain rate loaded fitted M-W models of studied PVB and EVA interlayers in various temperatures respect the viscoelastic nature of polymers – reduced shear stiffness at elevated temperature or lowered loading rate. Analytical stress-strain relations given by presented strain rate loaded M-W models are, in values, consistent with experiment to engineering shear strain of approx. 30% which is satisfactory.
- There is an analogy between short-term shear relaxation moduli given by DMTA and initial shear moduli given by static single-lap shear tests of small-scale specimen for both EVA and PVB based interlayers. The analogy is in values apparent for 10 s shear relaxation modulus G(t = 10s) for temperatures around or above T_g, $T \geq T_g$. For temperature below T_g, $T < T_g$, static single-lap shear test provides lower but safe value of this relaxation modulus. Therefore, if 10 s shear relaxation modulus of PVB or EVA interlayer is desirable, relatively simple static single-lap shear test with simple evaluation of G_{init} can be performed. The need of complicated DMTA is then eliminated because G_{init} reliably substitutes G(t = 10 s, T) as follows: G_{init}(loading rate $\epsilon < 2.0, 0.125 >$ mm/min, T) ≈ G(t = 10 s, T), see Tab. 30.
- Coincidence of experimental and analytical relations for large-scale Trosifol BG, EVA L, and SG 5000 specimens, loaded in four-point bending destructive tests in temperature range 19 °C and 24 °C, indicates the value of G_{init} given by presented static single-lap shear tests at 20 °C is a sufficient input for the calculation of short-term loaded 1D double LG panels in bending at room temperature by enhanced analytical methods.

Tab. 30: Analogy between 10 s shear relaxation modulus by DMTA and initial shear modulus G_{init} by static single-lap shear tests of small-scale specimens

Trosifol BG (T_g = +26 °C)				
	DMTA (shear)	Static single-lap shear tests		
Temperature	Relax. shear modulus Time 10 s	Initial shear modulus 2.0 mm/min	Initial shear modulus 0.5 mm/min	Initial shear modulus 0.125 mm/min
[°C]	[MPa]	[MPa]	[MPa]	[MPa]
0	240.2	144.13	103.32	--
+20	3.27	1.71	1.09	0.80
+40	0.56	0.46	0.45	0.31
+60	0.32	0.27	0.15	0.12

Trosifol BG (T_g = +26 °C)				
	DMTA (shear + torsion)	Static single-lap shear tests		
Temperature	Relax. shear modulus Time 10 s	Initial shear modulus 2.0 mm/min	Initial shear modulus 0.5 mm/min	Initial shear modulus 0.125 mm/min
[°C]	[MPa]	[MPa]	[MPa]	[MPa]
0	3051	144.13	103.32	--
+20	1.89	1.71	1.09	0.80
+40	0.42	0.46	0.45	0.31
+60	0.27	0.27	0.15	0.12

Trosifol ES (T_g = +41 °C)				
	DMTA (shear)	Static single-lap shear tests		
Temperature	Relax. shear modulus Time 10 s	Initial shear modulus 2.0 mm/min	Initial shear modulus 0.5 mm/min	Initial shear modulus 0.125 mm/min
[°C]	[MPa]	[MPa]	[MPa]	[MPa]
0	2281.69	1887.94	1887.94	--
+20	224.77	225.47	105.23	61.31
+40	1.37	0.90	--	0.61
+60	1.10	0.47	--	0.37

EVA L ($T_g < 0$ °C)				
	DMTA (shear + torsion)	Static single-lap shear tests		
Temperature	Relax. shear modulus Time 10 s	Initial shear modulus 2.0 mm/min	Initial shear modulus 0.5 mm/min	Initial shear modulus 0.125 mm/min
[°C]	[MPa]	[MPa]	[MPa]	[MPa]
0	6.61	7.46	6.52	--
+20	3.26	4.13	2.93	2.37
+40	1.57	0.98	--	0.84
+60	0.75	0.44	--	0.21

EVA S (T_g = -28 °C)				
	DMTA (shear)	Static single-lap shear tests		
Temperature	Relax. shear modulus Time 10 s	Initial shear modulus 2.0 mm/min	Initial shear modulus 0.5 mm/min	Initial shear modulus 0.125 mm/min
[°C]	[MPa]	[MPa]	[MPa]	[MPa]
0	10.79	13.26	13.28	--
+20	6.73	6.86	6.39	6.22
+40	2.94	3.43	--	3.09
+60	1.87	1.64	--	1.44

8. Numerical part of the thesis

Numerical part aims at verification of shear stiffness modulus *G* and constructed M-W models of selected interlayers obtained from experimental and analytical part of the thesis. This verification is performed on large-scale specimens loaded in four-point bending tests from sections 6.3 - 6.5. Numerical simulation was made in FE software RFEM®5 and ANSYS®18 APDL. The former enables only linear elastic analysis (LE). The latter enables, in addition, linear viscoelastic analysis (LVE). The choice of software was governed by the complexity of input data. Numerical results were compared with experimental data from four-point bending tests. Midspan tensile stress in glass and vertical deflections were in major attention, see Fig. 120. Designation of sensors remains the same as in section 6.3.

Note: Supposing small strain theory, plotted stress in the models is represented by engineering values.

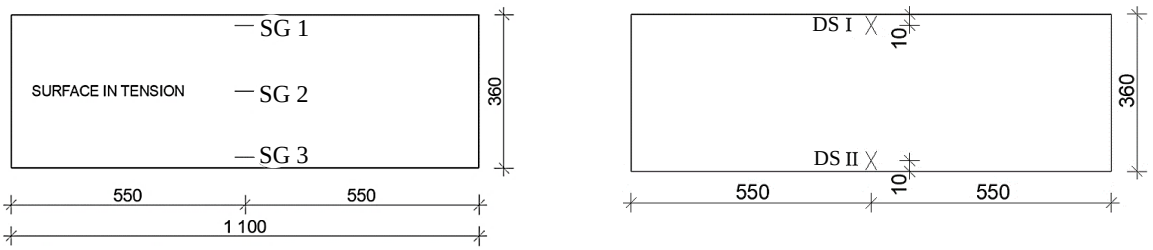

a) Strain gauges on lower ply of lower surface b) Displacement sensors

Fig. 120: Sensors of four-point bending tests whose data were used for comparison with num. results

8.1. LE analysis of four-point bending destructive tests

Conclusions from analytical part 7 suggesting the shear modulus G_{init}(T = 20 °C) of interlayer from static single-lap shear tests as an input into analytical calculation of short-term loaded 1D double LG panels in bending at room temperature, evoked the idea to perform simple linear elastic (LE) analysis of four-point bending destructive tests. Analysis was made in RFEM®5 using G_{init}(T = 20 °C, loading rate 0.125 mm/min) input. Creation of the model was rather quick and simple. Glass and interlayers were considered as homogeneous elastic isotropic materials with the following moduli of elasticity *E*, *G*, and Poisson ratio υ:

- Glass: E = 70 GPa; υ = 0.23
- Trosifol BG: G = 0.8 MPa; υ = 0.49
- EVA L: G = 2.4 MPa; υ = 0.49
- SG 5000: G = 206.0 MPa; υ = 0.49

Material isotropy and Poisson ratio of interlayers were based on recommendation stated in European standard EN 16613 [30] aimed at determination of interlayer mechanical properties. The model was created from the individual layers of nominal dimensions. This meant plane dimensions of 360 × 1000 mm (1000 mm distance of the supports), 2 × 10 mm thickness of glass, 0.76 mm thickness of Trosifol BG and EVA L, and 0.89 mm thickness of SG 5000. Since the static schema reminds simply supported panel, shorter bottom edges were supported by line hinge preventing the displacement in a vertical *z* direction. Additional hinge supports in horizontal *x* and *y* directions were added to the individual corner nodes to prevent numerical instabilities. The load in [kN] was applied in the form of line load in [kN/m] acting across the entire width of the panel. Its location correlated with the position of MTS loading apparatus, see Fig. 83a). Entire numerical model with boundary conditions and location of applied line load is shown in Fig. 121.

The model was meshed using 3D 8-node elements with linear displacement behaviour, each node with assigned three degrees of freedom in *x*, *y*, and *z* direction. A sensitivity study of meshing steps in range of < 5; 30 > mm did not show pronounced differences in results, therefore basic step of the mesh was chosen as 10 mm. The interlayer was modelled with one element and glass was modelled with two elements in a vertical sense. Details of used elements are shown in Fig. 122. The model was loaded with discrete values of measured force *F* recalculated to line load, and midspan normal stress and deflections were calculated by small strain 1st order LE analysis.

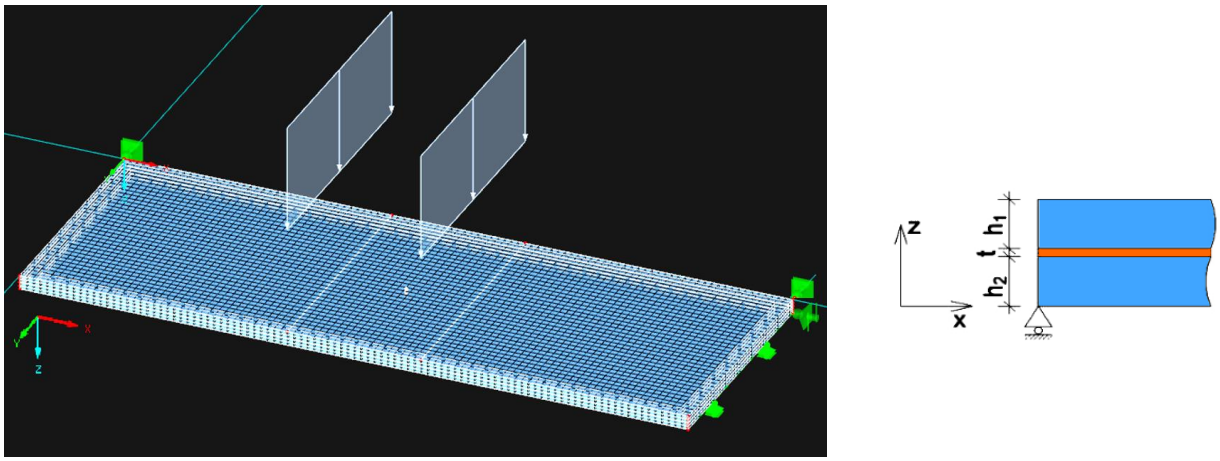

a) Entire numerical model with boundary conditions and mesh b) Line hinge along 360 mm edge

Fig. 121: Numerical model of four-point bending test in RFEM 5, plane dimensions 360 × 1000 mm

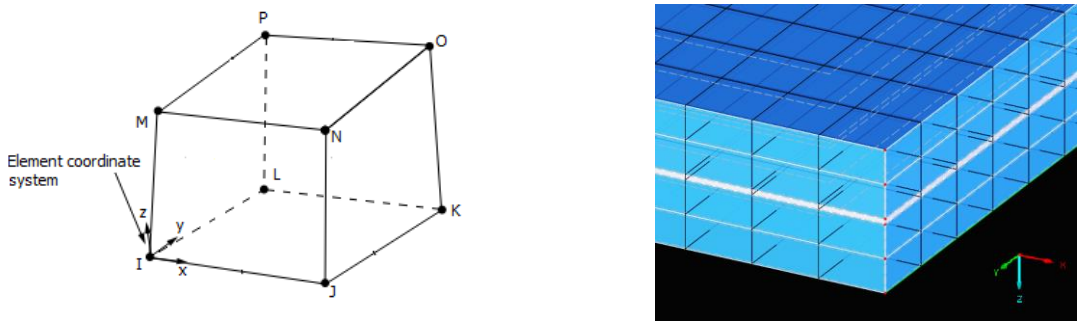

a) 8-node linear solid element used in the model b) FE mesh over the cross section

Fig. 122: Details of FE mesh used in the model

Numerical tensile stress at SG 3 and midspan vertical deflections are consistent with those by experiment, see Fig. 123. Experimental relations in Fig. 123 are shown for the same specimens plotted in section 7.3. (Fig. 119). Strain gauge SG 3 located near bottom edge in tension, was of main interest. Numerical and analytical values are similar, see their comparison with experimental data at the end of 1st loading phase in Tab. 31.

Tab. 31: Comparison of numerical and analytical calculation with experiment at certain value of force

Measured quantity	Analytical calculation by EET	Numerical calculation in RFEM 5	Experimental data
Trosifol BG Force at breakage 13.1 kN			
Normal stress in glass SG 3 [MPa]	+152.2	+158.5	+167.3
Normal stress in glass SG 6 [MPa]	-152.2	-153.2	-154.1
Midspan vertical deflection [mm]	34.3	34.4	37.0
EVA L Force at breakage 15.4 kN			
Normal stress in glass SG 3 [MPa]	+144.1	+150.5	+143.1
Normal stress in glass SG 6 [MPa]	-144.1	-146.3	-136.6
Midspan vertical deflection [mm]	27.0	27.2	26.6
SG 5000 Force at breakage 21.0 kN			
Normal stress in glass SG 3 [MPa]	+161.6	+166.7	+162.2
Normal stress in glass SG 6 [MPa]	-161.6	-163.8	-155.8
Midspan vertical deflection [mm]	22.0	22.3	23.9

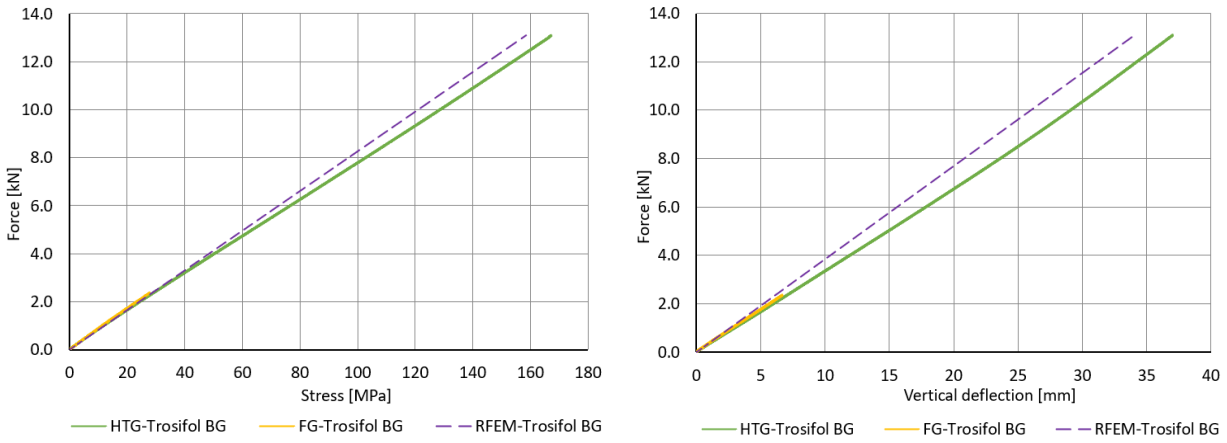

a) Trosifol BG: normal stress by SG 3 and vertical deflection (average by DS I and DS II)

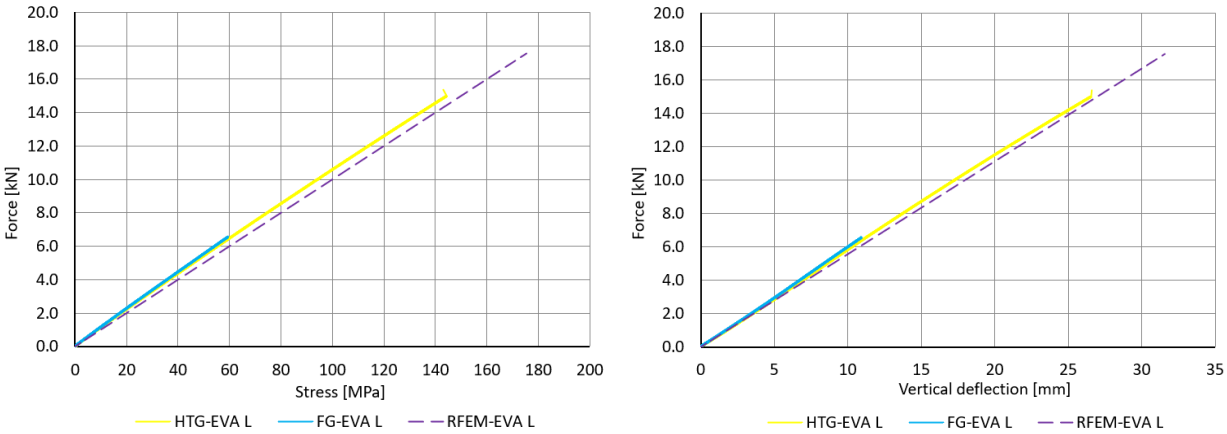

b) EVA L: normal stress by SG 3 and vertical deflection (average by DS I and DS II)

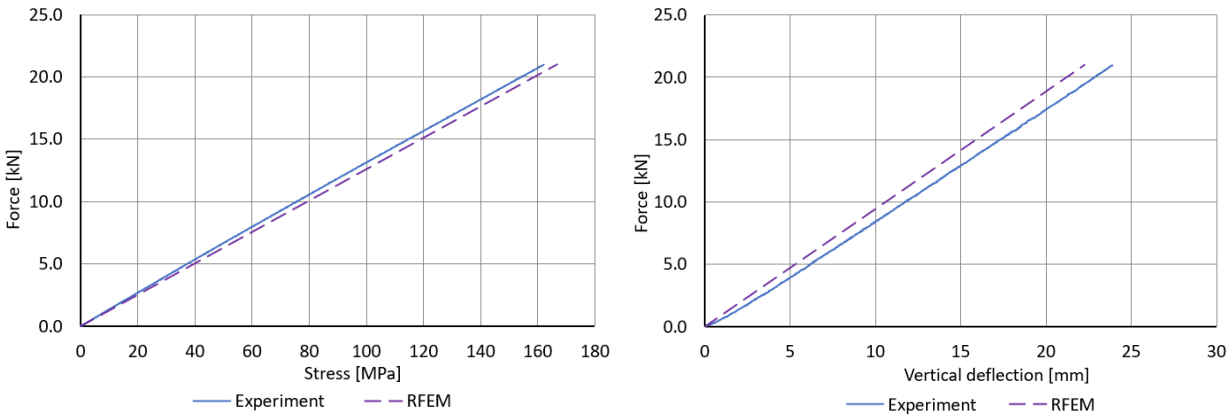

c) SG 5000: normal stress by SG 3 and vertical deflection (average by DS I and DS II)

Fig. 123: Comparison of numerical relations using G_{init} input at +20 °C with experimental data from four-point bending destructive tests in sections 6.3.2 (Trosifol ES, EVA L) and 6.4.2 (SG 5000)

Simple LE calculation also illustrated that relatively stiff interlayer SG 5000 ($G_{SG\ 5000}$ = 206.0 MPa) ensured linear distribution of normal stress over the entire midspan cross section meaning glass plies were fully shear coupled. On the other hand, shear modulus of Trosifol BG (G_{BG} = 0.8 MPa) caused nonlinear distribution of normal stress over the cross section meaning limited shear coupling of glass plies. These findings are graphically shown in Fig. 124 and are consistent with performed experiments. Correlation of numerical and experimental relations shows, relatively quick numerical model in RFEM 5 with G_{init}(20 °C) input of Trosifol BG, EVA L, and SG 5000 is also a good tool for the calculation of these short-term loaded 1D double LG panels at room temperature.

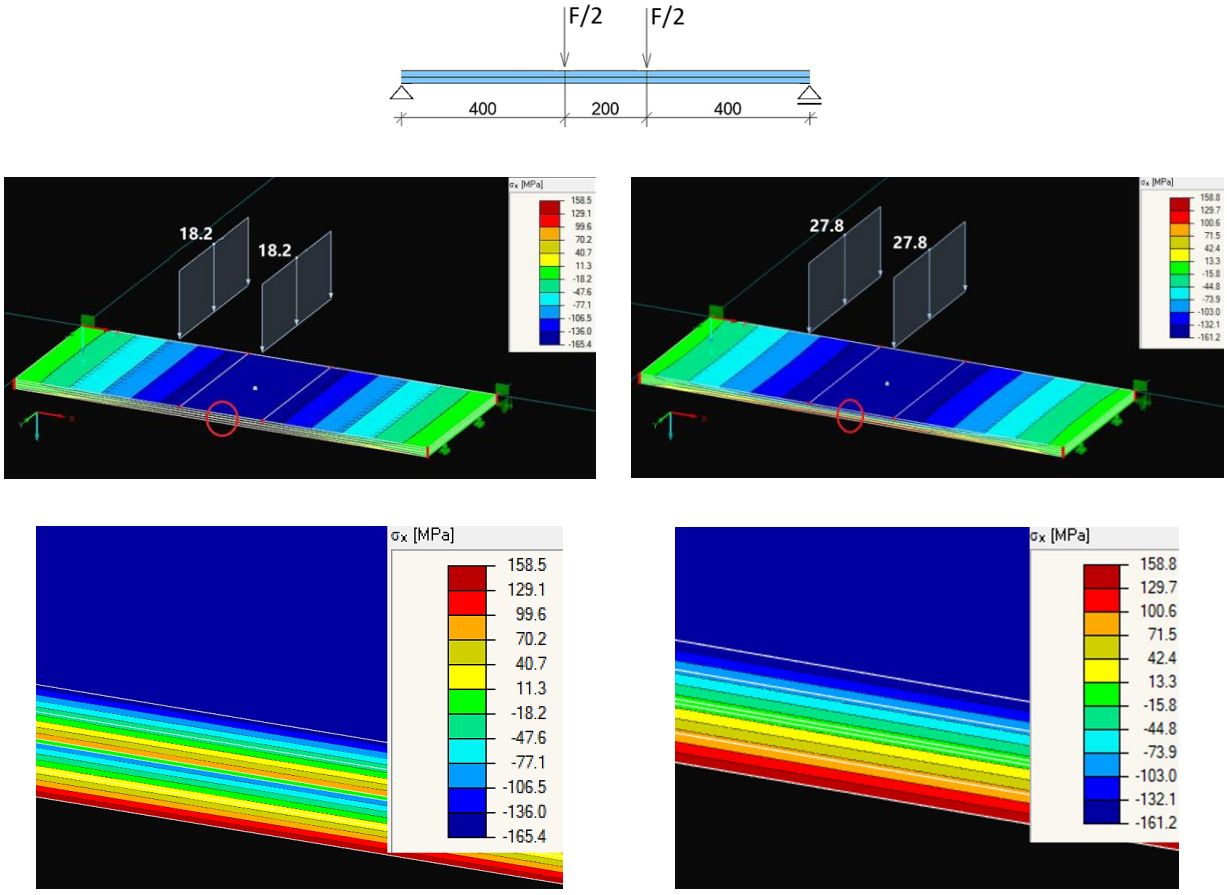

a) Trosifol BG, input G_{init} = 0.8 MPa, F = 13.1 kN b) SG 5000, input G_{init} = 206.0 MPa, F = 20.0 kN

Fig. 124: Midspan normal stress σ_x [MPa] over the testing specimen´s cross section by RFEM 5

Note: Vertical force F [kN] was in the model substituted by line load [kN/m] acting on the upper glass ply. F = 13.1 kN → 18.2 kN/m, F = 20.0 kN → 27.8 kN/m

8.2. Loading rate sensitivity of Maxwell models in LVE analysis of four-point bending destructive tests in various loading rates

Mechanical properties of selected interlayers were described by M-W models with a reference calling for the need of their verifications, especially in terms of DMTA testing modes these models were constructed on. To verify presented M-W models of Trosifol BG and EVA L in section 7, numerical LVE analysis of large-scale bending destructive tests in various loading rates from section 6.4, using these models as an input, was performed in ANSYS.

3D model in ANSYS was created using bottom-up technique as follows: First, spatial keypoints defining the corners of the individual layers were defined. These keypoints were connected by lines bordering the individual areas. Then, the individual volumes bordered by already defined areas, representing each layer of the specimen, were created. Values of all dimensions were modelled the same as in section 8.1 (e.g., 2 × 10 mm glass + 0.76 mm EVA or PVB). Boundary conditions were also modelled in the same way, i.e., line hinge in vertical *y* direction along the bottom shorter 360 mm edge with added individual corner hinge supports in horizontal *x* and *z* directions. Load was applied on the top surface where the panel was in contact with steel MTS loading bars, see Fig. 83a). Created model with boundary conditions, positions of load, and highlighted midspan by red strip are shown in Fig. 125.

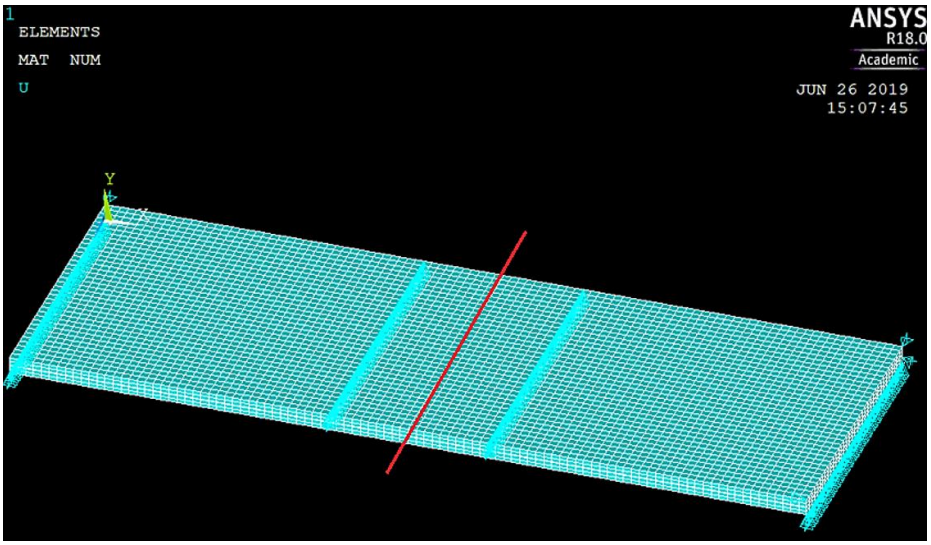

Fig. 125: Numerical model of four-point bending test in ANSYS, plane dimensions 360 × 1000 mm

Glass was defined as linear elastic, isotropic material with Young modulus $E = 70{\times}10^3$ MPa and Poisson ratio $v = 0.23$. Interlayers were defined as viscoelastic homogeneous isotropic material with Poisson ratio $v = 0.49$ [30] by constructed M-W models. LVE analysis is, in this context, materially nonlinear analysis, assuming linear viscoelastic material model of interlayer. Isotropy of interlayers enables to define the interrelations between their instantaneous elastic tensile/compressive E_{inst}, shear G_{inst}, and bulk K_{inst} moduli by M-W models as follows: $G_{inst} = E_{inst}/2{\cdot}(1+v)$; $K_{inst} = E_{inst}/3{\cdot}(1-2v) = 2{\cdot}G_{inst}{\cdot}(1+v)/3{\cdot}(1-2v)$. These equations are also valid for

every *i*-th elastic spring in M-W model, e.g., $K_i = 2 \cdot G_i \cdot (1+v)/3 \cdot (1-2v)$ [45]. Shear $G(t)$ and bulk $K(t)$ relaxation moduli of interlayer may be then written as

$$\text{a)} \quad G(t) = G_{inst} \cdot [a_\infty^G + \sum_{i=1}^{M} a_i^G \cdot \exp(-t/\theta_i^G)],$$
$$\text{b)} \quad K(t) = K_{inst} \cdot [a_\infty^K + \sum_{i=1}^{M} a_i^K \cdot \exp(-t/\theta_i^K)], \tag{68}$$

where G_{inst} and K_{inst} are defined by the sum of elastic components as $G_{inst} = \sum G_i + G_\infty$, $K_{inst} = \sum K_i + K_\infty$ and represent the stiffness of material without any relaxation effects. Relative shear and bulk moduli a_i of the individual elements are defined as $a_i^G = G_i/G_{inst}$ and $a_i^K = K_i/K_{inst}$. Symbols θ_i^G and θ_i^K represent relaxation times of individual Maxwell models as a ratio of damper viscosity and spring stiffness as $\theta_i^G = \eta_i^G/G_i$, $\theta_i^K = \eta_i^K/K_i$, see Fig. 126.

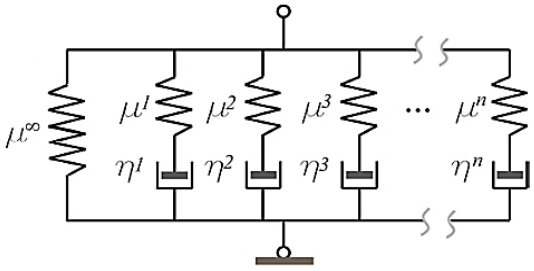

Fig. 126: Prony series of M-W model as an input into ANSYS – μ_i represents shear modulus G_i or bulk modulus K_i of an elastic spring, η_i represents a viscosity of a damper [45]

In the sense of linear viscoelasticity, ANSYS uses isotropy of a viscoelastic interlayer in the decomposition of its total strain into volumetric and deviatoric part. Stress-strain relation of interlayer in time is then expressed as follows [45]

$$\{\sigma(t)\} = \int_0^t [E(t-t')] \frac{\mathrm{d}\{\varepsilon\}}{\mathrm{d}t'} \mathrm{d}t' =$$
$$= \int_0^t 2G(t-t') \cdot [P] \frac{\mathrm{d}\{e\}}{\mathrm{d}t'} \mathrm{d}t' + \int_0^t K(t-t') \cdot \{j\} \frac{\mathrm{d}\varepsilon_V}{\mathrm{d}t'} \mathrm{d}t', \tag{69}$$

$$\{j\} = \{1,1,1,0,0,0\}^T, \qquad [P] = \begin{vmatrix} 1 & 0 & 0 & 0 & 0 & 0 \\ 0 & 1 & 0 & 0 & 0 & 0 \\ 0 & 0 & 1 & 0 & 0 & 0 \\ 0 & 0 & 0 & 0.5 & 0 & 0 \\ 0 & 0 & 0 & 0 & 0.5 & 0 \\ 0 & 0 & 0 & 0 & 0 & 0.5 \end{vmatrix} \tag{70}$$

where $\{e\}$ denotes deviatoric part of strain tensor in Voigt notation, ε_V represents volumetric part of strain tensor, G(t) represents shear relaxation modulus, K(t) is bulk relaxation modulus, t is evaluated time, time t' lies in interval $< 0; t >$, and $\{\sigma(t)\}$ represents stress tensor in Voigt notation. Scaling matrix [P] and vector $\{j\}$ are noted in Eq. (70). By means of Eq. (69), Prony input needs to be defined using both shear G_i and bulk K_i moduli of each Maxwell model, see Fig. 126. Example of this input for Trosifol BG at 20 °C is shown in Tab. 32. Supposing the deviatoric and volumetric part of stress relaxes in the same manner, number of Maxwell models as well as their shear and bulk relaxation times (θ_i^G, θ_i^K) were considered identical [73]. Prony input for other studied interlayers into ANSYS was made using the same procedure described herein. In case the deviatoric and volumetric parts of stress follow different relaxation behaviour, the number of Maxwell models and relaxation times $\theta_i^{G,K}$ for shear and volumetric response need not be the same but this fact must be demonstrated by an experiment [45].

Tab. 32: Prony series of Trosifol BG based on combined DMTA results in shear + torsion as LVE input

WLF model					
T_{ref}	+20 °C	C_1	8.635	C_2	42.422
Maxwell-Weichert model at T_{ref} = +20 °C					
E_{inst} [MPa]	9196.23	G_{inst} [MPa]	3085.98	K_{inst} [MPa]	153270.49
E_∞ [MPa]	0.69	G_∞ [MPa]	0.23	K_∞ [MPa]	11.54
E_i [MPa]	G_i [MPa]	a_i^G [-]	K_i [MPa]	a_i^K [-]	$\theta_i^K = \theta_i^G$ [s]
5310.73	1782.12	0.5774	88512.17	0.5775	1.00E-05
1547.24	519.21	0.1682	25787.37	0.1682	1.00E-04
1627.61	546.18	0.1770	27126.78	0.1770	1.00E-03
646.34	216.89	0.0703	10772.36	0.0703	1.00E-02
40.58	13.62	0.0044	676.38	0.0044	1.00E-01
14.87	4.99	0.0016	247.75	0.0016	1.00E+00
4.96	1.66	0.0005	82.64	0.0005	1.00E+01
1.75	0.59	0.0002	29.16	0.0002	1.00E+02
0.77	0.26	8.360E-05	12.81	8.360E-05	1.00E+03
0.19	0.06	2.067E-05	3.17	2.067E-05	1.00E+04
0.50	0.17	5.457E-05	8.36	5.457E-05	1.00E+05

The model was meshed using 3D elements SOLID 186 with reduced integration. This 20-node hexahedron with 3 degrees of freedom (displacements x, y, z) in each node ensures quadratic displacement behaviour and supports, besides linear elasticity, also linear viscoelasticity. Moreover, quadratic displacement behaviour of this element reduces unfavourable volumetric locking effects [74]. Geometry of chosen hexahedron with modifications are shown in Fig. 127a). Basic step of the mesh 10 mm was the same as in LE analysis. Glass was modelled with two elements and interlayer with one element in a vertical sense, see Fig. 127b).

The model was loaded with prescribed node displacement in vertical y direction. Displaced nodes were located on the top surface across the width of the specimen. The line of displaced nodes was located at the same position where MTS steel loading bars were in contact with glass, see

Fig. 83a) and Fig. 125. Prescribed vertical displacement of nodes respected prescribed MTS cross-head loading rate such as 2.0 mm/min; 0.5 mm/min; or 0.125 mm/min.

Source text file was constructed parametrically to enable the change of all parameters defining the geometry of the specimen and viscoelastic material of an interlayer. Hence, it will be, in the future, possible to perform LVE analysis using this source file for other types of interlayers. Complete ANSYS source files of these large-scale four-point bending destructive tests at various loading rates for studied interlayers are in the attachment of this thesis.

Solution settings in ANSYS were set as follows:

- static analysis,
- time linear vertical displacement of loaded nodes in 56 loading steps,
- small strain analysis,
- 10 Substeps in each loading step,
- all supports fixed in their directions,
- full Newton-Raphson method of nonlinear solution applied.

Time dependence of interlayer´s stiffness and load made the complete task time dependent. In Voigt matrix notation written as $[K(t)]\{r\} = \{f(t)\}$, where $[K(t)]$ is global stiffness matrix of the structure, $\{r\}$ is the vector of nodal displacements, and $\{f(t)\}$ is the vector of nodal loads. Therefore, the load was applied on structure in increments and the solution in every loading step respected the principle of virtual displacement, see Eq. (38). Totally 56 loading steps were applied. Numerical force-tensile stress in glass and force-vertical deflection relations for both Trosifol BG and EVA L interlayers, plotted over those by experiment, are shown in Fig. 128 and Fig. 129.

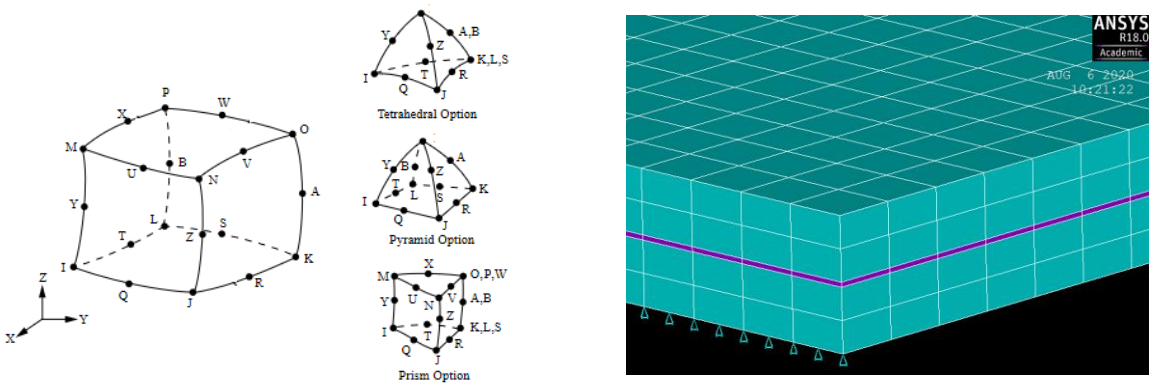

a) 20-node linear SOLID 186 with modifications b) FE mesh over the cross section

Fig. 127: Geometry of chosen element SOLID 186 and FE mesh

All numerical relations react to the loading rate applied and show reduced bending stiffness of the specimen as soon as the prescribed loading rate decreases. Closer comparison of numerical and experimental relations of Trosifol BG shows that global fit from combined DMTA results in shear + torsion provided M-W model whose Prony series react to the loading rate and plotted numerical relations match well with those by experiment, see Fig. 128c) and d). Contrary, DMTA in shear provided M-W model whose Prony series delivered rather unsafe numerical results and overestimated the bending stiffness of the specimen, see Fig. 128a) and b). Noteworthy deviation from experiment was obtained for applied force 10 kN at cross-head loading rate 0.125 mm/min (tensile stress deviated for 14% and deflection deviated for 26%). This comparison shows global fit of M-W model from combined DMTA results fits better to short-term loaded LG panel in bending at room temperature.

Numerical relations using constructed M-W model of EVA L delivered slightly higher values of tensile stress and deflections meaning more compliant numerical specimen, see Fig. 129. Noticeable deviation from experiment was detected at force 14 kN and loading rate 2.0 mm/min (tensile stress deviated to 10% and deflection deviated to 7%) which is satisfactory.

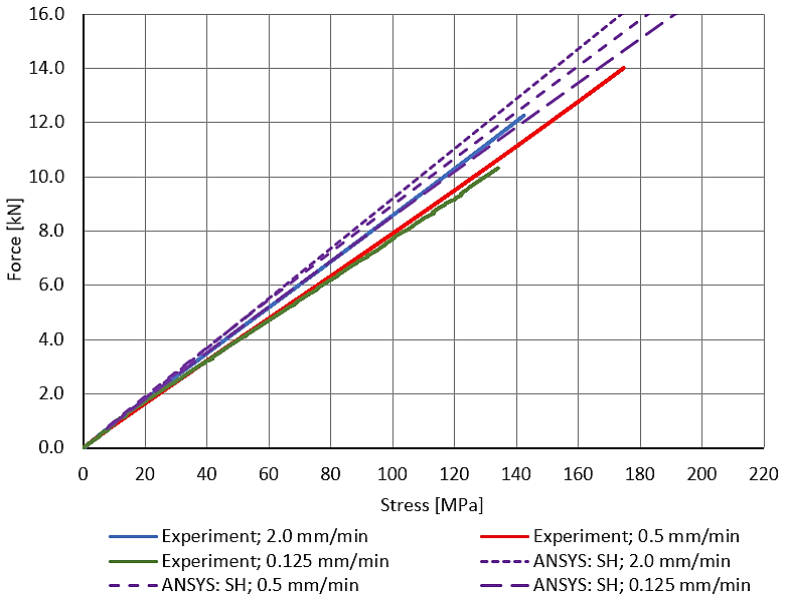

a) Normal stress by SG 3; M-W model based on DMTA in shear (SH)

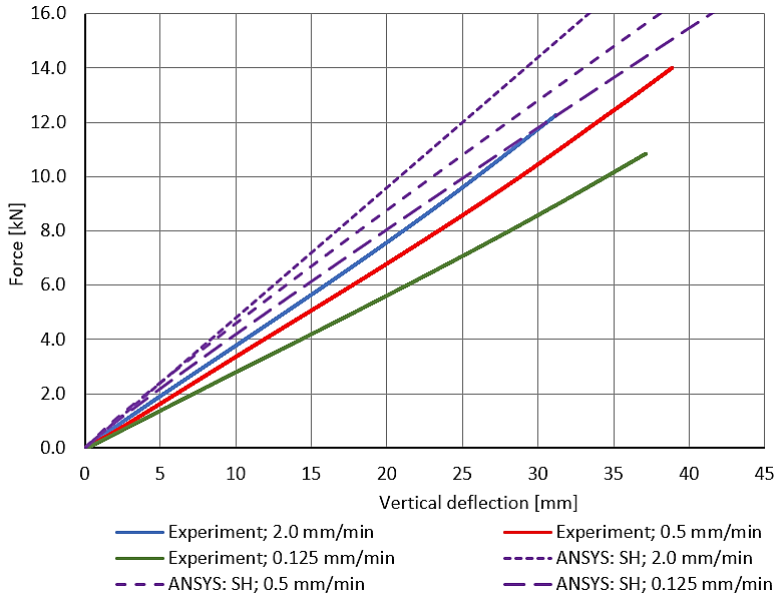

b) Vertical deflection (average by DS I and DS II); M-W model based on DMTA in shear (SH)

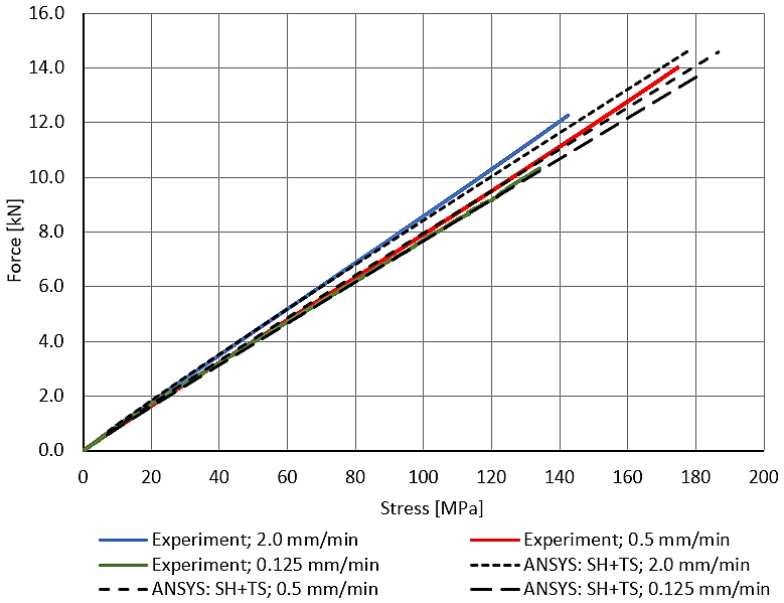

c) Normal stress by SG 3; M-W model based on combined DMTA results in shear + torsion (SH+TS)

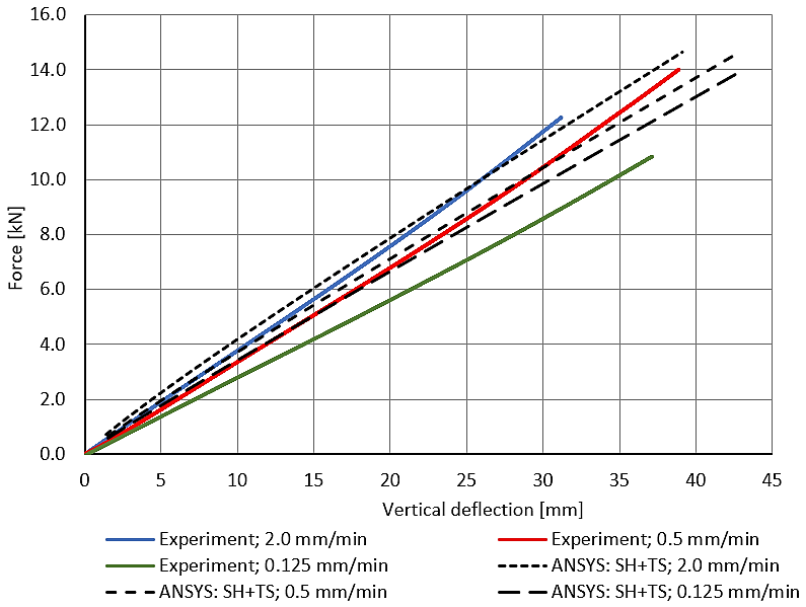

d) Vertical deflection (average by DS I and DS II); M-W model based on combined DMTA results in shear + torsion (SH+TS)

Fig. 128: Comparison of experimental and numerical midspan tensile stress in glass and vertical deflections using various M-W models of Trosifol BG from Tab. 22 and Tab. 25, T = +20 °C

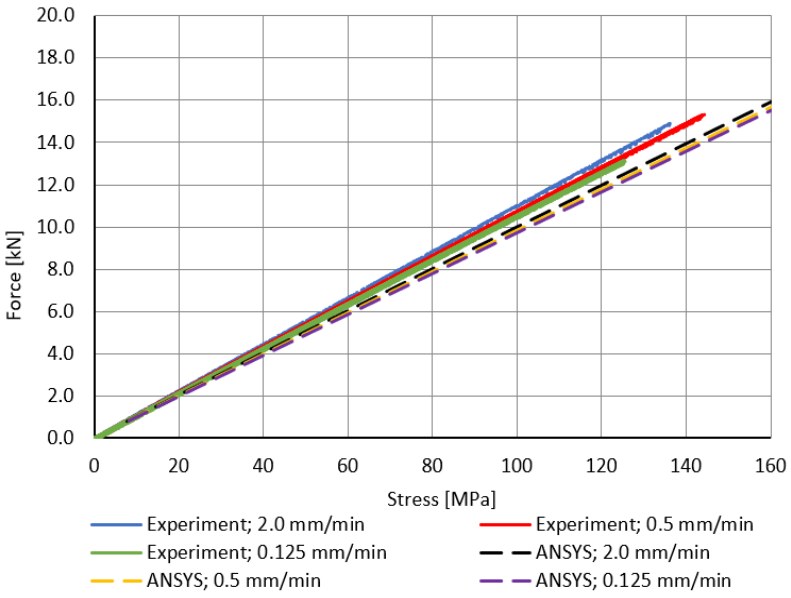

a) Normal stress by SG 3

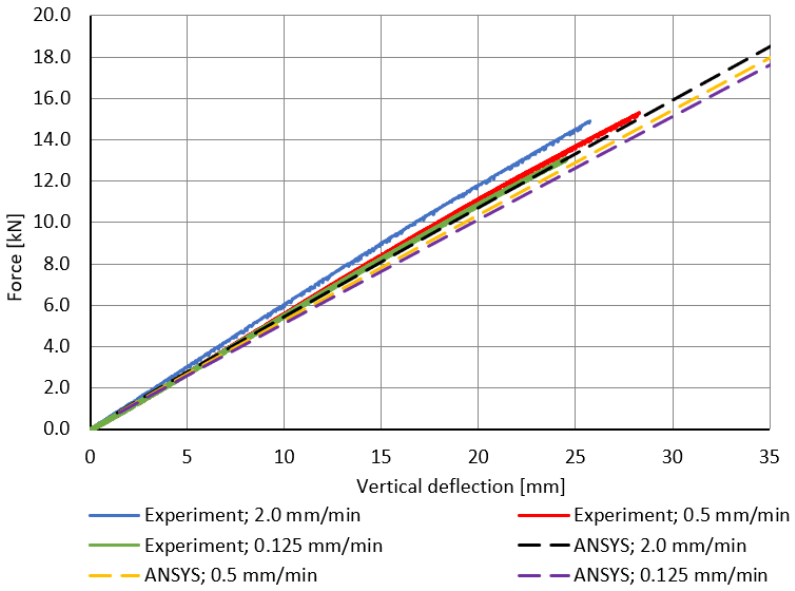

b) Vertical deflection (average by DS I and DS II)

Fig. 129: Comparison of experimental and numerical midspan tensile stress in glass and vertical deflections using fitted M-W model of EVA L from Tab. 25, T = +20 °C

Fig. 130 illustrates the numerical distribution of midspan normal tensile stress in glass over the width of the specimen´s cross section by use of fitted M-W models of Trosifol BG and EVA L at certain load. Experimental data is also provided. Both models deliver conservative values of tensile stress in glass and react to reduced loading rate by increasing value of stress. This correlates with the experiment in sense of pronounced relaxation effects of the specimen loaded at slower loading rate. Isolines of normal stress acting on the lower surface of lower glass ply for both interlayers, plotted in Fig. 131, show the entire surface was in tension with peaks of stress between loading MTS steel bars. This correlates with the course of bending moments along the span of the specimen according to the loading schema in Fig. 83a).

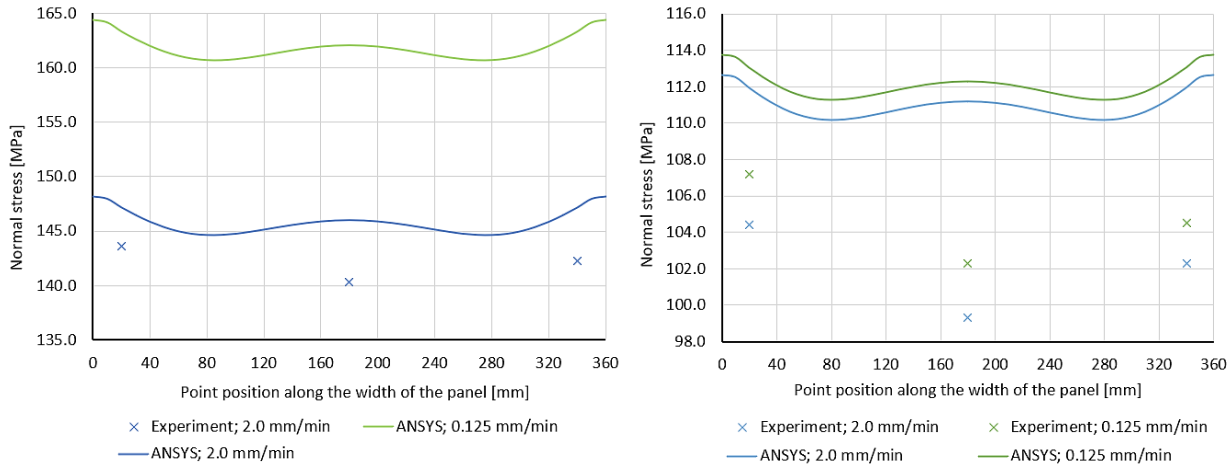

a) Trosifol BG: Force F = 12.0 kN

b) EVA L: Force F = 11.0 kN

Fig. 130: Comparison of experimental and numerical midspan tensile stress in glass σ_x over lower surface of lower glass ply, M-W models based on combined DMTA results in shear + torsion (SH+TS) in Tab. 25.

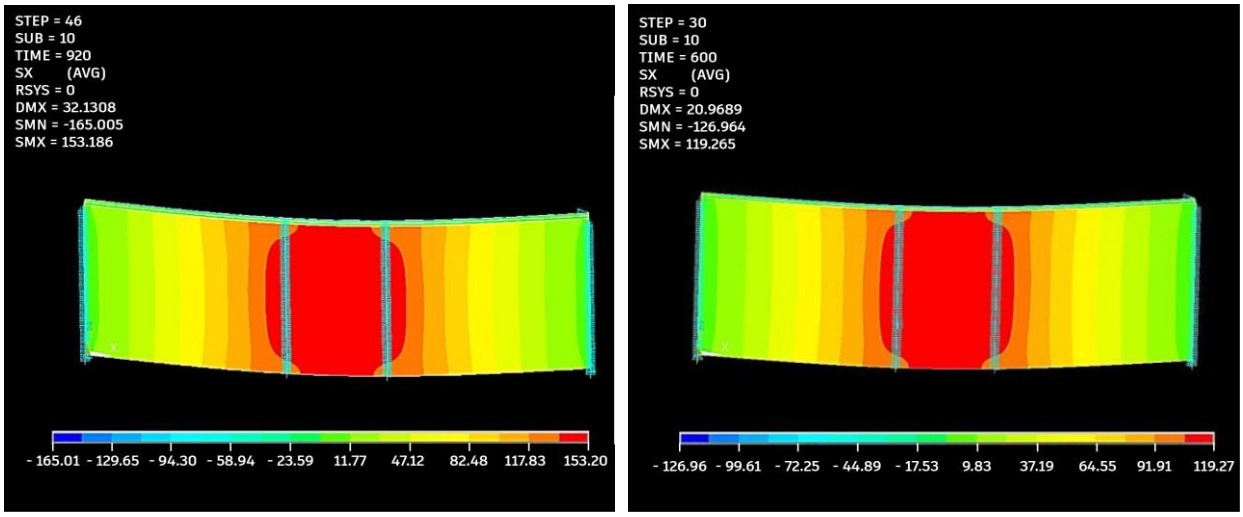

a) Trosifol BG: Force F = 12.0 kN; loading rate 2.0 mm/min

b) EVA L: Force F = 11.0 kN; loading rate 2.0 mm/min

Fig. 131: Numerical results of normal stress in horizontal direction σ_x [MPa] in glass – lower ply, lower surface; M-W models based on combined DMTA results in shear + torsion (SH+TS) in Tab. 25

8.3. LVE analysis of four-point bending creep tests

Creep tests of Trosifol BG and EVA L panels from section 6.5 were other subject of LVE analysis in ANSYS. To put the creep results into the context with DMTA results, relaxation functions of Trosifol BG and EVA L are plotted in Fig. 132 to 10^6 s ~ 270 h. Comparison of these functions shows that for every plotted temperature holds $G_{EVA\,L}(t, T) > G_{BG}(t, T)$. This was also confirmed at creep experiments.

Glass and interlayers were, in the model, defined by the same material parameters as in four-point bending destructive tests, see section 8.2. Moreover, effect of temperature needed to be included by modification of all relaxation times $\theta_i(T)$ in M-W model of interlayer by Eq. (28) with one common temperature shift coefficient $a_T(T)$ using appropriate WLF constants C_1 and C_2.

Numerical model was created by the same procedure as in section 8.2 using the same elements, meshing, nominal dimensions, and boundary conditions, see Fig. 125 (e.g., 2 × 10 mm glass + 0.76 mm EVA or PVB).

Total applied force F = 1.12 kN at experiment was on the model applied in the form of an equivalent pressure 0.1555 N/mm^2 acting on 10 × 360 mm strips, see Fig. 133. The load was applied on the specimen and remained constant in time. As soon as the loading time had passed, the specimen was unloaded.

The time of loading matched with the experiments. Creep phase with applied load was divided up to max. 61-time steps, unloading phase was divided up to max. 27-time steps with denser time division right after loading and unloading.

Source text file in ANSYS was constructed parametrically to enable the change of all parameters defining the geometry of the specimen and material of the interlayer. Complete source files of these four-point bending creep tests with studied interlayers are in the attachment of this thesis.

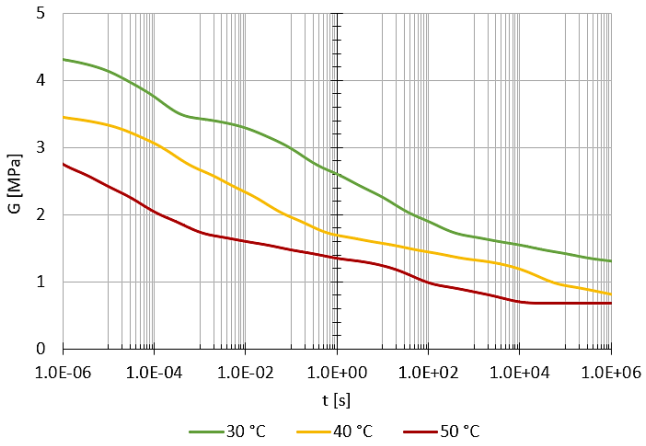

a) EVA L: M-W Prony input from Tab. 25

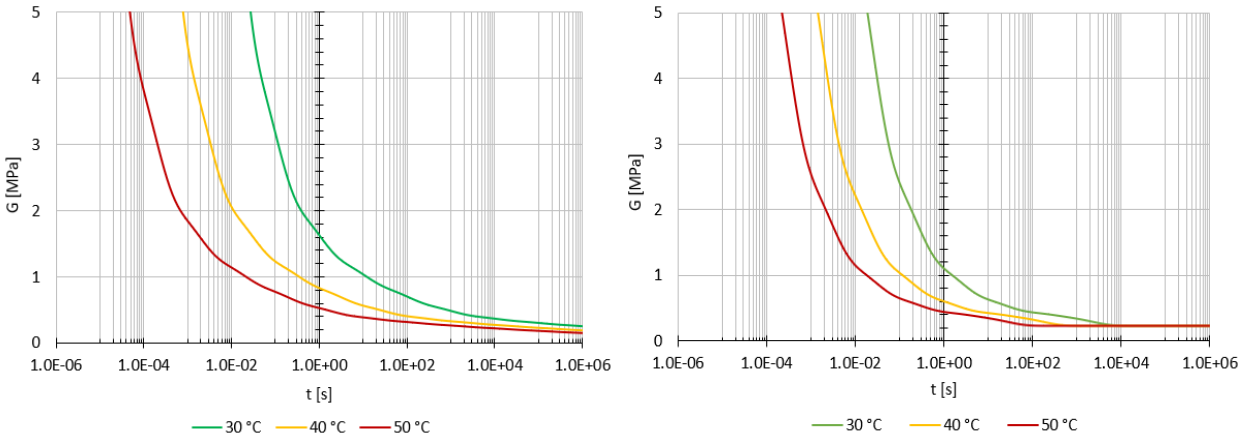

b) Trosifol BG: M-W Prony input from Tab. 22 (from DMTA results in shear)

c) Trosifol BG: M-W Prony input from Tab. 25 (from combined DMTA results in shear + torsion)

Fig. 132: Relaxation functions at testing temperatures of both tested interlayers given by M-W models

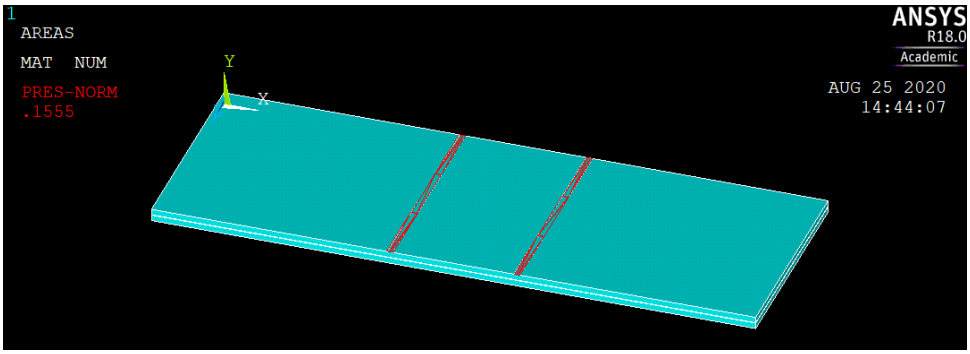

Fig. 133: Pressure 0.1555 N/mm^2 acting on both 10 × 360 mm red strips located 100 mm far from symmetry axis as an equivalent of applied force 1.12 kN

Solution settings were in ANSYS set as follows:

- static analysis,
- time constant value of applied load,
- small strain analysis,
- time of loading divided up to 61 steps,
- time of unloading divided up to 27 steps,
- 10 substeps in each time step,
- all supports fixed in their directions,
- full Newton-Raphson method of nonlinear solution applied.

Set of algebraic equations [K(t)]{r**}** = {f(t)} was solved iteratively in each time step. Numerical results of midspan normal tensile stress in glass at lower surface and vertical deflections are plotted over experimental relations in Fig. 134 for Trosifol BG and in Fig. 135 for EVA L.

All numerical results respect the physical nature of creep – increase of calculated values at constant load in time. In case of fixed time and elevated temperature, tensile stress and deflections

also increase (shear modulus of interlayer G is reduced). The inequality of Trosifol BG and EVA L shear relaxation moduli in Fig. 132, $G_{EVA\,L}(t, T) > G_{BG}(t, T)$, is reflected by their absolute values of both calculated quantities – EVA L specimen always achieved lower values of tensile stress and deflections at certain time of loading and certain temperature (e.g., $w_{EVA\,L}(t, T) < w_{BG}(t, T)$). This was also confirmed by experiments.

Comparison of coincidence between experimental and numerical creep results of specimens with Trosifol BG shows that M-W model based on DMTA results in shear (FE: SH), as ANSYS input, matches better with creep experiment than that based on combined DMTA results in shear + torsion (FE: SH+TS), in both loading and unloading parts. M-W model from combined DMTA results in shear + torsion gives relatively quick equilibrium shear stiffness at 30 °C: G_∞ = 0.23 MPa after 10^4 s ~ 2.7 h. At higher temperatures, this time is even shorter. Numerical values at loading based on this model (FE: SH+TS) at all testing temperatures, in Fig. 134, are therefore nearly identical. After unloading, both stress and deflections drop rapidly and turn to zero which is not consistent with the residual values measured by experiment. Contrary, shear modulus given by M-W model from DMTA in shear decreases smoothly from 1.7 MPa to 0.1 MPa between 1 s and 10^6 s at the range of testing temperatures. The state of stress and deflections of double LG panels in bending change rapidly in the interval of interlayer´s shear stiffness G = 1.0 – 0.1 MPa [68], therefore, time and temperature sensitivity of numerical relations (FE: SH) is justified. Pronounced relaxation effects in time were calculated at 30 °C using M-W model from DMTA in shear (FE: SH): tensile stress in glass at SG 2 increased for 22% and midspan vertical deflection increased for 42% between the time of loading (0.01 h) and right before unloading. The effect of increasing temperature from 30 °C to 50 °C is illustrated, e.g., by growth of numerical values (FE: SH) at 119 h of loading: midspan deflection increased for 10.5% and tensile stress in glass at SG 2 increased for 6.5%.

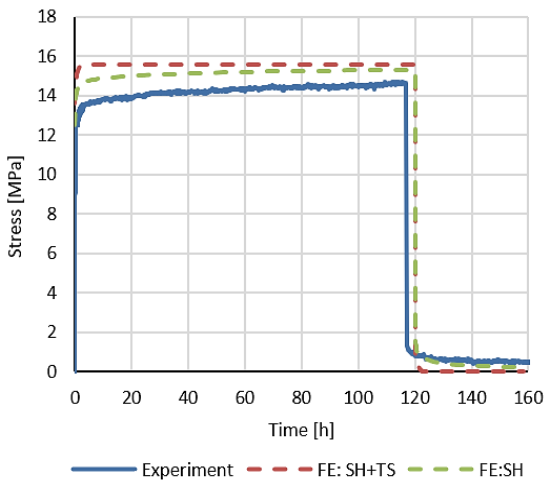

a) +30 °C; Normal stress by SG 2

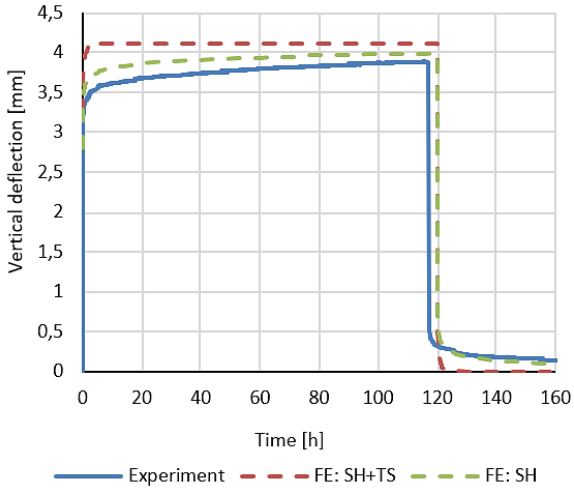

b) +30 °C; Deflection by DS I

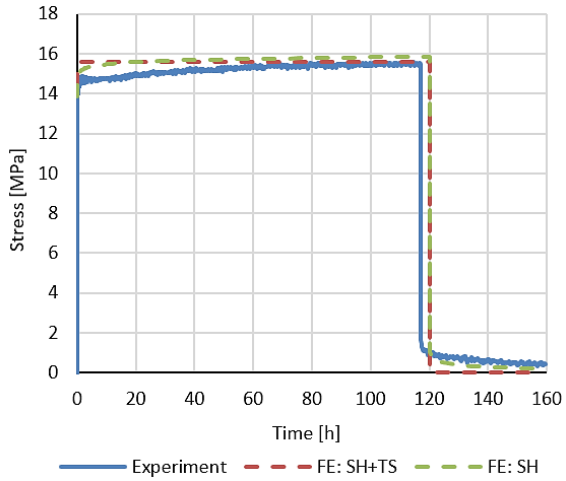

c) +40 °C; Normal stress by SG 2

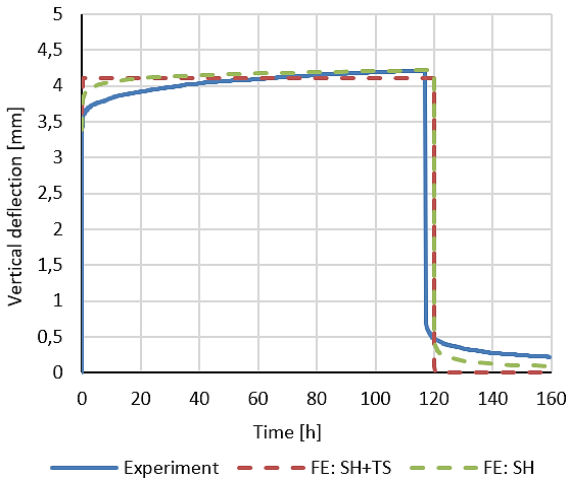

d) +40 °C; Deflection by DS I

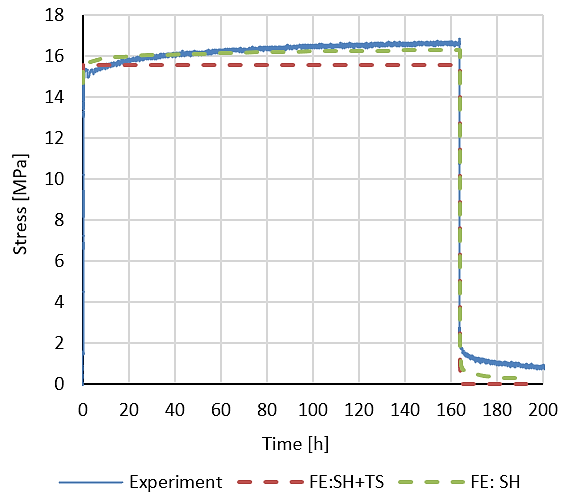

e) +50 °C; Normal stress by SG 2

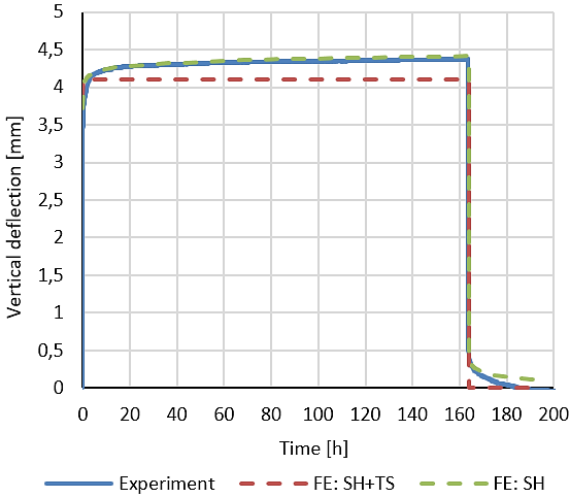

f) +50 °C; Deflection by DS I

Fig. 134: Comparison of experimental and numerical (FE) midspan tensile stress in glass and vertical deflections of LG specimen with Trosifol BG from creep test, numerical values by ANSYS

Comparison of creep experimental and numerical values in time of EVA L specimen show, numerical model provided results that match well with the experiment.

At loading phase, both numerical stress and deflections are conservative except for tensile stress at 50 °C. Noteworthy deviation of numerical results from experimental vertical deflections was recorded at 30 °C and 140 h of loading (to 17%), and from tensile stress in glass at 40 °C and 210 h of loading (to 8%). Numerical relations increase smoothly in time at 30 °C and 40 °C which reflects continuously decreasing shear stiffness of EVA L in tested time interval, see Fig. 132a). Numerical tensile stress in glass and deflection are stabilized at 50 °C already after 10^4 s ~ 2.5 h meaning the equilibrium relaxation shear stiffness G_∞ of EVA L has been achieved. Noteworthy time sensitivity of numerical results was recorded at 40 °C by the growth of tensile stress in glass

(SG 2) for 23% and midspan deflections for 18% between loading (0.01 h) and right before unloading (210 h). This was caused by continuous change of shear modulus $G_{EVA\,L}$(t, 40 °C) falling from 1.7 MPa to 0.8 MPa.

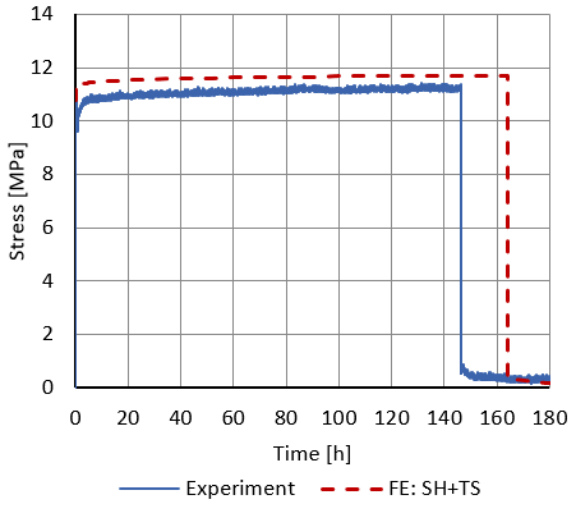

a) +30 °C; Normal stress by SG 2

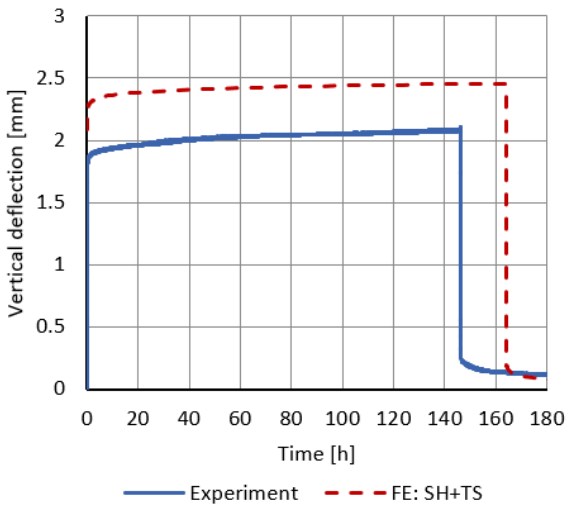

b) +30 °C; Deflection by DS I

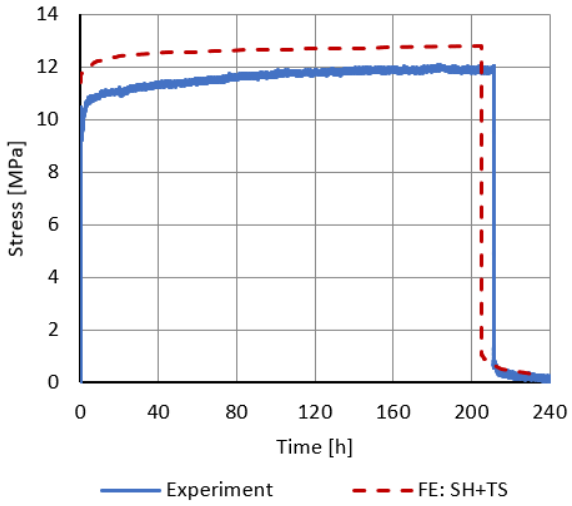

c) +40 °C; Normal stress by SG 2

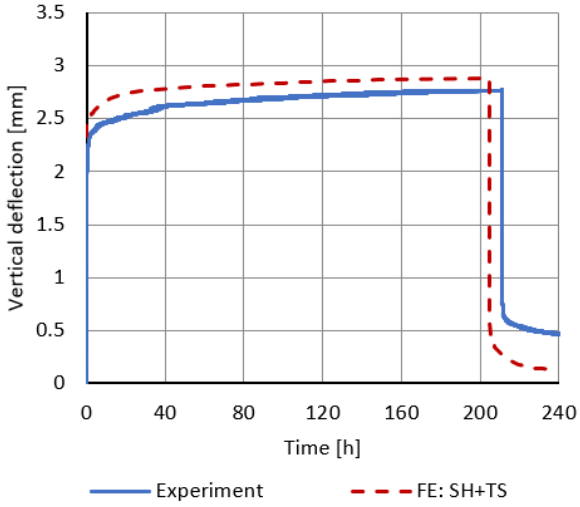

d) +40 °C; Deflection by DS I

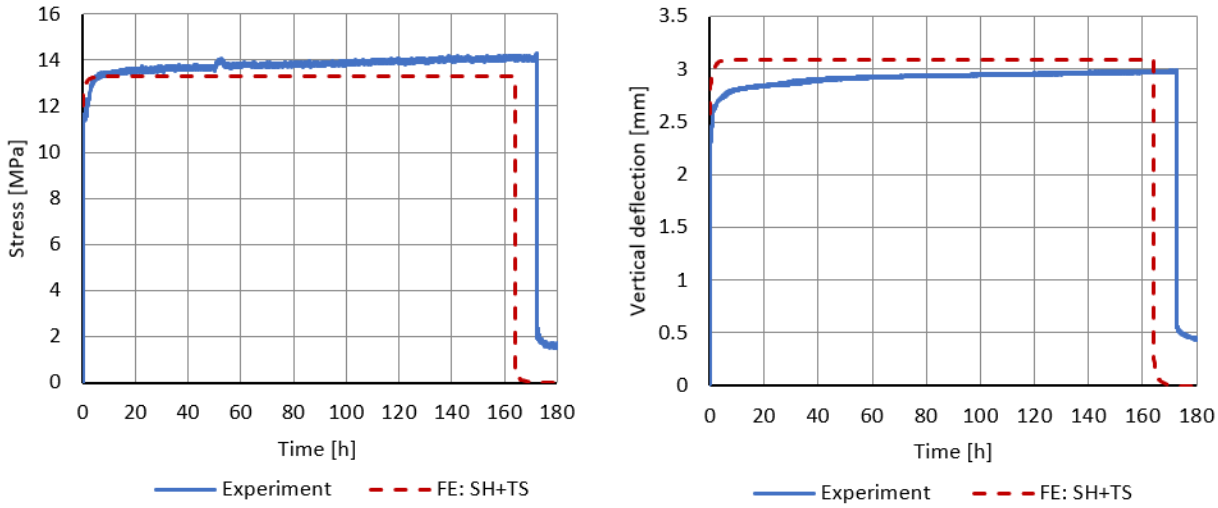

e) +50 °C; Normal stress by SG 2

f) +50 °C; Deflection by DS I

Fig. 135: Comparison of experimental and numerical (FE) midspan tensile stress in glass and vertical deflections of LG specimen with EVA L from creep test, numerical values by ANSYS

Presented numerical and experimental data before unloading, at all studied temperatures, are shown in Tab. 33. Numerical and analytical values of Trosifol BG specimen in Tab. 33 are based on its M-W model from DMTA in shear (SH). Following Kuntsche et al. [9], discrete values of interlayer´s shear modulus before unloading $G(t, T)$ from their relaxation curves in Fig. 132, were used as an input into EET method for simply supported midspan loaded 1D panel [58], and appropriate Effective Thickness with subsequent midspan tensile stress in glass and vertical deflections were calculated. These analytical results, also shown in Tab. 33, are, in all cases, higher than those by ANSYS with maximum deviation to 2.5% and reflect the suitability of EET method with discrete value of G to be used in calculation of LG panel in creep. Time courses of midspan tensile stress in glass and vertical deflections by LE calculation using EET with one discrete value of $G_{EVA\,L}(211\text{ h}, 40\text{ °C}) = 0.83$ MPa and by LVE calculation made in ANSYS using EVA L M-W Prony series input at 40 °C (FE: SH+TS), are shown in Fig. 136. In both LE and LVE analysis, time constant load $F = 1.12$ kN was applied. This graph illustrates the delayed response of viscoelastic material by the time growth of both quantities whereas LE calculation is instantaneous, constant response to the applied load. However, both analytical and numerical values of EVA L at 40 °C, before unloading, almost coincide (deviation to 1.1%). The coincidence of analytical and numerical results with experiment before unloading is satisfactory for both Trosifol BG and EVA L.

Tab. 33: Comparison of analytical and numerical results with experimental data shortly before unloading

Load F = 1.12 kN	Time [h]	Analytical calculation EET	Numerical calculation ANSYS	Percentage deviation analyt./num.	Experiment
+30 °C					
Trosifol BG		G = 0.27 MPa	by M-W		
Tensile stress in glass SG 2 [MPa]	117.0	15.64	15.32	2.1	14.57
Midspan vertical deflection DS I [mm]	117.0	4.00	3.90	2.5	3.81
EVA L		G = 1.33 MPa	by M-W		
Tensile stress in glass SG 2 [MPa]	140.0	11.83	11.70	1.1	11.10
Midspan vertical deflection DS I [mm]	140.0	2.45	2.44	0.4	2.07
+40 °C					
Trosifol BG		G = 0.21 MPa	by M-W		
Tensile stress in glass SG 2 [MPa]	117.0	16.20	15.84	2.2	15.36
Midspan vertical deflection DS I [mm]	117.0	4.23	4.21	0.4	4.21
EVA L		G = 0.83 MPa	by M-W		
Tensile stress in glass SG 2 [MPa]	211.0	12.92	12.78	1.1	11.84
Midspan vertical deflection DS I [mm]	211.0	2.90	2.88	0.7	2.76
+50 °C					
Trosifol BG		G = 0.16 MPa	by M-W		
Tensile stress in glass SG 2 [MPa]	160.0	16.69	16.30	2.3	16.41
Midspan vertical deflection DS I [mm]	160.0	4.42	4.40	0.4	4.36
EVA L		G = 0.68 MPa	by M-W		
Tensile stress in glass SG 2 [MPa]	160.0	13.42	13.28	1.0	14.05
Midspan vertical deflection DS I [mm]	160.0	3.10	3.09	0.3	2.96

Note: M-W model of Trosifol BG (EVA L) is based on DMTA in shear from Tab. 22 (in shear + torsion from Tab. 25)

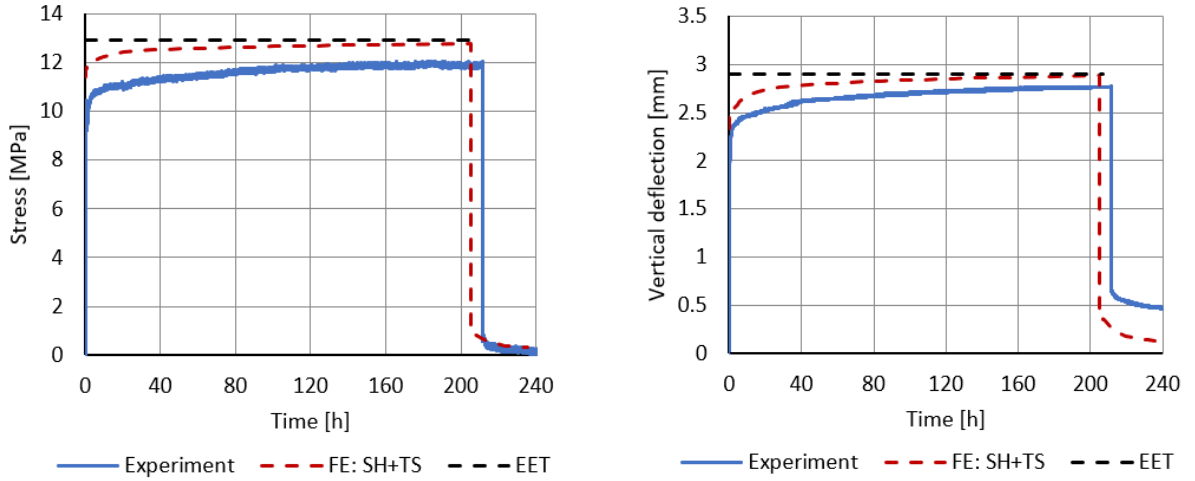

a) EVA L: +40 °C; Normal stress by SG 2

b) EVA L: +40 °C; Deflection by DS I

Fig. 136: Time course of calculated quantities by analytical EET using G(t = 211 h; 40 °C) = 0.83 MPa of EVA L, comparison with LVE in ANSYS and experiment, constant load F = 1.12 kN at loading phase

Mentioned inequality $G_{EVA\ L}$(t, 50 °C) > G_{BG}(t, 50 °C) given by relaxation functions in Fig. 132, is documented by the numerical values of normal stress in glass at 60 s and at 164 h of loading at 50 °C in Fig. 137 and Fig. 138. The values of shear moduli are the following: $G_{EVA\ L}$(60 s, 50 °C) = 1.05 MPa, $G_{EVA\ L}$(164 h, 50 °C) = 0.68 MPa; G_{BG}(60 s, 50 °C) = 0.33 MPa, G_{BG}(164 h, 50 °C) = 0.16 MPa. Since M-W model from DMTA in shear fits better the experimental creep data, numerical results are displayed in Fig. 137 and Fig. 139a) using this mechanical model. Comparison of plotted normal stresses shows EVA L specimen always achieved lower values of both tensile and compressive normal stress in glass than specimen with Trosifol BG. Moreover, numerical model well shows the relaxation effects of both interlayers by time increasing normal stress in glass.

Midspan vertical deflection 4.4 mm at 164 h of loading at 50 °C, see Fig. 139, calculated for Trosifol BG specimen is higher than 3.1 mm of EVA L specimen. Numerical models of both interlayers at 10 min after unloading show nonzero values of residual deflections which is typical for thermoplastics: Trosifol BG specimen achieved higher residual deflection than EVA specimen, 0.43 mm vs. 0.35 mm, which reflects the ratio of their cross-link densities (Trosifol BG 0% vs. EVA L 3%).

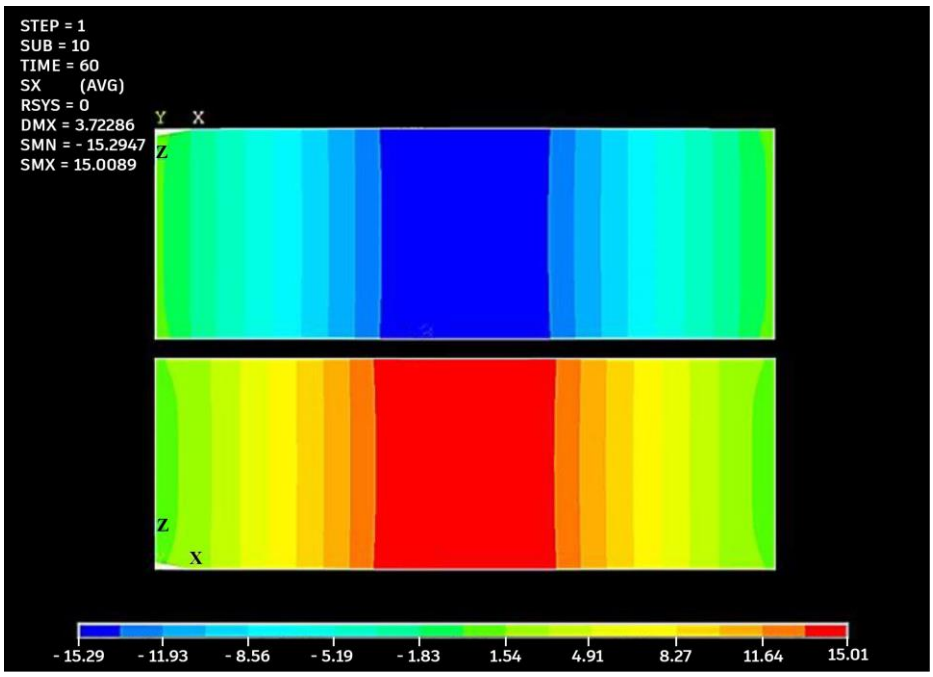

a) +50 °C; t = 60 s; upper ply-upper surface (upper picture); lower ply-lower surface (lower picture)

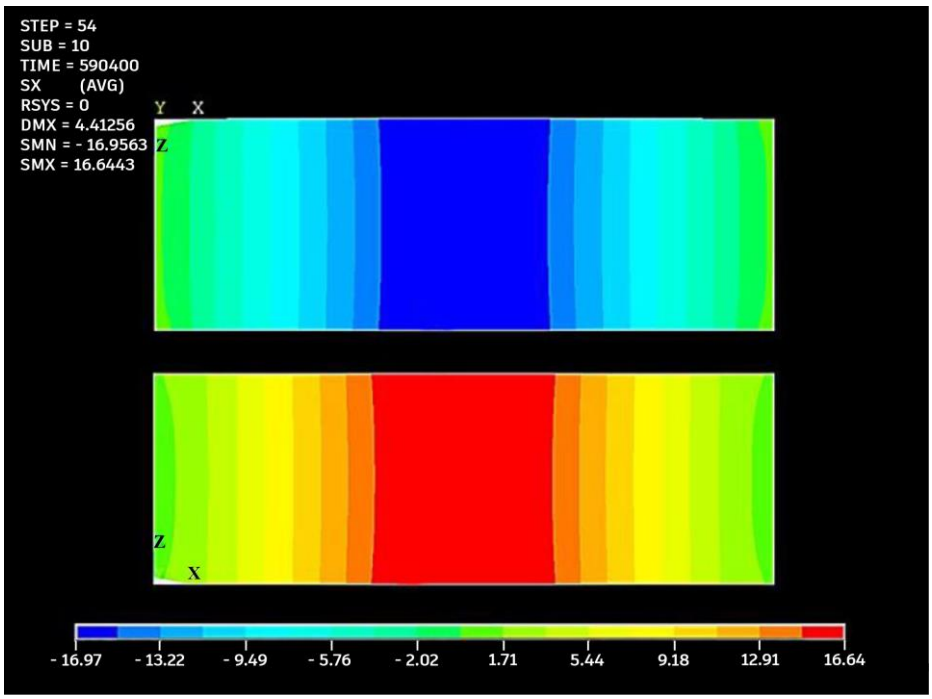

b) +50 °C; t = 164 h; upper ply-upper surface (upper picture); lower ply-lower surface (lower picture)

Fig. 137: Normal stress in glass σ_x [MPa] at creep test, LVE numerical results using M-W model as input of Trosifol BG from DMTA in shear (SH) from Tab. 22

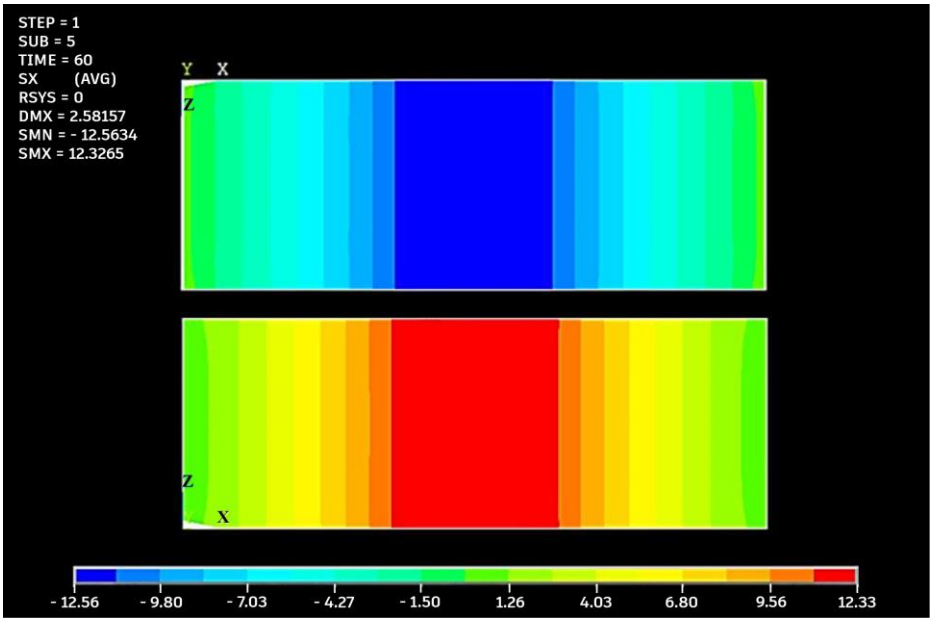

a) +50 °C; t = 60 s; upper ply-upper surface (upper picture); lower ply-lower surface (lower picture)

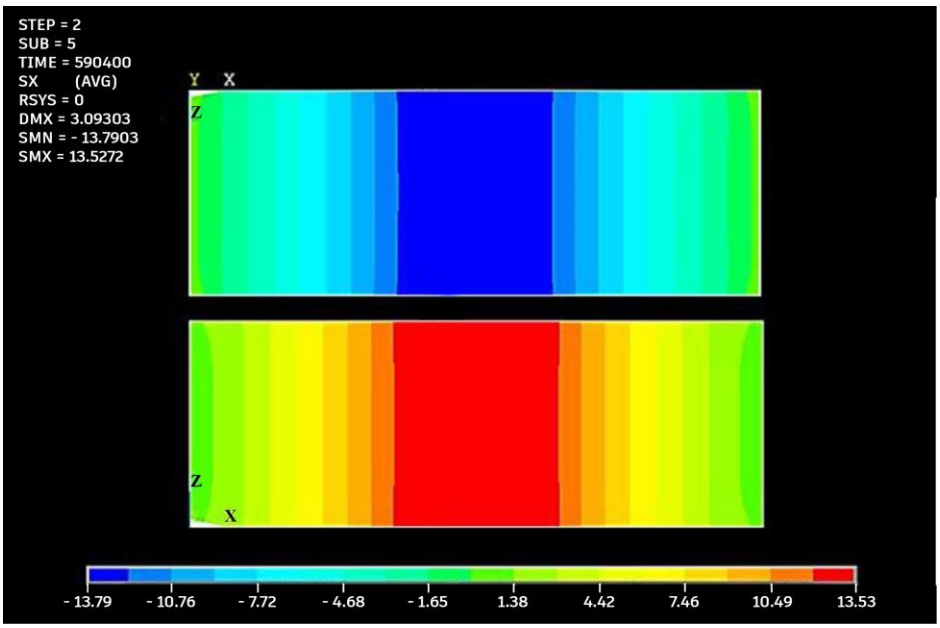

b) +50 °C; t = 164 h; upper ply-upper surface (upper picture); lower ply-lower surface (lower picture)

Fig. 138: Normal stress in glass σ_x [MPa] at creep, LVE numerical results using M-W model as input of EVA L from Tab. 25.

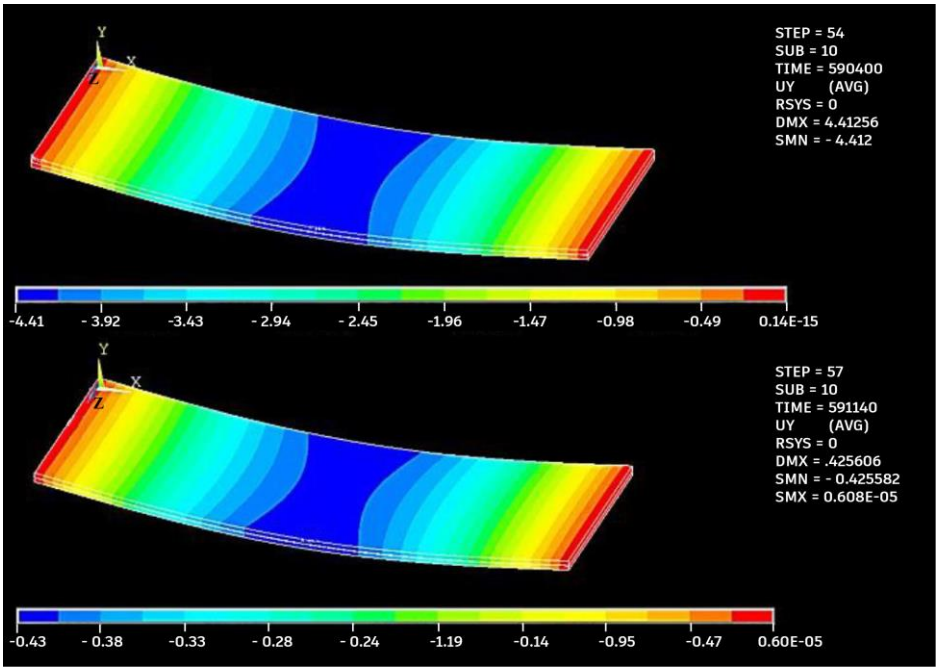

a) Trosifol BG (DMTA in SH): +50 °C; upper picture t = 164 h; lower picture time 10 min after unloading

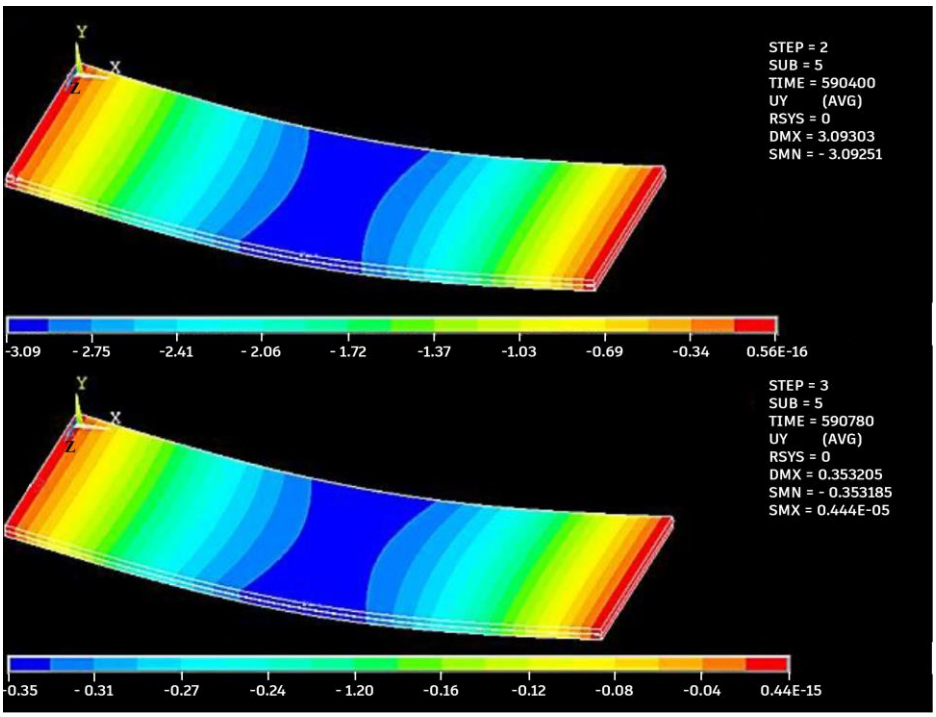

b) EVA L: +50 °C; upper picture t = 164 h; lower picture time 10 min after unloading

Fig. 139: Vertical deflections in [mm] before and after unloading in creep test, LVE numerical results using M-W models (Trosifol BG from Tab. 22, EVA L from Tab. 25) as inputs

Measurement of normal stress at the interface of glass and interlayer is technically demanding but numerical model enables to plot the distribution of normal stress over the cross section. The example is in Fig. 140 where the midspan normal stress over the specimen´s cross section, loaded at 164 h and at 50 °C, is plotted. Model shows that both interlayers ensured, in this loading case, only limited shear coupling of glass plies which is documented by nonuniform distribution of normal stress over the midspan cross section and by mutual displacement of glass plies above the support in Fig. 140. Upper glass ply was also in tension but peaks of tensile stress were, in both cases, concentrated along the bottom edge of lower glass ply. Lower shear stiffness of Trosifol BG than EVA L (0.16 MPa vs 0.68 MPa at 164h and 50 °C) means higher peaks of tensile stress acting on Trosifol BG specimen, see Fig. 140.

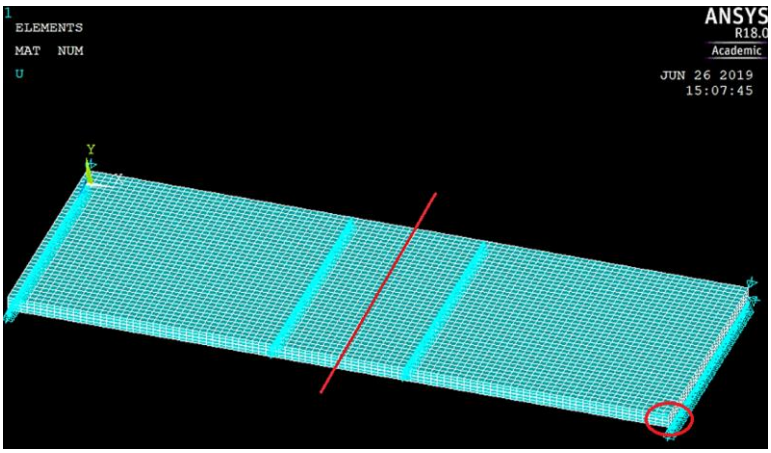

a) Coordinate system and points of interest highlighted by red strips

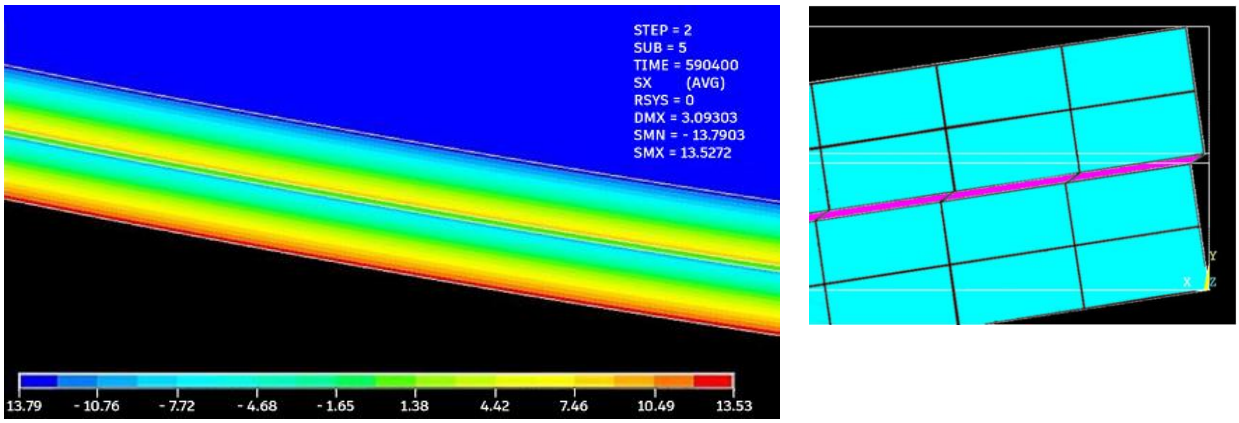

b) EVA L: +50 °C; t = 164 h

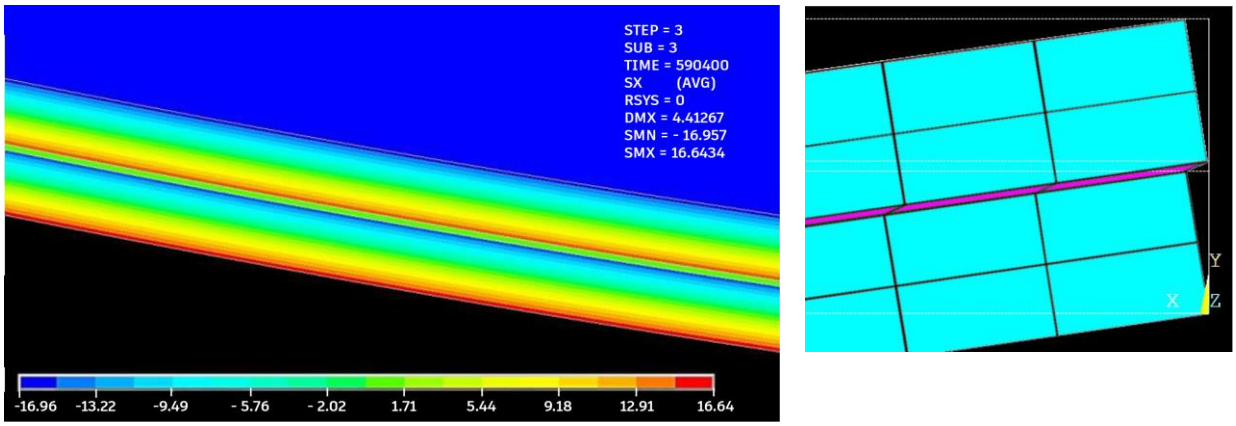

c) Trosifol BG (DMTA in SH): +50 °C; t = 164 h

Fig. 140: Creep; Normal stress σ_x [MPa] over the midspan cross section and displacement of glass plies above the support of specimen, LVE results using M-W models (Trosifol BG-Tab. 22, EVA L-Tab. 25)

8.4. Numerical part – conclusions

Numerical part aimed at verification of initial shear stiffness G_{init} and M-W models of Trosifol BG, EVA L, and SG 5000. Numerical models simulated large-scale LG specimens loaded in four-point bending tests from sections 6.3 - 6.5. The simulation, performed in RFEM®5 and ANSYS®18 APDL, included:

- LE calculation of the specimen using G_{init} inputs of Trosifol BG, EVA L, and SG 5000 measured at static small-scale single-lap shear tests at 20 °C,
- LVE calculation of the specimen loaded in various loading rates of vertical displacement using constructed M-W models of Trosifol BG and EVA L,
- LVE calculation of creep tests using constructed M-W models of Trosifol BG and EVA L.

The main findings from numerical part are listed below.

- Relatively quick and simple LE calculation in RFEM®5 using G_{init} inputs at 20 °C of Trosifol BG, EVA L, and SG 5000 provides, from an engineering point of view, sufficiently accurate results of short-term loaded 1D double LG panels. The load duration should not exceed a few minutes.
- Both constructed M-W models of Trosifol BG (based on DMTA in shear and torsion modes) were able to describe certain type of large-scale experiment (creep or destructive test). It cannot be then clearly said which mode of DMTA testing is more relevant.
- Numerical models using constructed M-W model of EVA L matched well with both destructive and creep bending tests and provided reliable results.
- Simple LE analytical calculation by EET method of presented bending creep tests using one discrete $G(t, T)$ value of EVA L and Trosifol BG interlayers delivered, before unloading, almost accurate results of both tensile stress in glass and deflections. Complicated LVE analysis of LG panel loaded in creep is then not necessary.
- Numerical model confirmed the experimental finding regarding LG panel laminated with SG 5000 in short-term out of plane loading: extreme stiffness of SG 5000 ensured full shear coupling of individual glass plies.

9. Parametric study

As stated before, LE analysis of LG in bending is mostly preferred method and it may be basically performed using enhanced analytical methods or numerical solution. Whether quick and simple LE calculation of LG panel is desirable, analytical solution using one certain value of interlayer´s shear stiffness *G*, as an input, is in hand. Currently used enhanced analytical methods for calculation of LG in bending determine the Effective Thickness of *i*-th glass ply as the thickness of glass monolith with equivalent bending properties. Effective Thickness is used in LE assessment of this monolith, in terms of stress and deflections, loaded in identical loading and boundary conditions as the original LG panel.

9.1. Purpose of study

The purpose of this parametric study is to compare the values of Effective Thickness using W-B and EET analytical methods to those calculated from numerical simulation performed in RFEM®5 for double LG panels loaded in various boundary conditions. The choice of boundary conditions was based on glazing applications in common practice. Numerical model with dense FE mesh enables to detect the peaks of tensile stress in glass and to calculate the Effective Thickness of *i*-th glass ply so that numerical peaks and analytical peaks (using glass monolith with the so defined Effective Thickness) of tensile stress would coincide. Due to this fact, numerically determined Effective Thickness will be, in the sequel, considered as reference.

Parametric study consists of calculation of Effective Thickness while changing the discrete value of interlayer´s shear modulus *G* between 0.01 MPa to 140 MPa for two types double LG panels: a) panel as 1D problem, b) panel as 2D problem, see Fig. 141.

In both cases, the cross section consisted of 10 mm glass + 0.76 mm interlayer + 10 mm glass ($h_1 = h_2 = 10$ mm; $t = 0.76$ mm). Panels were different in dimensions. 1D panel: span $l = 3000$ mm and width of the cross section $b = 800$ mm; 2D panel with horizontal dimensions 2500 × 2500 mm, see Fig. 141. Designation of material and dimensional input parameters keeping the same notation as in section 2.6.1, is shown in Fig. 142. Investigated cases of 1D problem were considered as follows: (i) simply supported panel under uniform load; (ii) simply supported panel under concentrated load; (iii) fixed-ended panel under uniform load; (iv) double-span simply supported panel under uniform load. 2D problems were considered as follows: (i) four-sides simply supported panel under uniform load; (ii) four-sides simply supported panel under concentrated load; (iii) two-sides simply supported panel under uniform load; (iv) one edge fixed ended panel under uniform load.

Simple support was modelled as a line hinge preventing edge´s vertical displacement in *z* direction. Fixed ended edge was, in addition, modelled by horizontal supports, see Fig. 143.

Both glass and interlayer were considered as linear elastic isotropic materials. Young modulus of glass $E = 70\,000$ MPa and Poisson ratio $\upsilon = 0.23$. Interlayer´s shear modulus $G \in \langle 0.01; 140 \rangle$ MPa with Poisson ratio $\upsilon = 0.49$.

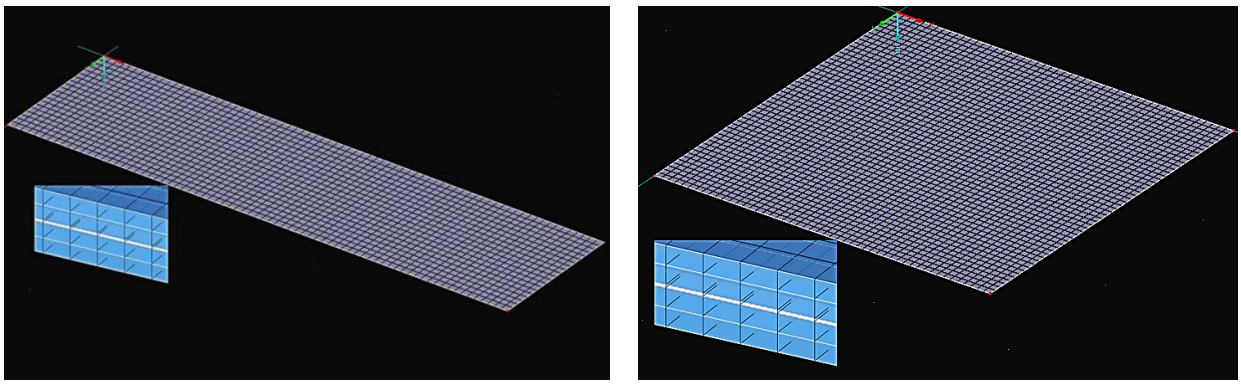

a) 1D problem: 800 × 3000 mm b) 2D problem: 2500 × 2500 mm

Fig. 141: Types of double LG panels modelled in RFEM 5 investigated in parametric study

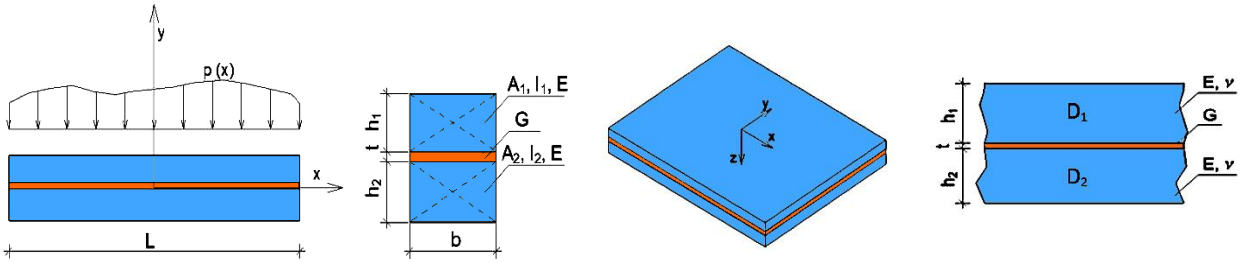

a) Input parameters for 1D problem b) Input parameters for 2D problem

Fig. 142: Input parameters for the calculation of Effective Thickness of LG panels by analytical W-B and EET methods

a) Simply supported edge b) Fixed ended edge

Fig. 143: Type of line constraint in the numerical model

As stated before, W-B method was originally intended for 1D uniformly loaded simply supported double LG panels but, in practice, it is used for various boundary conditions calling for verification in this matter [57]. Hence, W-B was here applied also for 2D panels supposing cross section of 2D panel has the same notation of dimensions as 1D panel in Fig. 142a), e.g., b = 2500 mm.

Analytical procedure: Given the geometry and material parameters of glass and interlayer, coefficients of shear forces (Γ using W-B, and η using EET) were defined using Eq. (30) (W-B), Eq. (35) (1D EET), and Eq. (36) (2D EET). Boundary conditions coefficient β in W-B method was

considered by value 9.6 [57]. The shape coefficient of boundary conditions ψ in EET, suggested by Galuppi et al. [58], for the calculation of η, was for 1D panels taken as: (i) $168/17l^2$, (ii) $10/l^2$, (iii) $42/l^2$, (iv) $21/l^2$ and for 2D panels taken as: (i) 3.18×10^{-6} mm^{-2}, (ii) 12.02×10^{-6} mm^{-2}, (iii) 1.49×10^{-6} mm^{-2}, (iv) 0.44×10^{-6} mm^{-2}. By use of panels geometry and calculated shear forces coefficients Γ and η for discrete values of shear stiffness of interlayer G, the corresponding Effective Thickness for deflection $h_{ef,w}$, and for normal stress $h_{ef,\sigma}$, were determined using Eq. (31) and Eq. (32) for W-B method, and using Eq. (33) and Eq. (34) for EET method. There is no difference between the Effective Thickness of upper and lower glass ply as they are of the same thickness.

Numerical procedure: All investigated cases were numerically modelled in RFEM®5 using analogical procedure as in section 8.1: 8-node spatial linear element with three degrees of freedom, see Fig. 122a). Basic step of the mesh was set as 10 mm. Meshing over the thickness of the cross section is shown in Fig. 141. Material parameters have been defined above.

Uniform load was in the model always applied in the form of 1.0 kN/m^2 acting on the panel. Midspan local force 1 kN was substituted by uniform load in [kN/m^2] acting on the track of 50 × 50 mm on the top of 2D panel or by a midspan line load in [kN/m] acting across the width of 1D panel. Examples are shown in Fig. 144. The value of load was chosen with respect to panel´s geometry not to allow for geometrical nonlinearities [52]. Small strain analysis was then enabled. This was an important fact since presented analytical methods also suppose geometrical linearity. Given the applied load, geometry, FE mesh, and discrete value of interlayer´s shear stiffness G, 1st order LE analysis was performed and maximal peaks of stress and deflections were calculated. Further, corresponding values of Effective Thickness $h_{ef,w}$ and $h_{ef,\sigma}$ for monolithic panel, under the same loading and boundary conditions, were calculated assuming this monolithic panel (defined by $h_{ef,w}$ and $h_{ef,\sigma}$) has identical peaks of tensile stress and deflections as laminated panel in the numerical model. This procedure was made using ordinary linear elastic analytical formulas from literature respecting Navier beam or plate theory. For example, maximum bending moment M and midspan vertical deflection w for 1D simply supported uniformly loaded monolithic panel (defined by $h_{ef,w}$ and $h_{ef,\sigma}$) having span l, line load f, Young modulus of glass E, and moment of inertia I, are calculated using Eq. (71), and maximum bending moment m and midspan vertical deflection w for uniformly loaded 2D four-sides simply supported monolithic panel (defined by $h_{ef,w}$ and $h_{ef,\sigma}$) having dimensions a; b, uniform load f, and flexural rigidity D, are determined according to Eq. (72). Details are given by Weller et al. [75].

Values of calculated Effective Thickness using both analytical and numerical procedures for all investigated cases are shown in Fig. 145 and Fig. 146.

$$M = f \cdot l^2/8;\ \ w = 5 \cdot f \cdot l^4/(384 \cdot E \cdot I)\,, \tag{71}$$

$$m = \xi \cdot a \cdot b \cdot f;\ \ w = \frac{a^2 \cdot b^2}{D} \cdot \eta_f \cdot f, \tag{72}$$

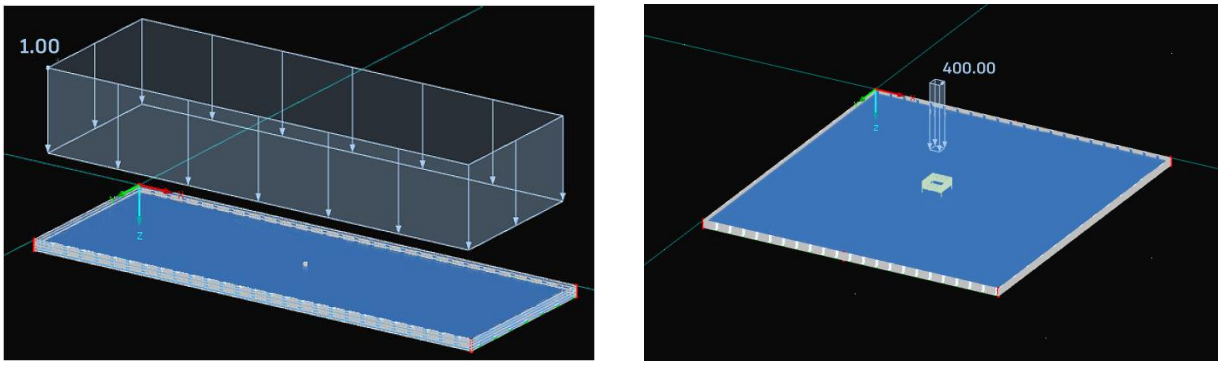

a) 1D problem: uniform load 1.0 kN/m^2

b) 2D problem: force 1 kN subsituted by uniform load 400 kN/m^2 acting on the track 50 × 50 mm

Fig. 144: Types of loads in kN/m^2 applied on LG panels in RFEM 5

1D problem

Parametric study of (i) uniformly loaded simply supported panel shows Effective Thicknesses by both analytical methods match well with the numerical solution. This is relevant since W-B method was aimed at this loading case and boundary conditions.

Results of (ii) simply supported panel under concentrated load are similar with the previous load case (i) in terms of deflection. Both analytical methods a bit underestimate the peak of normal tensile stress under concentrated load providing higher values of Effective Thickness for stress, the deviation from RFEM is to 5%.

The situation becomes rather different in case of fixed-ended panel under uniform load (iii). There is an evident unsafe deviation of W-B from EET for both stress and deflections. W-B roughly underestimates the peak of tensile stress at fixed-ended edge. Peaks of tensile stress in glass at fixed ended edge by RFEM do not react to the shear stiffness parameter for $G > 1.0$ MPa providing almost constant value of Effective Thickness for stress. EET method is not so stable in this matter and underestimates the value of tensile stress at fixing by giving higher values of Effective Thickness for stress than RFEM, the deviation is to 20%. Midspan vertical deflections by EET and RFEM match well for $G > 0.1$ MPa which is a common stiffness of an interlayer in practice.

Parametric results in case of double-span simply supported panel under uniform load (iv) are similar with the previous loading case (iii) but the deviation of analytical from numerical Effective Thickness for stress is lower. Double-span static schema does not hold for W-B method as this underestimates the peaks of normal tensile stress in glass above the support, deviation of its Effective Thickness for stress from RFEM is to 15%. The similar manner applies for midspan deflections. EET enables to calculate the midspan vertical deflections precisely but in case of normal tensile stress in glass above the support, the situation is less favourable as EET gives higher values of Effective Thickness for stress than RFEM, the deviation is to 10%.

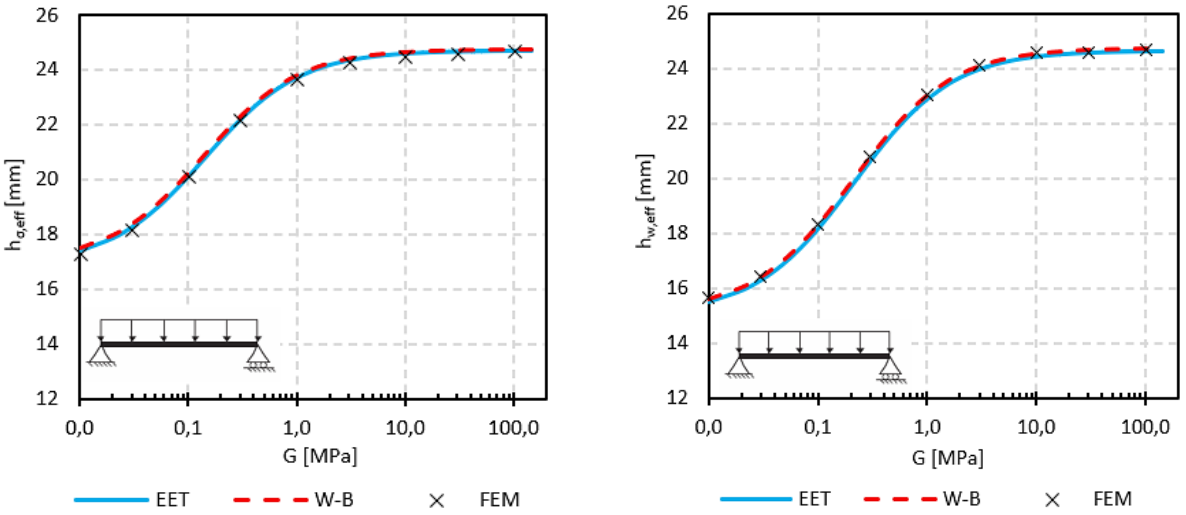

a) Simply supported panel under uniform load

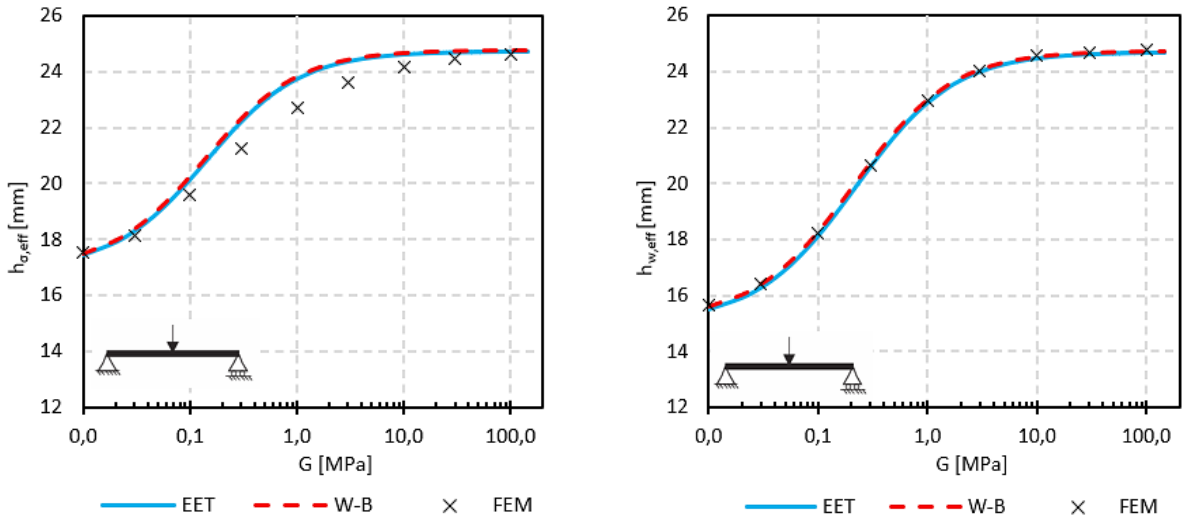

b) Simply supported panel under concentrated load

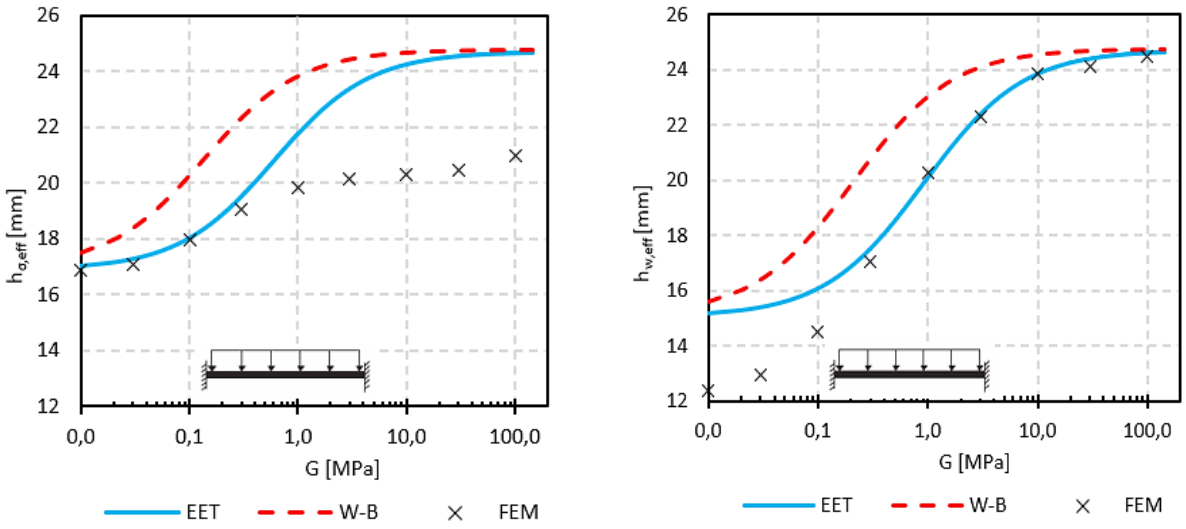

c) Fixed ended panel under uniform load

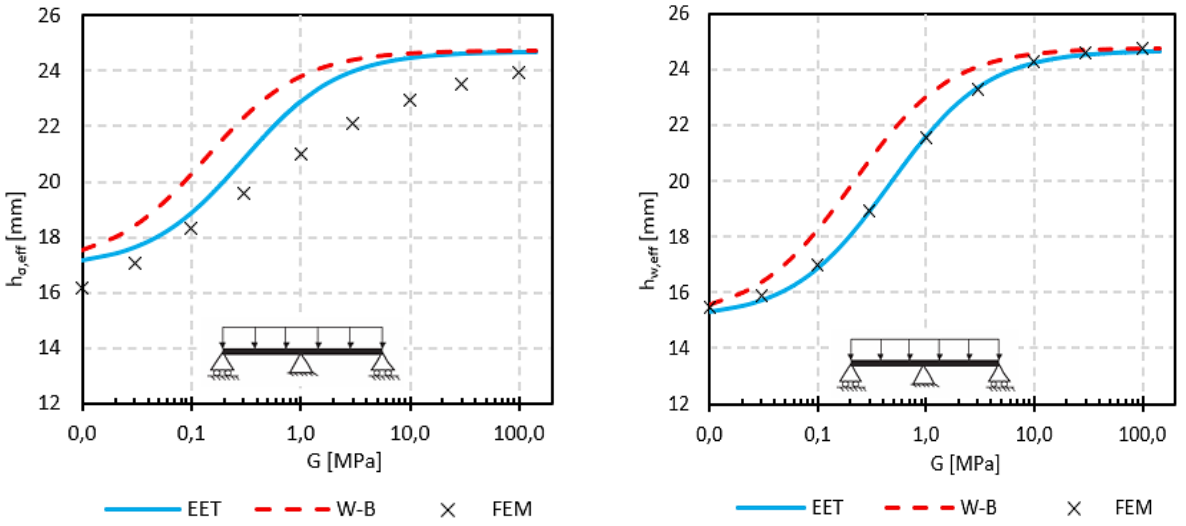

d) Double-span simply supported panel under uniform load

Fig. 145: Effective Thickness calculated using analytical and numerical LE solution for discrete values of interlayer´s shear stiffness *G*, double LG panels loaded in various boundary conditions as 1D problem

2D problem

Both analytical methods provide slightly higher Effective Thickness for stress in case of four-sides simply supported panel under uniform load (i) – deviations from RFEM are to 10% by W-B and to 5% by EET. Midspan vertical deflections by EET are consistent with RFEM. W-B is rather unsafe in this matter with the deviation from RFEM to 10%.

W-B method also in case four-sides simply supported panel under concentrated load (ii) underestimates both midspan tensile stress in glass and vertical deflection. The deviation of Effective Thickness for stress and for deflection from RFEM is to 17% and 12%, respectively. EET method is conservative in midspan normal stress for interlayer´s shear stiffness *G* up to

1.0 MPa. For higher values of *G*, the situation is inverse – Effective Thickness for stress by EET deviates from RFEM to 8%. Midspan vertical deflections by EET copy those by RFEM with a systematic safe deviation of Effective Thickness to 10%.

Results of parametric study for two-sides simply supported uniformly loaded panel (iii) show, both analytical methods match well with RFEM in both tensile stress in glass and deflections. Even though the solved panel is now a 2D problem, its deflected shape is still cylindrical, and W-B method delivered accurate results.

Numerical peaks of tensile stress in glass at fixed ended edge, for cantilever (iv), were insensitive of interlayer´s shear stiffness *G*. This meant both analytical methods overestimated Effective Thickness for stress for $G > 0.1$ MPa, e.g., EET deviates from RFEM to 22%. EET matched well with RFEM in task of free edge vertical deflection whereas W-B delivered safe deviation of Effective Thickness for deflection from RFEM to 15%.

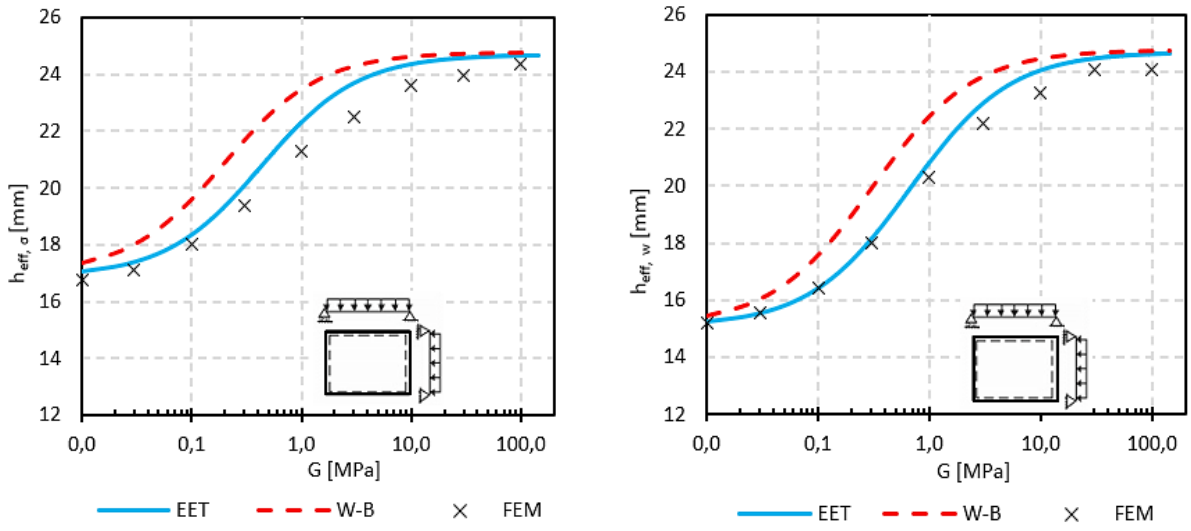

a) Four-sides simply supported panel under uniform load

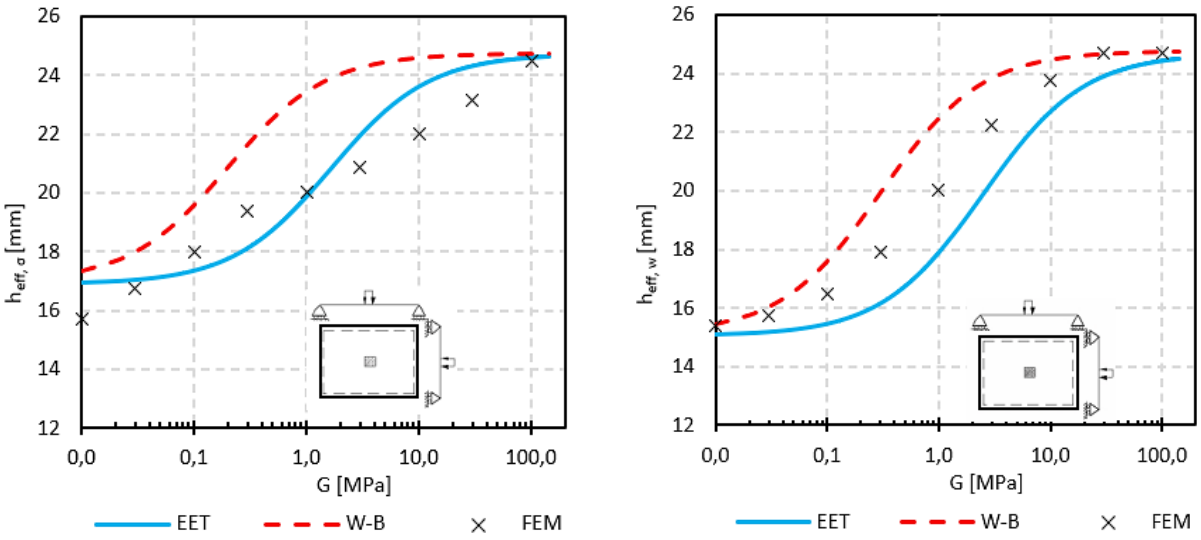

b) Four-sides simply supported panel under concentrated load

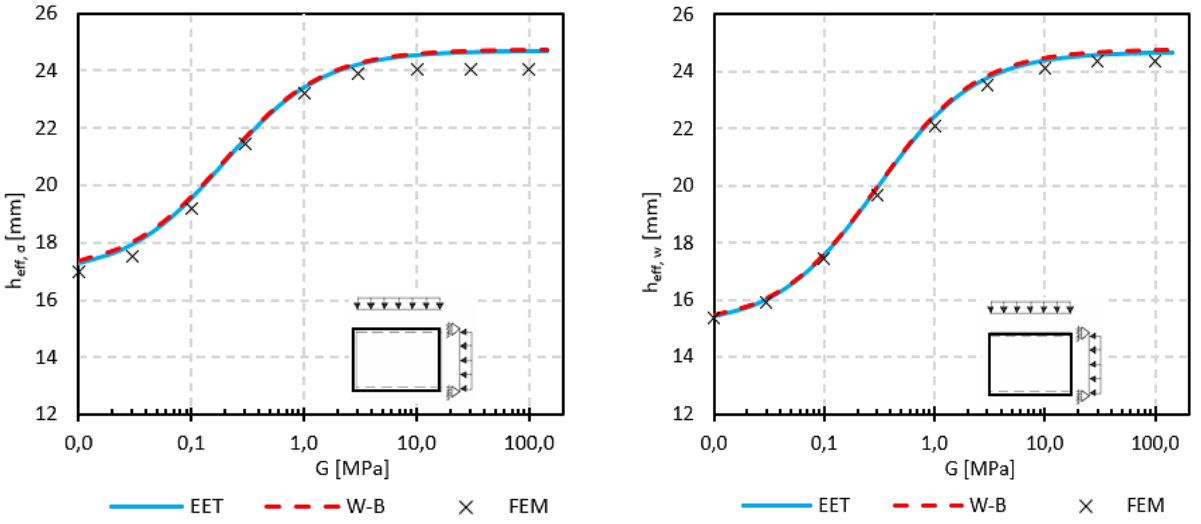

c) Two-sides simply supported panel under uniform load

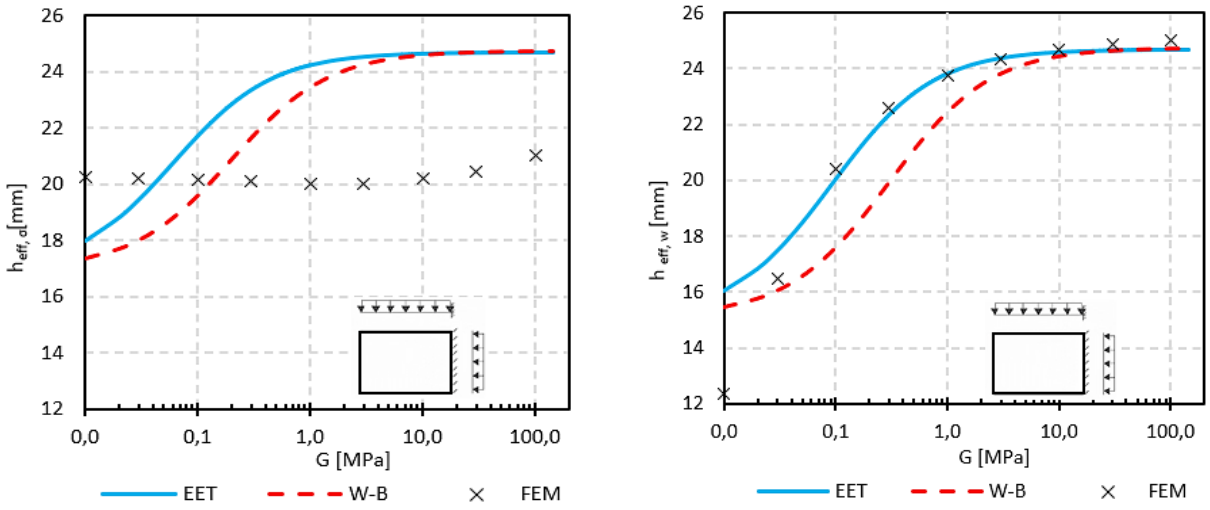

d) One edge fixed ended panel under uniform load

Fig. 146: Effective Thickness calculated using analytical and numerical LE solution for discrete values of interlayer´s shear stiffness *G*, double LG panels loaded in various boundary conditions as 2D problem

9.2. Parametric study – conclusions

Enhanced analytical LE methods for calculation of LG panels in bending, including the interlayer´s shear stiffness, are mostly preferred due to simple and time-saving procedure. These methods must be used correctly with respect to the loading case and boundary conditions of the problem which is, in practice, rather underestimated. The aim of this study was to analytically calculate the value of Effective Thickness for several practical examples of double LG panels in bending while varying the discrete value of interlayer´s shear elastic modulus *G*, and to compare this value with LE numerical simulation made in RFEM 5. This study enables to compare the calculated values with real experiments in the future. For this purpose, Wölfel-Bennison (W-B) and Enhanced Effective Thickness (EET) analytical methods were chosen. Four studied cases of 1D and 2D double LG panels loaded by uniform load or locally concentrated load, were chosen. The main findings from investigated cases are concluded below.

- W-B method gave values of Effective Thickness which correlated with EET and numerical solution only for uniformly loaded single span simply supported 1D panel or uniformly loaded two-sides simply supported 2D panel. It means, the cylindrical shape of vertical deflection ensures correct results. When used in other investigated boundary conditions, the simplicity of this method mostly results in overestimation of Effective Thickness.
- EET method delivers good results of Effective Thickness in most cases of practical relevance (single span simply supported 1D or 2D panels under uniform or local load) and demonstrates its suitability for use in practice. For cases of fixed ended panels, this method must be used with caution as normal stress at fixing is underestimated.

10. Practical calculation of load effects acting on double laminated glass panel according to EN 16612

The following part shows the assessment of linearly simply supported double LG panel loaded by uniformly distributed load. The panel is a part of office building in the Czech Republic belonging into class of consequences CC2. The analytical calculation will be made according to European standard EN 16612 [76] (supplied by EN 16613 [30]), which aims at the determination of load bearing capacity of uniformly loaded linearly supported glass elements used as infill panels. Even though EN 16612 itself covers glass non-structural infill panels, in the class of consequences lower than CC1 (e.g. windows) according to ČSN EN 1990 [77], it is in practice also used for linearly supported load bearing glass elements such as floor panels, roof panels, etc., belonging into higher class of consequences. The validity of this approach needs to be approved. Obtained results of the assessment will be compared to LE numerical calculation.

Two examples of structural double LG panels are considered

a) Vertical glazing as a part of a glass façade loaded by wind
b) Horizontal roof panel loaded by snow and self-weight

Double LG panels with nominal dimensions 900 × 2000 mm and composition 10.10.4: **10 mm HSG + 1.52 mm PVB (Trosifol® BG R20) + 10 mm HSG** loaded by uniformly distributed load will be assessed. The composition and static schemas are shown in figures below. The designation of variables, in the subsequent calculation, will be consistent with EN 16612 [76]. With respect to the given geometry and load, the analytical calculation of bending moments, normal stress, and vertical deflection will be made assuming Navier bending hypothesis for slender beams.

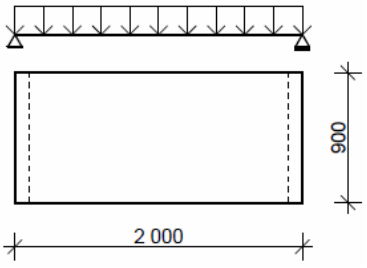

Roof panel 900 × 2000 mm

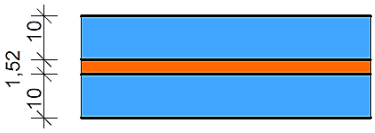

Composition of the panel 10.10.4

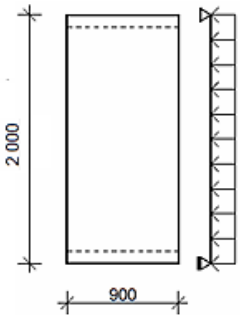

Facade panel 900 × 2000 mm

Types of applied loads at specific conditions

- Self-weight of the panel
- Wind gust load – duration of 3 seconds at 20 °C
- Snow loads – duration of 5 days at 20 °C (roof of heated building)

Material parameters

- Type of glass: Soda-lime heat strengthened glass (HSG)
- Young modulus of glass: E = 70 000 MPa
- Poisson ratio of glass: v = 0.23
- Density of glass: ρ = 2500 kg/m^3

Determination of glass tensile strength – HSG

- Design value of tensile strength

$$f_{g,d} = \frac{k_{mod} \cdot k_{sp} \cdot f_{g,k}}{\gamma_{M,A}} + \frac{k_v \cdot (f_{b,k} - f_{g,k})}{\gamma_{M,v}}$$

- Factor of the load duration k_{mod}
  Wind – 3 seconds k_{mod} = 1.0
  Snow – 5 days k_{mod} = 0.49

- Glass surface profile factor k_{sp}
  No surface treatment of glass k_{sp} = 1.0

- Strengthening factor of HSG resulting from manufacturing process k_v
  Glass panel was toughened horizontally k_v = 1.0

- Characteristic value of glass tensile strength
  Heat strengthened glass (HSG) $f_{b,k}$ = 70 MPa
  Float glass (FG) $f_{g,k}$ = 45 MPa

- Material partial factors
  Heat strengthened glass (HSG) $\gamma_{M,V}$ = 1.2
  Float glass (FG) $\gamma_{M,A}$ = 1.8

- Design value of glass tensile strength
  Structure loaded by wind

$$f_{g,d} = \frac{1.0 \cdot 1.0 \cdot 45}{1.8} + \frac{1.0 \cdot (70 - 45)}{1.2} = 45.8 \text{ MPa}$$

  Structure loaded by snow and self-weight

$$f_{g,d} = \frac{0.49 \cdot 1.0 \cdot 45}{1.8} + \frac{1.0 \cdot (70 - 45)}{1.2} = 33.1 \text{ MPa}$$

Note: When loads with different durations need to be treated in combination, the proposed k_{mod} associated with the shortest load duration must be used to determine the design value of glass tensile strength.

Acting loads

- Self-weight of the panel
  Density of glass $\rho = 25$ kN/m^3
  Thickness of one glass ply $h = 10$ mm
  Thickness of both glass plies $2 \times h = 20$ mm
  Uniformly distributed surface load

$$g_k = 25 \cdot 0.02 = 0.5 \text{ kN/m}^2$$

- Wind pressure at 20 °C and 3 s duration (wind area I according to ČSN EN 1991-1-4 [78])

$$q_k = 1.2 \text{ kN/m}^2$$

- Snow load – roof of heated building at 20 °C and duration of 5 days (snow area II according to EN 1991-1-3 [79])

$$q_k = 0.8 \text{ kN/m}^2$$

Combinations of actions

1. Ultimate limit state (ULS)
   Partial load factor of variable load $\gamma_Q = 1.50$
   Partial load factor of permanent load $\gamma_G = 1.35$
   Design value of wind load

$$f_d = \gamma_Q \cdot q_k = 1.5 \cdot 1.2 = 1.8 \text{ kN/m}^2$$

   Design value of self-weight and snow load

$$f_d = \gamma_G \cdot g_k + \gamma_Q \cdot q_k = 1.35 \cdot 0.5 + 1.5 \cdot 0.8 = 1.9 \text{ kN/m}^2$$

2. Serviceability limit state (characteristic SLS)
   Design value of wind load

$$f_d = 1.0 \cdot q_k = 1.0 \cdot 1.2 = 1.2 \text{ kN/m}^2$$

   Design value of self-weight and snow load

$$f_d = 1.0 \cdot g_k + 1.0 \cdot q_k = 1.0 \cdot 0.5 + 1.0 \cdot 0.8 = 1.3 \text{ kN/m}^2$$

Note: For determination of partial load factors γ_G, γ_Q for design values of load regarding glass panels in the class of consequences CC2, EN 16612 [76] refers to those listed in ČSN EN 1990 [77].
Façade panel is in vertical position. Self-weight acts in the plane of the panel and its effect on bending moments is, in this example, not considered (buckling of the panel is neglected). Roof panel is in horizontal position. Self-weight acts out of plane of the panel and directly bends the panel along the weak axis. Therefore, its effect is included into appropriate ULS and SLS combinations.

Coefficient of shear forces transfer and Effective Thickness of the panel

- Interlayer Trosifol BG R20 is made of polyvinyl butyral (PVB)
- Wind pressure at 20 °C, load duration of 3 s => "stiffness family" **1**
  Coefficient of shear transfer $\boldsymbol{\omega = 0.3}$

- Snow load – roof of heated building at 20 °C, load duration of 5 days => "stiffness family" **1**
  Coefficient of shear transfer $\boldsymbol{\omega = 0}$

- Determination of Effective Thickness
  Thickness of one glass ply h_k = 10 mm
  Thickness of interlayer h_f = 1.52 mm
  Distance of the midpane of the glass ply from the midpane of the laminated panel
  $h_{m,k}$ = 5.76 mm

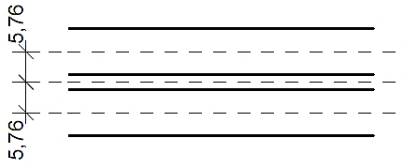

- Effective Thickness for calculation of vertical deflection

$$h_{ef,w} = \sqrt[3]{\sum_k h_k^3 + 12 \cdot \omega \cdot (\sum_i h_k \cdot h_{m,k}^2)}$$

Wind:

$$h_{ef,w} = \sqrt[3]{2 \cdot 10^3 + 12 \cdot 0.3 \cdot (2 \cdot 10 \cdot 5.76^2)} = 16.4 \text{ mm}$$

Snow:

$$h_{ef,w} = \sqrt[3]{2 \cdot 10^3 + 12 \cdot 0 \cdot (2 \cdot 10 \cdot 5.76^2)} = 12.6 \text{ mm}$$

- Effective Thickness for calculation of normal stress

$$h_{ef,\sigma} = \sqrt[2]{\frac{h_{ef,w}^3}{h_k + 2 \cdot \omega \cdot h_{m,k}}}$$

Note: Both glass plies are of the same thickness => both have identical value of $h_{ef,\sigma}$

Wind:

$$h_{ef,\sigma} = \sqrt[2]{\frac{16.4^3}{10 + 2 \cdot 0.3 \cdot 5.76}} = 18.1 \text{ mm}$$

Snow:

$$h_{ef,\sigma} = \sqrt[2]{\frac{12.6^3}{10 + 2 \cdot 0 \cdot 5.76}} = 14.1 \text{ mm}$$

Assessment of the panel to the applied load

Note: For analytical calculation of load effects, the surface load in kN/m^2 will substituted to line load in kN/m acting in direction of main *z* vertical axis.

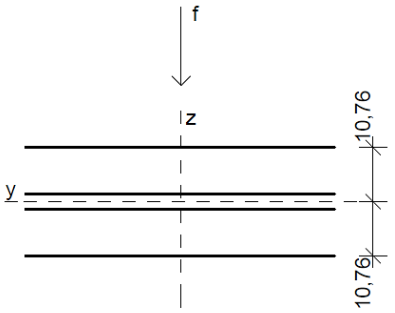

- Span of the panel L = 2.0 m
- Width of the panel b = 0.9 m

I. Façade panel loaded by wind

ULS

Design value of line load

$$f_d = 1.8 \cdot b = 1.8 \cdot 0.9 = 1.6\ \text{kN/m}$$

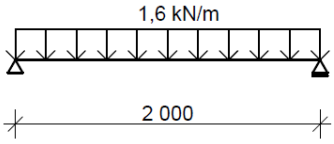

Midspan bending moment

$$M_{y,Ed} = \frac{1}{8} \cdot f_d \cdot L^2 = \frac{1}{8} \cdot 1.6 \cdot 2^2 = 0.8\ \text{kNm}$$

Effective moment of inertia for normal stress

$$I_{y,ef,\sigma} = \frac{1}{12} \cdot b \cdot h_{ef,\sigma}^3 = \frac{1}{12} \cdot 0.9 \cdot 0.018^3 = 4.374 \cdot 10^{-7}\ \text{m}^4$$

Effective cross section modulus for normal stress

$$W_{y,ef,\sigma} = \frac{I_{y,ef,\sigma}}{h_{ef,\sigma}/2} = 4.374 \cdot \frac{10^{-7}}{0.00905} = 4.86 \cdot 10^{-5}\ \text{m}^3$$

Design value of normal stress at the midspan

$$\sigma_{Ed} = \frac{M_{y,Ed}}{W_{y,ef,\sigma}} = \frac{0.8 \cdot 10^{-3}}{4.86 \cdot 10^{-5}} = 16.5\ \text{MPa}$$

Assessment

$$\sigma_{Ed} = 16.5\ \text{MPa} < f_{g,d} = 45.8\ \text{MPa} \quad \text{OK}$$

SLS

Design value of line load

$$f_d = 1.2 \cdot b = 1.2 \cdot 0.9 = 1.1\ \text{kN/m}$$

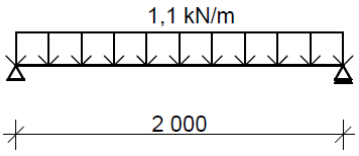

Effective moment of inertia for deflection

$$I_{y,ef,w} = \frac{1}{12} \cdot b \cdot h_{ef,w}^3 = \frac{1}{12} \cdot 0.9 \cdot 0.016^3 = 3.072 \cdot 10^{-7}\ \text{m}^4$$

Deflection at the midspan

$$w = \frac{5}{384} \cdot \frac{f_d \cdot L^4}{E \cdot I_{y,ef,w}} = \frac{5}{384} \cdot \frac{1.1 \cdot 2^4}{70 \cdot 10^6 \cdot 3.072 \cdot 10^{-7}} = 10.7\ \text{mm}$$

Assessment

$$w = 10.7\ \text{mm} < \min\left(\frac{L}{65}; 50\right) = 30.8\ \text{mm} \qquad \text{OK}$$

II. Roof panel loaded by snow and self-weight

ULS

Design value of line load

$$f_d = 1.9 \cdot b = 1.9 \cdot 0.9 = 1.7\ \text{kN/m}$$

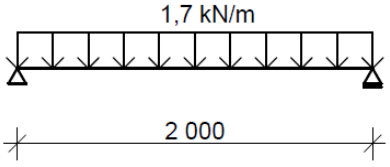

Midspan bending moment

$$M_{y,Ed} = \frac{1}{8} \cdot f_d \cdot L^2 = \frac{1}{8} \cdot 1.7 \cdot 2^2 = 0.85\ \text{kNm}$$

Effective moment of inertia for normal stress

$$I_{y,ef,\sigma} = \frac{1}{12} \cdot b \cdot h_{ef,\sigma}^3 = \frac{1}{12} \cdot 0.9 \cdot 0.014^3 = 2.058 \cdot 10^{-7}\ \text{m}^4$$

Effective cross section modulus for normal stress

$$W_{y,ef,\sigma} = \frac{I_{y,ef,\sigma}}{h_{ef,\sigma}/2} = 2.058 \cdot \frac{10^{-7}}{0.007} = 2.94 \cdot 10^{-5}\ \mathrm{m}^3$$

Design value of normal stress at the midspan

$$\sigma_{Ed} = \frac{M_{y,Ed}}{W_{y,ef,\sigma}} = \frac{0.85 \cdot 10^{-3}}{2.94 \cdot 10^{-5}} = 28.9\ \mathrm{MPa}$$

Assessment

$$\sigma_{Ed} = 28.9\ \mathrm{MPa} < f_{g,d} = 33.1\ \mathrm{MPa} \quad \mathrm{OK}$$

SLS

Design value of line load

$$f_d = 1.3 \cdot b = 1.3 \cdot 0.9 = 1.2\ \mathrm{kN/m}$$

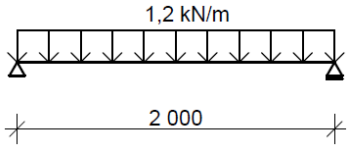

Effective moment of inertia for deflection

$$I_{y,ef,w} = \frac{1}{12} \cdot b \cdot h_{ef,w}^3 = \frac{1}{12} \cdot 0.9 \cdot 0.0126^3 = 1.5 \cdot 10^{-7}\ \mathrm{m}^4$$

Vertical deflection at the midspan

$$w = \frac{5}{384} \cdot \frac{f_d \cdot L^4}{E \cdot I_{y,ef,w}} = \frac{5}{384} \cdot \frac{1.2 \cdot 2^4}{70 \cdot 10^6 \cdot 1.5 \cdot 10^{-7}} = 24.0\ \mathrm{mm}$$

Assessment

$$w = 24.0\ \mathrm{mm} < \min\left(\frac{L}{65}; 50\right) = 30.8\ \mathrm{mm} \quad \mathrm{OK}$$

Conclusion

Analytical assessment of given double LG panels with PVB interlayer Trosifol BG R20, as a part of façade and roof, made according to EN 16612 [76], proved their reliability in ULS and SLS.

Comparison of analytically calculated values with numerical simulation in RFEM 5

To show the comparison with illustrated analytical calculation according to EN 16612 [76], studied example was numerically modelled. Applied load, geometry, and materials were the same as in analytical part above. Trosifol BG R20 was modelled as linear elastic material. The shear modulus of Trosifol BG R20 was assumed by discrete value given by its relaxation function from section 7.1.1, see Fig. 101 in this thesis.

For investigated load cases, the shear moduli and Poisson ratio of Trosifol BG R20 in RFEM 5 are the following:

- Wind: G(3 s; 20 °C) = 4.75 MPa, υ = 0.49
- Snow + self-weight: G(5 days; 20 °C) = 0.40 MPa, υ = 0.49

Basic step of the mesh was set as 10 mm, surface load applied in [kN/m^2]. Small strain, 1st order, LE analysis was performed for every loading case. The numerical results are the following:

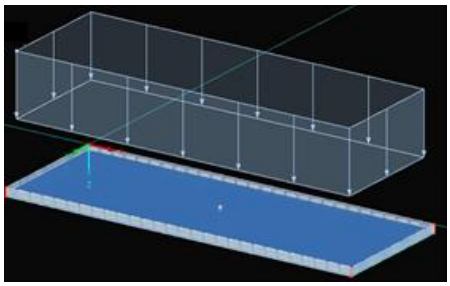

I. Facade panel loaded by wind (3 s, 20 °C)

ULS

Design value of load

$$f_d = 1.8\ \text{kN/m}^2$$

Normal stress – lower ply, surface in tension, $\sigma_{x,\,max}$ = 12.6 MPa

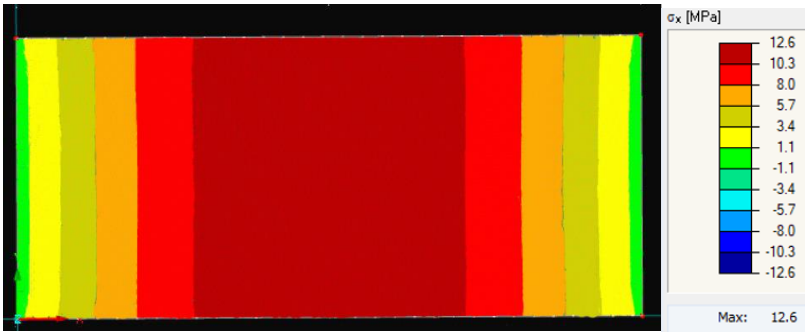

SLS

Design value of load

$$f_d = 1.2\ \mathrm{kN/m^2}$$

Vertical deflection $u_{z,\,max}$ = 5.3 mm

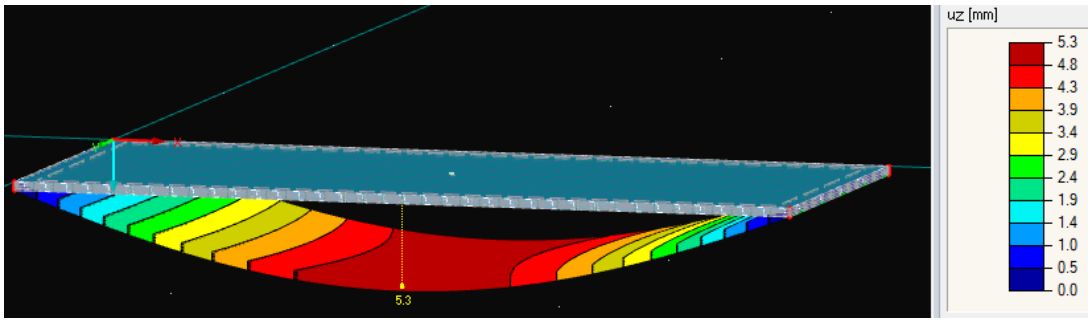

II. Facade panel loaded by snow and self-weight (5 days, 20 °C)

ULS

Design value of load

$$f_d = 1.9\ \mathrm{kN/m^2}$$

Normal stress – lower ply, surface in tension, $\sigma_{x,\,max}$ = 18.8 MPa

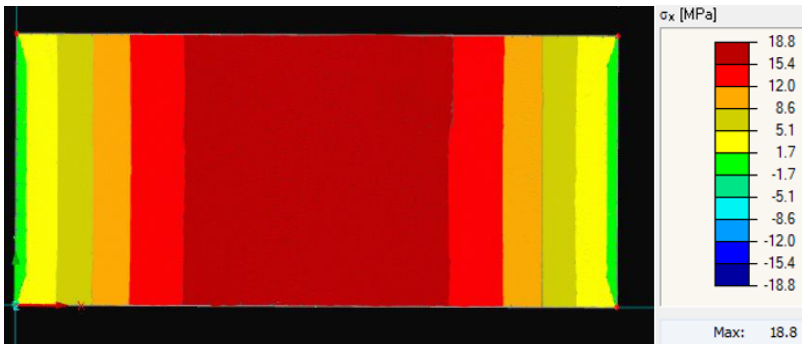

SLS

Design value of load

$$f_d = 1.3\ \mathrm{kN/m^2}$$

Vertical deflection $u_{z,\,max}$ = 12.1 mm

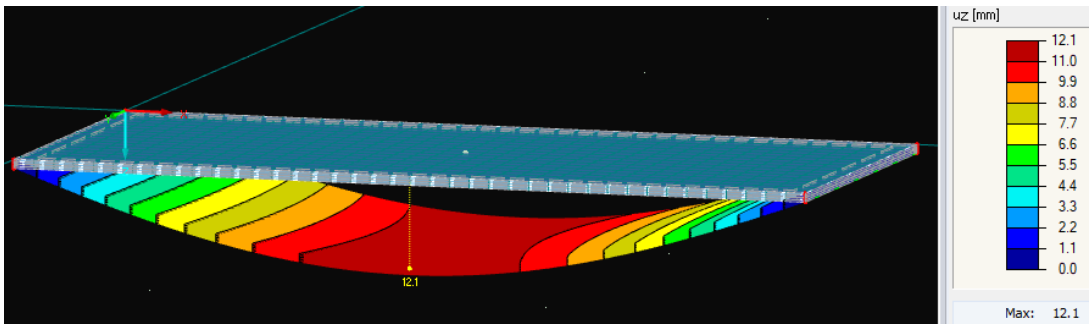

Comparison of analytical and numerical results

Normal tensile stress in glass at the midspan ULS

Load case	Analytical value [MPa] EN 16612	Numerical value [MPa] RFEM	Limit value [MPa] EN 16612
I. Wind (ω = 0.3)	16.5	12.6	45.8
II. Snow + self weight (ω = 0)	28.9	18.8	33.1

Vertical deflection of the panel at the midspan SLS

Load case	Analytical value [mm] EN 16612	Numerical value [mm] RFEM	Limit value [mm] EN 16612
I. Wind (ω = 0.3)	10.7	5.3	30.8
II. Snow + self weight (ω = 0)	24.0	12.1	30.8

Conclusion

Numerical values of midspan tensile stress in glass and vertical deflections are in both studied load cases lower than those calculated analytically according to EN 16612. This finding means the level of shear coupling given by Trosifol BG is underestimated and this interlayer could be assessed with higher shear transfer coefficients ω than those stated in current EN 16612. Table below suggests the values of ω for better coincidence between analytical and numerical values for studied load cases and used Trosifol BG.

Normal tensile stress in glass at the midspan ULS

Load case	Analytical value [MPa] EN 16612 (ω modified)	Numerical value [MPa] RFEM	Limit value [MPa] EN 16612
I. Wind (ω = 0.7)	12.7	12.6	45.8
II. Snow + self weight (ω = 0.2)	19.4	18.8	33.1

Vertical deflection of the panel at the midspan SLS

Load case	Analytical value [mm] EN 16612 (ω modified)	Numerical value [mm] RFEM	Limit value [mm] EN 16612
I. Wind (ω = 0.7)	5.8	5.3	30.8
II. Snow + self weight (ω = 0.2)	13.3	12.1	30.8

The analogy in short-term shear modulus given by static and dynamic (DMTA) single-lap shear tests, presented in section 7.4, allows for taking G_{init}(20 °C) as an input parameter into the numerical model for wind load. Table below shows numerical results by taking $G_{BG} = G_{init,BG}$(loading rate 2.0 mm/min, 20 °C) = 1.7 MPa from Tab. 7 simulating the response of investigated double LG panel loaded by 3 s wind. Results are similar to those using input in form of G_{BG}(3 s, 20 °C) = 4.75 MPa based on DMTA in shear. Concomitantly, EN 16612 is still conservative and shear transfer coefficient ω should be doubled from 0.3 to 0.6 to obtain similar results with the numerical model using $G_{init,BG}$(20 °C) = 1.7 MPa. This demonstrates the inapplicability of the current standard EN 16612 for practical use.

Conservatism of EN 16612 in case of investigated wind load for assessed midspan values

Load case	EN 16612	Numerical value	Numerical value
3s Wind at +20 °C	ω = 0.6 (modified)	G = G_{init} = 1.70 MPa (based on static tests)	G = 4.75 MPa (based on DMTA)
Tensile stress in glass [MPa] ULS	13.3	13.8	12.6
Vertical deflection [mm] SLS	6.4	6.7	5.3

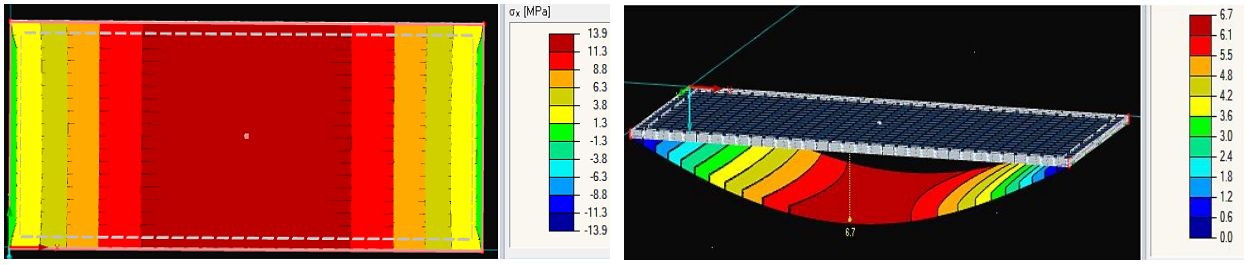

Analogy between G inputs for Trosifol BG used in short-term loaded panel by 3 s wind at +20 °C, left chart: stress-strain relation from static tests, right chart: relaxation function based on DMTA in shear

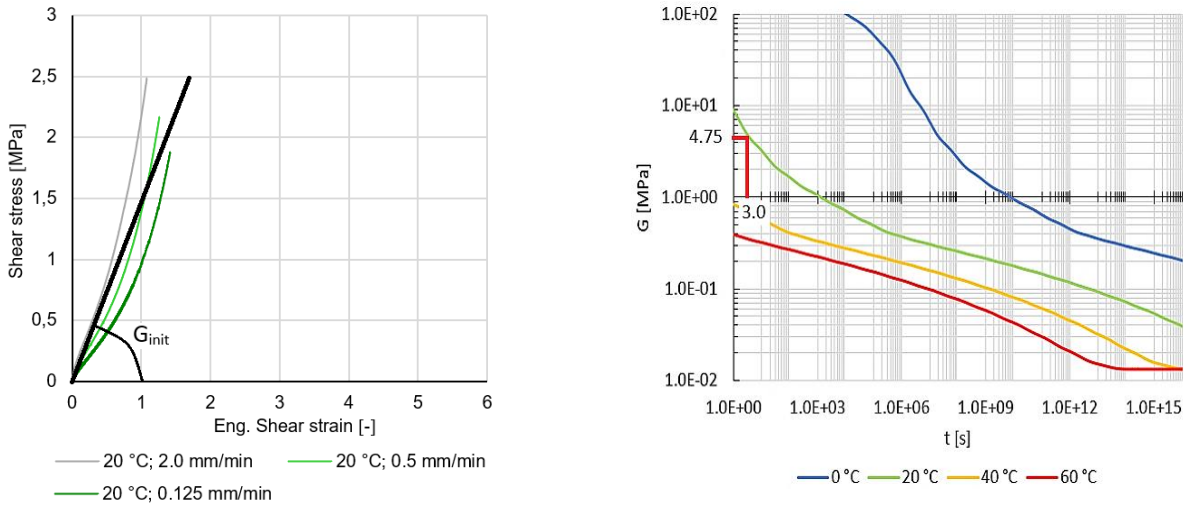

11. Conclusion of the thesis

Submitted thesis maps author´s research aimed at laminated glass (LG) used as load bearing structural element in civil structures. A key factor affecting the distribution of stress in out of plane loaded laminated glass, is the shear stiffness of an interlayer.

Small-scale static and dynamic single-lap shear experiments of common PVB based (**Trosifol® BG R20** and **Trosifol® Extra Strong**) and EVA based (**Evalam® 80/120** and **Evasafe®**) interlayers, and less extended ionomer (**SentryGlas® 5000**) and TPU (**Krystalflex® PE399**) based interlayers in various temperatures and loading rates enabled to get the basic understanding of their time and temperature-stiffness characteristics. Experiments showed that identical chemical base of two interlayers does not automatically predetermine their identical stiffness at certain time and temperature. This fact is often neglected by engineers who do not recognize between the individual trademarks of interlayers. Moreover, the analogy between short-term 10 s shear relaxation modulus $G(t = 10\ s, T)$ given by DMTA experiments and initial shear modulus G_{init} given by static single-lap shear tests of studied PVB and EVA interlayers indicates that relatively simple and quick small-scale static single-lap shear test provides reliable and sufficient value of this modulus. The need of complicated DMTA is then eliminated. This finding shows the way how the experimental testing of interlayers will be simplified in the future.

Presented research showed the interlayer can effectively form a shear coupling element of individual glass plies in LG panel. This means increase of the load bearing capacity of the panel by reduction of tensile stress in glass. Since producers of interlayers usually do not provide shear relaxation functions of their products, the research delivered these functions for studied PVB and EVA based interlayers via their mechanical models. To enable a simple design of LG panels loaded at certain temperature and defined duration of static load, including the shear stiffness of interlayer, without the need of complicated computer programs, Enhanced Effective Thickness [60] method (EET) was used in the analytical model. This method represents simple and relatively precise tool for the calculation of single span simply supported 1D and 2D LG panels under uniform or local load. Whether the entire loading history of LG panel is assumed, viscoelastic solution is necessary. Presented mechanical models of PVB and EVA interlayers then serve as input parameters.

Experimental research also proved indisputable meaning of polymeric interlayer in terms of safety. PVB, EVA, and ionomer interlayers, in all bending destructive tests, prevented the abrupt collapse of LG panel when overloaded and kept the shards adhered. Individual glass plies in bending broke gradually until total failure of the entire panel. This fact means increased safety giving structure users sufficient time to leave an endangered area in comparison to monolithic glass. Type of used interlayer even affected the unfavourable effect of HTG panel being susceptible to falling down the support after total failure. In this matter, stiff ionomer interlayer SG 5000 was unique because glass panels with this interlayer stayed on the support even after total failure.

At the end of the thesis, presented example of practical analytical calculation of wind and snow loaded 1D simply supported double LG panel 10.10.4 with dimensions 900 x 2000 mm, laminated with PVB interlayer Trosifol BG R20, performed according to European standard EN 16612 [76], showed this standard was too conservative. Evaluation of glass plies shear coupling level only through the coefficient ω neglecting the shape of the panel and boundary conditions makes this standard unsuitable for LG panels with a dominant beam effect (beam shaped LG panels act differently than square LG panels – the original aim of EN 16612). This fact opens the way how LG panels may be assessed in the future – EET method respecting the shape and boundary conditions of the panel will be preferred.

Submitted thesis brought insight into author´s research in the field of polymeric interlayers and laminated glass in out of plane static loading. The research has not been currently finished. It should be noted here that presented shear stiffness of all interlayers is quantified for non-aged materials and experimental results and conclusions do not include the effects of cyclic loading acting on LG panels, increased humidity, or UV radiation.

12. Main achieved outputs for engineering practice

1. Complete description of time and temperature dependent shear stiffness of common PVB (**Trosifol® BG R20** and **Trosifol® Extra Strong**) and EVA (**Evalam® 80/120** and **Evasafe®**) polymeric interlayers used in laminated glass panels.
2. Research showed how the experimental testing of polymeric interlayers can be simplified. Initial shear stiffness of PVB or EVA interlayer obtained from static single-lap shear test presented in this thesis, at temperature T around or above glass transition temperature, reliably substitutes the value of short-term 10 seconds shear relaxation modulus as $\boldsymbol{G_{init}(T \geqq T_g) \approx G(t = 10\ s, T \geqq T_g)}$. For temperatures T below glass transition temperature, static single-lap shear test provides lower value of this short-term shear relaxation modulus, $\boldsymbol{G_{init}(T < T_g) < G(t = 10\ s, T < T_g)}$, but extreme stiffness of interlayer at $\boldsymbol{T < T_g}$ ensures full shear coupling of glass plies in bending. Therefore, complicated dynamic mechanical thermal analysis (DMTA) is in terms of PVB or EVA $\boldsymbol{G(t = 10\ s, T)}$ not necessary.
3. It cannot be generally said which DMTA testing method of small-scale specimens is more appropriate (DMTA in shear mode vs. DMTA in torsion mode). Constructed relaxation functions of interlayer given by both methods still need to be verified by real experiments.
4. Ionomer interlayer **SentryGlas® 5000** at room temperature ensures full shear coupling of glass plies in short-term loaded laminated glass panel. Moreover, its extreme stiffness favourably affects the post-breakage behaviour of laminated heat toughened glass (HTG) panel as this panel does not fall down the support after total failure. On the other hand, special attention must be paid to the width and structural solution of the supporting structure in case of HTG panels laminated with **Trosifol® BG R20** and **Evalam® 80/120** interlayers to prevent the panel from slipping out of the supports when all glass plies get broken.

5. Analytical Enhanced Effective Thickness method (EET) is suitable for economical design of single span simply supported double LG panels under uniform or local load. This method may replace current European standard EN 16612 which, apart from EET, does not include the shape and boundary conditions into the assessment of the panel.

13. Aims of the future research

This thesis shows the topic of polymer engineering science and viscoelasticity as well as behaviour of laminated glass in bending is very complex. Since there is a wide spectrum of polymeric interlayers on the market without specified stiffness, the need of experimental research is desirable. To bring new knowledge into this engineering area, author is going to keep searching in the following fields:

1. Mechanical models of interlayers

Author intends to work over mechanical models using broader spectrum of polymeric interlayers. Various DMTA methods or creep tests of other types of, e.g., PVB or EVA interlayers such as Butacite® G, EVA Crystal, etc., allow to obtain their time-temperature dependent shear stiffness, and enable their categorization into stiffness families according to EN 16613 [30].

2. The effect of cyclic out of plane loading on the response of laminated glass

Ambient temperature and duration of static load are the main factors according to which laminated glass in bending is designed [76]. Load bearing laminated glass is, over its lifecycle, usually exposed to many types of variable loads with various durations. This fact is often neglected. Viscoelasticity of interlayers means LG panel reacts with the delay to the applied load and loading history affects its current state of stress and deflections. This effect is more pronounced for uncross-linked thermoplastic interlayers with residual viscoplastic strains. Fig. 147 schematically shows how the vertical deflections and tensile stress in LG increase when out of plane load in time is varied. This is due to viscoelastic nature of interlayer [20]. Implementation of the loading history into the reliable design of LG is other topic for the future research.

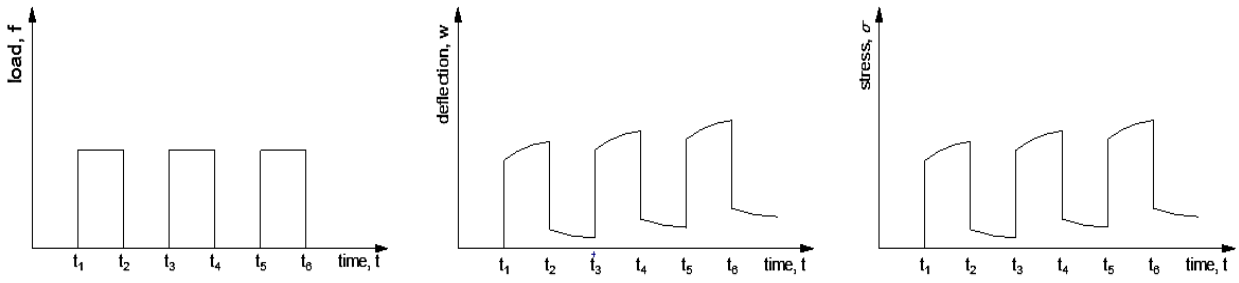

Fig. 147: Schematic effect of cyclic loading on the response of LG panel with uncross-linked interlayer

3. Effect of aging on the mechanical properties of polymeric interlayers

Aging of polymeric material as the consequence of UV radiation, change of temperature or humidity, is generally manifested by the change of its mechanical properties [80]. It is then desirable to test mechanical properties of aged interlayers subjected to these effects to see the difference of shear stiffness between their aged and non-aged structure. The example is shown in Fig. 148, where EVA S interlayer was subjected to artificial aging and was tested in single-lap shear tests at 0 °C. Mechanical properties of aged interlayers are the next topic for author´s research.

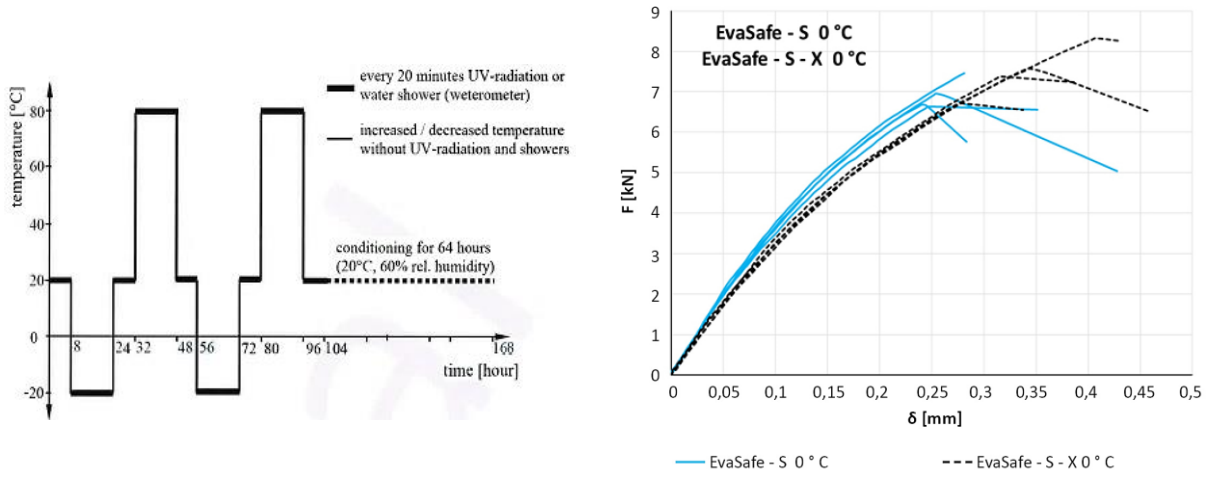

a) Aging cycle (UV + temperature changes) b) Static single-lap shear test at l. rate 2.0 mm/min

Fig. 148: Aging cycle and force-displacement relations of non-aged (full) and aged (dotted) EVA S interlayer measured from static single-lap shear tests identical with those shown in section 6.1

14. Valuable outcomes

Results of research and the entire experimental campaign were continuously presented at many international conferences, and they were also published in technical journals. Main outcomes from the thesis are listed below.

1. Guide for a practical design of laminated glass railing and floor according to valid German standard DIN 18008 [5] – example of analytical calculation is accessible at: https://ocel-drevo.fsv.cvut.cz/rpmt/?page_id=90

2. Journals with impact factor:
   - Hána, T.; Vokáč, M.; Eliášová, M.; Machalická, K.V
     Experimental investigation of temperature and loading rate effects on the initial shear stiffness of polymeric interlayers
     Engineering Structures. 2020, 223, ISSN 0141-0296.
   - Hána, T.; Janda, T.; Schmidt, J.; Zemanová, A.; Šejnoha, M.; Eliášová, M.; Vokáč, M.
     Experimental and Numerical Study of Viscoelastic Properties of Polymeric Interlayers Used for Laminated Glass: Determination of Material Parameters
     Materials. 2019, 12(14), ISSN 1996-1944.

3. Articles included into SCOPUS database:
   - Hána, T.; Eliášová, M.; Vokáč, M.; Machalická, K.V.
     Current analytical computational methods of laminated glass panels in comparison to FEM simulation
     In: 4th International Conference on Structures and Architecture ICSA, Lisabon, 2019-07-24/2019-08-26. Leiden: CRC Press/Balkema, 2019. p. 619-627. ISBN 978-1-138-03599-7.
   - Hána, T.; Eliášová, M.; Vokáč, M.; Vokáč Machalická, K.
     Viscoelastic properties of EVA interlayer used in laminated glass structures
     In: 5th International Conference on New Advances in Civil Engineering (ICNACE 2019). Melville, NY: AIP Publishing, APL, the American Institute of Physics, 2020. IOP Conference Series: Materials Science and Engineering. Vol. 800. ISSN 17578981
   - Hána, T.; Vokáč, M.; Machalická, K.V.; Eliášová, M.
     Dynamic Mechanical Thermal Analysis of EVA and PVB Polymeric Interlayers in Low Temperatures
     In: IOP Conference Series: Materials Science and Engineering. Bristol: IOP Publishing Ltd., 2019. Vol. 471. ISSN 1757-899X.

- Vokáč, M.; Hána, T.; Machalická, K.V.; Eliášová, M.
  Viscoelastic Properties of PVB Interlayer for Laminated Glass Structures Used in Building Reconstructions
  Key Engineering Materials, 2019. P. 115-122. Vol. 808. ISSN 1013-9826.
- Hána, T.; Sokol, Z.; Eliášová, M.; Vokáč, M.; Machalická, K.V.
  Four-point bending tests of double laminated glass panels with PVB in different loading rates
  In: Advances and Trends in Engineering Sciences and Technologies III: Proceedings of the 3rd International Conference on Engineering Sciences and Technologies. Boca Raton: CRC Press, 2019. P. 89-95. ISBN 9780367075095.
- Hána, T.; Vokáč, M.; Vokáč Machalická, K.; Eliášová, M.
  Material Properties of Polymeric Interlayers under Static and Dynamic Loading with Respect to the Temperature
  In: Challenging Glass 6 – International Conference on the Architectural and Structural Application of Glass. Delft: TU Delft, 2018. P. 417-426. Vol. 6. ISBN 978-94-6366-044-0.
- Hána, T.; Machalická, K.; Eliášová, M.; Vokáč, M.
  Safety Design of Laminated Glass Regarding PVB Interlayer Stiffness
  Key Engineering Materials, 2017. P. 279-285. Vol. 755. ISSN 1013-9826.

4. Author was cited in SCOPUS database by:

- Santo, D., Mattei, S., Bedon, C.
  Elastic critical moment for the lateral-torsional buckling (LTB) analysis of structural glass beams with discrete mechanical lateral restraints (2020) Materials, 13 (11), art. No. 2492, doi: 10.3390/ma13112492
- Schmidt, J., Zemanová, A.
  Euler and exponential algorithm in viscoelastic analyses of laminated glass (2020) Acta Polytechnica CTU Proceedings, 26, pp. 86-93, doi: 10.14311/APP.2020.26.0086
- Bedon, C.
  Issues on the vibration analysis of in-service laminated glass structures: Analytical, experimental and numerical investigations on delaminated beams (2019) Applied Sciences (Switzerland), 9 (18), art. No. 3928, doi: 10.3390/app9183928
- Yang, Z.G., Zang, M.Y., Cheng, Y.L.
  Simulation of Impact Fracture Behavior of Laminated Glass Based on DEM/FEM and Cohesive Model (2019) Strength of Materials, 51 (4), pp. 520-533, doi: 10.1007/s11223-019-00097-2
- Schmidt, J., Zemanová, A., Zeman, J., Šejnoha, M.
  Phase-field fracture modelling of thin monolithic and laminated glass plates under quasi-static bending (2020) Materials, 13 (22), pp. 1-29, doi: 10.3390/ma13225153

- Hänig, J., Weller, B.
  Experimental investigations and numerical simulations of innovative limeweight glass-plastic-composite panels made of thin glass and PMMA (2021) Glass Structures and Engineering, pp. 249-271, doi: 10.1007/s40940-021-00153-x
- Lu, Y., Chen, S., Shao, X.
  Shear modulus of ionomer interlayer: Effects of time, temperature and strain rate (2021) Construction and Building Materials, 302, doi: 10.1016/j.conbuildmat.2021.124224
- Zhang, Z., Fu, Q., Wang, J., Yang, R., Xiao, P., Ke, F., Lu, C.
  Interaction between the edge dislocation dipole pair and interfacial misfit dislocation network in Ni-based single crystal superalloys (2021) International Journal of Solids and Structures, 228, doi: 10.1016/j.ijsolstr.2021.111128
- Galuppi, L., Nizich, A.J.
  Cantilevered laminated glass balustrades: the Conjugate Beam Effective Thickness method – Part 1 The analytical model (2021) Glass Structures and Engineering, doi: 10.1007/s40940-021-00156-8
- Schmidt, J., Janda, T., Zemanová, A., Zeman, J., Šejnoha, M.
  Newmark algorithm for dynamic analysis with Maxwell chain model (2020) Acta Polytechnica, 60, pp. 502-511, doi: 10.14311/AP.2020.60.0502
- Vedrtnam, A., Bedon, C., Youssef, M.A., Chaturvedi, S.
  Effect of non-uniform temperature exposure on the out-of-plane bending performance of ordinary laminated glass panels (2021) Composite Structures, 275,
  doi: 10.1016/j.compstruct.2021.114517
- Centelles, X., Martín, M., Solé, A., Castro, J.R., Cabeza, L.F.
  Tensile test on interlayer materials for laminated glass under diverse ageing conditions and strain rates (2020) Constructions and Building Materials, 243,
  doi: 10.1016/j.conbuildmat.2020.118230
- Yang, J., Wang, Y., Wang, X., Hou, X., Zhao, Ch., Ye, J.
  Local bridging effect of fractured laminated glass with EVA based hybrid interlayers under weathering actions (2021) Construction and Building Materials, 314,
  doi: 10.1016/j.conbuildmat.2021.125595
- Zemanová, A., Hála, P., Konrád, P., Janda, T., Hlůžek, R.
  The influence of interlayer properties on the response of laminated glass to low-velocity hard-object impact (2022) International Journal of Impact Engineering, 159,
  doi: 10.1016/j.ijimpeng.2021.104036
- Lu, Y., Chen, S., Shao, X.
  Shear modulus ionomer interlayer: Effects of time, temperature and strain rate (2021) Construction and Building Materials, 302,
  doi: 10.1016/j.conbuildmat.2021.124224

15. References

List of references cited in this thesis

[1] M. Eliášová et al., *Sklo - materiál pro nosné konstrukce = Glass - material for load-bearing structures*. V Praze: České vysoké učení technické, 2014.

[2] Institution of Structural Engineers, Ed., *Structural use of glass in buildings*. London: SETO, 1999.

[3] J. Wurm, *Glass structures: design and construction of self-supporting skins*. Basel: Boston : Birkhäuser, 2007.

[4] M. Eliášová, *Nosné konstrukce ze skla*. Praha: ČVUT, 2005.

[5] *DIN 18008-1: Glass in civil engineering - Design and Construction rules, Part 1: Conditions and general principles*. Berlin: German Institute für Normung, 2011.

[6] W. Laufs and A. Luible, *Introduction on Use of Glass in Modern Buildings*. Lausanne: EPFL-ICOM, 2003.

[7] D. Delincé et al., 'Post-breakage behaviour of laminated glass in structural applications', in *Challenging glass conference*, Amsterdam, The Netherlands, 2008.

[8] T. Hána et al., 'Determination of PVB interlayer's shear modulus and its effect on normal stress distribution in laminated glass panels', presented at the 3rd International Conference on Innovative Materials, Structures and Technologies, Bristol, 2017.

[9] J. Kuntsche et al., 'Engineering design of laminated safety glass considering the shear coupling: a review', *Glass Struct Eng*, no. 4, pp. 209–228, 2019.

[10] M. Haldimann et al., *Structural use of glass*. Zürich, Switzerland: International Association for Bridge and Structural Engineering, 2008.

[11] L. Sable et al., 'Influence of EVA, PVB and Ionoplast Interlayers on the Structural Behaviour and Fracture Pattern of Laminated Glass', *Int J Struct Glass Adv Mat Research*, no. 3, pp. 62–78, 2019.

[12] *Post-Breakage Performance of Laminated Safety Glass*, Kuraray Technical sheet. [Online]. Available: https://www.curbellplastics.com/Research-Solutions/Technical-Resources/Technical-Resources/Breakage-Performance-of-Laminated-Safety-Glass.

[13] B. Hoffmeister et al., 'Innovative steel-glass components for high performance building skins: testing of full-scale prototypes', *Glass Struct Eng*, no. 2, pp. 57–78, 2017.

[14] B. Kassnel-Henneberg, 'Connections in Glass', in *Challenging Glass 5 - Conf. on Architectural and Structural Applications of Glass*, Belgium - Gent, 2016.

[15] (2020, August.11), *Strut Channel Systems-For Less*. [Online]. Available: http://www.strutchannelfittings.com/THK-11615-SHADE-ATRIUM-SHADING-PV--THIN-FILM-40-30-20-OR-10-TRANSPARENT-MODULES-WITH-ALUMINUM-RACKING-DESIGNED-TO-ATTACH-TO-EXISTING-ATRIUM-FRAMING-ON-ROOF_p_1222.html.

[16] (2020, August.11), *Best Stairs Lighting images*. [Online]. Available: https://www.google.com/imgres?imgurl=https://i.pinimg.com/236x/f1/9b/39/f19b3929e30df0406e68ae0e7a0f4e58--floating-stairs-glass-stairs.jpg&imgrefurl=https://in.pinterest.com/amardeepdugar/stairs-lighting/&h=177&w=236&tbnid=8U2oIQNG44q4oM&tbnh=177&tbnw=236&usg=AI4_-kRPnrFuLlq5SJPeG_Xk861bG1uzsQ&vet=1&docid=02ymoKn85SE4EM&hl=cs.

[17] (2020, August.20), *GlasSpace-StructuralGlass*. [Online]. Available: https://www.google.com/imgres?imgurl=https://www.glasspace.com/wp-content/uploads/2019/12/glass-roof-1.jpg&imgrefurl=https://www.glasspace.com/glass-roof-lights/&h=508&w=508&tbnid=uLkdaN-4s-LIiM&tbnh=225&tbnw=225&usg=AI4_-kQUKBdyMcEthtTW-fWWioDzjNafbQ&vet=1&docid=bwi_AMeymIuOMM&hl=cs.

[18] *EN 1991-1-1: Eurocode 1, Actions on structures – Part 1-1: General actions – Densities, self-weight, imposed loads for buildings*. Brussels: European Committee for Standardization CEN, 2002.

[19] J. Kuntsche et al., 'Viscoelastic properties of laminated glass interlayers – theory and experiments', in *Glass Performance Days*, Tampere, 2015.

[20] R. S. Lakes, *Viscoelastic materials*. Cambridge ; New York: Cambridge University Press, 2009.

[21] *Physical properties of SentryGlas and Butacite, Technical data Sheet*, Kuraray Technical sheet. [Online]. Available: https://www.trosifol.com/fileadmin/user_upload/Kuraray_4_1_Physical_Properties_of_Sentryglas.pdf.

[22] H. F. Brinson and L. C. Brinson, *Polymer engineering science and viscoelasticity: an introduction*. Springer Science, 2015.

[23] J. D. Ferry, *Viscoelastic properties of polymers*, 3d ed. New York: Wiley, 1980.

[24] (2020, May.14), *How polymers work: Thoughts on thermoplastic elastomers*. [Online]. Available: https://pslc.ws/macrog/tpe.htm.

[25] X. Xu et al., 'Experimental Studies on Viscoelasticity of Film Materials in Laminated Glass Sheets', *SAE International*, 2015.

[26] L. Andreozzi et al., 'Dynamic torsion tests to characterize the termo-viscoelastic properties of polymeric interlayers for laminated glass', *Constr Build Mat*, no. 65, pp. 1–13, 2014.

[27] P. Hooper et al., 'The mechanical behaviour of poly(vinyl butyral) at different strain magnitudes and strain rates', *J Mat Sci*, no. 47, pp. 3564–3576, 2012.

[28] L. Biolzi et al., 'Long term response of glass-PVB double-lap joints', *Comp Part B: Eng*, pp. 41–49, 2014.

[29] M. Botz et al., 'Experimental determination of the shear modulus of polymeric interlayers used in laminated glass', in *GlassCon Global*, Chicago, vol. 2018, pp. 31–38.

[30] *EN 16613: Glass in building - Laminated glass and laminated safety glass-Determination of interlayer viscoelastic properties*. Brussels: European Commitee for Standardization, CEN, 2019.

[31] Z. Bittnar et al., *Numerical methods of mechanics I*. Praha: České vysoké učení technické, 1992.

[32] W. Grellmann et al., Eds., *Kunststoffprüfung*, 2. Aufl. München: Hanser, 2011.

[33] M. A. Kraus et al., 'Parameter identification methods for visco- and hyperelastic material models', *Glass Struct Eng*, no. 2, pp. 147–167, 2017.

[34] N. P. Cheremisinoff, *Condensed Encyclopedia of Polymer Engineering Terms*. 2012.

[35] H. Leaderman, 'Textile Materials and the Time Factor: Mechanical Behaviour of Textile Fibers and Plastics', *Text Res J*, no. 11, p. 171, 1941.

[36] F. Kohlrausch, 'Experimental-Untersuchung uber die elastische Nachwirkungbel der Torsion', *Fogg Ann Physik*, no. 8, p. 337, 1876.

[37] F. R. Schwarzl, *Polymermechanik*. Springer Berlin Heidelberg, 1990.

[38] M. Schuster et al., 'Investigations on the thermorheologically complex material behaviour of the laminated safety glass interlayer ethylene-vinyl-acetate', *Glass Struct Eng*, no. 3, pp. 373–388, 2018.

[39] M. Williams et al., 'The Temperature Dependence of Relaxation Mechanisms in Amorphous Polymers and Other Glass-forming Liquids', *J Am Chem Soc*, no. 77, pp. 3701–3707, 1955.

[40] J. S. Cartner and H. F. Brinson, 'The nonlinear Viscoelastic Behaviour of Adhesives and Chopped Fiber Composites'. Virginia Tech. Report, 1978.

[41] M. A. Kraus et al., 'Rheological modelling of linear viscoelastic materials for strengthening in bridge engineering', in *Proceedings of the 11th German Japanese Bridge Symposium*, Osaka, 2016.

[42] A. J. Malkin and A. I. Isayev, *Rheology: concepts, methods, and applications*, 2. ed. Toronto: CP, ChemTec Publ, 2012.

[43] M. Jirásek, 'Lectures to Přetváření a porušování Materiálů at CTU, Part: Viscoelasticity of materials'. 2020[Online]. Availablehttp://bilakniha.cvut.cz/cs/predmet24825905.html.

[44] H. Poincaré, *Science and Hypothesis*. New York: The Walter Scott Publishing Co, 1905.

[45] S. P. Panchenko, 'Numerical simulation of viscoelastic materials'. National University of Railway Transport, 2014[Online]. Availablehttps://www.researchgate.net/publication/276395700_NUMERICAL_SIMULATION_OF_VISCOELASTIC_MATERIALS/fulltext/5627769908ae2b313c54e579/NUMERICAL-SIMULATION-OF-VISCOELASTIC-MATERIALS.pdf.

[46] B. Weller et al., ‘Experimental Study on Different Interlayer Materials for Laminated Glass’, in *Glass Processing Days*, Tampere, 2005, pp. 120–123.

[47] A. Rühl et al., ‘Characterization and modeling of poly(methyl methacrylate) and thermoplastic polyurethane for the application in laminated setups’, *Mech Mat*, no. 113, pp. 102–111, 2017.

[48] D. Callewaert et al., ‘Influence of Temperature and Load Duration on Glass/Ionomer Laminates Torsion and Bending Stiffness’, in *International Symposium on the Application of Architectural Glass*, Munich, 2008, pp. 51–63.

[49] E. Wölfel, ‘Nachgiebiger Verbund Eine Nächerungslösung und deren Anwendungsmöglichkeiten’, *Stahlbau*, pp. 173–180, 1987.

[50] T. Serafinavicius et al., ‘Bending Behaviour of Structural Glass Laminated With different Interlayers’, *Mech Comp Mat*, no. 49, pp. 437–446, 2013.

[51] *EN 1288-3: Glass in building. Determination of the bending strength of glass. Part 3: Test with specimen supported at two points*, Brussels. European Committee for Standardization CEN, 2000.

[52] G. Molnár et al., ‘Finite element analysis of laminated structural glass plates with polyvinyl butyral (PVB) interlayer’, *Periodica Pol*, no. 56, pp. 35–42, 2012.

[53] T. Serafinavicius et al., ‘Long-term laminated glass four point bending test with PVB, EVA, and SG interlayers at different temperatures’, *Proc Eng*, no. 57, pp. 996–1004, 2013.

[54] S. J. Bennison et al., ‘Structural Performance of Laminated Glass Made With a Stiff interlayer’, *The Use Glass Build*, pp. 57–65, 2002.

[55] *ASTM: E1300-09 Standard Practice for Determining Load Resistance of Glass in Buidings*. Americal Society Testing of Materials, 2009.

[56] S. J. Bennison and I. Stelzer, ‘Structural properties of laminated glass’, in *Glass Performance Days*, Finland, 2009.

[57] I. Calderone et al., ‘Effective laminate thickness for the design of laminated glass’, in *Glass Performance Days*, Finland, 2009.

[58] L. Galuppi et al., ‘Practical expressions for the design of laminated glass’, *Comp Part B*, no. 45, pp. 1677–1688, 2013.

[59] *CNR-DT-210: Instructions for the design, execution, and control of buildings with structural glass elements*. Roma: National Research Council of Italy, 2012.

[60] L. Galuppi and G. Royer Carfagni, ‘Effective thickness of laminated glass beams: New expression via a variational approach’, *Eng Struct*, no. 38, pp. 53–67, 2012.

[61] L. Galuppi et al., ‘The Effective Thickness of Laminated Glass Plates’, *J Mech Mat Struct*, no. 7, pp. 375–400, 2012.

[62] L. Galuppi and G. Royer Carfagni, ‘Laminated beams with viscoelastic interlayer’, *Int J Sol Struct*, no. 49, pp. 2637–2645, 2012.

[63] *Z-70.3-230: Allgemeine bauaufsichtliche Zulassung der Verbundsicherheitsglas aus der Produktfamilie SAFLEX DG mit Schubverbund*. Berlin: Deutsches Institut für Bautechnik, 2016.

[64] Y. J. Juang et al., ‘Rheological analysis of polyvinyl butyral near the glass transition temperature’, *Polymer Eng Sci*, no. 41, pp. 275–292, 2001.

[65] G. Hidalgo, (2020,), *Our Expertise: Glass Laminated Structures with EVA or PVB. A Comparison Analysis*. [Online]. Available: https://www.novogenio.com/blog/glass-laminated-structures-with-eva-or-pvb.-a-comparison-analysis.

[66] S. H. Schulze et al., ‘Influence of Vacuum Lamination Process on Laminate Properties-Simulation and Test Results’, presented at the 24th European Photovoltaic Solar Energy Conference, Germany, 2009.

[67] (2019,), *BASF. Ellastolan material properties. Technical sheet*. [Online]. Available: http://www.polyurethanes.basf.de/pu/Elastollan/Elastollan_Materialeigenschaften.

[68] L. Galuppi and G. Royer Carfagni, ‘The effective thickness of laminated glass: Inconsistency of the formulation in a proposal of EN-standards’, *Comp Part B: Eng*, no. 55, pp. 109–118, 2013.

[69] J. Kuntsche, *Mechanisches Verhalten von Verbundglas unter zeitabhängiger Belastung und Explosionsbeanspruchung*. Berlin: Springer Vieweg, 2015.

[70] J. Schmidt et al., 'Calibration of model for laminated glass polymer interlayer based on rheometer data', in *55th Conference on experimental stress analysis*, Slovakia, 2017.

[71] J. A. Nelder and R. Mead, 'A Simplex Method for Function Minimization', *Comput J*, no. 7, pp. 308–313, 1965.

[72] R. A. Schapery, 'Application of Thermodynamics to Thermomechanical Fracture and Birefringent Phenomena in Viscoelastic Media', *J Applied Ph*, no. 35, pp. 1451–1465, 1964.

[73] A. Zbiciak and W. Grzesikiewicz, 'Identification of constitutive model for asphalt-aggregate mixes using linear rheological schemes', *Polio Komp Wspom Proj*, no. 10, pp. 187–196, 2012.

[74] P. Y. Rohan et al., 'Finite element modelling of nearly incompressible materials and volumetric locking: a case study', *Comp Meth Biomech Biomed Eng*, no. 17, pp. 192–193, 2014.

[75] R. Weller et al., *Glasbau Praxis - Konstruktion und Bemessung*, 3rd ed. Berlin: Beuth Verlag GmbH, 2013.

[76] *EN 16612: Glass in building - Determination of the lateral load resistance of glass panes by calculation*. Brussels: European Commitee for Standardization, 2019.

[77] *ČSN EN 1990: Zásady navrhování konstrukcí*. Český Normalizační Institut, 2015.

[78] *ČSN EN 1991-1-4: Zatížení konstrukcí - Zatížení větrem*. Český Normalizační Institut, 2007.

[79] *ČSN EN 1991-1-3: Zatížení konstrukcí - Zatížení sněhem*. Český Normalizační Institut, 2005.

[80] J. Verdu, 'Effect of Aging on the Mechanical Properties of Polymeric Materials', *J Macro Sci*, no. 31, 1994 [Online]. Available: doi.org/10.1080/10601329409350099.

Complete list of author´s publications related to this thesis

- **Hána, T.; Vokáč, M.; Eliášová, M.; Machalická, K.V.**
  Experimental investigation of temperature and loading rate effects on the initial shear stiffness of polymeric interlayers
  Engineering Structures. 2020, 223, ISSN 0141-0296.
- **Hána, T.; Janda, T.; Schmidt, J.; Zemanová, A.; Šejnoha, M.; Eliášová, M.; Vokáč, M.**
  Experimental and Numerical Study of Viscoelastic Properties of Polymeric Interlayers Used for Laminated Glass: Determination of Material Parameters
  Materials. 2019, 12(14), ISSN 1996-1944.
- **Hána, T.; Vokáč, M.; Eliášová, M.; Sokol, Z.; Machalická, K.V.**
  Four-point bending tests of PVB double laminated glass panels – experiments and numerical analysis
  In: Challenging Glass 7 – Conference on Architectural and Structural Applications of Glass. 2020, ISBN 978-94-6366-296-3.
- **Vokáč, M.; Hána, T.; Machalická, K.V.; Eliášová, M.**
  Viscoelastic Properties of Selected PVB Interlayers for Laminated Glass
  In: Acta Materialia Turcica. 2020, 4, 37-42, ISSN 2630-5909.
- **Hána, T.; Eliášová, M.; Vokáč, M.; Machalická, K.V.**
  Viscoelastic properties of EVA interlayer used in laminated glass structures
  In: 5th International Conference on New Advances in Civil Engineering, Kyrenia, 2019-11-08/2019-11-10. Melville, NY: AIP Publishing, APL, the American Institute of Physics, 2020. IOP Conference Series: Materials Science and Engineering. vol. 800. ISSN 17578981.
- **Hána, T.; Vokáč, M.; Eliášová, M.; Machalická, K.V.**
  Advanced computational methods of perpendicularly loaded laminated glass panes
  In: Modern Building Materials, Structures and Technicques MBMST 2019. The 13th International Conference Modern Building Materials, Structures and Techniques, Vilnius, 2019-05-16/2019-05-17. VGTU Press, 2019. p. 336-343. ISSN 2029-9915. ISBN 978-609-476-197-3.
- **Hána, T.; Eliášová, M.; Vokáč, M.; Machalická, K.V.**
  Current analytical computational methods of laminated glass panels in comparison to FEM simulation
  In: CRUZ, P.J.J., ed. Structures and Architecture: Bridging the Gap and Crossing Borders. 4th International Conference on Structures and Architecture, Lisabon, 2019-07-24/2019-08-26. Leiden: CRC Press/Balkema, 2019. p. 619-627. vol. 1. ISBN 978-1-138-03599-7.
- **Hána, T.; Sokol, Z.; Eliášová, M.; Vokáč, M.; Machalická, K.V.**
  Four-point bending tests of double laminated glass panels with PVB in different loading rates
  In: Advances and Trends in Engineering Sciences and Technologies III: Proceedings of the 3rd International Conference on Engineering Sciences and Technologies. Boca Raton: CRC Press, 2019. p. 89-95. ISBN 9780367075095.
- **Hána, T.**
  Viskoleastické vlastnosti PVB Fólie používané do konstrukcí vrstvených skel
  In: STUDNIČKA, J. and J. FÍLA, eds. Sborník semináře doktorandů katedry ocelových a dřevěných konstrukcí 2019. Praha: Czech Technical University in Prague, 2019. p. 60-66. ISBN 978-80-01-06601-0.
- **Vokáč, M.; Hána, T.; Machalická, K.V.; Eliášová, M.**
  Viscoelastic Properties of PVB Interlayer for Laminated Glass Structures Used in Building Reconstructions
  Key Engineering Materials, 2019. p. 115-122. vol. 808. ISSN 1013-9826.

- **Hána, T.; Sokol, Z.; Eliášová, M.; Vokáč, M.**
  Four-Point Bending Test of Double Laminated Glass Panels with EVA Interlayer in Various Loading Rates
  In: ZOLOTAREV, I. and V. RADOLF, eds. Engineering Mechanics 2019: Book of full texts. Engineering Mechanics 2019, Svratka, 2019-05-13/2019-05-16. Prague: Institute of Thermomechanics, AS CR, v.v.i., 2019. p. 145-148. ISSN 1805-8248. ISBN 978-80-87012-71-0.
- **Hána, T.; Vokáč, M.; Machalická, K.V.; Eliášová, M.**
  Dynamic Mechanical Termal Analysis of EVA and PVB Polymeric Interlayers in Low Temperatures
  In: IOP Conference Series: Materials Science and Engineering . 3rd World Multidisciplinary Civil Engineering, Architecture, Urban Planning Symposium, Praha, 2018-06-18/2018-06-22. Bristol: IOP Publishing Ltd., 2019. vol. 471. ISSN 1757-899X.
- **Hána, T.**
  Vliv polymerních folií na chování vrstvených skel při zatížení
  In: STUDNIČKA, J. and J. FÍLA, eds. Sborník semináře doktorandů katedry ocelových a dřevěných konstrukcí 13.2. a 20.9. 2018. Praha: ČVUT, Fakulta stavební, Katedra ocelových a dřevěných konstrukcí, 2018. p. 31-34. ISBN 978-80-01-06448-1.
- **Hána, T.; Vokáč, M.; Machalická, K.V.; Sokol, Z.; Eliášová, M.**
  Influence of loading rate on double laminated glass panels performance in four-point bending tests
  In: ESaT 2018. 3rd International Conference on Engineering Sciences and Technologies, Tatranské Matliare, 2018-09-12/2018-09-14. Košice: Technická univerzita v Košiciach, Stavebná fakulta, 2018. ISBN 978-80-553-2982-6.
- **Hána, T.; Eliášová, M.; Sokol, Z.**
  Structural Performance of Double Laminated Glass Panels with EVA and PVB Interlayer in Four-Point Bending Tests
  International Journal of Structural Glass and Advanced Materials Research. 2018, ISSN 2616-4515.
- **Hána, T.; Machalická, K.V.; Eliášová, M.; Vokáč, M.**
  Výpočet napjatosti ohýbaných nosných prvků z vrstveného skla v závislosti na tuhosti folie PVB a EVA
  TZB-info: portál pro technická zařízení budov. 2018, 20(10.09.2018), ISSN 1801-4399.
- **Hána, T.; Eliášová, M; Sokol, Z.**
  Four Point Bending Tests of Double Laminated Glass Panels
  In: Engineering Mechanics 2018: Book of Full Texts. 24th International Conference Engineering Mechanics 2018, Svratka, 2018-05-14/2018-05-17. Praha: Ústav teoretické a aplikované mechaniky AV ČR, v. v. i., 2018. p. 285-288. ISSN 1805-8248. ISBN 978-80-86246-88-8.
- **Hána, T.; Vokáč, M.; Machalická, K.V.; Eliášová, M.**
  Material Properties of Polymeric Interlayers under Static and Dynamic Loading with Respect to the Temperature
  In: LOUTER, Ch., et al., eds. Challenging Glass 6 - International Conference on the Architectural and Structural Application of Glass. Challenging Glass 6, Delft: TU Delft, 2018. p. 417-426. vol. 6. ISBN 978-94-6366-044-0.
- **Hána, T.; Eliášová, M.; Machalická, K.V.; Vokáč, M.**
  Stanovení smykového modulu folií PVB a EVA v závislosti na teplotě a rychlosti zatížení
  TZB info. 2018, 20(30.04.2018), ISSN 1801-4399.

- **Hána, T.; Eliášová, M.; Machalická, K.V.; Vokáč, M.**

  Determination of PVB interlayer´s shear modulus and its effect on normal stress distribution in laminated glass panels

  In: IOP Conference Series: Materials Science and Engineering . 3rd International Conference on Innovative Materials, Structures and Technologies, Riga, 2017-09-27/2017-09-29. Bristol: IOP Publishing Ltd, 2017. vol. 251. ISSN 1757-899X.

- **Hána, T.**

  Vliv polymerních folií na chování vrstvených skel při zatížení

  In: STUDNIČKA, J. and J. FÍLA, Seminář doktorandů katedry ocelových a dřevěných konstrukcí, Praha, 2017-02-16. Praha: ČVUT, Fakulta stavební, Katedra ocelových a dřevěných konstrukcí, 2017. p. 13-14. ISBN 978-80-01-06167-1.

- **Hána, T.; Machalická, K.V.; Eliášová, M.; Vokáč, M.**

  Safety Design of Laminated Glass Regarding PVB Interlayer Stiffness

  Key Engineering Materials, 2017. p. 279-285. vol. 755. ISSN 1013-9826.

Expert reports on practical problems written by author

- **Hána, T.; Vokáč, M.**

  Expert report n. 1800J236: Monitoring of temperature field on façade panel made of double laminated glass installed in building construction "Na Dlaskově 129; Velké Popovice"

  Issued by: Klokner Institute CTU, August 2020.

- **Hána, T.; Šimůnek, I.**

  Expert report n. 2100J055: Assessment of load bearing glass awning placed above main entrance of elementary school Kamenice, Prague region

  Issued by: Klokner Institute CTU, March 2021.

Abroad internship related to autor´s research

Time period: 1.9.2019 – 29.2.2020
Destination: Ghent University – Belgium
Supervision: prof. Jan Belis, Ph.D.
Purpose: Preparation and performance of destructive and creep loading tests with large-scale LG specimens laminated with studied interlayers. Destructive tests were performed in four-point bending mode at room temperature. Creep tests were performed in three-point bending mode in the climatic chamber.

16. Appendix

Appendix A: Technical sheets of studied interlayers

Note: Technical sheets of all studied interlayers provided by the manufacturers are listed below. The lists include available technical data.

DATA SHEET EVALAM 80/120

INFORMATION

TEMPERATURE	ºc	135
TIME	Minutes	Total_Thickn._Glass x 3'
VACUUM		ACTIVATED

PROPERTIES

THICKNESS	(mm)	0.38 +-5%
WIDTH	(mm)	2100
LENGTH	(m)	100
COLOR		Transparent
WATER ABSORTION -23^{O}C, 24hr	(%)	0.1
ANTI-AGING outdoor during 1 moth		Normal
ANTI-AGING UV Radiation Test 2000hr		< 1.5%
RESISTANCE TO HEAT 100^{O}C, 2hr		Normal
FREEZING RESISTANCE -40^{O}C 2hr		Excellent
HARDNESS	(Shore)	75
ADHESION STRENGTH	(N/cm)	94
LIGHT TRANSMITTANCE 1 Layer	(%)	90.7
HAZE 1 Layer	(%)	0.8
UV FILTERING	(%)	99.8
TENSILE	Mpa	13.9

CERTIFICATIONS

EVALAM 80/120 has all regulations required by the law of laminated glass for the construction required by the ECC for the outside glazing :

- TEMPERATURE UNE-EN 12543-4:1998	Satisfactory
- HUMIDITY UNE-EN 12543-4:1988	Satisfactory
- HIGH TEMPERATURE UNE-EN 12543-4:1988	Satisfactory
- IMPACT TEST UNE EN-356-2001	1B1 (4T+4T.3) o (8T+8T.2)
- IMPACT TEST UNE EN-356-2001	P1A (5+5.1)
- Flexión N/mm2 UNE-EN 1288-3	37 N/mm2
- Compatibility test silicones	Satisfactory

Evalam® 80/120 by PUJOL™

Properties	Unit	Testing method	Type G7140
Tensile strength	MPa	JIS K 7127	26
Extensibility	%	JIS K 7127	350
Young modulus (23 °C)	MPa	JIS K 7127	18
Poisson ratio	-		0.32
Hardness	Shore A	-	82
Glass transition temperature	°C	DSC	-28
Melting point	°C	DSC	79
Internal resistance	Ω x cm		5.4×10^{15}
Dielectric constant (1kHz)			3.4
Breakdown voltage	kV/mm		19
Refractive index		-	1.491
Limit wavelength UV	nm	-	380
Thermal conductivity	kcal/mh°C	-	0.1
Thermal expansion	1/K	-	3.5×10^{-4}
Absorbtion	%	JIS K 7209	< 0.01
Water permeability	g/m^2 x 24h	-	64.3
Gelatinization time	%	-	95

Evasafe® by BRIDGESTONE™

kuraray

TROSIFOL
PVB film for laminated safety glass

Specification
TROSIFOL BG R 20
Film thickness 0,76mm – 1,52mm

Property		Value	Tolerance	Unit	Method TROSIFOL
Film thickness > Certificate <		0,78 1,14 1,52	+ 0,04 - 0,04 + 0,06 - 0,04 + 0,07 - 0,05	mm	**Test method PAPB001**
Roughness R_z λ 2,5mm > Certificate <		40	± 12	µm	**Test method PAPB002** DIN EN ISO 4287
Moisture content > Certificate <		0,45	± 0,07	%	**Test method PAPB003** IR - Measurement)
Pummel test > Certificate <		≥ 6			**Test method PAPB004** based auf 2mm float glass
Compressive **Shear Strength** > Certificate <	0,76mm 1,14mm 1,52mm	≥ 16,0 ≥ 15,0 ≥ 14,0		N/mm^2	**Test method PAPB007** based auf 2mm float glass
Shrinkage MD > Certificate <		≤ 2,0		%	**Test method PAPB005** at 20°C and 10 min. storage

QM TROSIFOL
Rev. 04.2008

Trosifol® BG R20 by KURARAY™

TROSIFOL® ES

TROSIFOL® ES				
Product	Colour	Thickness [mm]	Roll width [cm]	Roll length [m]
TROSIFOL ES	Clear	0.76	45-321	250

PHYSICAL DATA TROSIFOL ES			
Properties	Unit	Test method	Value
Density	g/cm³	DIN 53479	1.081
Refractive index	-	DIN 53491	1.4872
Thermal conductivity	W/mK	DIN EN 12939	0.152
Thermal expansion coefficient	1/K x 10 $^{-4}$	ISO 11359	1.6
Specific heat	J/gK	ISO 11357	0.351
Thermal resistance	m² x K/W	DIN EN 12665	0.0056
Tear resistance	N/mm²	ISO 527	≥ 32
Elongation at break*	%	ISO 527	≥ 180

* General approval from the building authorities for laminated safety glass pending from the German institute for Construction Engineering, Berlin, Germany

LIGHT DATA TO DIN EN 410**		
Properties	Unit	Value
Light transmittance	%	90
Light reflectance 8°	%	8
Radiation transmittance	%	75
Radiation reflectance	%	7
Radiation absorption	%	18
UV transmittance	%	0.15
g-value	%	79
Shading coefficient	%	99

**All data measured in accordance with EN 410:2011-04 on laminated safety glass with two plies of 4 mm float glass

Trosifol® Extra Strong by KURARAY™

SentryGlas® Elastic Properties (SG5000)

In general, 0,76 mm (30 mil) is specified for easy processing when double stacking and not intended to be used as a single ply. Single ply use has not been tested to determine performance against any safety glazing codes or standards. 0,89 mm (35 mil) interlayers typically require high quality tempered glass for flatness. 1.52 mm (60 mil) interlayers are specified as the standard thickness for minimally supported applications. 2.28 mm (90 mil) thickness interlayers are normally specified for anti-intrusion, hurricane and other types of security applications. Glass producers and laminators require interlayers to be supplied either in sheet form or on rolls. SentryGlas® Ionoplast interlayers are available in both formats. For faster deliveries, SentryGlas® ionoplast interlayer is stocked in standard thicknesses (calipers) of 0.89 mm (35 mil), 1.52 mm (60 mil) and 2.28 mm (90 mil) sheets. SentryGlas® ionoplast interlayer on roll is available in 0,76 mm (30 mil) and 0.89 mm (35 mil) thickness.

TABLE 1 — LAMINATE PROPERTIES

Property	Units Metric (English)	Value	Test
Haze	%	< 2	ASTM D1003
Impact test 0,23 kg (0.5 lb)	m (ft)	> 9.14 (> 30)	ANSI Z26.1
Boil test 2 hr	-	No defects	ANSI Z26.1
Bake test 2 hr / 100 °C	-	No defects	ANSI Z26.1

TABLE 2 — INTERLAYER TYPICAL PROPERTIES

Property	Units Metric (English)	Value	ASTM Test
Young's Modulus	Mpa (kpsi)	300 (43.5)	D5026
Tear Strength	MJ/m3 (ft lb/in3)	50 (604)	D638
Tensile Strength	Mpa (kpsi)	34.5 (5.0)	D638
Elongation	% (%)	400 (400)	D638
Density	g/cm3 (lb/in3)	0.95 (0.0343)	D792
Flex Modulus 23 °C (73 °F)	Mpa (kpsi)	345 (50)	D790
Heat Deflection Temperature (HDT) @ 0.46 MPa	°C (°F)	43 (110)	D648
Melting Point	°C (°F)	94 (201)	(DSC)
Coeff. of Thermal Expansion (-20 °C to 32 °C)	10-3 cm/cm °C (mils/in °C)	10 - 15 (0.10 - 0.15)	D696
Thermal Conductivity	W/M-K (BTU-in/hr-ft2 °F)	0.246 (1.71)	

SentryGlas® 5000 by KURARAY™

kuraray

trosifol™
world of interlayers

Physical properties*

Property	Test Method/ ASTM Test	Unit	BG	Colour	HR100	SC	SC+	ES	SentryGlas®
Density	DIN 53479/D792	g/cm³	1.065	1.065	1.065	1.058	1.06	1.081	0.95
Refractive index	DIN 53491	-	1.482	1.482	1.482	1.478	-	1.4872	-
Thermal conductivity	DIN EN 12939	W/mK	0.20	0.20	0.20	0.14	0.20	0.152	0.246
Thermal expansion coefficient	-	1/K x 10^{-4}	2.20	2.20	2.20	4.14	2.20	-	-
Thermal expansion coefficient	ISO 11359	1/K x 10^{-4}	-	-	-	-	-	1.60	-
Thermal expansion coefficient	D696	10-5 cm/cm °C	-	-	-	-	-	-	10-15
Specific heat	DIN 52616	J/gK	1.85	1.85	1.85	-	1.85	-	-
Specific heat	ISO 11357	J/gK	-	-	-	-	-	0.351	-
Thermal resistance	DIN EN 12664	m² x K/W	-	-	-	-	-	0.0056	-
Tear resistance	ISO 527	N/mm²	-	-	-	-	-	≥ 32	-
Surface resitivity	DIN 53482	Ω x 10^{11}	2.00	2.00	2.00	2.00	2.00	-	-
Tensile strength	ISO 527/D638	N/mm²	> 23	> 23	> 23	> 14	> 20	-	34.50
Tensile elongation	ISO 527/D638	%	> 280	> 280	> 280	> 300	> 250	≥ 180	400
Young's modulus	D5026	MPa	-	-	-	-	-	-	300
Flex modulus 23 °C	D790	MPa	-	-	-	-	-	-	345
Heat deflection temperature at 0.46 Mpa	D648	°C	-	-	-	-	-	-	43
Melting point	(DSC)	°C	-	-	-	-	-	-	94

Additional technical data of Trosifol® ES/BG and SentryGlas® 5000 by KURARAY™

PRODUCT DATA

KRYSTALFLEX® PE399
Thermoplastic Polyurethane Film

INTRODUCTION

KRYSTALFLEX® PE399 is a high performance aliphatic polyether film intended for processing by lamination with a range of glass and plastic components.

KRYSTALFLEX® PE399 is part of the HUNTSMAN film and sheet product range for glass, polycarbonate, acrylic, CAB lamination applications. It is used in aerospace, transportation, security, and architectural markets.

PERFORMANCE FEATURES

- Excellent laminated transparency
- Excellent hydrolysis & microbial resistance
- Good low temperature flexibility
- Enhanced UV stability
- Medium durometer
- Contains adhesion promoter
- Medium modulus
- Excellent cold impact

APPLICATIONS

- Prison containment glazing
- Ballistic / Blast / Intrusion
- Vehicle armoring
- Retail kiosks
- Hurricane / Vandal glazing
- Zoos
- Liquid crystal laminates
- Computer screens

Table 1: Typical Physical Properties

Property	Key	DIN	Unit	Value	ASTM	Unit	Value
Hardness	M	53505	Shore A	80	D-2240	Shore A	80
Tensile Strength	E	53504	MPa	45	D-412	psi	6500
Elongation @ break	E	53504	%	500	D-412	%	500
100% Modulus	E	53504	MPa	2	D-412	psi	300
300% Modulus	E	53504	MPa	7	D-412	psi	1000
Tear Resistance	E	53515	N/mm	37	D-624	pli	210
Specific Gravity	E	53478		1.07	D-792		1.07
Softening Range Low	E	Huntsman TMA	°C	80	Huntsman TMA	°F	175
Softening Range High	E	Huntsman TMA	°C	140	Huntsman TMA	°F	285
Midpoint Tg by DSC	E	Huntsman DSC	°C	-36	D-3418	°F	-33

E = 0.050" extruded film cut to ASTM requirements
M = Injection moulded parts to meet DIN & ASTM requirements
ASTM measurements were tested at 20 in/min.
DIN measurements were tested at 500 mm/min.

HUNTSMAN
Enriching lives through innovation

Krystalflex® PE399 by HUNTSMAN™

Appendix B: Experimental stress-strain relations of small-scale static single-lap shear tests

Note: Experimental data from small-scale static single-lap shear tests in the climatic chamber of all tested interlayers are listed below. Shear stress and shear strain are stated as engineering values.
Example of the legend **TP-20M-04** means Krystalflex PE399 tested in 20 °C and loaded with TEMPOS cross-head vertical loading rate 0.5 mm/min. Last number 04 denotes the number of tested specimen. Key to the legend in presented charts is below.

0	= temperature 0 °C
20	= temperature 20 °C
40	= temperature 40 °C
60	= temperature 60 °C

S	= TEMPOS cross-head loading rate 2.0 mm/min
M	= TEMPOS cross-head loading rate 0.5 mm/min
L	= TEMPOS cross-head loading rate 0.125 mm/min

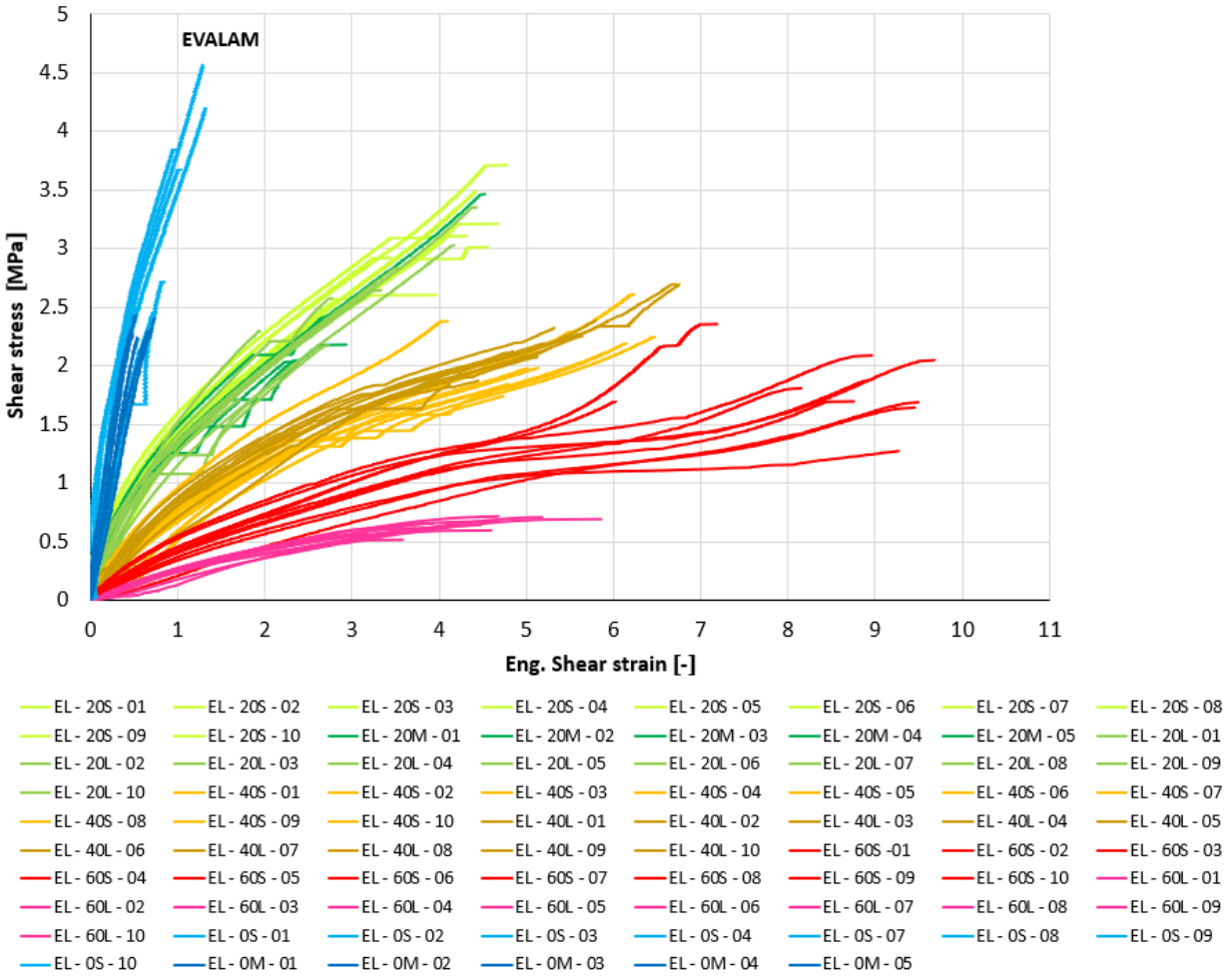

Evalam 80/120

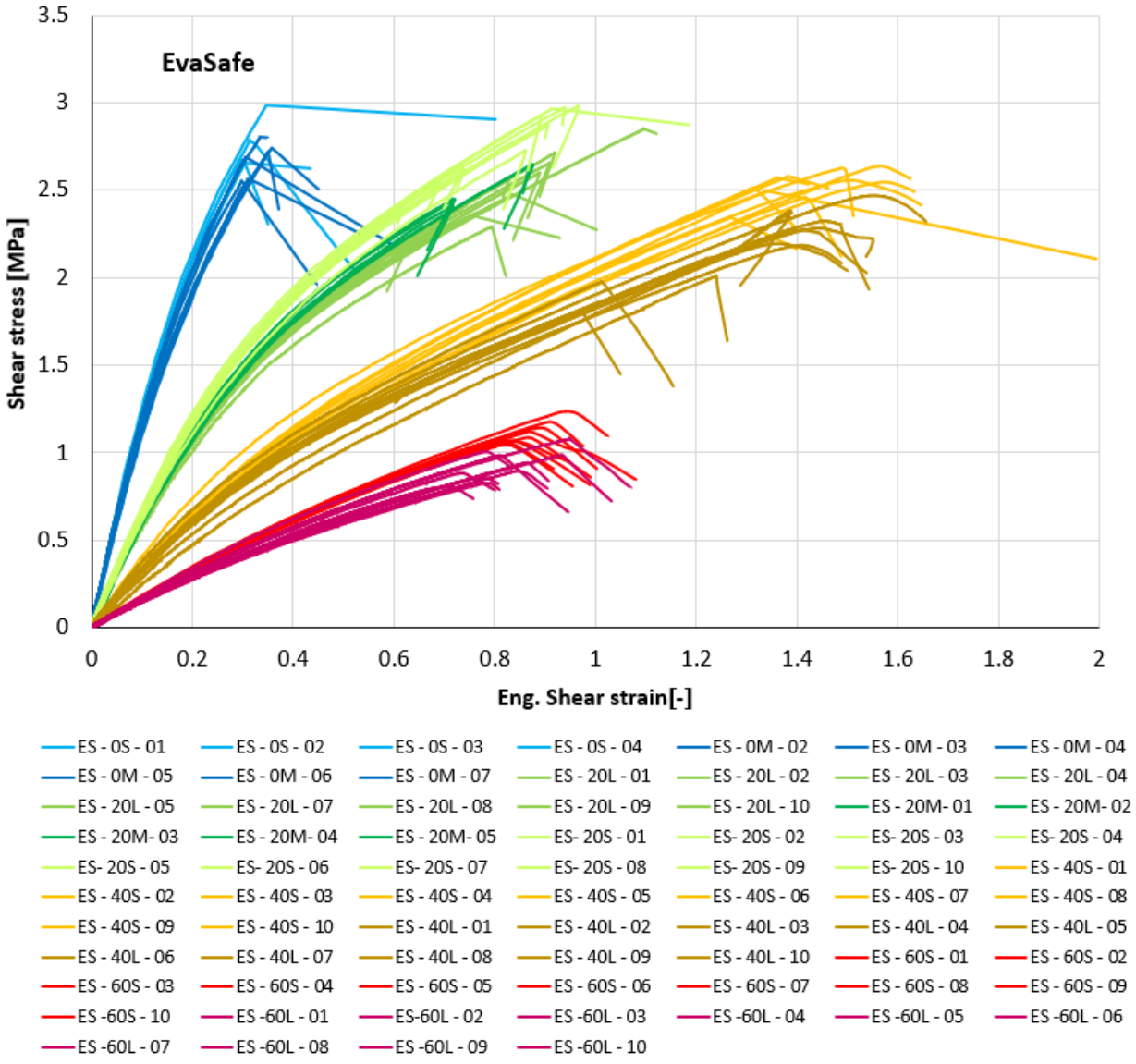
EvaSafe
Shear stress [MPa]
Eng. Shear strain[-]
0
0.5
1
1.5
2
2.5
3
3.5
0
0.2
0.4
0.6
0.8
1
1.2
1.4
1.6
1.8
2
ES - 0S - 01
ES - 0S - 02
ES - 0S - 03
ES - 0S - 04
ES - 0M - 02
ES - 0M - 03
ES - 0M - 04
ES - 0M - 05
ES - 0M - 06
ES - 0M - 07
ES - 20L - 01
ES - 20L - 02
ES - 20L - 03
ES - 20L - 04
ES - 20L - 05
ES - 20L - 07
ES - 20L - 08
ES - 20L - 09
ES - 20L - 10
ES - 20M- 01
ES - 20M- 02
ES - 20M- 03
ES - 20M- 04
ES - 20M- 05
ES- 20S - 01
ES- 20S - 02
ES- 20S - 03
ES- 20S - 04
ES- 20S - 05
ES- 20S - 06
ES- 20S - 07
ES- 20S - 08
ES- 20S - 09
ES- 20S - 10
ES - 40S - 01
ES - 40S - 02
ES - 40S - 03
ES - 40S - 04
ES - 40S - 05
ES - 40S - 06
ES - 40S - 07
ES - 40S - 08
ES - 40S - 09
ES - 40S - 10
ES - 40L - 01
ES - 40L - 02
ES - 40L - 03
ES - 40L - 04
ES - 40L - 05
ES - 40L - 06
ES - 40L - 07
ES - 40L - 08
ES - 40L - 09
ES - 40L - 10
ES - 60S - 01
ES - 60S - 02
ES - 60S - 03
ES - 60S - 04
ES - 60S - 05
ES - 60S - 06
ES - 60S - 07
ES - 60S - 08
ES - 60S - 09
ES -60S - 10
ES -60L - 01
ES-60L - 02
ES -60L - 03
ES -60L - 04
ES -60L - 05
ES -60L - 06
ES -60L - 07
ES -60L - 08
ES -60L - 09
ES -60L - 10

Evasafe

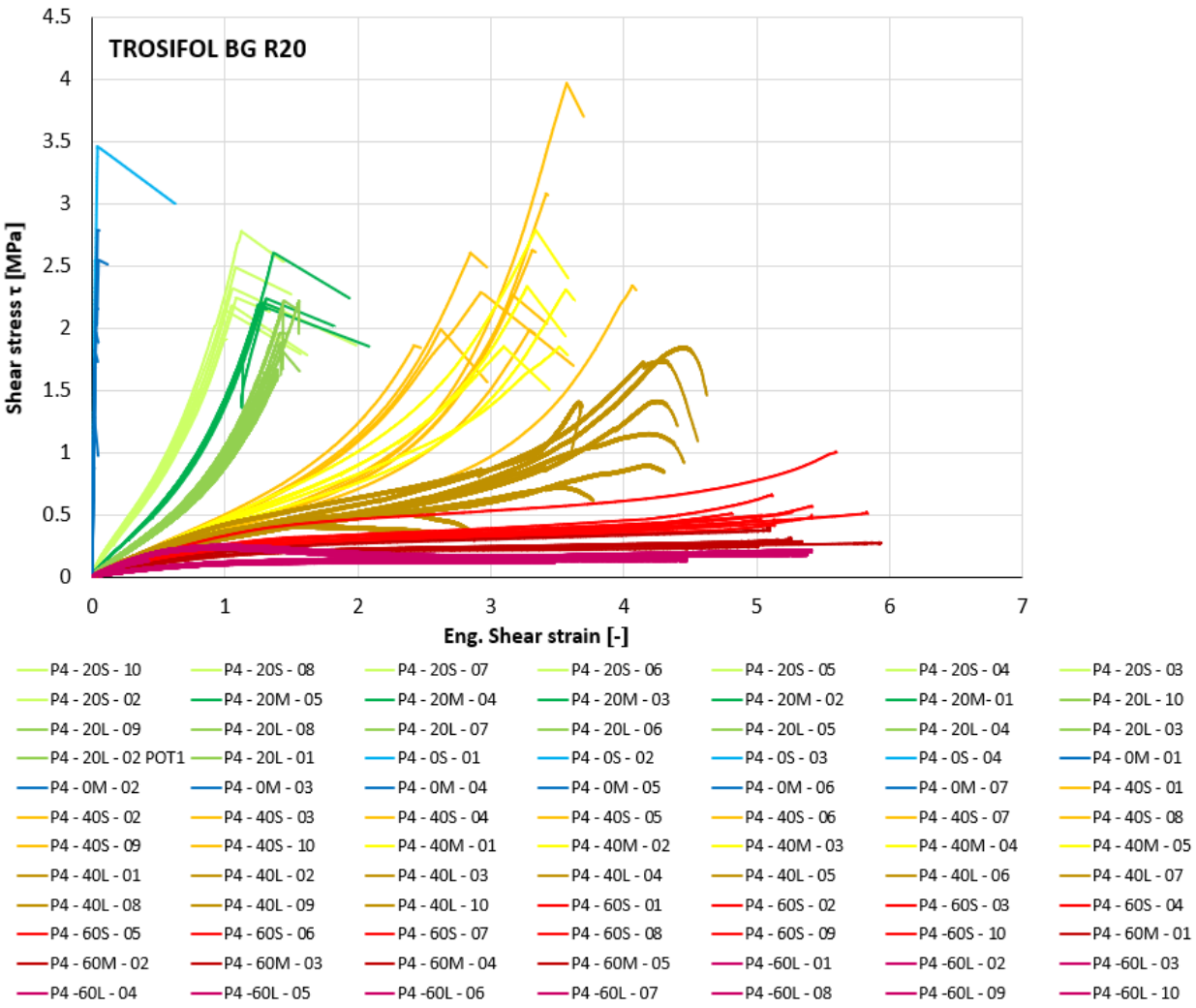

Trosifol BG R20

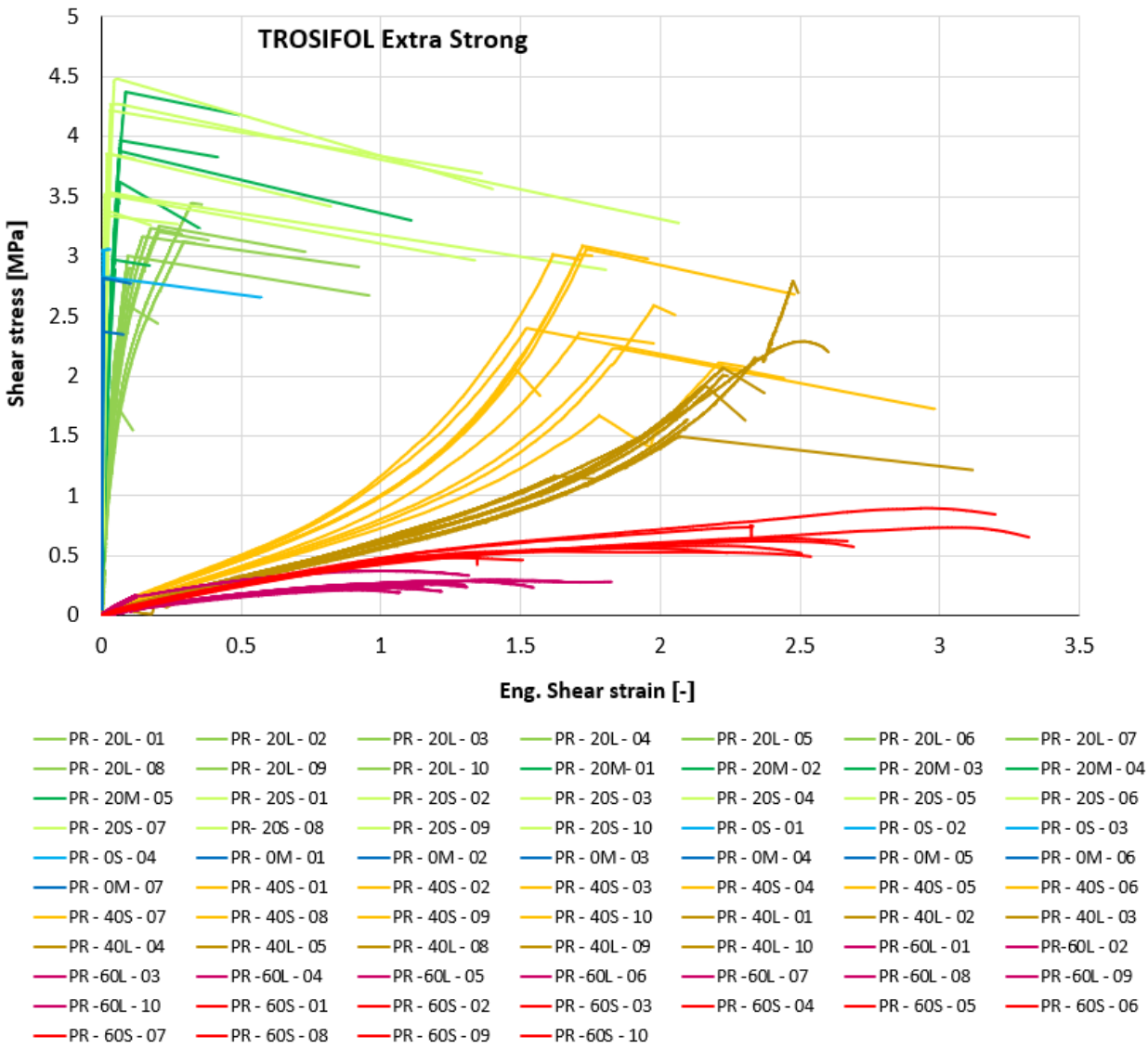

Trosifol Extra Strong

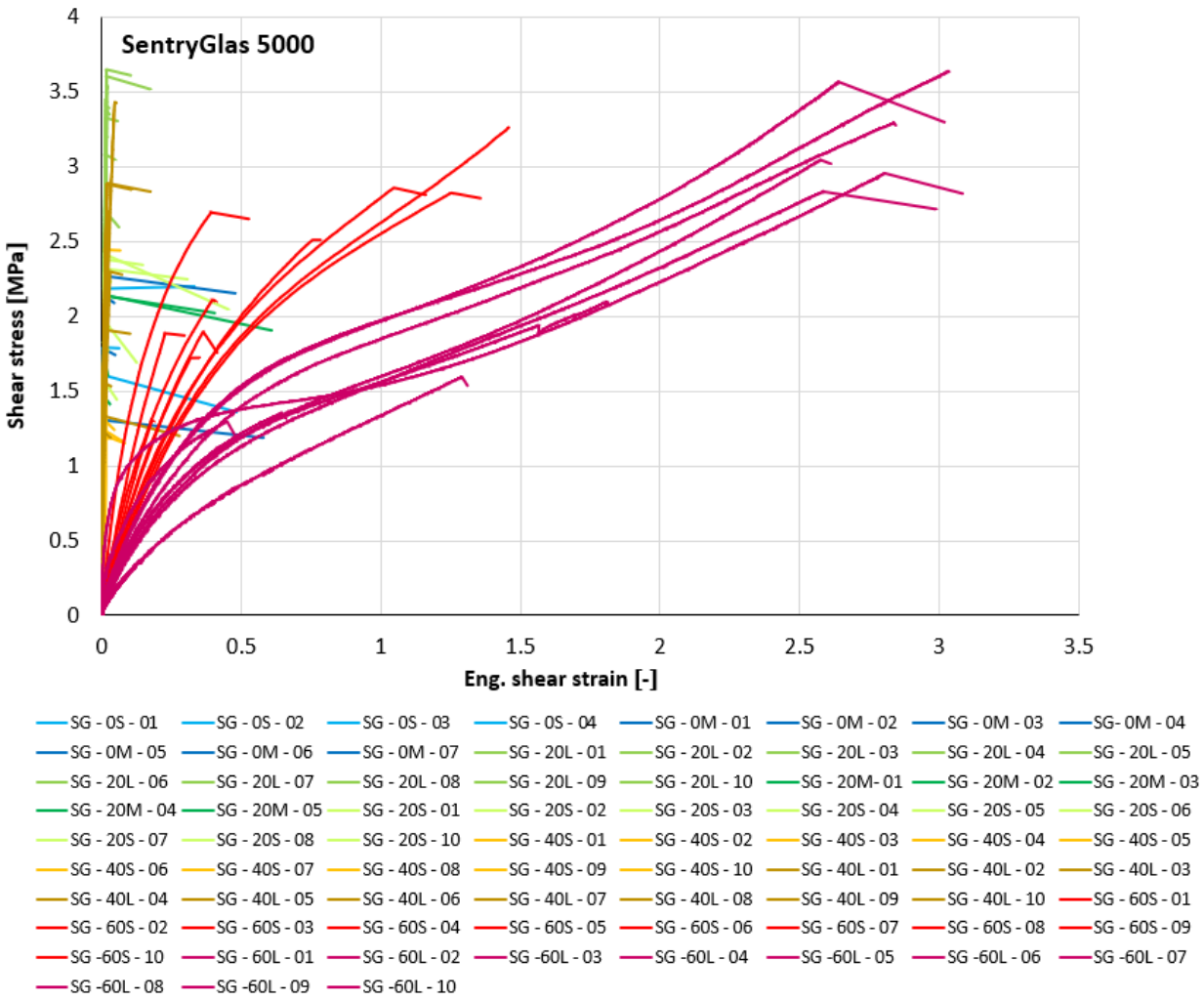

SentryGlas 5000

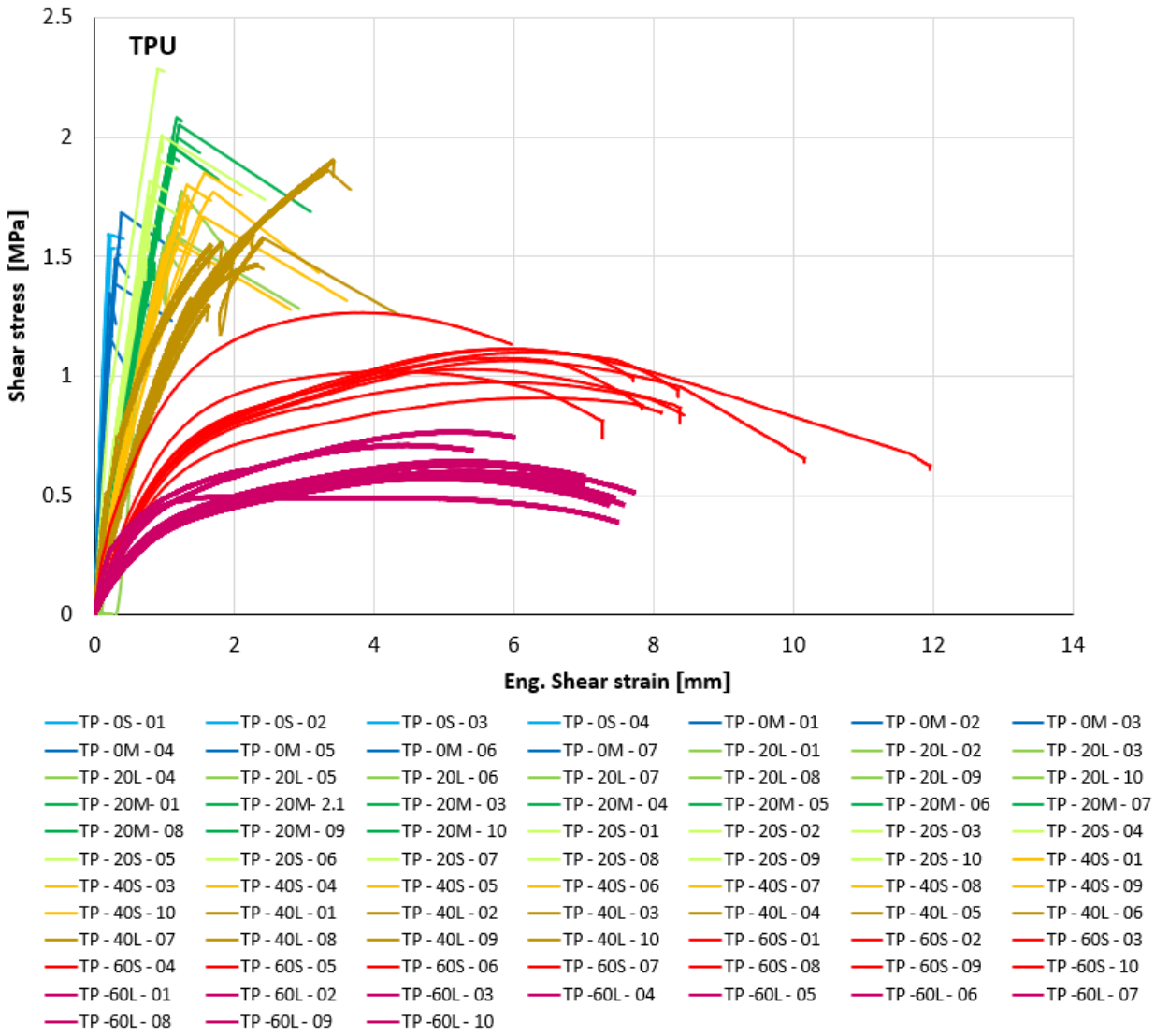

Krystalflex PE399

Appendix C: Experimental relations measured at small-scale dynamic DMTA single-lap shear tests

Note: Experimental data of DMTA in shear performed on small-scale single-lap specimens in the climatic chamber are listed below. Particularly, shear storage modulus G' and shear loss modulus G'' of all tested interlayers against frequency f are plotted. Relations show the dominancy of storage modulus G' over loss modulus G'' measured at experiments.

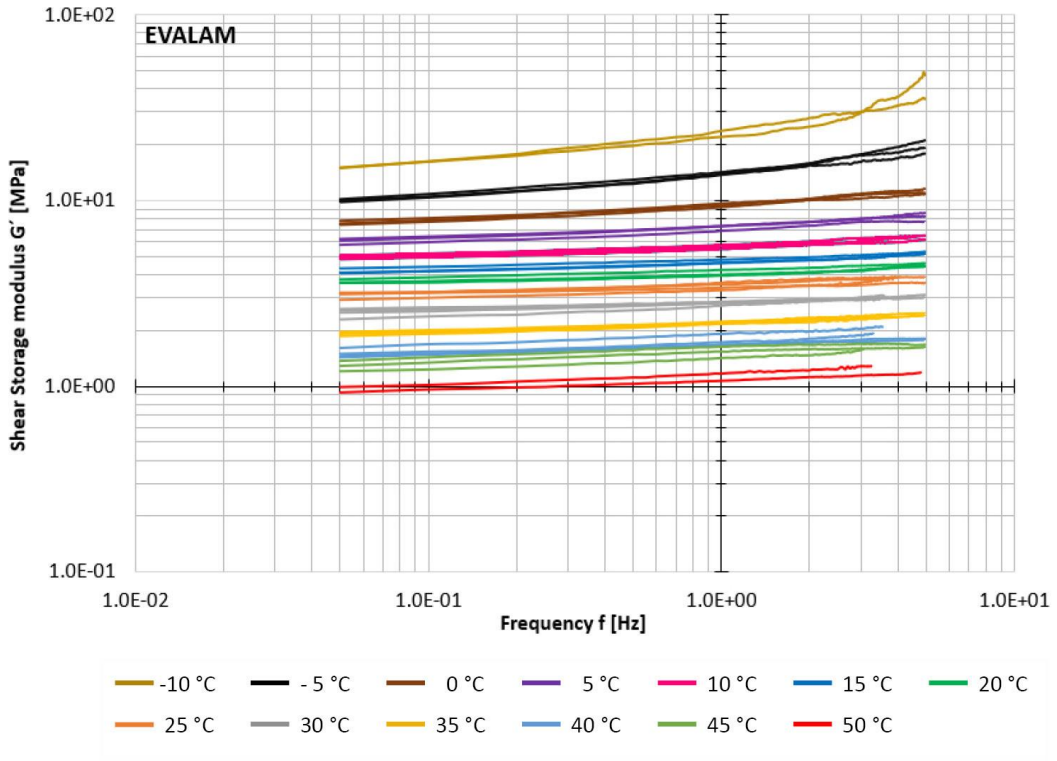

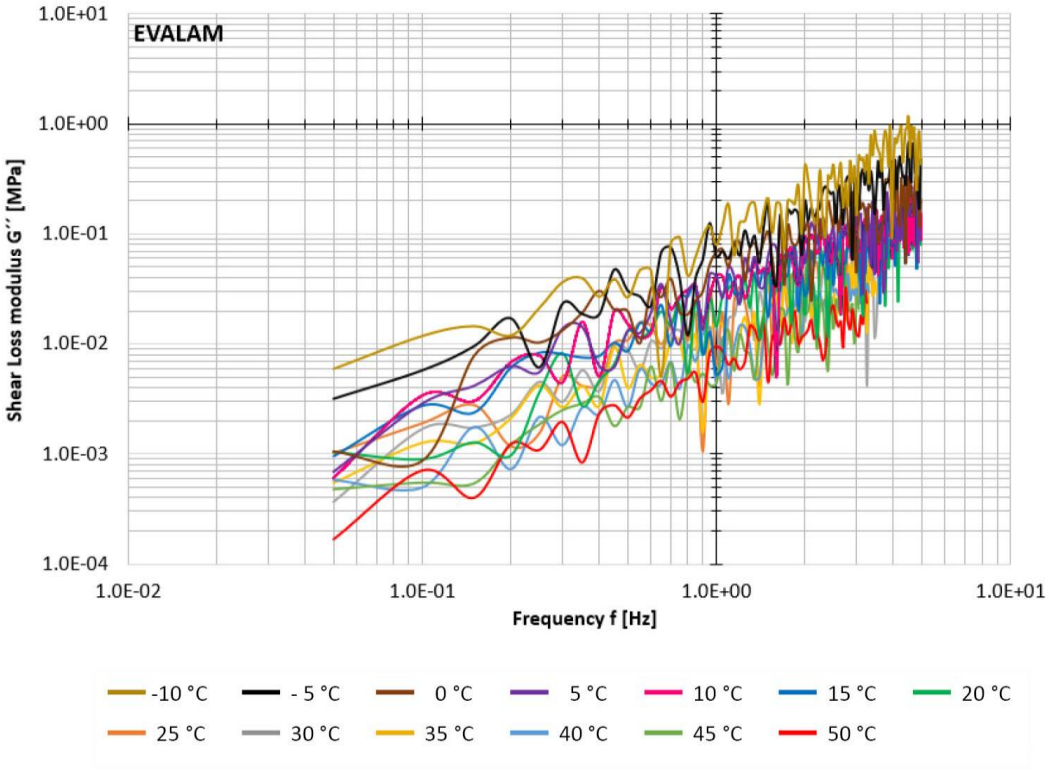

Evalam 80/120

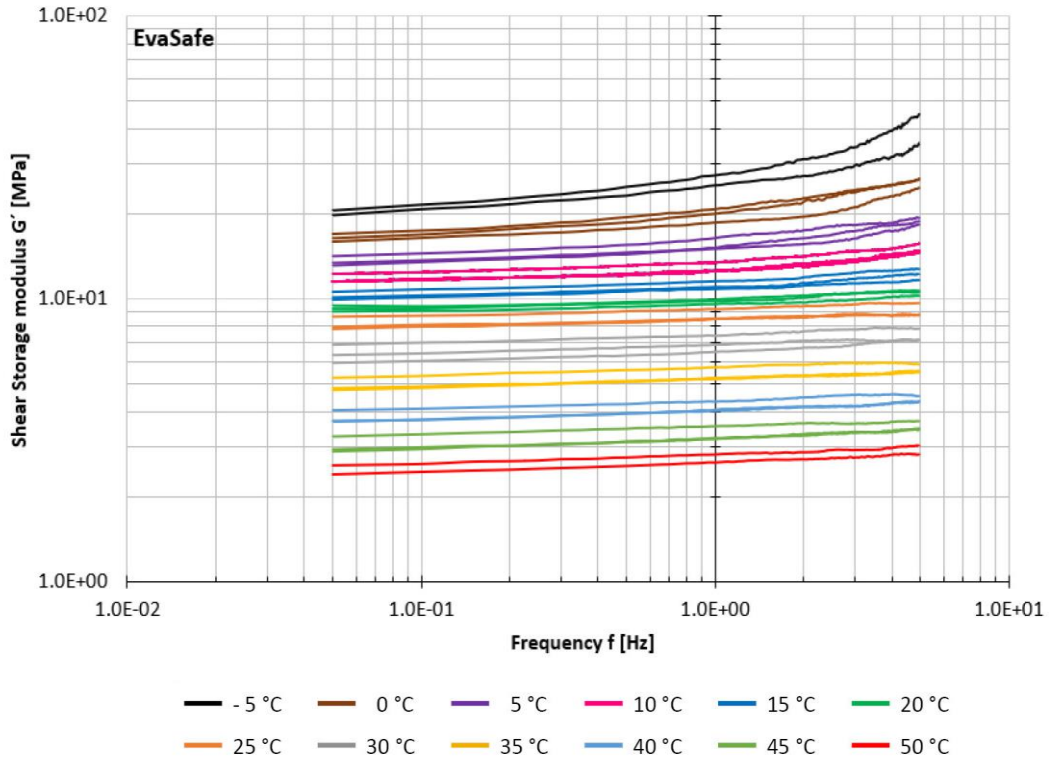

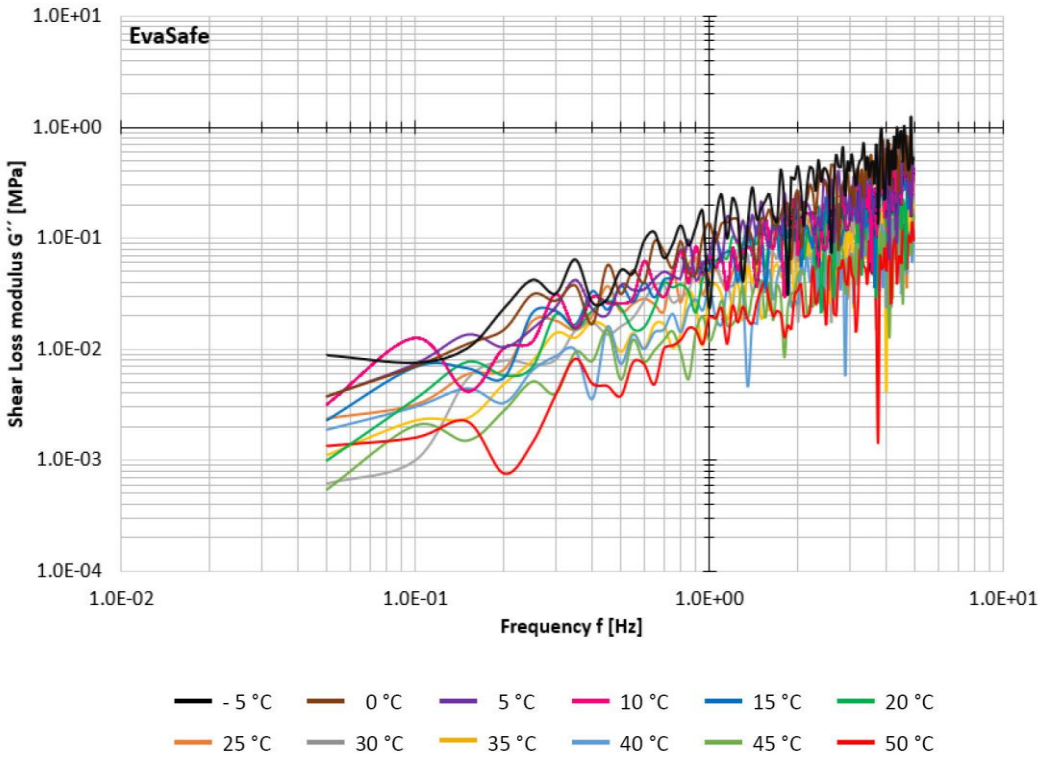
EvaSafe
Shear Loss modulus G'' [MPa]
1.0E+01
1.0E+00
1.0E-01
1.0E-02
1.0E-03
1.0E-04
1.0E-02
1.0E-01
1.0E+00
1.0E+01
Frequency f [Hz]
- 5 °C
0 °C
5 °C
10 °C
15 °C
20 °C
25 °C
30 °C
35 °C
40 °C
45 °C
50 °C

Evasafe

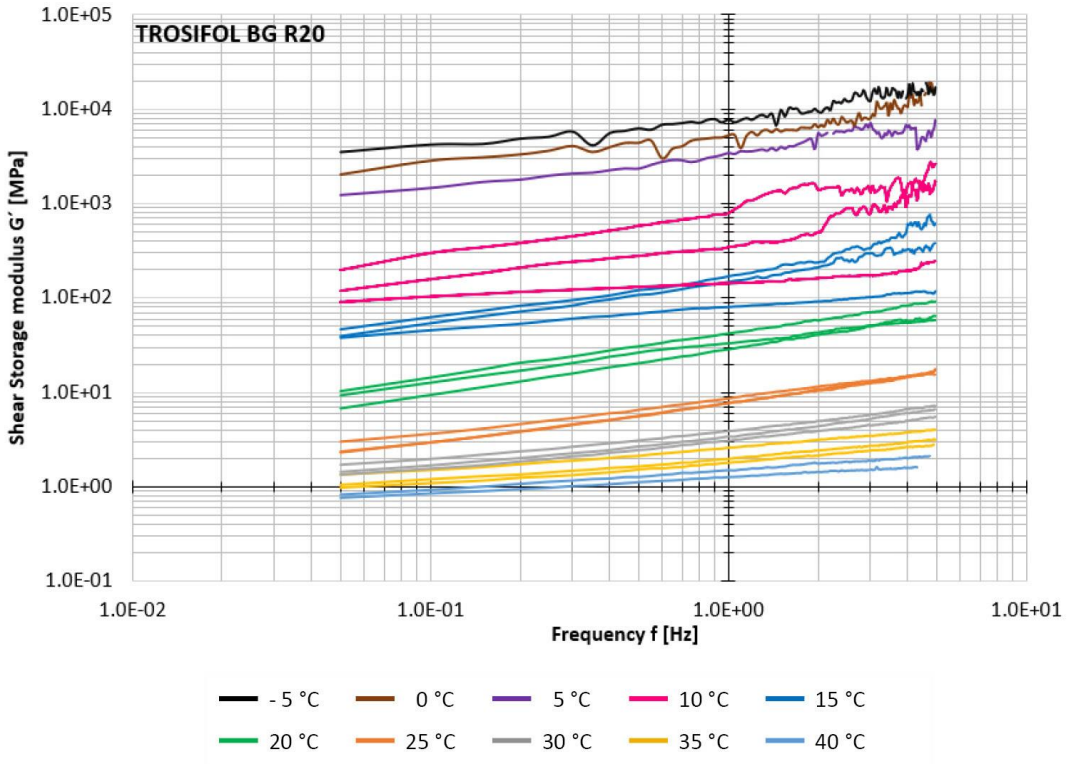
TROSIFOL BG R20
Shear Storage modulus G' [MPa]
1.0E+05
1.0E+04
1.0E+03
1.0E+02
1.0E+01
1.0E+00
1.0E-01
1.0E-02
1.0E-01
1.0E+00
1.0E+01
Frequency f [Hz]
- 5 °C
0 °C
5 °C
10 °C
15 °C
20 °C
25 °C
30 °C
35 °C
40 °C

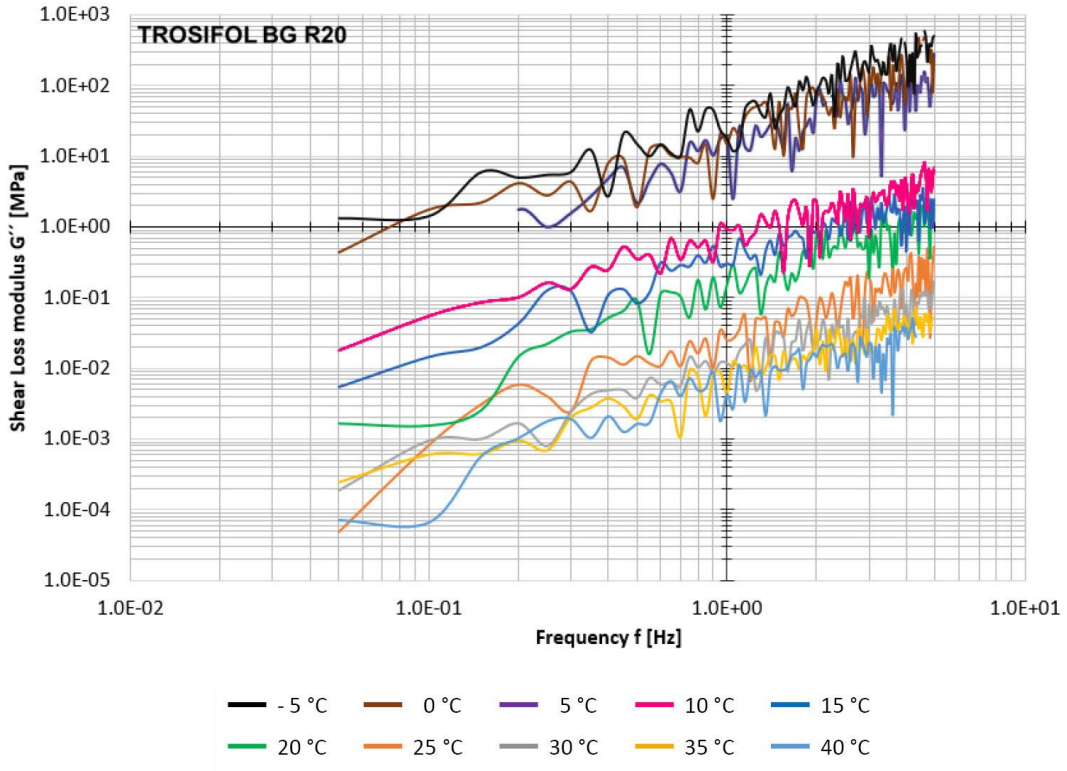

Trosifol BG R20

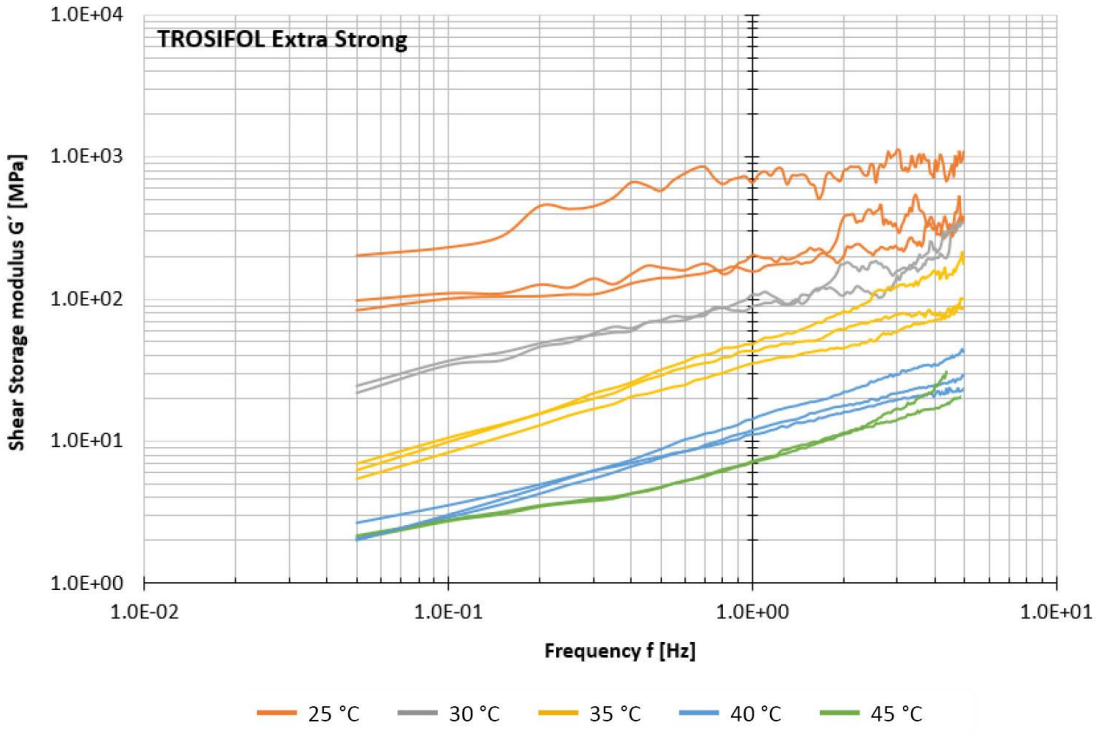

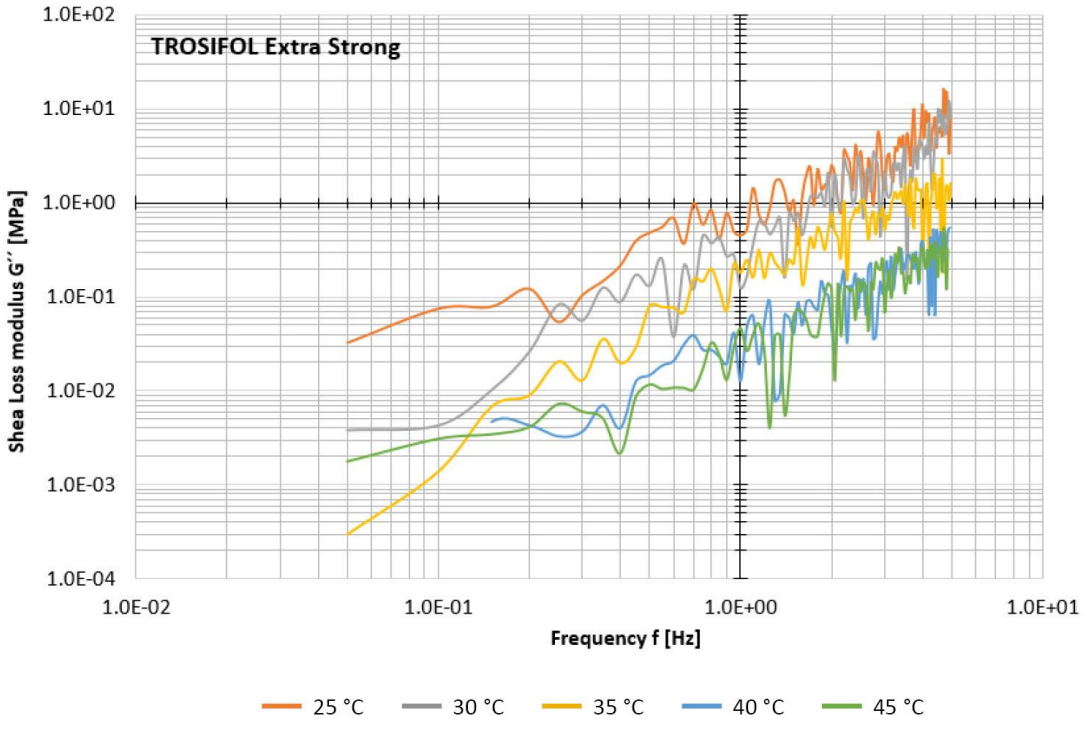

Trosifol Extra Strong

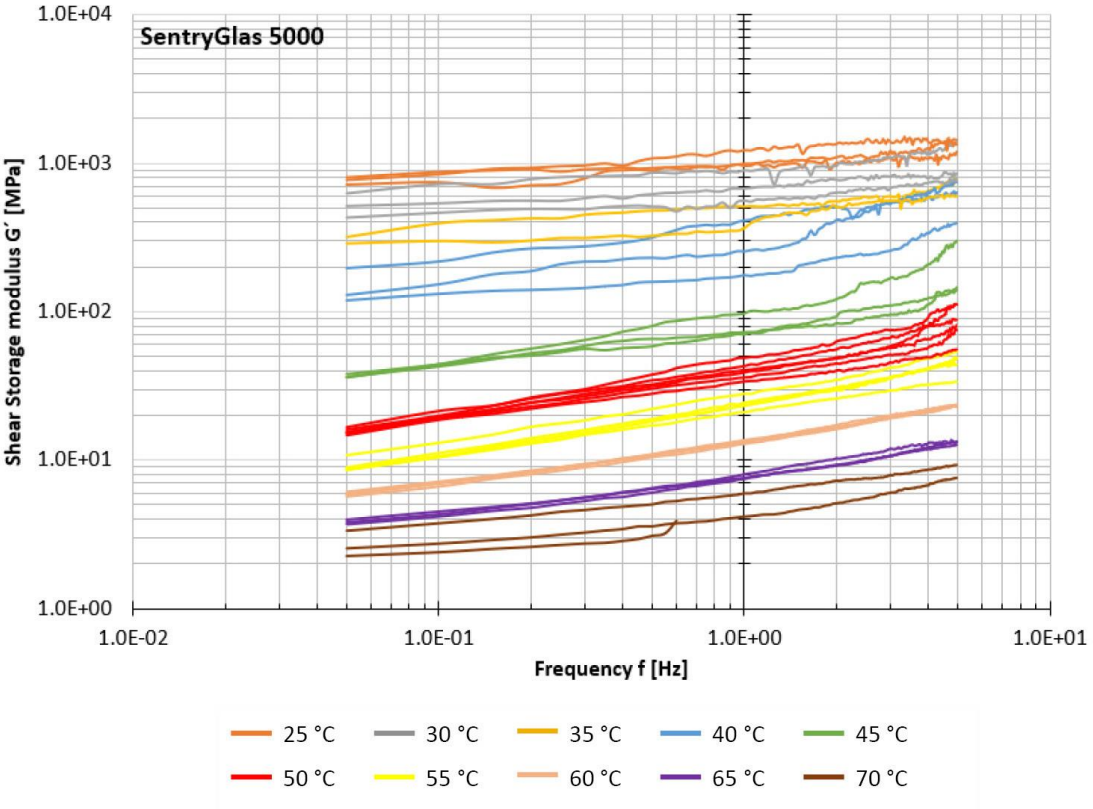

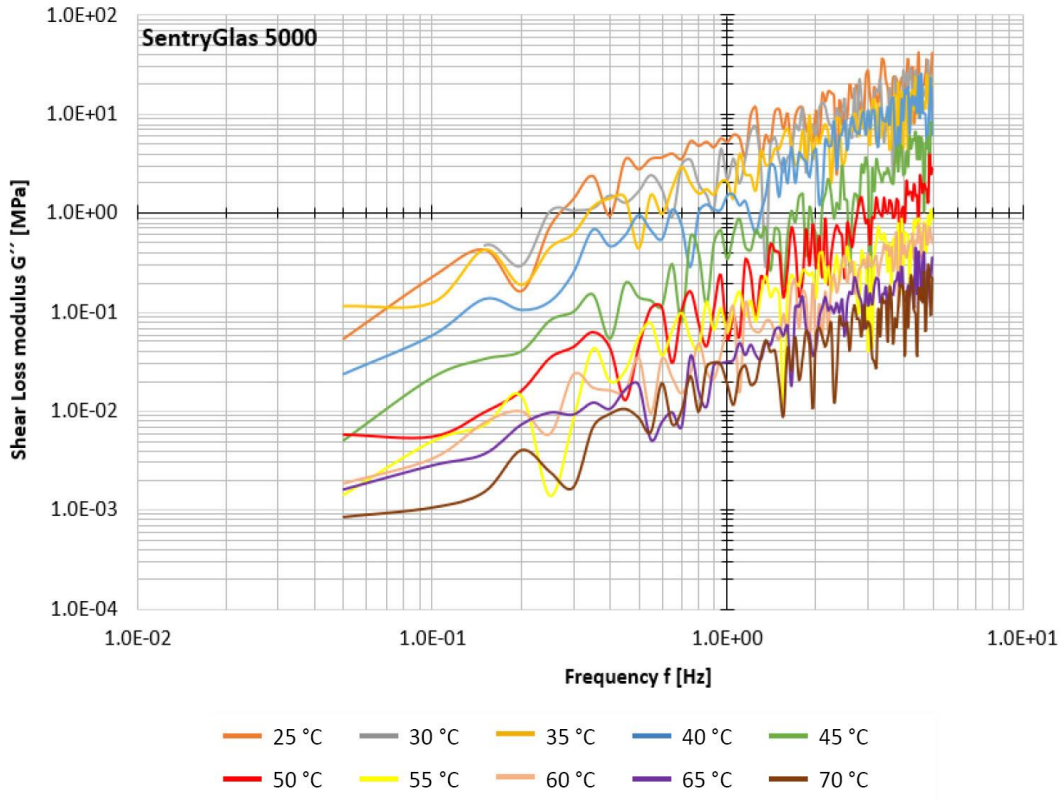

SentryGlas 5000

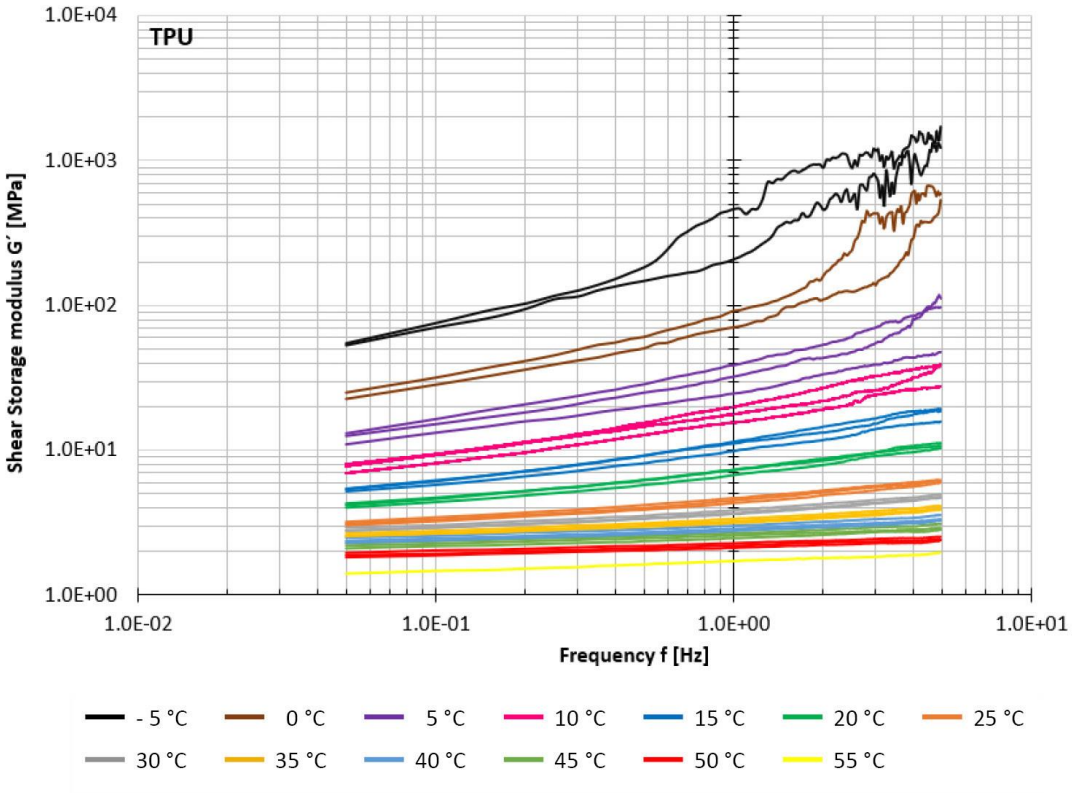

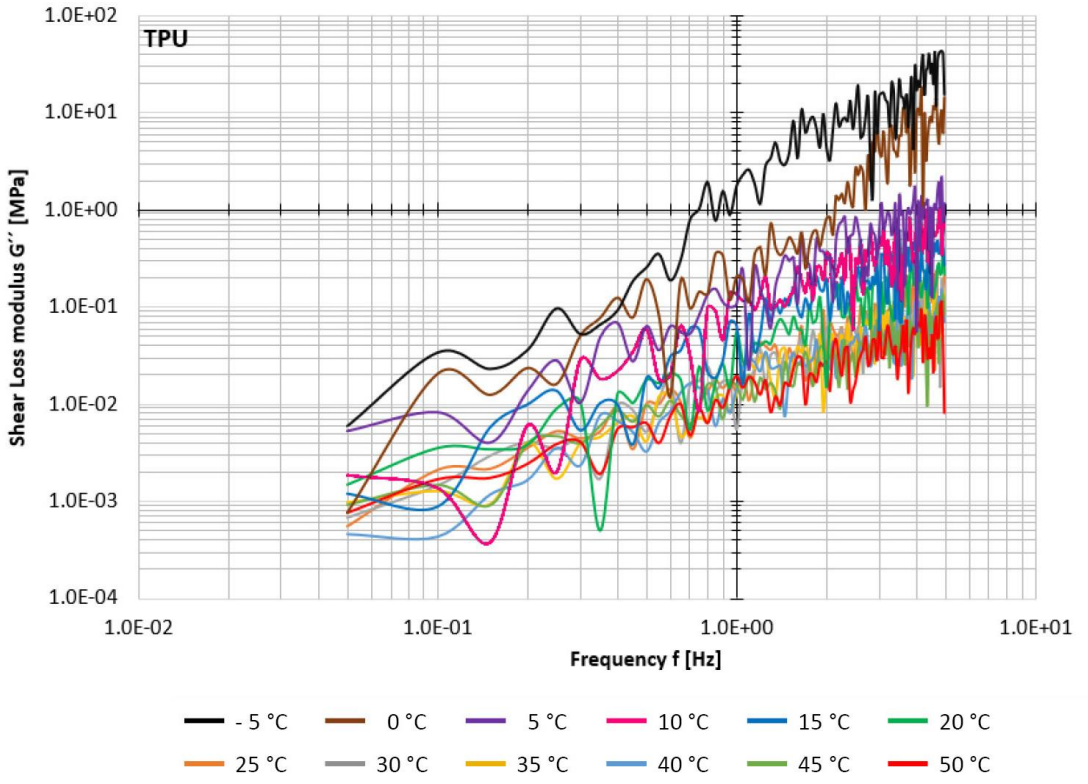

Krystalflex PE399

Appendix D: Four-point bending destructive tests of large-scale specimens at one loading rate

Note: Experimental data measured at bending destructive tests are plotted below. Temperature range of glass during the tests was +19 °C to +23 °C. Tests were controlled with constant MTS vertical cross-head loading rate 1.8 mm/min. Results are plotted for 1st loading phase (loading until breakage of lower glass ply).

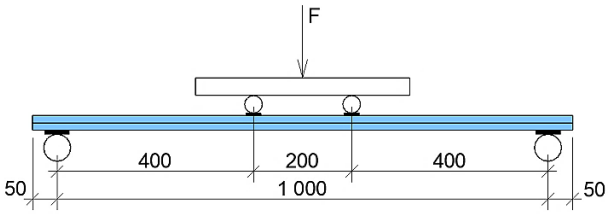

Static schema of the test

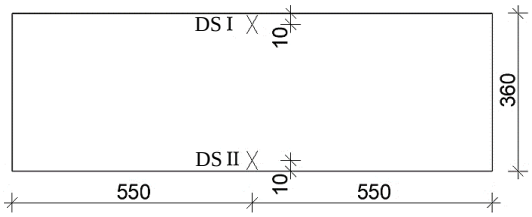

Position of displacement sensors on the specimen

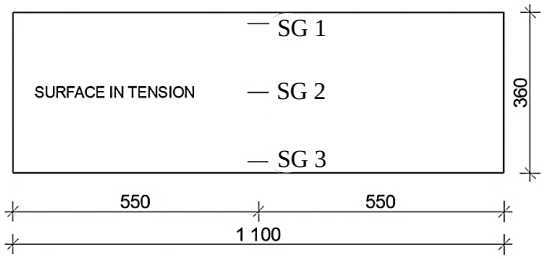

Strain gauges: Lower glass ply, lower surface

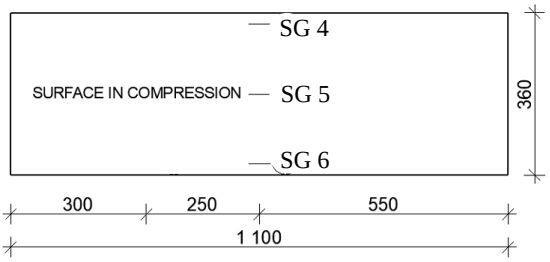

Strain gauges: Upper glass ply, upper surface

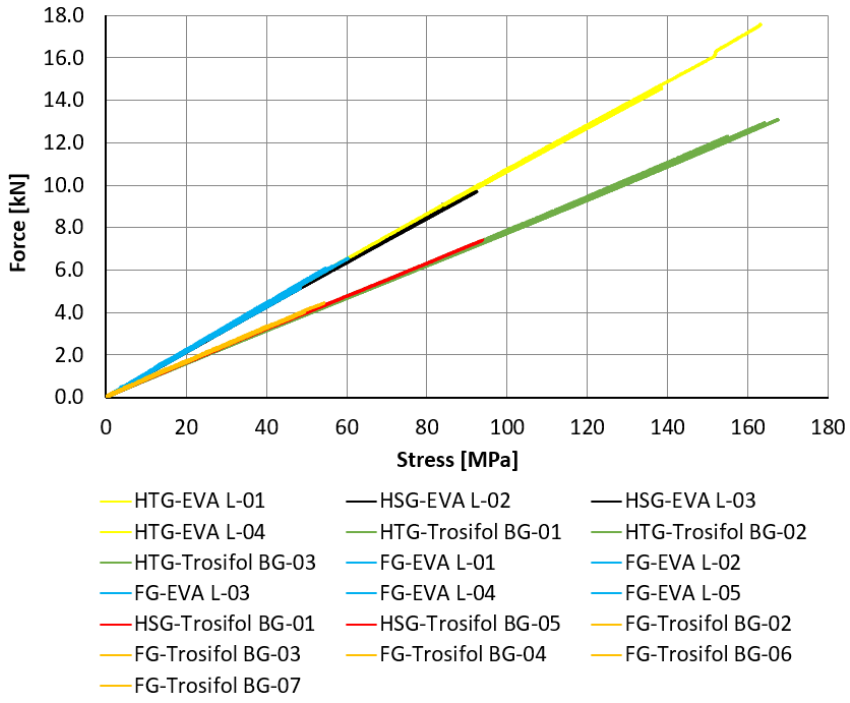

Normal stress in glass by SG 1

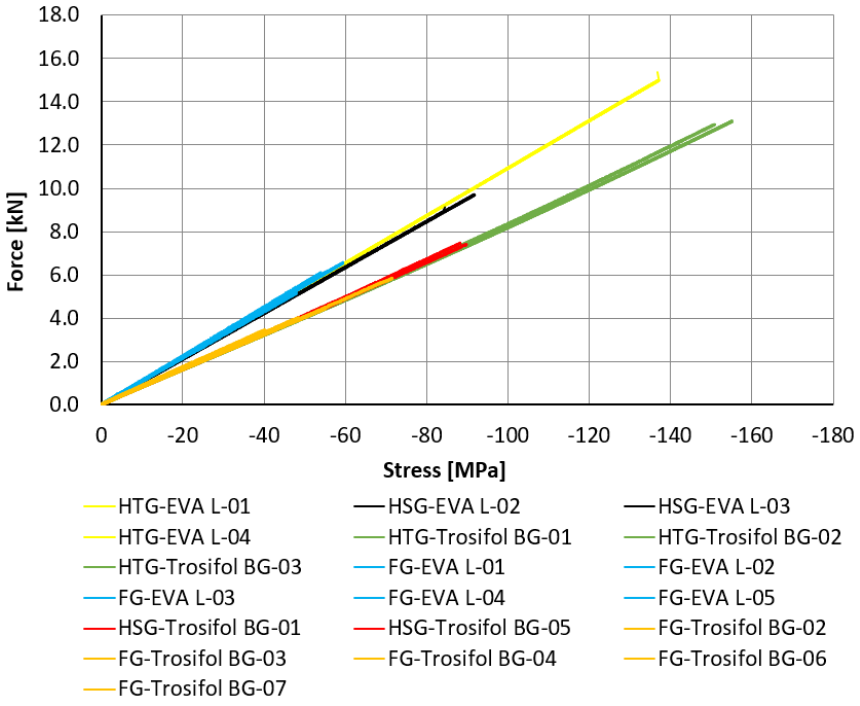

Normal stress in glass by SG 4

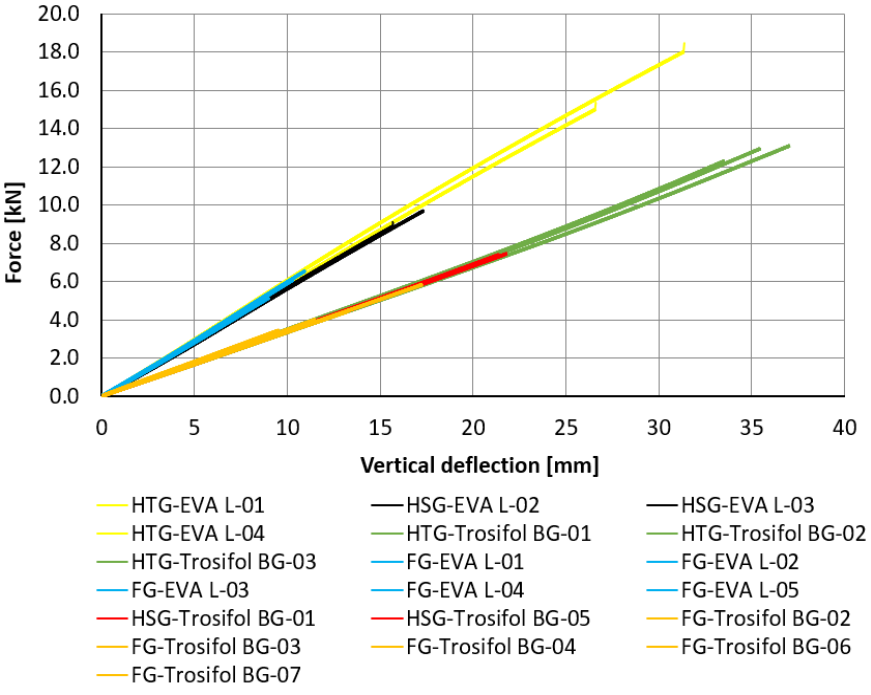

Vertical deflection (average by DS I and DS II)

Appendix E: Four-point bending destructive tests of large-scale specimens at various loading rates

Note: Experimental data measured at bending destructive tests are plotted below. Measured temperature range of glass during the tests was from +19 °C to +24 °C. Tests were controlled by MTS cross-head vertical loading rates 2.0 mm/min, 0.5 mm/min, and 0.125 mm/min. Prescribed loading rate was kept constant during the test. Results are plotted for 1st loading phase (loading until breakage of lower glass ply).

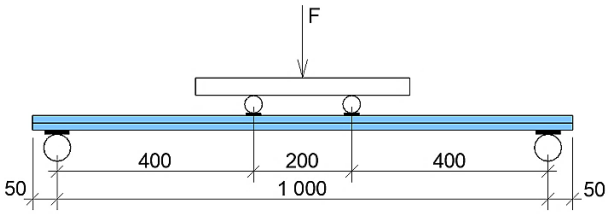

Static schema of the test

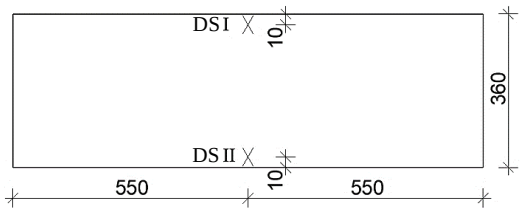

Position of displacement sensors on the specimen

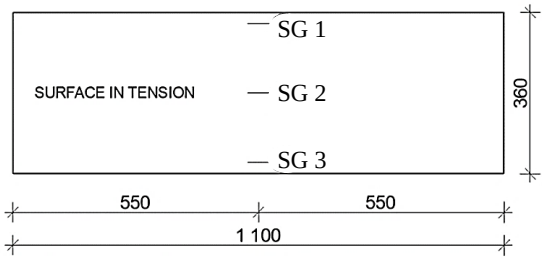

Strain gauges: Lower glass ply, lower surface

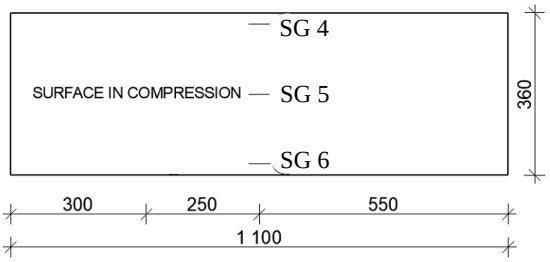

Strain gauges: Upper glass ply, upper surface

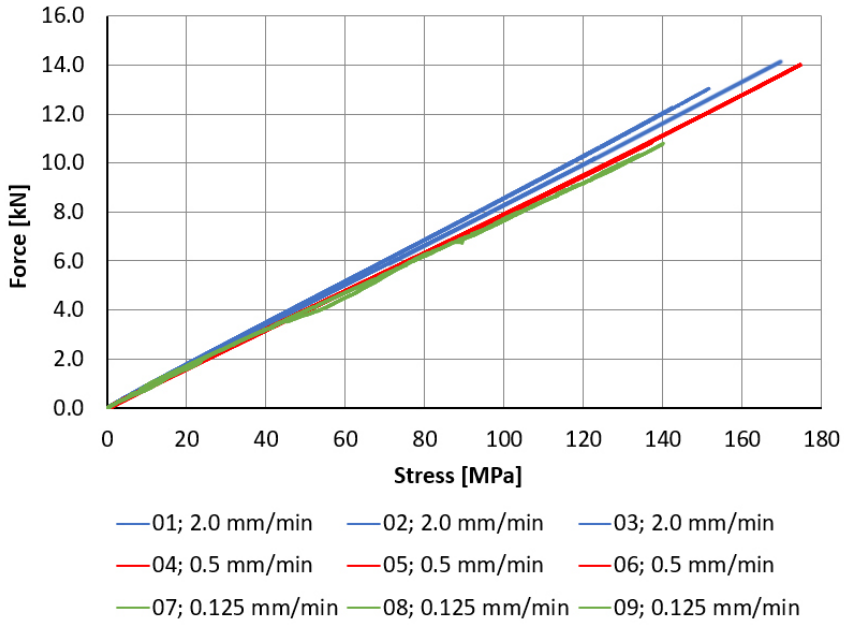

Trosifol BG R20: Normal stress in glass by SG 3

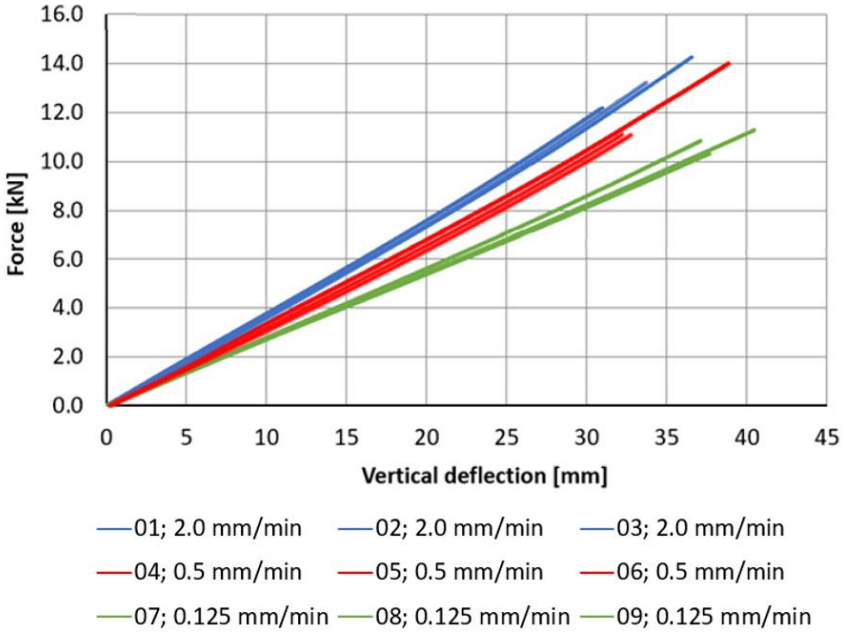

Trosifol BG R20: Vertical deflection (average by DS I and DS II)

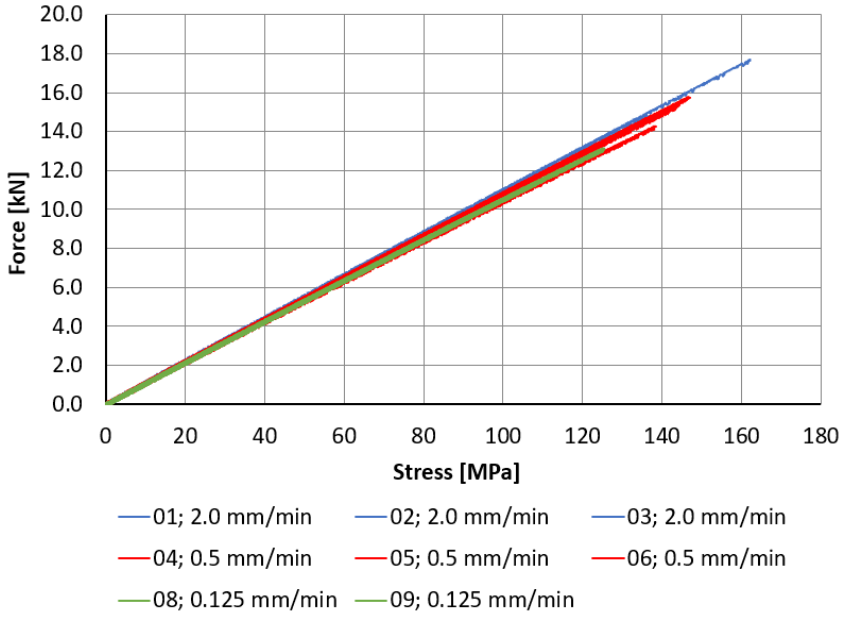

Evalam 80/120: Normal stress in glass by SG 3

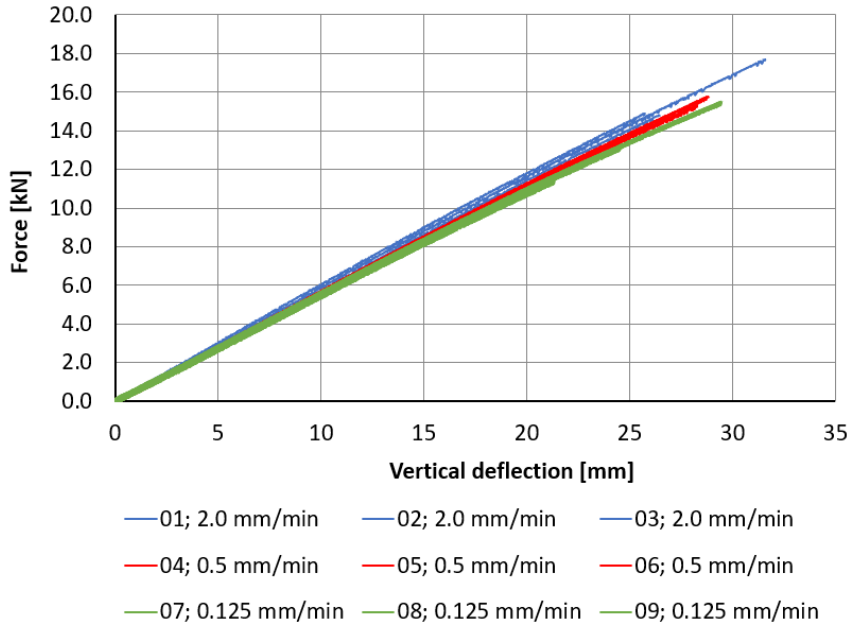

Evalam 80/120: Vertical deflection (average by DS I and DS II)

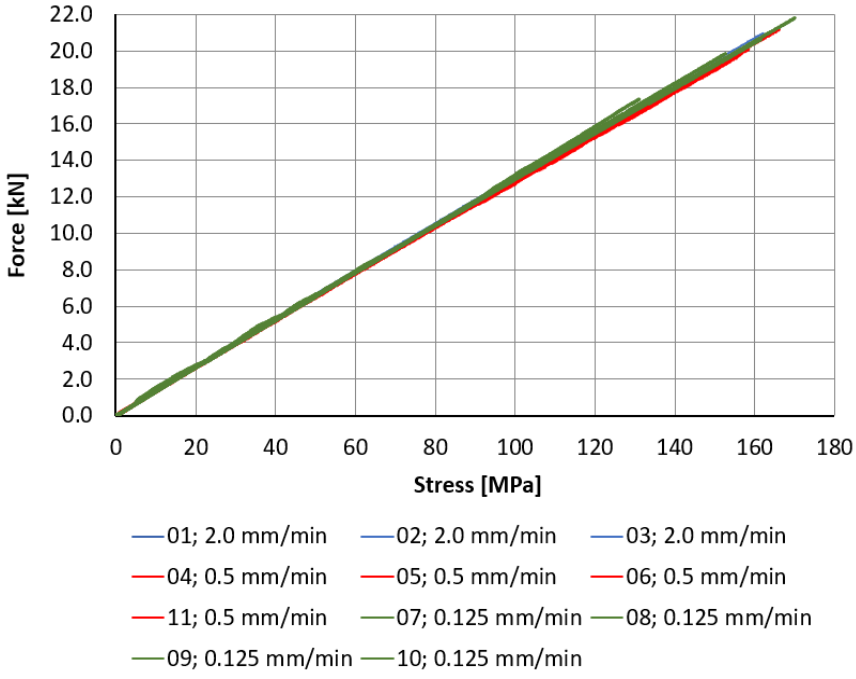

SentryGlas 5000: Normal stress in glass by SG 3

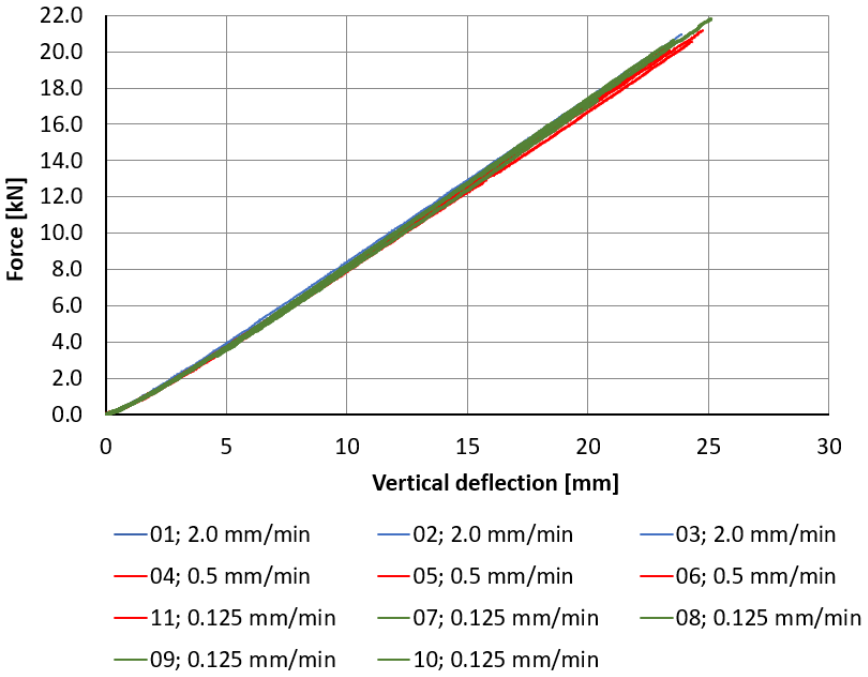

SentryGlas 5000: Vertical deflection (average by DS I and DS II)

Appendix F: Four-point bending creep tests in the climatic chamber

Note: Experimental data measured at bending creep tests in the climatic chamber are plotted below. Value of applied load *F* was 1.12 kN. Load was kept constant during the test until unloading. Temperature in the climatic chamber was kept constant during the entire test.

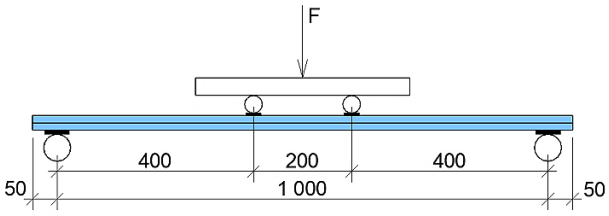

Static schema of the test

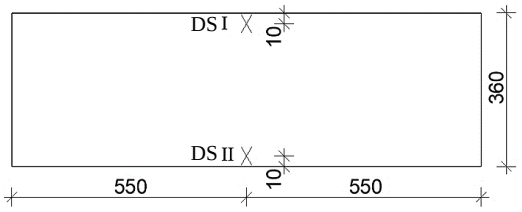

Position of displacement sensors on the specimen

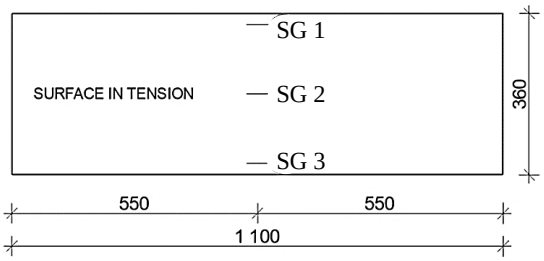

Strain gauges: Lower glass ply, lower surface

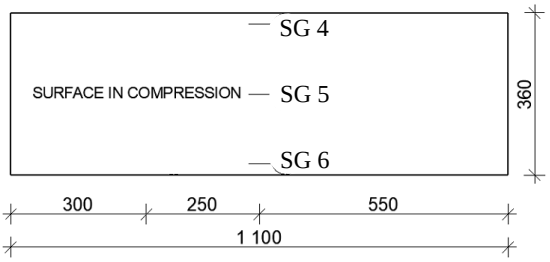

Strain gauges: Upper glass ply, upper surface

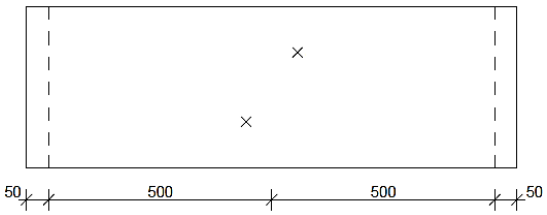

Position of Pt 100 sensors glued on the glass

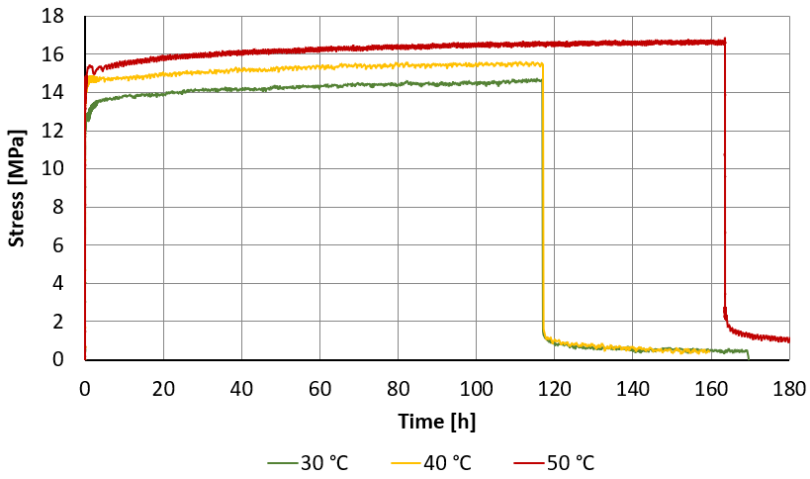

Trosifol BG R20: Normal stress in glass by SG 2

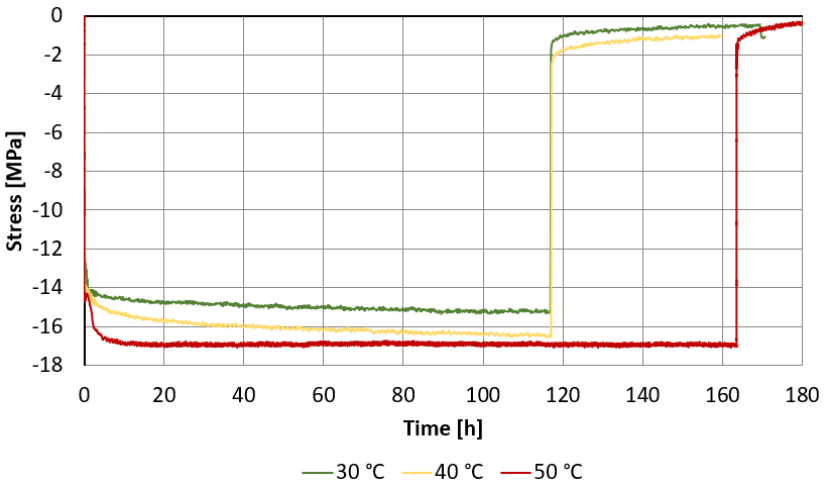

Trosifol BG R20: Normal stress in glass by SG 5

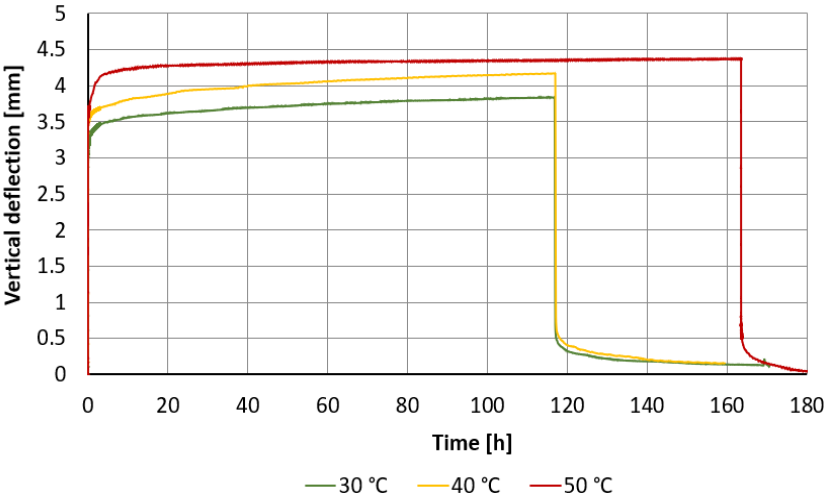

Trosifol BG R20: Vertical deflection measured by DS I

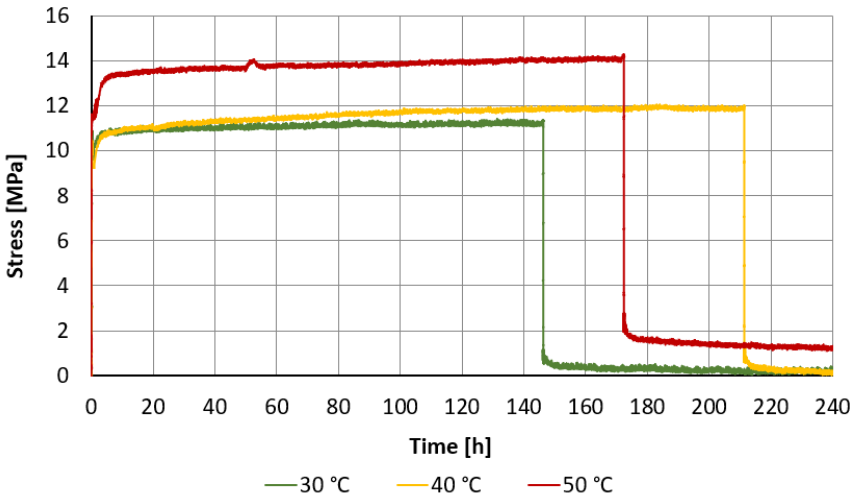

Evalam 80/120: Normal stress in glass by SG 2

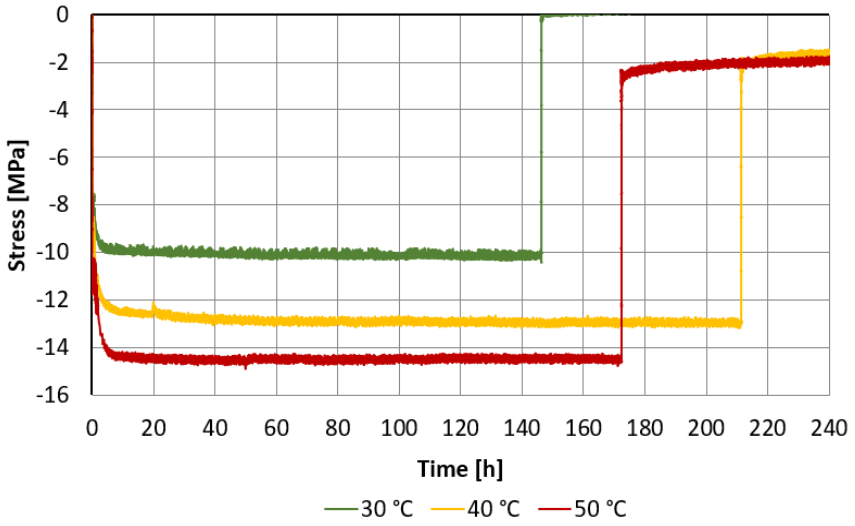

Evalam 80/120: Normal stress in glass by SG 5

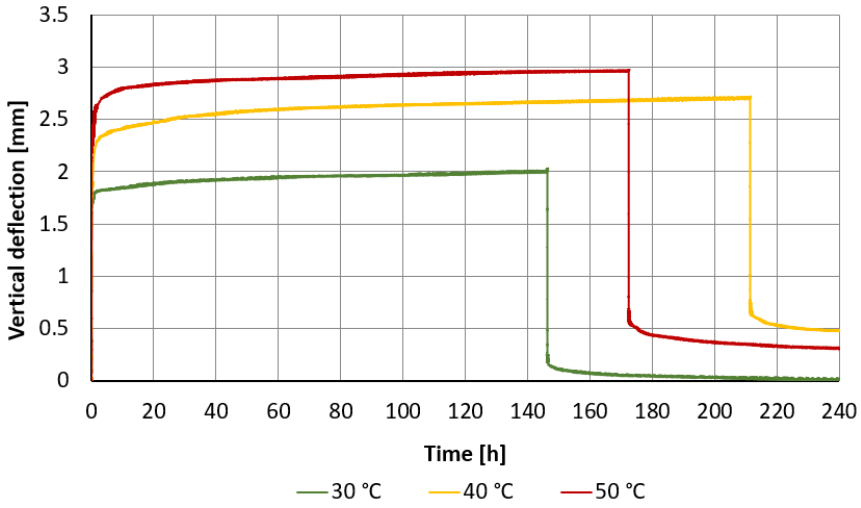

Evalam 80/120: Vertical deflection measured by DS I

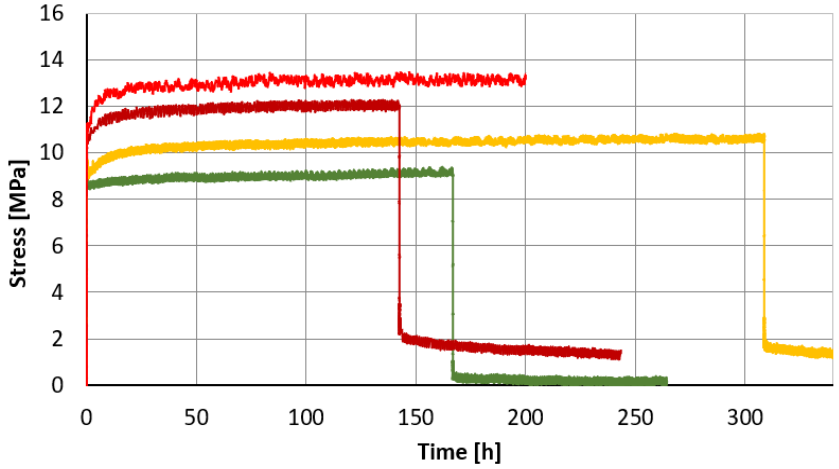

SentryGlas 5000: Normal stress in glass by SG 2

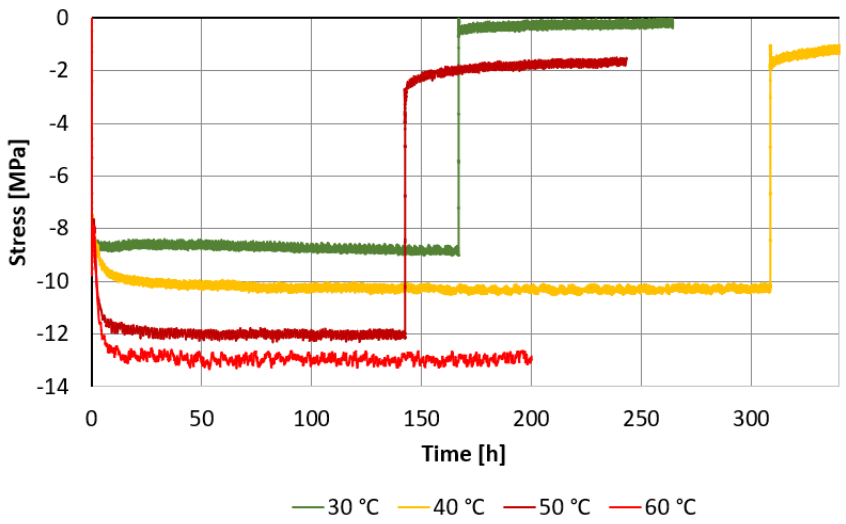

SentryGlas 5000: Normal stress in glass by SG 5

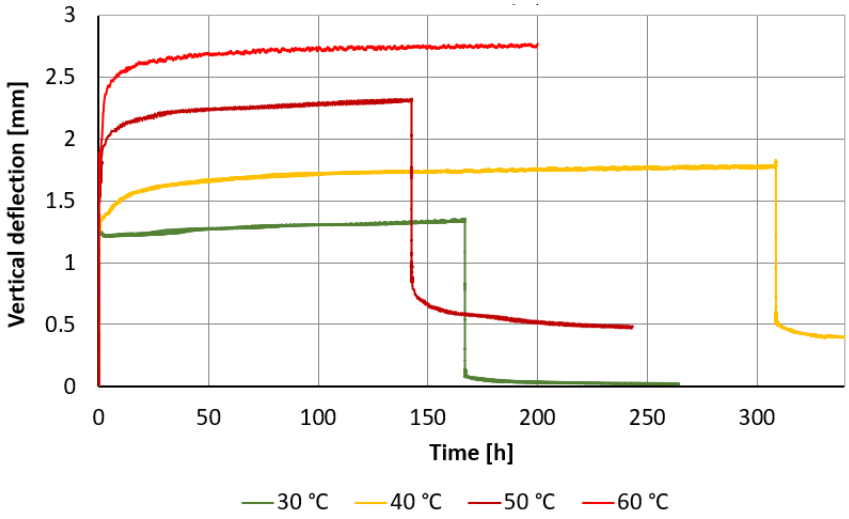

SentryGlas 5000: Vertical deflection measured by DS I

Appendix G: ANSYS codes for LVE analysis of large-scale four-point bending tests

- **Destructive bending tests at various loading rates**

Note: ANSYS code for LVE analysis of four-point bending destructive tests of large-scale specimens from section 8.2 using fitted M-W Prony series of Trosifol BG R20 and Evalam 80/120 at 20 °C – numerical simulation of experiment. Inputs and outputs are in [mm, N, MPa].

```
!Input parameters for Static displacement analysis
l=1000                  !span of the panel
b=360                   !width of the panel
a=400                   !distance between support and applied force
s=200                   !distance between applied MTS forces (steel rollers)
tg=10                   !thickness of glass
ti=0.76                 !thickness of interlayer
e1=70000                !Young modulus of glass
nu1=0.23                !Poisson ratio of glass

/PREP 7

!Key points definition
K,1,0,0,b
K,2,l,0,b
K,3,l,0,0
K,4,0,0,0
K,5,0,tg,b
K,6,l,tg,b
K,7,l,tg,0
K,8,0,tg,0
K,9,0,tg+ti,b
K,10,l,tg+ti,b
K,11,l,tg+ti,0
K,12,0,tg+ti,0
K,13,0,2*tg+ti,b
K,14,a,2*tg+ti,b
K,15,a+s,2*tg+ti,b
K,16,l,2*tg+ti,b
K,17,l,2*tg+ti,0
K,18,a+s,2*tg+ti,0
K,19,a,2*tg+ti,0
K,20,0,2*tg+ti,0

!volumes definition

V,1,2,3,4,5,6,7,8                   !Volume 1 (lower glass plate)
V,5,6,7,8,9,10,11,12                !Volume 2 (interlayer)

LSTR,       14,       19            !Lines for displacement input
LSTR,       15,       18            !Lines for displacement input

V,9,10,11,12,13,16,17,20            !Volume 3 (upper glass plate)

!Material properties
MP,ex,1,e1                          !Define Young modulus of glass
MP,nuxy,1,nu1                       !Define Poisson ratio of glass
```

```
!Evalam 80/120 Viscoelastic definition by Prony, temperature 20 °C
!*
MPDE,ALL,2
TBDE,ALL,2
MPTEMP,,,,,,,
MPTEMP,,,,,,,,
MPTEMP,1,0
MPDATA,EX,2,,66.50669
MPDATA,PRXY,2,,0.49
TB,PRONY,2,1,22,SHEAR
TBTEMP,0
TBDATA,,0.310691,1.00E-09,0.174687,1.00E-08,0.102573,1.00E-07
TBDATA,,0.07495,1.00E-06,0.034125,1.00E-05,0.107583,1.00E-04
TBDATA,,0.002921,1.00E-03,0.011112,1.00E-02,0.025791,1.00E-01
TBDATA,,0.002523,1.00,0.008451,1.00E+01,0.019944,1.00E+02
TBDATA,,0.013447,1.00E+03,0.017995,1.00E+04,0.015597,1.00E+05
TBDATA,,0.005001,1.00E+06,0.0057,1.00E+07,0.006174,1.00E+08
TBDATA,,0.002263,1.00E+09,0.014468,1.00E+10,0.004481,1.00E+11
TBDATA,,0.008957,1.00E+12
TB,PRONY,2,1,22,BULK
TBTEMP,0
TBDATA,,0.310691,1.00E-09,0.174687,1.00E-08,0.102573,1.00E-07
TBDATA,,0.07495,1.00E-06,0.034125,1.00E-05,0.107583,1.00E-04
TBDATA,,0.002921,1.00E-03,0.011112,1.00E-02,0.025791,1.00E-01
TBDATA,,0.002523,1.00,0.008451,1.00E+01,0.019944,1.00E+02
TBDATA,,0.013447,1.00E+03,0.017995,1.00E+04,0.015597,1.00E+05
TBDATA,,0.005001,1.00E+06,0.0057,1.00E+07,0.006174,1.00E+08
TBDATA,,0.002263,1.00E+09,0.014468,1.00E+10,0.004481,1.00E+11
TBDATA,,0.008957,1.00E+12

!Trosifol BG R20 Viscoelastic definition by Prony based on DMTA results in shear (SH), temperature 20 °C
!*
MPTEMP,,,,,,,,
MPTEMP,1,0
MPDATA,EX,2,,1622.092
MPDATA,PRXY,2,,0.49
TB,PRONY,2,1,30,SHEAR
TBTEMP,0
TBDATA,,0.126064,1.00E-10,0.114159,1.00E-09,0.114159,1.00E-08
TBDATA,,0.114159,1.00E-07,0.093271,1.00E-06,0.093271,1.00E-05
TBDATA,,0.080889,1.00E-04,0.079419,1.00E-03,0.079419,1.00E-02
TBDATA,,0.075855,1.00E-01,0.01997,1,0.005173,1.00E+01
TBDATA,,0.001708,1.00E+02,0.000795,1.00E+03,0.00055,1.00E+04
TBDATA,,0.00035,1.00E+05,0.000148,1.00E+06,0.000106,1.00E+07
TBDATA,,8.63E-05,1.00E+08,7.39E-05,1.00E+09,6.45E-05,1.00E+10
TBDATA,,5.65E-05,1.00E+11,4.94E-05,1.00E+12,4.3E-05,1.00E+13
TBDATA,,3.7E-05,1.00E+14,3.13E-05,1.00E+15,2.57E-05,1.00E+16
TBDATA,,2.01E-05,1.00E+17,1.4E-05,1.00E+18,5.89E-06,1.00E+19
TB,PRONY,2,1,30,BULK
TBTEMP,0
TBDATA,,0.126064,1.00E-10,0.114159,1.00E-09,0.114159,1.00E-08
TBDATA,,0.114159,1.00E-07,0.093271,1.00E-06,0.093271,1.00E-05
TBDATA,,0.080889,1.00E-04,0.079419,1.00E-03,0.079419,1.00E-02
TBDATA,,0.075855,1.00E-01,0.01997,1,0.005173,1.00E+01
TBDATA,,0.001708,1.00E+02,0.000795,1.00E+03,0.00055,1.00E+04
TBDATA,,0.00035,1.00E+05,0.000148,1.00E+06,0.000106,1.00E+07
TBDATA,,8.63E-05,1.00E+08,7.39E-05,1.00E+09,6.45E-05,1.00E+10
TBDATA,,5.65E-05,1.00E+11,4.94E-05,1.00E+12,4.3E-05,1.00E+13
```

```
TBDATA,,3.7E-05,1.00E+14,3.13E-05,1.00E+15,2.57E-05,1.00E+16
TBDATA,,2.01E-05,1.00E+17,1.4E-05,1.00E+18,5.89E-06,1.00E+19

!Trosifol BG R20 Viscoelastic definition by Prony based on combined DMTA results in shear and torsion (SH+TS), temperature 20 °C
!*
MPTEMP,,,,,,,,
MPTEMP,1,0
MPDATA,EX,2,,5310.73
MPDATA,PRXY,2,,0.49
TB,PRONY,2,1,30,SHEAR
TBTEMP,0
TBDATA,,0.5775,1.00E-05,0.1682,1.00E-04,0.1770,1.00E-03
TBDATA,,0.0703,1.00E-02,0.0044,1.00E-01,0.0016,1.00E+00
TBDATA,,0.0005,1.00E+01,0.0002,1.00E+02,8.360E-05,1.00E+03
TBDATA,,2.067E-05,1.00E+04,5.457E-05,1.00E+05
TB,PRONY,2,1,30,BULK
TBTEMP,0
TBDATA,,0.5775,1.00E-05,0.1682,1.00E-04,0.1770,1.00E-03
TBDATA,,0.0703,1.00E-02,0.0044,1.00E-01,0.0016,1.00E+00
TBDATA,,0.0005,1.00E+01,0.0002,1.00E+02,8.360E-05,1.00E+03
TBDATA,,2.067E-05,1.00E+04,5.457E-05,1.00E+05

!Element type
ET,1,SOLID186

!Material assignment to the individual volumes
TYPE,      1
MAT,            1
REAL,
ESYS,           0
SECNUM,
!*
CM,_Y,VOLU
VSEL, , , ,             2
CM,_Y1,VOLU
CMSEL,S,_Y
!*
CMSEL,S,_Y1
VATT,           2, ,      1,            0
CMSEL,S,_Y
CMDELE,_Y
CMDELE,_Y1
!*
!Mesh options

ESIZE,10,0,                    !Global mesh size 10 mm
!Mesh volumes

FLST,5,3,6,ORDE,2
FITEM,5,1
FITEM,5,-3
CM,_Y,VOLU
VSEL, , , ,P51X
CM,_Y1,VOLU
CHKMSH,'VOLU'
CMSEL,S,_Y
!*
VMESH,_Y1
```

```
!*
CMDELE,_Y
CMDELE,_Y1
CMDELE,_Y2
!*

!Stress analysis

/SOLU
ANTYPE,0                    !Static analysis

FLST,2,2,4,ORDE,2
FITEM,2,20
FITEM,2,22
!*
/GO
DL,P51X, ,UY,0              !Support kept strained in vertical y direction

FLST,2,2,3,ORDE,2
FITEM,2,17
FITEM,2,20
!*
/GO
DK,P51X, ,0, ,0,UZ, , , , , ,      !Keypoints strained in z direction

FLST,2,1,3,ORDE,1
FITEM,2,16
!*
/GO
DK,P51X, ,0, ,0,UX, , , , , ,      !Keypoint strained in x direction

!Solution setting
KBC,0                       !Ramped loading
NLGEOM,0                    !Small displacement analysis
NROPT,1                     !Full Newton-Raphson method applied
LNSRCH,0                    !Line search in Newton-Raphson method off
AUTOTS,0                    !Automatic time stepping off
```

Loading rate 2.0 mm/min	Loading rate 0.5 mm/min	Loading rate 0.125 mm/min
!1.step	!1.step	!1.step
FLST,2,2,4,ORDE,2	FLST,2,2,4,ORDE,2	FLST,2,2,4,ORDE,2
FITEM,2,33	FITEM,2,33	FITEM,2,33
FITEM,2,-34	FITEM,2,-34	FITEM,2,-34
!*	!*	!*
/GO	/GO	/GO
DL,P51X, ,UY,-0.66	DL,P51X, ,UY,-0.72	DL,P51X, ,UY,-0.72
!Time at the end of the load step	!Time at the end of the load step	!Time at the end of the load step
TIME,20	TIME,90	TIME,360
!Solution setting	!Solution setting	!Solution setting
NSUBST,10,0,0 !number of substeps	NSUBST,10,0,0 !number of substeps	NSUBST,10,0,0 !number of substeps
LSWRITE,1, !Write to LS file	LSWRITE,1, !Write to LS file	LSWRITE,1, !Write to LS file

```
!Delete the set line displacement

FLST,2,2,4,ORDE,2
FITEM,2,33
FITEM,2,-34
DLDELE,P51X,UY

!2. step

FLST,2,2,4,ORDE,2
FITEM,2,33
FITEM,2,-34
!*
/GO
DL,P51X, ,UY,-1.32
!Time at the end of the load step
TIME,40

LSWRITE,2,    !Write to LS file

!Delete the set line displacement

FLST,2,2,4,ORDE,2
FITEM,2,33
FITEM,2,-34
DLDELE,P51X,UY

!3. step

FLST,2,2,4,ORDE,2
FITEM,2,33
FITEM,2,-34
!*
/GO
DL,P51X, ,UY,-1.98
!Time at the end of the load step
TIME,60

LSWRITE,3,    !Write to LS file

!Delete the set line displacement

FLST,2,2,4,ORDE,2
FITEM,2,33
FITEM,2,-34
DLDELE,P51X,UY

!4. step

FLST,2,2,4,ORDE,2
FITEM,2,33
FITEM,2,-34
!*
/GO
DL,P51X, ,UY,-2.64
```

```
!Delete the set line displacement

FLST,2,2,4,ORDE,2
FITEM,2,33
FITEM,2,-34
DLDELE,P51X,UY

!2. step

FLST,2,2,4,ORDE,2
FITEM,2,33
FITEM,2,-34
!*
/GO
DL,P51X, ,UY,-1.44
!Time at the end of the load step
TIME,180

LSWRITE,2,    !Write to LS file

!Delete the set line displacement

FLST,2,2,4,ORDE,2
FITEM,2,33
FITEM,2,-34
DLDELE,P51X,UY

!3. step

FLST,2,2,4,ORDE,2
FITEM,2,33
FITEM,2,-34
!*
/GO
DL,P51X, ,UY,-2.16
!Time at the end of the load step
TIME,270

LSWRITE,3,    !Write to LS file

!Delete the set line displacement

FLST,2,2,4,ORDE,2
FITEM,2,33
FITEM,2,-34
DLDELE,P51X,UY

!4. step

FLST,2,2,4,ORDE,2
FITEM,2,33
FITEM,2,-34
!*
/GO
DL,P51X, ,UY,-2.88
```

```
!Delete the set line displacement

FLST,2,2,4,ORDE,2
FITEM,2,33
FITEM,2,-34
DLDELE,P51X,UY

!2. step

FLST,2,2,4,ORDE,2
FITEM,2,33
FITEM,2,-34
!*
/GO
DL,P51X, ,UY,-1.44
!Time at the end of the load step
TIME,720

LSWRITE,2,    !Write to LS file

!Delete the set line displacement

FLST,2,2,4,ORDE,2
FITEM,2,33
FITEM,2,-34
DLDELE,P51X,UY

!3. step

FLST,2,2,4,ORDE,2
FITEM,2,33
FITEM,2,-34
!*
/GO
DL,P51X, ,UY,-2.16
!Time at the end of the load step
TIME,1080

LSWRITE,3,    !Write to LS file

!Delete the set line displacement

FLST,2,2,4,ORDE,2
FITEM,2,33
FITEM,2,-34
DLDELE,P51X,UY

!4. step

FLST,2,2,4,ORDE,2
FITEM,2,33
FITEM,2,-34
!*
/GO
DL,P51X, ,UY,-2.88
```

```
!Time at the end of the load step
TIME,80

LSWRITE,4,    !Write to LS file

!Delete the set line displacement

FLST,2,2,4,ORDE,2
FITEM,2,33
FITEM,2,-34
DLDELE,P51X,UY

                …
                …
                …
!30. step

FLST,2,2,4,ORDE,2
FITEM,2,33
FITEM,2,-34
!*
/GO
DL,P51X, ,UY,-19.8
!Time at the end of the load step
TIME,600

LSWRITE,30,    !Write to LS file

!Delete the set line displacement

FLST,2,2,4,ORDE,2
FITEM,2,33
FITEM,2,-34
DLDELE,P51X,UY

!31. step

FLST,2,2,4,ORDE,2
FITEM,2,33
FITEM,2,-34
!*
/GO
DL,P51X, ,UY,-20.46
!Time at the end of the load step
TIME,620

LSWRITE,31,    !Write to LS file

!Delete the set line displacement

FLST,2,2,4,ORDE,2
FITEM,2,33
FITEM,2,-34
DLDELE,P51X,UY
```

```
!Time at the end of the load step
TIME,360

LSWRITE,4,    !Write to LS file

!Delete the set line displacement

FLST,2,2,4,ORDE,2
FITEM,2,33
FITEM,2,-34
DLDELE,P51X,UY

                …
                …
                …
!30. step

FLST,2,2,4,ORDE,2
FITEM,2,33
FITEM,2,-34
!*
/GO
DL,P51X, ,UY,-21.6
!Time at the end of the load step
TIME,2700

LSWRITE,30,    !Write to LS file

!Delete the set line displacement

FLST,2,2,4,ORDE,2
FITEM,2,33
FITEM,2,-34
DLDELE,P51X,UY

!31. step

FLST,2,2,4,ORDE,2
FITEM,2,33
FITEM,2,-34
!*
/GO
DL,P51X, ,UY,-22.32
!Time at the end of the load step
TIME,2790

LSWRITE,31,    !Write to LS file

!Delete the set line displacement

FLST,2,2,4,ORDE,2
FITEM,2,33
FITEM,2,-34
DLDELE,P51X,UY
```

```
!Time at the end of the load step
TIME,1440

LSWRITE,4,    !Write to LS file

!Delete the set line displacement

FLST,2,2,4,ORDE,2
FITEM,2,33
FITEM,2,-34
DLDELE,P51X,UY

                …
                …
                …
!30. step

FLST,2,2,4,ORDE,2
FITEM,2,33
FITEM,2,-34
!*
/GO
DL,P51X, ,UY,-21.6
!Time at the end of the load step
TIME,10800

LSWRITE,30,    !Write to LS file

!Delete the set line displacement

FLST,2,2,4,ORDE,2
FITEM,2,33
FITEM,2,-34
DLDELE,P51X,UY

!31. step

FLST,2,2,4,ORDE,2
FITEM,2,33
FITEM,2,-34
!*
/GO
DL,P51X, ,UY,-22.32
!Time at the end of the load step
TIME,11160

LSWRITE,31,    !Write to LS file

!Delete the set line displacement

FLST,2,2,4,ORDE,2
FITEM,2,33
FITEM,2,-34
DLDELE,P51X,UY
```

```
!32. step

FLST,2,2,4,ORDE,2
FITEM,2,33
FITEM,2,-34
!*
/GO
DL,P51X, ,UY,-21.12
!Time at the end of the load step
TIME,640

LSWRITE,32,    !Write to LS file

!Delete the set line displacement

FLST,2,2,4,ORDE,2
FITEM,2,33
FITEM,2,-34
DLDELE,P51X,UY
                …
                …
                …
!55. step

FLST,2,2,4,ORDE,2
FITEM,2,33
FITEM,2,-34
!*
/GO
DL,P51X, ,UY,-36.3
!Time at the end of the load step
TIME,1100

LSWRITE,55,    !Write to LS file

!Delete the set line displacement

FLST,2,2,4,ORDE,2
FITEM,2,33
FITEM,2,-34
DLDELE,P51X,UY

!56. step

FLST,2,2,4,ORDE,2
FITEM,2,33
FITEM,2,-34
!*
/GO
DL,P51X, ,UY,-36.96
!Time at the end of the load step
TIME,1120

LSWRITE,56,    !Write to LS file

!SOLVE all LS files COMMAND
```

```
!32. step

FLST,2,2,4,ORDE,2
FITEM,2,33
FITEM,2,-34
!*
/GO
DL,P51X, ,UY,-23.04
!Time at the end of the load step
TIME,2880

LSWRITE,32,    !Write to LS file

!Delete the set line displacement

FLST,2,2,4,ORDE,2
FITEM,2,33
FITEM,2,-34
DLDELE,P51X,UY
                …
                …
                …
!55. step

FLST,2,2,4,ORDE,2
FITEM,2,33
FITEM,2,-34
!*
/GO
DL,P51X, ,UY,-39.6
!Time at the end of the load step
TIME,4950

LSWRITE,55,    !Write to LS file

!Delete the set line displacement

FLST,2,2,4,ORDE,2
FITEM,2,33
FITEM,2,-34
DLDELE,P51X,UY

!56. step

FLST,2,2,4,ORDE,2
FITEM,2,33
FITEM,2,-34
!*
/GO
DL,P51X, ,UY,-40.32
!Time at the end of the load step
TIME,5040

LSWRITE,56,    !Write to LS file

!SOLVE all LS files COMMAND
```

```
!32. step

FLST,2,2,4,ORDE,2
FITEM,2,33
FITEM,2,-34
!*
/GO
DL,P51X, ,UY,-23.04
!Time at the end of the load step
TIME,11520

LSWRITE,32,    !Write to LS file

!Delete the set line displacement

FLST,2,2,4,ORDE,2
FITEM,2,33
FITEM,2,-34
DLDELE,P51X,UY
                …
                …
                …
!55. step

FLST,2,2,4,ORDE,2
FITEM,2,33
FITEM,2,-34
!*
/GO
DL,P51X, ,UY,-39.6
!Time at the end of the load step
TIME,19800

LSWRITE,55,    !Write to LS file

!Delete the set line displacement

FLST,2,2,4,ORDE,2
FITEM,2,33
FITEM,2,-34
DLDELE,P51X,UY

!56. step

FLST,2,2,4,ORDE,2
FITEM,2,33
FITEM,2,-34
!*
/GO
DL,P51X, ,UY,-40.32
!Time at the end of the load step
TIME,20160

LSWRITE,56,    !Write to LS file

!SOLVE all LS files COMMAND
```

- **LVE analysis of four-point bending creep tests**

Note: ANSYS code for LVE analysis of four-point bending creep tests from section 8.3 using fitted Prony series of Trosifol BG R20 and Evalam 80/120 interlayers at testing temperatures – numerical simulation of experiment. Inputs and outputs are in [mm, N, MPa].

```
!Input parameters for Static displacement analysis
l=1000                  !span of the panel
b=360                   !width of the panel
a=400                   !distance between support and applied force
s=200                   !distance between applied MTS forces (steel rollers)
tg=10                   !thickness of glass
ti=0.76                 !thickness of interlayer
e1=70000                !Young modulus of glass
nu1=0.23                !Poisson ratio of glass

/PREP 7

!Key points definition
K,1,0,0,b
K,2,l,0,b
K,3,l,0,0
K,4,0,0,0
K,5,0,tg,b
K,6,l,tg,b
K,7,l,tg,0
K,8,0,tg,0
K,9,0,tg+ti,b
K,10,l,tg+ti,b
K,11,l,tg+ti,0
K,12,0,tg+ti,0
K,13,0,2*tg+ti,b
K,14,a,2*tg+ti,b
K,15,a+s,2*tg+ti,b
K,16,l,2*tg+ti,b
K,17,l,2*tg+ti,0
K,18,a+s,2*tg+ti,0
K,19,a,2*tg+ti,0
K,20,0,2*tg+ti,0
K,21,a-10,2*tg+ti,b
K,22,a-10,2*tg+ti,0
K,23,a+s+10,2*tg+ti,b
K,24,a+s+10,2*tg+ti,0

!volumes definition

V,1,2,3,4,5,6,7,8               !Volume 1 (lower glass plate)
V,5,6,7,8,9,10,11,12            !Volume 2 (interlayer)
V,9,10,11,12,13,16,17,20        !Volume 3 (upper glass plate)
```

```
!Material properties

MP,ex,1,e1              !Define Young´s modulus of glass
MP,nuxy,1,nu1           !Define Poisson ratio of glass

!Evalam 80/120 Viscoelastic definition by Prony, temperature 30 °C
!*
MPDE,ALL,2
TBDE,ALL,2
MPTEMP,,,,,,,
MPTEMP,,,,,,,,
MPTEMP,1,0
MPDATA,EX,2,,66.50669
MPDATA,PRXY,2,,0.49
TB,PRONY,2,1,22,SHEAR
TBTEMP,0
TBDATA,,0.310691,1.46E-12,0.174687,1.46E-11,0.102573,1.46E-10
TBDATA,,0.07495,1.46E-09,0.034125,1.46E-08,0.107583,1.46E-07
TBDATA,,0.002921,1.46E-06,0.011112,1.46E-05,0.025791,1.46E-04
TBDATA,,0.002523,1.46E-03,0.008451,1.46E-02,0.019944,1.46E-01
TBDATA,,0.013447,1.46,0.017995,1.46E+01,0.015597,1.46E+02
TBDATA,,0.005001,1.46E+03,0.0057,1.46E+04,0.006174,1.46E+05
TBDATA,,0.002263,1.46E+06,0.014468,1.46E+07,0.004481,1.46E+08
TBDATA,,0.008957,1.46E+09
TB,PRONY,2,1,22,BULK
TBTEMP,0
TBDATA,,0.310691,1.46E-12,0.174687,1.46E-11,0.102573,1.46E-10
TBDATA,,0.07495,1.46E-09,0.034125,1.46E-08,0.107583,1.46E-07
TBDATA,,0.002921,1.46E-06,0.011112,1.46E-05,0.025791,1.46E-04
TBDATA,,0.002523,1.46E-03,0.008451,1.46E-02,0.019944,1.46E-01
TBDATA,,0.013447,1.46,0.017995,1.46E+01,0.015597,1.46E+02
TBDATA,,0.005001,1.46E+03,0.0057,1.46E+04,0.006174,1.46E+05
TBDATA,,0.002263,1.46E+06,0.014468,1.46E+07,0.004481,1.46E+08
TBDATA,,0.008957,1.46E+09

!Evalam 80/120 Viscoelastic definition by Prony, temperature 40 °C
!*
MPDE,ALL,2
TBDE,ALL,2
MPTEMP,,,,,,,
MPTEMP,,,,,,,,
MPTEMP,1,0
MPDATA,EX,2,,66.50669
MPDATA,PRXY,2,,0.49
TB,PRONY,2,1,22,SHEAR
TBTEMP,0
TBDATA,,0.310691,2.37E-15,0.174687,2.37E-14,0.102573,2.37E-13
TBDATA,,0.07495,2.37E-12,0.034125,2.37E-11,0.107583,2.37E-10
TBDATA,,0.002921,2.37E-09,0.011112,2.37E-08,0.025791,2.37E-07
TBDATA,,0.002523,2.37E-06,0.008451,2.37E-05,0.019944,2.37E-04
TBDATA,,0.013447,2.37E-03,0.017995,2.37E-02,0.015597,2.37E-01
TBDATA,,0.005001,2.37,0.0057,2.37E+01,0.006174,2.37E+02
TBDATA,,0.002263,2.37E+03,0.014468,2.37E+04,0.004481,2.37E+05
TBDATA,,0.008957,2.37E+06
```

```
TB,PRONY,2,1,22,BULK
TBTEMP,0
TBDATA,,0.310691,2.37E-15,0.174687,2.37E-14,0.102573,2.37E-13
TBDATA,,0.07495,2.37E-12,0.034125,2.37E-11,0.107583,2.37E-10
TBDATA,,0.002921,2.37E-09,0.011112,2.37E-08,0.025791,2.37E-07
TBDATA,,0.002523,2.37E-06,0.008451,2.37E-05,0.019944,2.37E-04
TBDATA,,0.013447,2.37E-03,0.017995,2.37E-02,0.015597,2.37E-01
TBDATA,,0.005001,2.37,0.0057,2.37E+01,0.006174,2.37E+02
TBDATA,,0.002263,2.37E+03,0.014468,2.37E+04,0.004481,2.37E+05
TBDATA,,0.008957,2.37E+06

!Evalam 80/120 Viscoelastic definition by Prony, temperature 50 °C
!*
MPDE,ALL,2
TBDE,ALL,2
MPTEMP,,,,,,,
MPTEMP,,,,,,,,
MPTEMP,1,0
MPDATA,EX,2,,66.50669
MPDATA,PRXY,2,,0.49
TB,PRONY,2,1,22,SHEAR
TBTEMP,0
TBDATA,,0.310691,4.29E-18,0.174687,4.29E-17,0.102573,4.29E-16
TBDATA,,0.07495,4.29E-15,0.034125,4.29E-14,0.107583,4.29E-13
TBDATA,,0.002921,4.29E-12,0.011112,4.29E-11,0.025791,4.29E-10
TBDATA,,0.002523,4.29E-09,0.008451,4.29E-08,0.019944,4.29E-07
TBDATA,,0.013447,4.29E-06,0.017995,4.29E-05,0.015597,4.29E-04
TBDATA,,0.005001,4.29E-03,0.0057,4.29E-02,0.006174,4.29E-01
TBDATA,,0.002263,4.29,0.014468,4.29E+01,0.004481,4.29E+02
TBDATA,,0.008957,4.29E+03
TB,PRONY,2,1,22,BULK
TBTEMP,0
TBDATA,,0.310691,4.29E-18,0.174687,4.29E-17,0.102573,4.29E-16
TBDATA,,0.07495,4.29E-15,0.034125,4.29E-14,0.107583,4.29E-13
TBDATA,,0.002921,4.29E-12,0.011112,4.29E-11,0.025791,4.29E-10
TBDATA,,0.002523,4.29E-09,0.008451,4.29E-08,0.019944,4.29E-07
TBDATA,,0.013447,4.29E-06,0.017995,4.29E-05,0.015597,4.29E-04
TBDATA,,0.005001,4.29E-03,0.0057,4.29E-02,0.006174,4.29E-01
TBDATA,,0.002263,4.29,0.014468,4.29E+01,0.004481,4.29E+02
TBDATA,,0.008957,4.29E+03

!Trosifol BG R20 Viscoelastic definition by Prony based on DMTA results in shear (SH), temperature 30 °C
!*
MPDE,ALL,2
TBDE,ALL,2
MPTEMP,,,,,,,
MPTEMP,,,,,,,,
MPTEMP,1,0
MPDATA,EX,2,,1622.092
MPDATA,PRXY,2,,0.49
TB,PRONY,2,1,30,SHEAR
TBTEMP,0
TBDATA,,0.126064,9.58E-13,0.114159,9.58E-12,0.114159,9.58E-11
TBDATA,,0.114159,9.58E-10,0.093271,9.58E-09,0.093271,9.58E-08
TBDATA,,0.080889,9.58E-07,0.079419,9.58E-06,0.079419,9.58E-05
TBDATA,,0.075855,9.58E-04,0.01997,9.58E-03,0.005173,9.58E-02
TBDATA,,0.001708,9.58E-01,0.000795,9.58,0.00055,9.58E+01
TBDATA,,0.00035,9.58E+02,0.000148,9.58E+03,0.000106,9.58E+04
```

```
TBDATA,,8.63E-05,9.58E+05,7.39E-05,9.58E+06,6.45E-05,9.58E+07
TBDATA,,5.65E-05,9.58E+08,4.94E-05,9.58E+09,4.3E-05,9.58E+10
TBDATA,,3.7E-05,9.58E+11,3.13E-05,9.58E+12,2.57E-05,9.58E+13
TBDATA,,2.01E-05,9.58E+14,1.4E-05,9.58E+15,5.89E-06,9.58E+16
TB,PRONY,2,1,30,BULK
TBTEMP,0
TBDATA,,0.126064,9.58E-13,0.114159,9.58E-12,0.114159,9.58E-11
TBDATA,,0.114159,9.58E-10,0.093271,9.58E-09,0.093271,9.58E-08
TBDATA,,0.080889,9.58E-07,0.079419,9.58E-06,0.079419,9.58E-05
TBDATA,,0.075855,9.58E-04,0.01997,9.58E-03,0.005173,9.58E-02
TBDATA,,0.001708,9.58E-01,0.000795,9.58,0.00055,9.58E+01
TBDATA,,0.00035,9.58E+02,0.000148,9.58E+03,0.000106,9.58E+04
TBDATA,,8.63E-05,9.58E+05,7.39E-05,9.58E+06,6.45E-05,9.58E+07
TBDATA,,5.65E-05,9.58E+08,4.94E-05,9.58E+09,4.3E-05,9.58E+10
TBDATA,,3.7E-05,9.58E+11,3.13E-05,9.58E+12,2.57E-05,9.58E+13
TBDATA,,2.01E-05,9.58E+14,1.4E-05,9.58E+15,5.89E-06,9.58E+16

!Trosifol BG R20 Viscoelastic definition by Prony based on DMTA results in shear (SH), temperature 40 °C

!*
MPDE,ALL,2
TBDE,ALL,2
MPTEMP,,,,,,,
MPTEMP,,,,,,,,
MPTEMP,1,0
MPDATA,EX,2,,1622.092
MPDATA,PRXY,2,,0.49
TB,PRONY,2,1,30,SHEAR
TBTEMP,0
TBDATA,,0.126064,2.76E-14,0.114159,2.76E-13,0.114159,2.76E-12
TBDATA,,0.114159,2.76E-11,0.093271,2.76E-10,0.093271,2.76E-09
TBDATA,,0.080889,2.76E-08,0.079419,2.76E-07,0.079419,2.76E-06
TBDATA,,0.075855,2.76E-05,0.01997,2.76E-04,0.005173,2.76E-03
TBDATA,,0.001708,2.76E-02,0.000795,2.76E-01,0.00055,2.76
TBDATA,,0.00035,2.76E+01,0.000148,2.76E+02,0.000106,2.76E+03
TBDATA,,8.63E-05,2.76E+04,7.39E-05,2.76E+05,6.45E-05,2.76E+06
TBDATA,,5.65E-05,2.76E+07,4.94E-05,2.76E+08,4.3E-05,2.76E+09
TBDATA,,3.7E-05,2.76E+10,3.13E-05,2.76E+11,2.57E-05,2.76E+12
TBDATA,,2.01E-05,2.76E+13,1.4E-05,2.76E+14,5.89E-06,2.76E+15
TB,PRONY,2,1,30,BULK
TBTEMP,0
TBDATA,,0.126064,2.76E-14,0.114159,2.76E-13,0.114159,2.76E-12
TBDATA,,0.114159,2.76E-11,0.093271,2.76E-10,0.093271,2.76E-09
TBDATA,,0.080889,2.76E-08,0.079419,2.76E-07,0.079419,2.76E-06
TBDATA,,0.075855,2.76E-05,0.01997,2.76E-04,0.005173,2.76E-03
TBDATA,,0.001708,2.76E-02,0.000795,2.76E-01,0.00055,2.76
TBDATA,,0.00035,2.76E+01,0.000148,2.76E+02,0.000106,2.76E+03
TBDATA,,8.63E-05,2.76E+04,7.39E-05,2.76E+05,6.45E-05,2.76E+06
TBDATA,,5.65E-05,2.76E+07,4.94E-05,2.76E+08,4.3E-05,2.76E+09
TBDATA,,3.7E-05,2.76E+10,3.13E-05,2.76E+11,2.57E-05,2.76E+12
TBDATA,,2.01E-05,2.76E+13,1.4E-05,2.76E+14,5.89E-06,2.76E+15

!Trosifol BG R20 Viscoelastic definition by Prony based on DMTA results in shear (SH), temperature 50 °C
!*
MPDE,ALL,2
TBDE,ALL,2
MPTEMP,,,,,,,
MPTEMP,,,,,,,,
```

```
MPTEMP,1,0
MPDATA,EX,2,,1622.092
MPDATA,PRXY,2,,0.49
TB,PRONY,2,1,30,SHEAR
TBTEMP,0
TBDATA,,0.126064,1.69E-15,0.114159,1.69E-14,0.114159,1.69E-13
TBDATA,,0.114159,1.69E-12,0.093271,1.69E-11,0.093271,1.69E-10
TBDATA,,0.080889,1.69E-09,0.079419,1.69E-08,0.079419,1.69E-07
TBDATA,,0.075855,1.69E-06,0.01997,1.69E-05,0.005173,1.69E-04
TBDATA,,0.001708,1.69E-03,0.000795,1.69E-02,0.00055,1.69E-01
TBDATA,,0.00035,1.69,0.000148,1.69E+01,0.000106,1.69E+02
TBDATA,,8.63E-05,1.69E+03,7.39E-05,1.69E+04,6.45E-05,1.69E+05
TBDATA,,5.65E-05,1.69E+06,4.94E-05,1.69E+07,4.3E-05,1.69E+08
TBDATA,,3.7E-05,1.69E+09,3.13E-05,1.69E+10,2.57E-05,1.69E+11
TBDATA,,2.01E-05,1.69E+12,1.4E-05,1.69E+13,5.89E-06,1.69E+14
TB,PRONY,2,1,30,BULK
TBTEMP,0
TBDATA,,0.126064,1.69E-15,0.114159,1.69E-14,0.114159,1.69E-13
TBDATA,,0.114159,1.69E-12,0.093271,1.69E-11,0.093271,1.69E-10
TBDATA,,0.080889,1.69E-09,0.079419,1.69E-08,0.079419,1.69E-07
TBDATA,,0.075855,1.69E-06,0.01997,1.69E-05,0.005173,1.69E-04
TBDATA,,0.001708,1.69E-03,0.000795,1.69E-02,0.00055,1.69E-01
TBDATA,,0.00035,1.69,0.000148,1.69E+01,0.000106,1.69E+02
TBDATA,,8.63E-05,1.69E+03,7.39E-05,1.69E+04,6.45E-05,1.69E+05
TBDATA,,5.65E-05,1.69E+06,4.94E-05,1.69E+07,4.3E-05,1.69E+08
TBDATA,,3.7E-05,1.69E+09,3.13E-05,1.69E+10,2.57E-05,1.69E+11
TBDATA,,2.01E-05,1.69E+12,1.4E-05,1.69E+13,5.89E-06,1.69E+14

!Trosifol BG R20 Viscoelastic definition by Prony based on combined DMTA results in shear and torsion (SH+TS), temperature 30 °C

!*
MPDE,ALL,2
TBDE,ALL,2
MPTEMP,,,,,,,
MPTEMP,,,,,,,,
MPTEMP,1,0
MPDATA,EX,2,,9196.229
MPDATA,PRXY,2,,0.49
TB,PRONY,2,1,11,SHEAR
TBTEMP,0
TBDATA,,0.57749,2.25E-07,0.168247,2.25E-06,0.176986,2.25E-05
TBDATA,,0.070283,2.25E-04,0.004413,2.25E-03,0.001616,2.25E-02
TBDATA,,0.000539,2.25E-01,0.00019,2.25E+00,8.36E-05,2.25E+01
TBDATA,,2.07E-05,2.25E+02,5.46E-05,2.25E+03,,
TB,PRONY,2,1,11,BULK
TBTEMP,0
TBDATA,,0.57749,2.25E-07,0.168247,2.25E-06,0.176986,2.25E-05
TBDATA,,0.070283,2.25E-04,0.004413,2.25E-03,0.001616,2.25E-02
TBDATA,,0.000539,2.25E-01,0.00019,2.25,8.36E-05,2.25E+01
TBDATA,,2.07E-05,2.25E+02,5.46E-05,2.25E+03,,

!Trosifol BG R20 Viscoelastic definition by Prony based on combined DMTA results in shear and torsion (SH+TS), temperature 40 °C
!*
MPTEMP,,,,,,,,
MPTEMP,1,0
MPDATA,EX,2,,9196.229
MPDATA,PRXY,2,,0.49
TB,PRONY,2,1,11,SHEAR
```

```
TBTEMP,0
TBDATA,,0.57749,1.71E-08,0.168247,1.71E-07,0.176986,1.71E-06
TBDATA,,0.070283,1.71E-05,0.004413,1.71E-04,0.001616,1.71E-03
TBDATA,,0.000539,1.71E-02,0.00019,1.71E-01,8.36E-05,1.71
TBDATA,,2.07E-05,1.71E+01,5.46E-05,1.71E+02,,
TB,PRONY,2,1,11,BULK
TBTEMP,0
TBDATA,,0.57749,1.71E-08,0.168247,1.71E-07,0.176986,1.71E-06
TBDATA,,0.070283,1.71E-05,0.004413,1.71E-04,0.001616,1.71E-03
TBDATA,,0.000539,1.71E-02,0.00019,1.71E-01,8.36E-05,1.71
TBDATA,,2.07E-05,1.71E+01,5.46E-05,1.71E+02,,

!Trosifol BG R20 Viscoelastic definition by Prony based on combined DMTA results in shear and torsion (SH+TS), temperature 50 °C

!*
MPTEMP,,,,,,,,
MPTEMP,1,0
MPDATA,EX,2,,9196.229
MPDATA,PRXY,2,,0.49
TB,PRONY,2,1,11,SHEAR
TBTEMP,0
TBDATA,,0.57749,2.65E-09,0.168247,2.65E-08,0.176986,2.65E-07
TBDATA,,0.070283,2.65E-06,0.004413,2.65E-05,0.001616,2.65E-04
TBDATA,,0.000539,2.65E-03,0.00019,2.65E-02,8.36E-05,2.65E-01
TBDATA,,2.07E-05,2.65,5.46E-05,2.65E+01,,
TB,PRONY,2,1,11,BULK
TBTEMP,0
TBDATA,,0.57749,2.65E-09,0.168247,2.65E-08,0.176986,2.65E-07
TBDATA,,0.070283,2.65E-06,0.004413,2.65E-05,0.001616,2.65E-04
TBDATA,,0.000539,2.65E-03,0.00019,2.65E-02,8.36E-05,2.65E-01
TBDATA,,2.07E-05,2.65,5.46E-05,2.65E+01,,

!Element type
ET,1,SOLID186

!Material assignment to the individual volumes

TYPE,     1
MAT,           1
REAL,
ESYS,          0
SECNUM,
!*

CM,_Y,VOLU
VSEL, , , ,            2
CM,_Y1,VOLU
CMSEL,S,_Y
!*
CMSEL,S,_Y1
VATT,          2, ,     1,          0
CMSEL,S,_Y
CMDELE,_Y
CMDELE,_Y1
!*
!Mesh options

ESIZE,10,0,                          !Global mesh size 10 mm
```

```
!Mesh volumes
FLST,5,3,6,ORDE,2
FITEM,5,1
FITEM,5,-3
CM,_Y,VOLU
VSEL, , , ,P51X
CM,_Y1,VOLU
CHKMSH,'VOLU'
CMSEL,S,_Y
!*
VMESH,_Y1
!*
CMDELE,_Y
CMDELE,_Y1
CMDELE,_Y2
!*

!Stress analysis

/SOLU
ANTYPE,0                    !New static analysis

FLST,2,2,4,ORDE,2
FITEM,2,20
FITEM,2,22
!*
/GO
DL,P51X, ,UY,0              !Supports kept strained in vertical sense

FLST,2,2,3,ORDE,2
FITEM,2,17
FITEM,2,20
!*
/GO
DK,P51X, ,0, ,0,UZ, , , , , ,   !Keypoints strained in z direction

FLST,2,1,3,ORDE,1
FITEM,2,16
!*
/GO
DK,P51X, ,0, ,0,UX, , , , , ,   !Keypoint strained in x direction

!Solution setting
KBC,0                       !Ramped loading
NLGEOM,0                    !Small displacement analysis
NROPT,1                     !Full Newton-Raphson method applied
LNSRCH,0                    !Line search in Newton-Raphson method off
AUTOTS,0                    !Automatic time stepping off
```

Evalam 80/120; 30 °C	Evalam 80/120; 40 °C	Evalam 80/120; 50 °C
!1. step	!1. step	!1. step
FLST,2,2,5,ORDE,2	FLST,2,2,5,ORDE,2	FLST,2,2,5,ORDE,2
FITEM,2,6	FITEM,2,6	FITEM,2,6
FITEM,2,19	FITEM,2,19	FITEM,2,19
/GO	/GO	/GO
!*	!*	!*

```
SFA,P51X,1,PRES,0.1555

!Time at the end of load step
TIME,60

!Solution setting
NSUBST,10,0,0 !Number of substeps

LSWRITE,1,
!Write to LS file

!Delete the loading (pressure on areas)

FLST,2,2,5,ORDE,2
FITEM,2,6
FITEM,2,19
SFADELE,P51X,1,PRES

!2. step

FLST,2,2,5,ORDE,2
FITEM,2,6
FITEM,2,19
/GO
!*
SFA,P51X,1,PRES,0.1555

!Time at the end of load step
TIME,360

LSWRITE,2,    !Write to LS file

!Delete the loading (pressure on areas)

FLST,2,2,5,ORDE,2
FITEM,2,6
FITEM,2,19
SFADELE,P51X,1,PRES

!3. step

FLST,2,2,5,ORDE,2
FITEM,2,6
FITEM,2,19
/GO
!*
SFA,P51X,1,PRES,0.1555

!Time at the end of load step
TIME,720

LSWRITE,3,    !Write to LS file
```


```
SFA,P51X,1,PRES,0.1555

!Time at the end of load step
TIME,60

!Solution setting
NSUBST,10,0,0 !Number of substeps

LSWRITE,1,
!Write to LS file

!Delete the loading (pressure on areas)

FLST,2,2,5,ORDE,2
FITEM,2,6
FITEM,2,19
SFADELE,P51X,1,PRES

!2. step

FLST,2,2,5,ORDE,2
FITEM,2,6
FITEM,2,19
/GO
!*
SFA,P51X,1,PRES,0.1555

!Time at the end of load step
TIME,360

LSWRITE,2,    !Write to LS file

!Delete the loading (pressure on areas)

FLST,2,2,5,ORDE,2
FITEM,2,6
FITEM,2,19
SFADELE,P51X,1,PRES

!3. step

FLST,2,2,5,ORDE,2
FITEM,2,6
FITEM,2,19
/GO
!*
SFA,P51X,1,PRES,0.1555

!Time at the end of load step
TIME,720

LSWRITE,3,    !Write to LS file
```



```
SFA,P51X,1,PRES,0.1555

!Time at the end of load step
TIME,60

!Solution setting
NSUBST,10,0,0 !Number of substeps

LSWRITE,1,
!Write to LS file

!Delete the loading (pressure on areas)

FLST,2,2,5,ORDE,2
FITEM,2,6
FITEM,2,19
SFADELE,P51X,1,PRES

!2. step

FLST,2,2,5,ORDE,2
FITEM,2,6
FITEM,2,19
/GO
!*
SFA,P51X,1,PRES,0.1555

!Time at the end of load step
TIME,360

LSWRITE,2,    !Write to LS file

!Delete the loading (pressure on areas)

FLST,2,2,5,ORDE,2
FITEM,2,6
FITEM,2,19
SFADELE,P51X,1,PRES

!3. step

FLST,2,2,5,ORDE,2
FITEM,2,6
FITEM,2,19
/GO
!*
SFA,P51X,1,PRES,0.1555

!Time at the end of load step
TIME,720

LSWRITE,3,    !Write to LS file
```

```
!Delete the loading (pressure on areas)

FLST,2,2,5,ORDE,2
FITEM,2,6
FITEM,2,19
SFADELE,P51X,1,PRES

!4. step

FLST,2,2,5,ORDE,2
FITEM,2,6
FITEM,2,19
/GO
!*
SFA,P51X,1,PRES,0.1555

!Time at the end of load step
TIME,1080

LSWRITE,4,    !Write to LS file

!Delete the loading (pressure on areas)

FLST,2,2,5,ORDE,2
FITEM,2,6
FITEM,2,19
SFADELE,P51X,1,PRES

                …
                …
                …

!54. step

FLST,2,2,5,ORDE,2
FITEM,2,6
FITEM,2,19
/GO
!*
SFA,P51X,1,PRES,0.1555

!Time at the end of load step
TIME,590400

LSWRITE,54,    !Write to LS file

!Delete the loading (pressure on areas)

FLST,2,2,5,ORDE,2
FITEM,2,6
FITEM,2,19
SFADELE,P51X,1,PRES

!!!! UNLOADING
```

```
!Delete the loading (pressure on areas)

FLST,2,2,5,ORDE,2
FITEM,2,6
FITEM,2,19
SFADELE,P51X,1,PRES

!4. step

FLST,2,2,5,ORDE,2
FITEM,2,6
FITEM,2,19
/GO
!*
SFA,P51X,1,PRES,0.1555

!Time at the end of load step
TIME,1080

LSWRITE,4,    !Write to LS file

!Delete the loading (pressure on areas)

FLST,2,2,5,ORDE,2
FITEM,2,6
FITEM,2,19
SFADELE,P51X,1,PRES

                …
                …
                …

!54. step

FLST,2,2,5,ORDE,2
FITEM,2,6
FITEM,2,19
/GO
!*
SFA,P51X,1,PRES,0.1555

!Time at the end of load step
TIME,738000

LSWRITE,54,    !Write to LS file

!Delete the loading (pressure on areas)

FLST,2,2,5,ORDE,2
FITEM,2,6
FITEM,2,19
SFADELE,P51X,1,PRES

!!!! UNLOADING
```

```
!Delete the loading (pressure on areas)

FLST,2,2,5,ORDE,2
FITEM,2,6
FITEM,2,19
SFADELE,P51X,1,PRES

!4. step

FLST,2,2,5,ORDE,2
FITEM,2,6
FITEM,2,19
/GO
!*
SFA,P51X,1,PRES,0.1555

!Time at the end of load step
TIME,1080

LSWRITE,4,    !Write to LS file

!Delete the loading (pressure on areas)

FLST,2,2,5,ORDE,2
FITEM,2,6
FITEM,2,19
SFADELE,P51X,1,PRES

                …
                …
                …

!54. step

FLST,2,2,5,ORDE,2
FITEM,2,6
FITEM,2,19
/GO
!*
SFA,P51X,1,PRES,0.1555

!Time at the end of load step
TIME,590400

LSWRITE,54,    !Write to LS file

!Delete the loading (pressure on areas)

FLST,2,2,5,ORDE,2
FITEM,2,6
FITEM,2,19
SFADELE,P51X,1,PRES

!!!! UNLOADING
```

```
!55. step

FLST,2,2,5,ORDE,2
FITEM,2,6
FITEM,2,19
/GO
!*
SFA,P51X,1,PRES,0

!Time at the end of load step
TIME,590420

LSWRITE,55,    !Write to LS file

!Delete the loading (pressure on areas)

FLST,2,2,5,ORDE,2
FITEM,2,6
FITEM,2,19
SFADELE,P51X,1,PRES

!56. step

FLST,2,2,5,ORDE,2
FITEM,2,6
FITEM,2,19
/GO
!*
SFA,P51X,1,PRES,0

!Time at the end of load step
TIME,590780

LSWRITE,56,    !Write to LS file

!Delete the loading (pressure on areas)

FLST,2,2,5,ORDE,2
FITEM,2,6
FITEM,2,19
SFADELE,P51X,1,PRES

!57. step

FLST,2,2,5,ORDE,2
FITEM,2,6
FITEM,2,19
/GO
!*
SFA,P51X,1,PRES,0

!Time at the end of load step
TIME,591140

LSWRITE,57,    !Write to LS file
```

```
!55. step

FLST,2,2,5,ORDE,2
FITEM,2,6
FITEM,2,19
/GO
!*
SFA,P51X,1,PRES,0

!Time at the end of load step
TIME,738020

LSWRITE,55,    !Write to LS file

!Delete the loading (pressure on areas)

FLST,2,2,5,ORDE,2
FITEM,2,6
FITEM,2,19
SFADELE,P51X,1,PRES

!56. step

FLST,2,2,5,ORDE,2
FITEM,2,6
FITEM,2,19
/GO
!*
SFA,P51X,1,PRES,0

!Time at the end of load step
TIME,738380

LSWRITE,56,    !Write to LS file

!Delete the loading (pressure on areas)

FLST,2,2,5,ORDE,2
FITEM,2,6
FITEM,2,19
SFADELE,P51X,1,PRES

!57. step

FLST,2,2,5,ORDE,2
FITEM,2,6
FITEM,2,19
/GO
!*
SFA,P51X,1,PRES,0

!Time at the end of load step
TIME,738740

LSWRITE,57,    !Write to LS file
```

```
!55. step

FLST,2,2,5,ORDE,2
FITEM,2,6
FITEM,2,19
/GO
!*
SFA,P51X,1,PRES,0

!Time at the end of load step
TIME,590420

LSWRITE,55,    !Write to LS file

!Delete the loading (pressure on areas)

FLST,2,2,5,ORDE,2
FITEM,2,6
FITEM,2,19
SFADELE,P51X,1,PRES

!56. step

FLST,2,2,5,ORDE,2
FITEM,2,6
FITEM,2,19
/GO
!*
SFA,P51X,1,PRES,0

!Time at the end of load step
TIME,590780

LSWRITE,56,    !Write to LS file

!Delete the loading (pressure on areas)

FLST,2,2,5,ORDE,2
FITEM,2,6
FITEM,2,19
SFADELE,P51X,1,PRES

!57. step

FLST,2,2,5,ORDE,2
FITEM,2,6
FITEM,2,19
/GO
!*
SFA,P51X,1,PRES,0

!Time at the end of load step
TIME,591140

LSWRITE,57,    !Write to LS file
```

```
!Delete the loading (pressure on areas)

FLST,2,2,5,ORDE,2
FITEM,2,6
FITEM,2,19
SFADELE,P51X,1,PRES

!58. step

FLST,2,2,5,ORDE,2
FITEM,2,6
FITEM,2,19
/GO
!*
SFA,P51X,1,PRES,0

!Time at the end of load step
TIME,591500

LSWRITE,58,    !Write to LS file

!Delete the loading (pressure on areas)

FLST,2,2,5,ORDE,2
FITEM,2,6
FITEM,2,19
SFADELE,P51X,1,PRES
                …
                …
                …

!78. step

FLST,2,2,5,ORDE,2
FITEM,2,6
FITEM,2,19
/GO
!*
SFA,P51X,1,PRES,0

!Time at the end of load step
TIME,685460

LSWRITE,78,    !Write to LS file

!Delete the loading (pressure on areas)

FLST,2,2,5,ORDE,2
FITEM,2,6
FITEM,2,19
SFADELE,P51X,1,PRES
```

```
!Delete the loading (pressure on areas)

FLST,2,2,5,ORDE,2
FITEM,2,6
FITEM,2,19
SFADELE,P51X,1,PRES

!58. step

FLST,2,2,5,ORDE,2
FITEM,2,6
FITEM,2,19
/GO
!*
SFA,P51X,1,PRES,0

!Time at the end of load step
TIME,739100

LSWRITE,58,    !Write to LS file

!Delete the loading (pressure on areas)

FLST,2,2,5,ORDE,2
FITEM,2,6
FITEM,2,19
SFADELE,P51X,1,PRES
                …
                …
                …

!78. step

FLST,2,2,5,ORDE,2
FITEM,2,6
FITEM,2,19
/GO
!*
SFA,P51X,1,PRES,0

!Time at the end of load step
TIME,833060

LSWRITE,78,    !Write to LS file

!Delete the loading (pressure on areas)

FLST,2,2,5,ORDE,2
FITEM,2,6
FITEM,2,19
SFADELE,P51X,1,PRES
```

```
!Delete the loading (pressure on areas)

FLST,2,2,5,ORDE,2
FITEM,2,6
FITEM,2,19
SFADELE,P51X,1,PRES

!58. step

FLST,2,2,5,ORDE,2
FITEM,2,6
FITEM,2,19
/GO
!*
SFA,P51X,1,PRES,0

!Time at the end of load step
TIME,591500

LSWRITE,58,    !Write to LS file

!Delete the loading (pressure on areas)

FLST,2,2,5,ORDE,2
FITEM,2,6
FITEM,2,19
SFADELE,P51X,1,PRES
                …
                …
                …

!78. step

FLST,2,2,5,ORDE,2
FITEM,2,6
FITEM,2,19
/GO
!*
SFA,P51X,1,PRES,0

!Time at the end of load step
TIME,685460

LSWRITE,78,    !Write to LS file

!Delete the loading (pressure on areas)

FLST,2,2,5,ORDE,2
FITEM,2,6
FITEM,2,19
SFADELE,P51X,1,PRES
```

!79. step	!79. step	!79. step
FLST,2,2,5,ORDE,2	FLST,2,2,5,ORDE,2	FLST,2,2,5,ORDE,2
FITEM,2,6	FITEM,2,6	FITEM,2,6
FITEM,2,19	FITEM,2,19	FITEM,2,19
/GO	/GO	/GO
!*	!*	!*
SFA,P51X,1,PRES,0	SFA,P51X,1,PRES,0	SFA,P51X,1,PRES,0
!Time at the end of load step	!Time at the end of load step	!Time at the end of load step
TIME,699860	TIME,847460	TIME,699860
LSWRITE,79, !Write to LS file	LSWRITE,79, !Write to LS file	LSWRITE,79, !Write to LS file
!SOLVE all LS files COMMAND	!SOLVE all LS files COMMAND	!SOLVE all LS files COMMAND

Trosifol BG R20; 30 °C	Trosifol BG R20; 40 °C	Trosifol BG R20; 50 °C
!1. step	!1. step	!1. step
FLST,2,2,5,ORDE,2	FLST,2,2,5,ORDE,2	FLST,2,2,5,ORDE,2
FITEM,2,6	FITEM,2,6	FITEM,2,6
FITEM,2,19	FITEM,2,19	FITEM,2,19
/GO	/GO	/GO
!*	!*	!*
SFA,P51X,1,PRES,0.1555	SFA,P51X,1,PRES,0.1555	SFA,P51X,1,PRES,0.1555
!Time at the end of load step	!Time at the end of load step	!Time at the end of load step
TIME,60	TIME,60	TIME,60
!Solution setting	!Solution setting	!Solution setting
NSUBST,10,0,0 !Number of substeps	NSUBST,10,0,0 !Number of substeps	NSUBST,10,0,0 !Number of substeps
LSWRITE,1,	LSWRITE,1,	LSWRITE,1,
!Write to LS file	!Write to LS file	!Write to LS file
!Delete the loading (pressure on areas)	!Delete the loading (pressure on areas)	!Delete the loading (pressure on areas)
FLST,2,2,5,ORDE,2	FLST,2,2,5,ORDE,2	FLST,2,2,5,ORDE,2
FITEM,2,6	FITEM,2,6	FITEM,2,6
FITEM,2,19	FITEM,2,19	FITEM,2,19
SFADELE,P51X,1,PRES	SFADELE,P51X,1,PRES	SFADELE,P51X,1,PRES
!2. step	!2. step	!2. step
FLST,2,2,5,ORDE,2	FLST,2,2,5,ORDE,2	FLST,2,2,5,ORDE,2
FITEM,2,6	FITEM,2,6	FITEM,2,6
FITEM,2,19	FITEM,2,19	FITEM,2,19
/GO	/GO	/GO
!*	!*	!*
SFA,P51X,1,PRES,0.1555	SFA,P51X,1,PRES,0.1555	SFA,P51X,1,PRES,0.1555
!Time at the end of load step	!Time at the end of load step	!Time at the end of load step
TIME,360	TIME,360	TIME,360
LSWRITE,2, !Write to LS file	LSWRITE,2, !Write to LS file	LSWRITE,2, !Write to LS file

!Delete the loading (pressure on areas)	!Delete the loading (pressure on areas)	!Delete the loading (pressure on areas)
FLST,2,2,5,ORDE,2	FLST,2,2,5,ORDE,2	FLST,2,2,5,ORDE,2
FITEM,2,6	FITEM,2,6	FITEM,2,6
FITEM,2,19	FITEM,2,19	FITEM,2,19
SFADELE,P51X,1,PRES	SFADELE,P51X,1,PRES	SFADELE,P51X,1,PRES
!3. step	!3. step	!3. step
FLST,2,2,5,ORDE,2	FLST,2,2,5,ORDE,2	FLST,2,2,5,ORDE,2
FITEM,2,6	FITEM,2,6	FITEM,2,6
FITEM,2,19	FITEM,2,19	FITEM,2,19
/GO	/GO	/GO
!*	!*	!*
SFA,P51X,1,PRES,0.1555	SFA,P51X,1,PRES,0.1555	SFA,P51X,1,PRES,0.1555
!Time at the end of load step	!Time at the end of load step	!Time at the end of load step
TIME,720	TIME,720	TIME,720
LSWRITE,3, !Write to LS file	LSWRITE,3, !Write to LS file	LSWRITE,3, !Write to LS file
!Delete the loading (pressure on areas)	!Delete the loading (pressure on areas)	!Delete the loading (pressure on areas)
FLST,2,2,5,ORDE,2	FLST,2,2,5,ORDE,2	FLST,2,2,5,ORDE,2
FITEM,2,6	FITEM,2,6	FITEM,2,6
FITEM,2,19	FITEM,2,19	FITEM,2,19
SFADELE,P51X,1,PRES	SFADELE,P51X,1,PRES	SFADELE,P51X,1,PRES
!4. step	!4. step	!4. step
FLST,2,2,5,ORDE,2	FLST,2,2,5,ORDE,2	FLST,2,2,5,ORDE,2
FITEM,2,6	FITEM,2,6	FITEM,2,6
FITEM,2,19	FITEM,2,19	FITEM,2,19
/GO	/GO	/GO
!*	!*	!*
SFA,P51X,1,PRES,0.1555	SFA,P51X,1,PRES,0.1555	SFA,P51X,1,PRES,0.1555
!Time at the end of load step	!Time at the end of load step	!Time at the end of load step
TIME,1080	TIME,1080	TIME,1080
LSWRITE,4, !Write to LS file	LSWRITE,4, !Write to LS file	LSWRITE,4, !Write to LS file
!Delete the loading (pressure on areas)	!Delete the loading (pressure on areas)	!Delete the loading (pressure on areas)
FLST,2,2,5,ORDE,2	FLST,2,2,5,ORDE,2	FLST,2,2,5,ORDE,2
FITEM,2,6	FITEM,2,6	FITEM,2,6
FITEM,2,19	FITEM,2,19	FITEM,2,19
SFADELE,P51X,1,PRES	SFADELE,P51X,1,PRES	SFADELE,P51X,1,PRES
…	…	…
…	…	…
…	…	…

```
!61. step

FLST,2,2,5,ORDE,2
FITEM,2,6
FITEM,2,19
/GO
!*
SFA,P51X,1,PRES,0.1555

!Time at the end of load step
TIME,432000

LSWRITE,61,  !Write to LS file

!Delete the loading (pressure on areas)

FLST,2,2,5,ORDE,2
FITEM,2,6
FITEM,2,19
SFADELE,P51X,1,PRES


!!!!UNLOADING

!62. step

FLST,2,2,5,ORDE,2
FITEM,2,6
FITEM,2,19
/GO
!*
SFA,P51X,1,PRES,0

!Time at the end of load step
TIME,432020

LSWRITE,62,  !Write to LS file

!Delete the loading (pressure on areas)

FLST,2,2,5,ORDE,2
FITEM,2,6
FITEM,2,19
SFADELE,P51X,1,PRES

!63. step

FLST,2,2,5,ORDE,2
FITEM,2,6
FITEM,2,19
/GO
!*
SFA,P51X,1,PRES,0
```

```
!61. step

FLST,2,2,5,ORDE,2
FITEM,2,6
FITEM,2,19
/GO
!*
SFA,P51X,1,PRES,0.1555

!Time at the end of load step
TIME,432000

LSWRITE,61,  !Write to LS file

!Delete the loading (pressure on areas)

FLST,2,2,5,ORDE,2
FITEM,2,6
FITEM,2,19
SFADELE,P51X,1,PRES


!!!!UNLOADING

!62. step

FLST,2,2,5,ORDE,2
FITEM,2,6
FITEM,2,19
/GO
!*
SFA,P51X,1,PRES,0

!Time at the end of load step
TIME,432020

LSWRITE,62,  !Write to LS file

!Delete the loading (pressure on areas)

FLST,2,2,5,ORDE,2
FITEM,2,6
FITEM,2,19
SFADELE,P51X,1,PRES

!63. step

FLST,2,2,5,ORDE,2
FITEM,2,6
FITEM,2,19
/GO
!*
SFA,P51X,1,PRES,0
```

```
!54. step

FLST,2,2,5,ORDE,2
FITEM,2,6
FITEM,2,19
/GO
!*
SFA,P51X,1,PRES,0.1555

!Time at the end of load step
TIME,590400

LSWRITE,54,  !Write to LS file

!Delete the loading (pressure on areas)

FLST,2,2,5,ORDE,2
FITEM,2,6
FITEM,2,19
SFADELE,P51X,1,PRES


!!!!UNLOADING

!55. step

FLST,2,2,5,ORDE,2
FITEM,2,6
FITEM,2,19
/GO
!*
SFA,P51X,1,PRES,0

!Time at the end of load step
TIME,590420

LSWRITE,55,  !Write to LS file

!Delete the loading (pressure on areas)

FLST,2,2,5,ORDE,2
FITEM,2,6
FITEM,2,19
SFADELE,P51X,1,PRES

!56. step

FLST,2,2,5,ORDE,2
FITEM,2,6
FITEM,2,19
/GO
!*
SFA,P51X,1,PRES,0
```

```
!Time at the end of load step
TIME,432380

LSWRITE,63,    !Write to LS file

!Delete the loading (pressure on areas)

FLST,2,2,5,ORDE,2
FITEM,2,6
FITEM,2,19
SFADELE,P51X,1,PRES

!64. step

FLST,2,2,5,ORDE,2
FITEM,2,6
FITEM,2,19
/GO
!*
SFA,P51X,1,PRES,0

!Time at the end of load step
TIME,432740

LSWRITE,64,    !Write to LS file

!Delete the loading (pressure on areas)

FLST,2,2,5,ORDE,2
FITEM,2,6
FITEM,2,19
SFADELE,P51X,1,PRES
                …
                …
                …
!87. step
FLST,2,2,5,ORDE,2
FITEM,2,6
FITEM,2,19
/GO
!*
SFA,P51X,1,PRES,0

!Time at the end of load step
TIME,555860

LSWRITE,87,    !Write to LS file

!Delete the loading (pressure on areas)

FLST,2,2,5,ORDE,2
FITEM,2,6
FITEM,2,19
SFADELE,P51X,1,PRES
```

```
!Time at the end of load step
TIME,432380

LSWRITE,63,    !Write to LS file

!Delete the loading (pressure on areas)

FLST,2,2,5,ORDE,2
FITEM,2,6
FITEM,2,19
SFADELE,P51X,1,PRES

!64. step

FLST,2,2,5,ORDE,2
FITEM,2,6
FITEM,2,19
/GO
!*
SFA,P51X,1,PRES,0

!Time at the end of load step
TIME,432740

LSWRITE,64,    !Write to LS file

!Delete the loading (pressure on areas)

FLST,2,2,5,ORDE,2
FITEM,2,6
FITEM,2,19
SFADELE,P51X,1,PRES
                …
                …
                …
!87. step
FLST,2,2,5,ORDE,2
FITEM,2,6
FITEM,2,19
/GO
!*
SFA,P51X,1,PRES,0

!Time at the end of load step
TIME,555860

LSWRITE,87,  !Write to LS file

!Delete the loading (pressure on areas)

FLST,2,2,5,ORDE,2
FITEM,2,6
FITEM,2,19
SFADELE,P51X,1,PRES
```

```
!Time at the end of load step
TIME,590780

LSWRITE,56,    !Write to LS file

!Delete the loading (pressure on areas)

FLST,2,2,5,ORDE,2
FITEM,2,6
FITEM,2,19
SFADELE,P51X,1,PRES

!57. step

FLST,2,2,5,ORDE,2
FITEM,2,6
FITEM,2,19
/GO
!*
SFA,P51X,1,PRES,0

!Time at the end of load step
TIME,591140

LSWRITE,57,    !Write to LS file

!Delete the loading (pressure on areas)

FLST,2,2,5,ORDE,2
FITEM,2,6
FITEM,2,19
SFADELE,P51X,1,PRES
                …
                …
                …
!78. step
FLST,2,2,5,ORDE,2
FITEM,2,6
FITEM,2,19
/GO
!*
SFA,P51X,1,PRES,0

!Time at the end of load step
TIME,685460

LSWRITE,78,    !Write to LS file

!Delete the loading (pressure on areas)

FLST,2,2,5,ORDE,2
FITEM,2,6
FITEM,2,19
SFADELE,P51X,1,PRES
```

!88. step	!88. step	!79. step
FLST,2,2,5,ORDE,2	FLST,2,2,5,ORDE,2	FLST,2,2,5,ORDE,2
FITEM,2,6	FITEM,2,6	FITEM,2,6
FITEM,2,19	FITEM,2,19	FITEM,2,19
/GO	/GO	/GO
!*	!*	!*
SFA,P51X,1,PRES,0	SFA,P51X,1,PRES,0	SFA,P51X,1,PRES,0
!Time at the end of load step	!Time at the end of load step	!Time at the end of load step
TIME,570260	TIME,570260	TIME,699860
LSWRITE,88, !Write to LS file	LSWRITE,88, !Write to LS file	LSWRITE,79, !Write to LS file
!SOLVE all LS files COMMAND	!SOLVE all LS files COMMAND	!SOLVE all LS files COMMAND